1-1-2011

# Comparison of progression of diffuse axonal injury with histology and diffusion tensor imaging

Nisrine Zakaria
*Wayne State University,*

Recommended Citation

# COMPARISON OF PROGRESSION OF DIFFUSE AXONAL INJURY WITH HISTOLOGY AND DIFFUSION TENSOR IMAGING

by

**NISRINE ZAKARIA**

**DISSERTATION**

Submitted to the Graduate School

of Wayne State University,

Detroit, Michigan

In partial fulfillment of the requirements

for the degree of

**DOCTOR OF PHILOSOPHY**

2011

MAJOR: BIOMEDICAL ENGINEERING

Approved by:

_____
Advisor                        Date

_____

_____

_____

# ACKNOWLEDGEMENTS

I would like to deeply thank Dr. John Cavanaugh for his patience, guidance, support and encouragement he has given me throughout the years.  Dr. John Cavanaugh's research experience and knowledge has helped me to tackle many problems in my research and continue to forge ahead to the completion of my work.  I would like to extend my sincere gratitude and appreciation to my PhD dissertation committee Drs. Mark Haacke, Randall Benson and King Yang for their valuable advice on my dissertation.  Also I would like to further thank Dr. Mark Haacke for teaching me MRI basics and inspiring me to further study this area.  Also I would like to express my gratitude to him for allowing me to utilize the MRI facilities to image my rats.  I would like to express my thanks to those at the MRI facilities specifically Drs. Yimin Shen, Zhifend Kou and Yi Zhong.

I am indebted to support i have received from many of my colleagues especially Dr. Srinivas Kallakuri, Sharath Baudaru, Gurjiwan Virk, Ke Feng, and Anuja Vedpathak.  As well as all the volunteers especially Abhijit Anil Munotthat, and Branden Anderson who have helped me in my endeavours throughout this project.  It is an honor for me to further thank Dr. Srinivas Kallakuri for teaching me many laboratory techniques and providing me technical assistance throughout the years.  I would like to express my gratitude to Dr. Bulent Ozkan for this help, advise, and guidance on my statistical analysis of my data.  I would like to thank Mrs. Charlotte Harman for kindly going through my thesis and making corrections.

Last but not least I would like to thank my family and friends who unwavering support throughout these years has been a source of strength and sanity for me.  I would like to express my deepest thanks to my mother and father were it not for their financial support over all my educational years this thesis would have undoubtedly not been possible.

# TABLE OF CONTENTS

iv

# LIST OF TABLES

# LIST OF FIGURES

xiii

xix

xxii

# CHAPTER 1 INTRODUCTION

Traumatic brain injury (TBI) is a significant global public health problem.  The Federal

Government's Individuals with Disabilities Education Act (IDEA) defined TBI as:

> [A]n acquired injury to the brain caused by an external physical force, resulting in total or partial functional disability or psychosocial impairment, or both that adversely affects a [person's] performance.  The  Term applies to open or closed head injuries resulting in impairment in one or more areas such as cognition; language; memory; attention' reasoning abstract thinking; judgment; problem-solving; sensory, perceptual, and motor abilities; psychosocial behavior; physical functions; information processing; and speech.  The term does not apply to brain injuries that congenital or degenerative, or to brain injuries induced by birth trauma. (Code of Federal Regulations, 2005)

In the United States approximately 1.4 million TBI cases are reported yearly (Langlois, Marr et al. 2005; Langlois, Rutland-Brown et al. 2006).  On a global scale the incidence of TBI still remains unknown (Corrigan, Selassie et al. 2010).   This estimate of TBI prevalence underestimates the true TBI cases in the United State, since individuals receiving medical care at an outpatient clinic or doctors' offices are not included in this estimate.  It is suggested that 200,000 American with TBI are treated in outpatient clinics or doctors' offices each year (Finkelstein, Corso et al. 2006).  Also, individuals with TBI who are treated at military facilities in the United States and abroad are not included in this estimate.  In addition, some cases of TBI are misdiagnosed, and the numbers of individuals who experience TBI and do not seek medical attention are unknown.  In spite of that, the estimated TBI cases are eight times greater than the occurrence of breast cancer cases and 37 times greater than the occurrence of HIV and Aids cases (Jiang, van Zijl et al. 2006; Jemal, Siegel et al. 2007).  From the estimated TBI cases who seek medical attention each year 235,000 individuals are hospitalized and survive, whereas 50,000 to 52,000 individuals die (1989; 1998; Thurman, Alverson et al. 1999; Ghajar 2000; Langlois, Rutland-Brown et al. 2004; Ashman, Gordon et al. 2006; Langlois, Rutland-Brown et al. 2006; Chua, Ng et al. 2007; Corrigan, Selassie et al. 2010).  In the US each year 80,000 to

90,000 individuals will experience permanent disabilities related to their TBI (1989; Thurman, Alverson et al. 1999; Langlois, Rutland-Brown et al. 2004; Ashman, Gordon et al. 2006; Chua, Ng et al. 2007). At least 5.3 million individuals or 2% of US population, in addition to 57 million individuals worldwide live with disability as an outcome of their TBI (Ashman, Gordon et al. 2006; Langlois, Rutland-Brown et al. 2006; Chua, Ng et al. 2007).

In the United States the major TBI risk factors are age, gender, and low socioeconomic status(Corrigan, Selassie et al. 2010). According to hospital discharge records the leading cause of TBI are falls (28%), motor vehicle crashes (20%), struck by or against events (19%), assault (11%), non motor vehicle crashes (3%), other (19%) (Langlois, Rutland-Brown et al. 2006). The highest occurrence of TBI is among adolescents and young adults (15- 24 years), and individuals older than 75 years, in addition a less striking incidence of TBI occurs in children 5 years and younger (1998; Burns and Hauser 2003; Chua, Ng et al. 2007; Corrigan, Selassie et al. 2010). Males tend to experience roughly double the risk factor of TBI in comparison to females; this could be an attributed to the males risk taking tendency and engagements with high-risk activities (Corrigan, Selassie et al. 2010). Additional, individual coming from low socioeconomic status tend to have higher risk in acquiring TBI (Corrigan, Selassie et al. 2010).

It is estimated that the annual economical cost of TBI in the United States is $60.4 billion; this estimate includes productivity losses of $51.2 billion (Finkelstein, Corso et al. 2006). However, this estimated economical cost is based on the medical treatment and does not account for the extended rehabilitation, support, and services required for long-term and lifelong disabilities (Corrigan, Selassie et al. 2010). Additionally, the estimate does not include the value of lost quality of life, or the indirect impact on friends, family, care givers and the community. Furthermore, it has been documented that TBI survivors tend to have an increased risk in other health conditions such as binge drinking , development of epilepsy, depression, Alzheimers, and experiencing early death (Langlois, Rutland-Brown et al. 2006). All these increased risks are

not part of the economical estimate as well. Thus, the economical cost of TBI is much greater than the estimated annual cost of $60.4 billion.

## Grading TBI Severities

To estimate the severity of the brain's physiological or anatomical damage as a result of TBI, healthcare professionals assign a level of injury severity in accordance to the common used indices of severity such as; Glasgow Coma Scale (GCS), Abbreviated Injury Severity Scale (AIS), Loss of Consciousness (LOC) and posttraumatic amnesia (Corrigan, Selassie et al. 2010). These injury indexes of TBI categorize the injury severity as a mild, moderate and severe (Table 1) (Rimel, Giordani et al. 1981; Rimel, Giordani et al. 1982). However, the boundaries of these severities are difficult to delineate especially when defining the minimum threshold of mild TBI (Corrigan, Selassie et al. 2010).

**Table 1:** TBI severity scales. The following min, h, and d represent minutes, hours and days respectively (Corrigan, Selassie et al. 2010)

|  |  | Severity Category | | |
| --- | --- | --- | --- | --- |
| **Index Severity** | **Measurement Approach** | **Mild** | **Moderate** | **Severe** |
| **Abbreviated Injury Severity** | Anatomic/Structural damage | 1-2 | 3 | 4-6 |
| **Glasgow Coma Scale** | Neurological deficit/mental status | 13-15 | 9-12 | 3-8 |
| **Loss of Consciousness** | Mental Status/alertness | <30 min | 30 min – 24 h | >24 h |
| **Posttraumatic Amnesia** | Mental Status/memory and recall | 0 – 1 d | >1 to ≤7 d | >7 d |

These indices of severity are a good predictor during acute care for the probability of mortality; however, they are a poor indicator of long term outcome (Corrigan, Selassie et al. 2010). Originally it was thought that the greater the severity score the more likely the occurrence of disability, however this assumption was found to be false. A population cohort study in Scotland reported that the disabilities acquired by individuals after 1 year being discharged from the hospital where 47% for mild TBI, 45% for moderate TBI, and 48% for sever

TBI (Thornhill, Teasdale et al. 2000), these initial TBI severities were measured by GCS and duration of LOC. This poor association between the initial TBI severity and the disability outcome has been also repeatedly reported by other smaller studies (Corrigan, Selassie et al. 2010). Therefore, the need for improved classification of TBI in order to enable and accurate prognosticate injury trajectory still is needed.

In order to better classify TBI and to predict its short and long term consequences one must look at the cellular level of the injury in a noninvasive manner. One method that may allow us to probe into the brain noninvasively is neuroimaging. However, clinical and neuroimaging assessment of TBI is remains a great challenge to clinicians. Currently conventional neuroimaging techniques underestimate or fail to recognize the extent of TBI. However, many clinical studies has utilized a nonconventional Magnetic Resonance Imaging (MRI) known as Diffusion Tensor Imaging (DTI) to investigate how different DTI parameters can detect pathological changes in TBI patients (Arfanakis, Haughton et al. 2002; Inglese, Makani et al. 2005; Le, Mukherjee et al. 2005; Newcombe, Williams et al. 2007; Xu, Rasmussen et al. 2007). In addition, some studies have further investigated how these changes can be a predictor of outcome in TBI patients (Huisman, Schwamm et al. 2004; Bazarian, Zhong et al. 2007; Benson, Meda et al. 2007; Kraus, Susmaras et al. 2007). Even though these studies have imaged patients days to even years post TBI they reported a change in the DTI parameters when compared to healthy volunteers (Arfanakis, Haughton et al. 2002; Inglese, Makani et al. 2005; Le, Mukherjee et al. 2005; Newcombe, Williams et al. 2007; Xu, Rasmussen et al. 2007). The DTI parameters where found to correlate with the Glasgow Coma Scale (GCS), Rankin score, post-concussive symptom, cognition and post-traumatic amnesia (Huisman, Schwamm et al. 2004; Bazarian, Zhong et al. 2007; Benson, Meda et al. 2007; Kraus, Susmaras et al. 2007). Therefore, this nonconventional neuroimaging method may play an important role in predicting the underlining pathology event occurring in the brain as consequence of TBI. In order to utilize

DTI to better improve classification of TBI and to accurately prognosticate injury trajectory one must understand the cellular injury effects on the DTI signals.  Thus, this study utilizes histological methods considered as the gold standard of axonal injury detection and compares them to DTI parameter changes as a result of TBI in an animal model.  This study focuses on diffuse axonal injury (DAI), a type of diffuse brain injury.  DAI is extremely difficult to be detected by current conventional neuroimaging technique (Arfanakis, Haughton et al. 2002) and it is believed to play a crucial role in neurological deficits. Thus, an increased understanding of the relationship between DTI and DAI is imperative.

## Hypothesis and specific aims

**Specific aim 1:**  To demonstrate if diffusion tensor imaging (DTI) parameters of fractional anisotropy (FA), apparent diffusion coefficient (ADC), axial diffusivity (AD) and radial diffusivity (RD) are significantly correlated with Diffuse Axonal Injury in the corpus callosum and optic chiasm at 4 time points (4 hours, 24 hours, 3 days, and 7 days) post-impact, in adult male Sprague Dawley rats subjected to severe TBI via an acceleration impact model.

*Method:*  In selected regions of interest (ROI), that is, corpus callosum and optic chiasm, the FA, ADC, RD and AD histogram distributions will be measured.  β-amyloid precursor protein (β-APP) and neurofilament immunocytochemistry will be carried out in the corresponding tissue and the number of retraction balls (RB) and axonal swellings will be quantified in the same ROIs.  The RB and axonal swelling quantification will be compared to the DTI parameters of the corresponding region at each time interval (4 hours, 24 hours, 3 days, and 7 days).  Additionally, the relationship between the location of injury and the ability of DTI to detect DAI at different time points will be investigated.

**Hypothesis 1**: The severity of axonal injury is characterized by the retraction ball and axonal swelling count.  Therefore, the severity of DAI will correlate with the DTI parameters (FA, ADC,

AD and RD).  The changes in retraction ball and swollen axons counts will correlate with the DTI parameter changes over time, since DTI parameter changes are dependent on the axonal integrity.

**Specific aim 2**:  To determine if the DTI parameters can effectively trace the injury profile as time progresses.

*Method:*  The progression of DAI will be monitored by DTI at four hours, twenty-four hours, three days and seven days.  At each time point, a group of animals (n = 6) will be sacrificed and histological analysis will be carried out to quantify: axonal swellings/retraction balls by amyloid precursor protein (β-APP) and neurofilament (NF-L) immunocytochemistry.  The variation in DTI parameters will be compared to the pathological changes of the tissue over time.

**Hypothesis 2**:  DAI is a secondary injury of TBI therefore, as time progresses the injury will become more prominent and more damage will become evident.  Therefore, the early detection of DTI parameter changes should be a good indicator of axonal injury progression as time increases.  As time progresses after induction of TBI, the pathology profile changes, where some recovery of axons will take place while other axons will become disconnected from their distal end.  This pathological profile should influence the DTI parameter changes over time.

## CHAPTER 2 TRAUMATIC BRAIN INJURY

TBI is produced by rapid head acceleration/deceleration during a traumatic event (Kelley, Farkas et al. 2006).  The rapid head acceleration/deceleration causes an internal stresses and strains upon the brain tissue and thereby induces diffuse brain injury.  All tissue components such as neurons, neuronal processes, transmitter mechanisms, glial cells and blood vessels are affected by the internal stresses and strains caused by rapid acceleration/deceleration (Reilly 2001) and can resulting in an alteration to the gray matter (GM) and white matter (WM) environments which in turn lead to neurological deficits.

### White Matter Structures

WM structures of the brain consist of axons, capillaries, glial cells, ependymal cells and endothelial cells.  Axons, extensions from the neuronal cell bodies found in the GM, convey signals from one nerve cell to another (Johansen-Berg and Behrens 2009).  The ependymal and endothelial cells line the ventricular system and blood vessels respectively.  Glial cells are subdivided into two categories known as macroglia and microglia.

Macroglial cells consist of astrocytes, oligodendrocytes, and NG2 positive cells (Figure 2.1).  NGE positive cells are precursors for mature oligodendrocytes and astrocytes in the developing adult brain.  Oligodendrocytes are the cells that produce the myelin sheath that gives the WM its white appearance.  The myelin sheaths are membranous, lipid and protein-rich structures that wraps around the axons.  The myelin sheaths insulate the axons and thus enable efficient electrical conduction.  Astrocytes, the other macroglial cells, play supporting roles in the central nervours system (CNS).  The astrocytes regulate the extracellular ion concentration, maintain the blood brain barrier (BBB) as well as providing a structural and trophic support to the neurons and oligodendrocytes.  The second category of glial cells is the microglial cells

which are  the immune cells of the CNS.  Microglial cells are phagocytic cells that engulf dying cells and waste product.
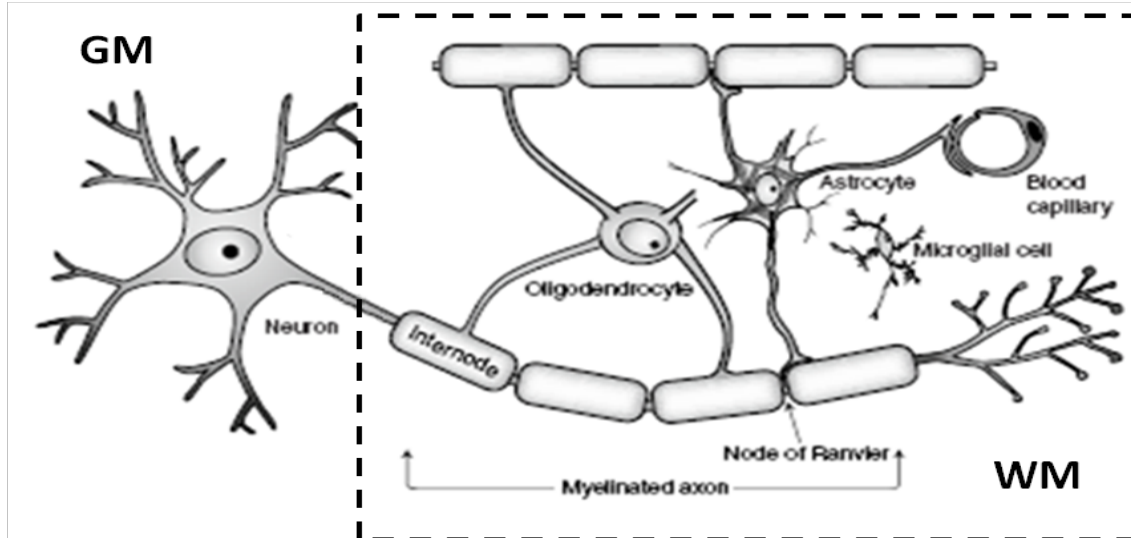


**Figure 1:** Representation of major cellular elements of the WM.   The neuron cell body is present in the GM  (Johansen-Berg and Behrens 2009).

## Gray Matter

GM structures of the brain consist of neuronal cell bodies, dendrites, axons, glial cells and capillaries (Purves 2008).  The neuronal  cell bodies are present only in the GM and are absent in the WM.  The axons extend from the neuronal cell bodies are present in the GM to the WM where they span in tracts to transmit information from one part of the brain to another (Kandel, Schwartz et al. 2000).  Similar to the WM, glial cells and capillaries are also present in the GM (Purves 2008).

## Neuron

The neuron is the communication cell within the CNS composed of dendrites, soma (cell body) and axon (Squire 2003).  The dendrites, afferent components of the neurons, are arranged around the soma (Siegel, Albers et al. 2006).  The soma is rich in organelles (Siegel, Albers et al. 2006).  The axons extend from the soma and lack biosynthesis machinery (Miller, Ackerley et al. 2002; Johansen-Berg and Behrens 2009).  Accordingly, in the neuron most

proteins are synthesized in or close to the soma and transported to their appropriate locations via the transport system (Miller, Ackerley et al. 2002; Roy, Zhang et al. 2005; Siegel, Albers et al. 2006). The transport system is composed of two components, molecular motors and rails (Miller, Ackerley et al. 2002; Brown 2003; Roy, Zhang et al. 2005). The molecular motors utilized in the axonal transport system to move cargo along the rails are kinesins and dyneins (Figure 2) (Miller, Ackerley et al. 2002; Brown 2003; Roy, Zhang et al. 2005). The rails are composed of a complex network of cytoskeleton, mainly microtubules and actin polymers (Brown 2003; Roy, Zhang et al. 2005). The motors transport the cargo along these rails bidirectionally. The kinesins and dyneins move the cargo anterogradely and retrogradely, respectively (Figure 2) (Brown 2003; Roy, Zhang et al. 2005).
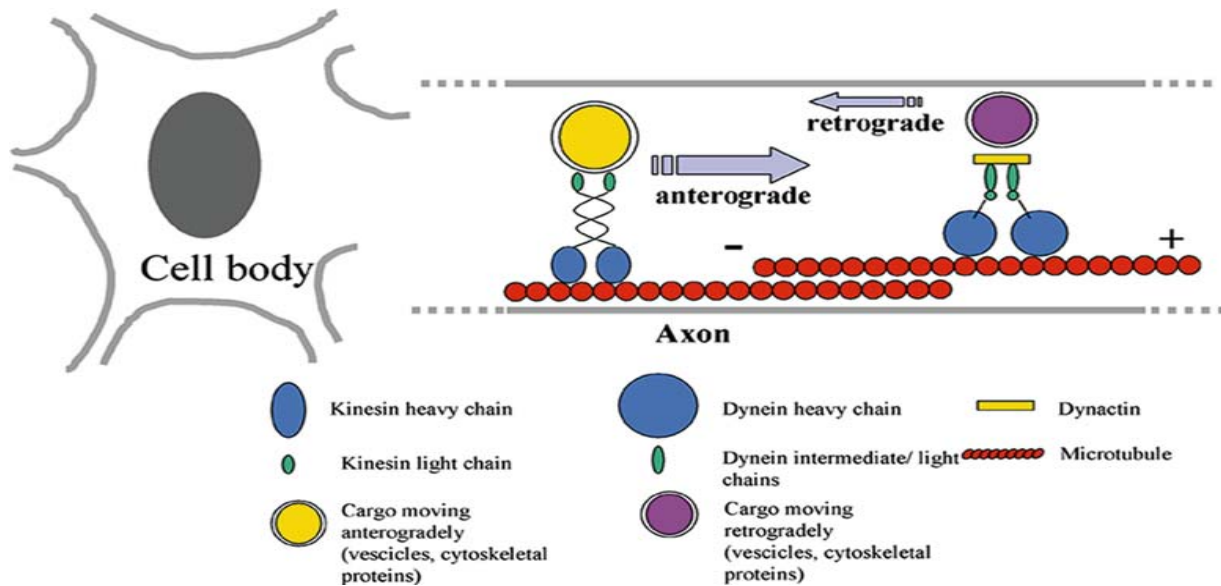


**Figure 2:** Bidirectional transports of cargo along an axon via molecular motors kinesin and dynein. The kinesins and dynein

If the cargo is a membra                                                                              nal

transport system whereas, if the                                                                      er

or cytosolic protein complex, it is                                                                    m

(Roy, Coffee et al. 2000; Wang,                                                                       by,

Zhang et al. 2005).  The fast and slow axonal transport systems move the cargo at a fast rate along the axons; however, the fast transport system moves the cargo continuously along the axon whereas the slow transport system moves the cargo along the system rapidly but with relatively infrequent movement (Roy, Coffee et al. 2000; Wang, Ho et al. 2000; Miller, Ackerley et al. 2002; Brown 2003; Roy, Zhang et al. 2005).  Hence, the transport systems in the neuron are very essential to the neuron's health because they are the highways in which cellular components are trafficked to their appropriate destination to serve their purposes.

## Brain Structures

The two anatomical WM brain structures the CC and Och of Sprague Dawley rats were investigated for axonal injury via histology and magnetic resonance imaging in the following chapters.

### Corpus Callosum

The CC, also referred to as the colossal commissure, is a WM anatomical structure of the brain.  The CC is composed of a broad thick plate of dense fiber that forms the roof of the lateral and third ventricles, transverses the floor of the hemispheric fissure, and fans out in a callosal radiation dispersing into various cortical regions (Carpenter 1991).  The CC is the largest commissure of the brain (Kandel, Schwartz et al. 2000) and it is divided into three sections, the genue, the body or truncus, and the splenium, to represent the anterior, middle and posterior part of the CC respectively (Figure 3).  The CC fibers reciprocally connect regions of the cerebral cortex in all lobes with corresponding regions of opposite hemispheres to allow communication between the two hemispheres (Carpenter 1991; Kandel, Schwartz et al. 2000). The genue connects the frontal lobe cortices, the body connects the remaining frontal lobe cortices and parietal lobe cortices, whereas the splenium connects the temporal lobe cortices and the occipital lobes cortices (Carpenter 1991).

**Optic Chiasm**

Axons from the retinal ganglion cells known as optic nerves enter the cranial cavity thru the optic foramina and come together to form the Och (Carpenter 1991). In the Och the optic fibers either cross the midline or remain uncrossed (Figure 3) (Carpenter 1991; Jeffery 2001). After the optic fibers have adopted a pathway in the Och, the fibers separate into two optic tracts that project into the brain hemispheres (Carpenter 1991; Jeffery 2001). Hence, the crossed and uncrossed fibers in the optic chiasm lead to a projection into the contralateral and ipsilateral hemispheres respectively (Figure 3) (Carpenter 1991; Jeffery 2001). The organization of the optic axons from each eye gives rise to both crossed and uncrossed hemispheric pathways in the Och thus generating binocular vision (Carpenter 1991; Jeffery 2001). As a result, the optic chiasm is responsible for perception of depth and visual measurement of distances.
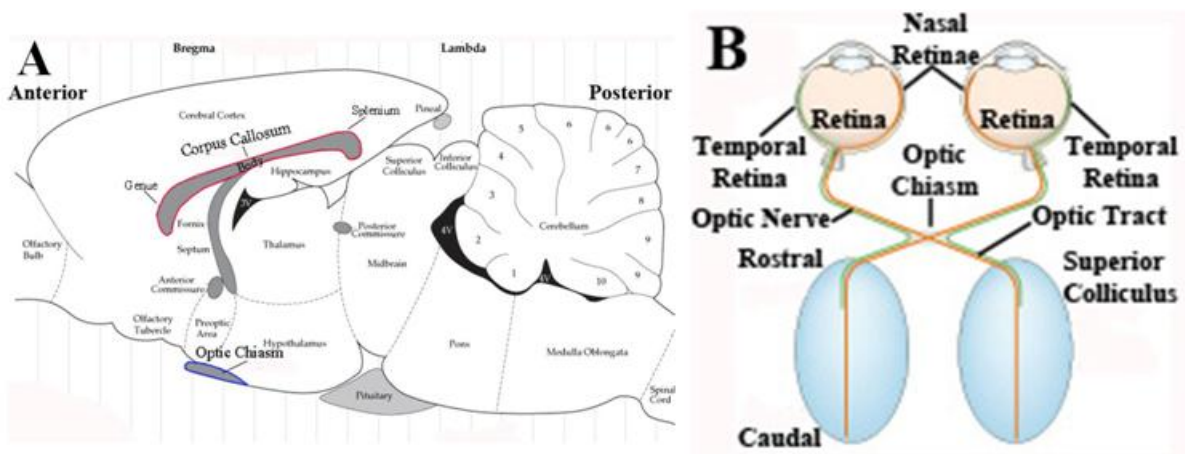


**Figure 3:**Schematic diagram of the (A) sagittal section of the rat's brain and (B) Visual pathway.(A) The CC and Och are outlined in red and blue respectively(Paxinos and Watson 2005). (B) In the Och some optic nerves cross while other do not, then the optic nerves continue as optic tracts into superior colliculus (Guan and Rao 2003).

**Traumatic Brain Injury Classification and Biomechanics**

TBI is a heterogeneous complex injury beginning with an impact and followed by four overlapping phases. These phases succeeding the initial impact are primary injury, evolution of the primary injury, secondary or additional injury, and recovery (Reilly 2001). In the scientific

literature, TBI is classified into two broad categories of injuries: focal injuries and diffuse injuries (Melvin, Lighthall et al. 1994; Mamelak, Pitts et al. 1996; Thurman, Alverson et al. 1999; Langlois, Rutland-Brown et al. 2004). Focal injuries consist of epidural hematomas, subdural hematomas, intracerebral hematomas, lacerations, and coup and countercoup contusion (Melvin, Lighthall et al. 1994; Mamelak, Pitts et al. 1996; Thurman, Alverson et al. 1999; Langlois, Rutland-Brown et al. 2004). Diffuse injuries consist of brain swelling, concussion and diffuse axonal injury (DAI) (Melvin, Lighthall et al. 1994; Mamelak, Pitts et al. 1996; Thurman, Alverson et al. 1999; Langlois, Rutland-Brown et al. 2004). Focal brain injuries are acquired as an outcome of a direct impacting force to the head (Adams, Graham et al. 1983; Graham, McLellan et al. 1983; Gennarelli 1993), whereas diffuse brain injuries are acquired as an outcome of internal forces acting on the brain as a result of acceleration and/or deceleration of the brain (Gennarelli, Thibault et al. 1982; Adams, Doyle et al. 1984; Adams, Doyle et al. 1989; Blumbergs, Jones et al. 1989; Margulies, Thibault et al. 1990; Grady, McLaughlin et al. 1993; Smith, Meaney et al. 2003). Focal and diffuse brain injuries are commonly present together during traumatic brain injury (Smith, Meaney et al. 2003) since an impacting force to the head may also lead to rapid acceleration and/or deceleration of the brain, therefore producing internal forces throughout the brain tissue. .

## Animal TBI Induction Models

To study TBI in the laboratory various animal trauma models have been designed and are currently being utilized. These various in-vivo animal brain injury models are: fluid percussion, cortical impact, rotational acceleration and impact acceleration models that have been developed to induce TBI. Fluid percussion and cortical impact have been reported to produce a focal brain contusion and are associated with relatively minimal supratentorial axonal injury. Genneralli et al in 1981 and Smith et al in 1997 developed rotational brain injury models that induced diffuse axonal injury in large animals (Gennarelli, Adams et al. 1981; Smith, Chen

et al. 1997).   Genneralli et al were able to produce DAI in subhuman primates through application of 10 - 20 ms single pulse rotational acceleration to the head (Gennarelli, Adams et al. 1981; Smith, Chen et al. 1997).  In 1997 Smith et al created a rotational acceleration model in miniature swine utilizing a pneumatic actuator and snout clamp (Smith, Chen et al. 1997). Induction of DAI in smaller animals became possible in 1994 when Marmarou et al developed a weight-drop model that induced DAI in rats (Marmarou, Foda et al. 1994).  In 2001 Gutierez et al induced DAI in rabbits by rotational acceleration of the rabbit's head (Gutierrez, Huang et al. 2001).  Also in 2000 Xiao-Shen was able to induce DAI in rats by lateral acceleration of the rat's head (Xiao-Sheng, Sheng-Yu et al. 2000).

**Marmarou Weight-Drop Model**

The Marmarou's weight-drop model is one of the most frequently used rodent impact acceleration models (Cernak 2005; Saatman, Serbest et al. 2009).  It has been extensively utilized to study neural and vascular changes associated with DAI because this model induces DAI with minimal focal brain lesions (Foda and Marmarou 1994; Marmarou, Foda et al. 1994). Since the overall purpose of this study is to assess the ability for DAI to be measured using DTI, Marmarou's weight-drop model was utilized to induce TBI.

The Marmarou's weight-drop model consists of a brass column weight that freely falls within a plexiglas tube from a designated drop height (Figure 4 A).  The brass weight column is dropped onto a stainless steel helmet (10 mm in diameters and 3 mm in depth) fixed with dental cement to the rat's skull between the lambda and bregma fissures and centered on the midline of the skull (Figure 4 B) (Marmarou, Foda et al. 1994).  The rat is positioned on a 10 cm foam bed contained in the plexiglas box (Figure 4 A).

In the Marmarou's weight-drop model it has been well established that the severity of the induced TBI is directly related to the weight-drop height (Foda and Marmarou 1994; Marmarou,

Foda et al. 1994; Ding, Yao et al. 2001; Kallakuri, Cavanaugh et al. 2003).  Varying the weight-drop height induces the same microscopic changes to neurons, astrocytes and small blood vessels; however; varying the drop height will vary the severity of these microscopic injuries (Foda and Marmarou 1994; Ding, Yao et al. 2001; Carre, Cantais et al. 2004).  As the weight-drop height increases, the more prominent the injuries becomes, i.e. an impact mass dropped from one-meter height induces mild TBI whereas an impact mass dropped from two-meter height induces severe TBI (Foda and Marmarou 1994; Ding, Yao et al. 2001; Kallakuri, Cavanaugh et al. 2003).  Therefore, the Marmarou's weight-drop model is capable of controlling the severity of induced injury by varying the magnitude of impact energy (Foda and Marmarou 1994; Marmarou, Foda et al. 1994; Ding, Yao et al. 2001; Kallakuri, Cavanaugh et al. 2003).

A shortcoming of Marmarou's weight-drop model is the change in the foam integrity over multiple uses.  The variation in the foam will cause a variation in the forces experienced by each impacted rat (Piper, Thomson et al. 1996).  Zhang et al investigated the characteristics of the foam utilized in the Marmaou weight-drop model via compression test (Zhang, Gurao et al. 2011).  Zhang reported that the stress resistance of used foam is reduced to 70% of new foam, and it was further reported that with enough recovery time the foam is capable of recovery to the stress level after initial degradation.  To ensure consistent mechanical foam behavior between impact a recovery time of at least one hour after compression of the foam was recommended (Zhang, Gurao et al. 2011). To minimize the impact variation caused by the foam, after each impact in this study the foam was not utilized for at least one week in order for it to elastically recover after each impact.  This recovery time is in line with Zhang et al recommendation.  In addition, any foam that exhibited any visible deformation was discarded and not used for any more impacts.
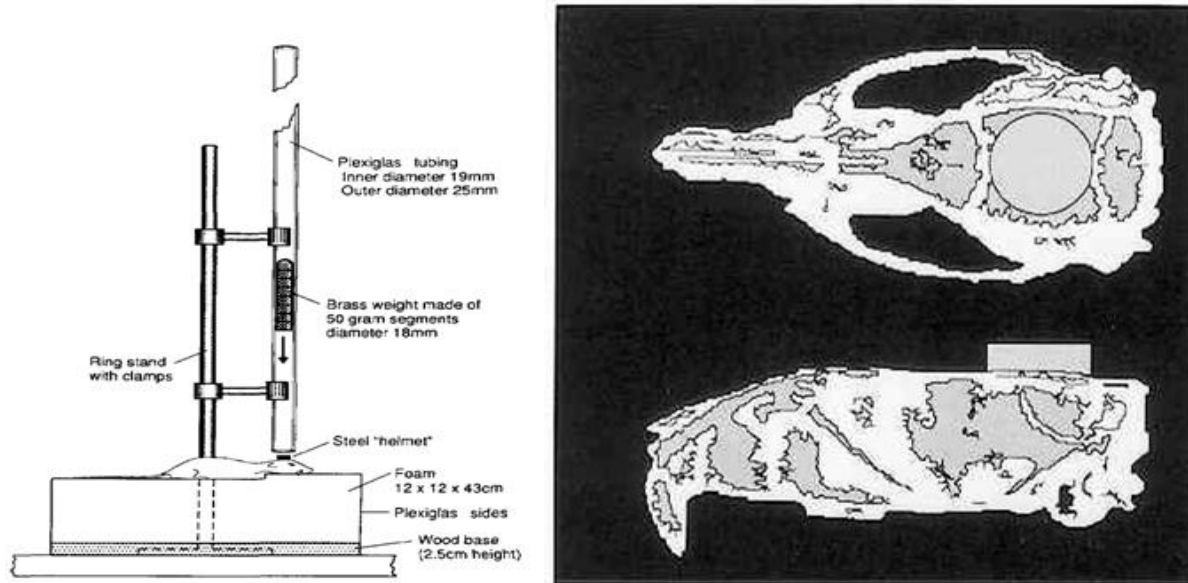
**Figure 4:** (A) Schematic diagram of (A) impact-acceleration injury model and (B) steel helmet placed on the rat skull. (A)The upper weight is attached to a string and the segmented weight column is elevated to the desired height. The bottom opening of the plexiglas cylinder is positioned in close proximity to the head of the rat and centered for the mass to strike directly upon the helmet. (B) The steel helmet placement on the rat skull at the midline between the bregma and lambdoid suture. (Marmarou, Foda et al. 1994)

## Cellular Response Post-TBI

The internal loading to the brain during TBI induces dynamic shear, tensile, and compressive strains onto the brain tissue which leads to dynamic tissue deformation (Smith, Meaney et al. 2003). During traumatic event the rapid uniaxial stretch of the axon results in damage to the cytoskeleton of the axons which is classified as DAI (Gennarelli, Thibault et al. 1989; Smith, Wolf et al. 1999; Wolf, Stys et al. 2001; Tang-Schomer, Patel et al. 2010)

## Traumatic Axonal Injury

DAI is a clinical diagnosis of axonal injury and since laboratory induced axonal injury is produced by an experimental traumatic insult to an animal the term traumatic axonal injury (TAI) (Saatman, Serbest et al. 2009) will be utilized henceforth to denote the laboratory-induced axonal injury.

*Neurofilament Compaction*
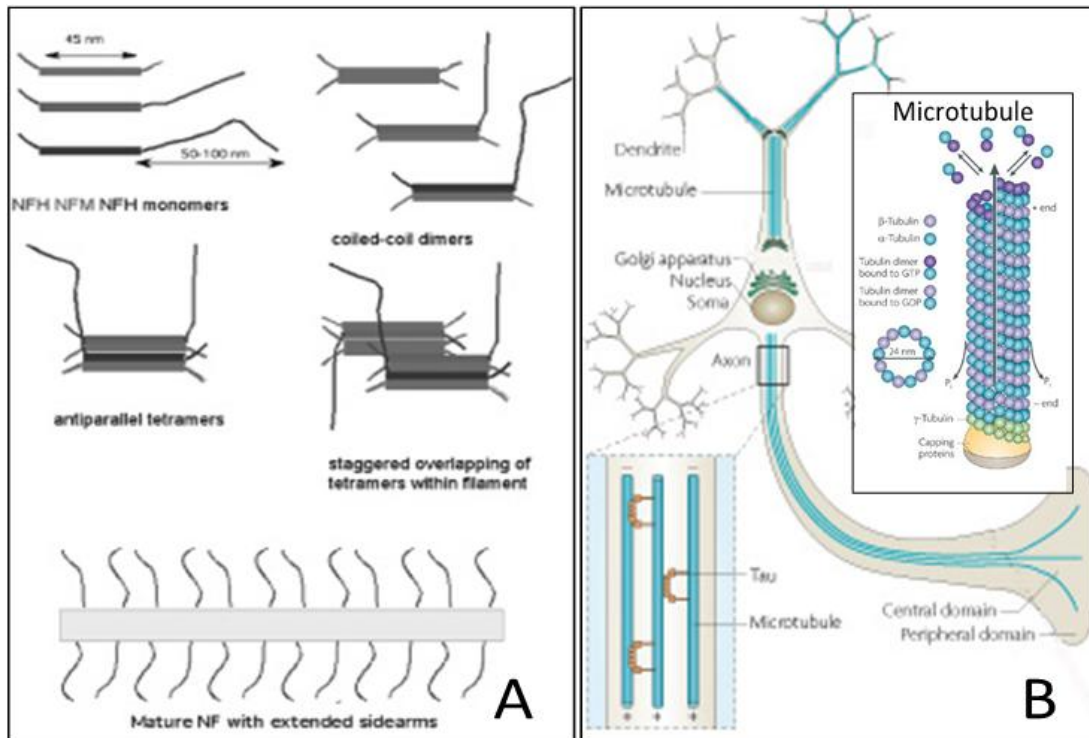


**Figure 5:** Schematic diagram of NF and Microtubule. (A) NF monomers and their assembly to a mature NF. (Janmeya, Leterrierb et al. 2003). (B) Microtubule assembly from tubulin monomers and their uniform tau-bound orientation in the axon (Conde and Caceres 2009)**.**

Neurofilaments (NFs) are intermediate filaments of 10nm diameter found in mature neurons (Alberts 1994; Hoffman 1995). The NFs are part of the neuron's cytoskeleton that provide mechanical stability (Huh, Laurer et al. 2002). They are composed of three protein subunits named NF-L (light molecular weight), NF-M (medium molecular weight) and NF-H (heavy molecular weight) (Figure 5) (Alberts 1994; Hoffman 1995). NF-L and NF-H are associated with NF core and sidearm respectively, whereas NF-M are irregularly localized along the core and the base of side arms (Hoffman 1995). NF proteins are synthesized in the soma and transported via a slow axonal transport (Alberts 1994; Hoffman 1995). The newly synthesized NFs, formed in the soma, are relatively sparsely phosphorylated, and become increasingly phosphorylated during their transport in the axon (Huh, Laurer et al. 2002).

As a result of brain injury, some neurofilament compaction occurs by either phosphorylation or calpain-mediated proteolysis of sidearms (Giza and Hovda 2001; Marmarou, Walker et al. 2005). NF-M and NF-H have a unique feature of extended carboxyterminal domain, which contains multiple repeats of lysine-serine-proline (KSP) motif (Alberts 1994; Hoffman 1995). After induction of injury it has been reported that an influx of the regular excluded tracer of plant protein horseradish peroxidase (HRP) enters the axon (Pettus, Christman et al. 1994; Pettus and Povlishock 1996; Povlishock, Marmarou et al. 1997; Okonkwo, Pettus et al. 1998; Povlishock, Buki et al. 1999). The HRP influx into the axon occurs because the forces exerted onto the axon during injury induction cause mechanical poration of the axolemma. This mechanoporation of the axolemma is believed to also permit an influx of normally excluded ions into the axon such as $Ca^{2+}$ and thereby elevating the intracellular $Ca^{2+}$ (Povlishock 1992; Maxwell and Graham 1997; Siesjo, Hu et al. 1999; Giza and Hovda 2001; Smith, Meaney et al. 2003; Marmarou, Walker et al. 2005). $Ca^{2+}$ ions are known to induce proteolytic pathways which are thought to be key players in axonal pathology (Buki and Povlishock 2006). The increased level of intracellular $Ca^{2+}$ activates calcineurin (calcium-activated phosphatase) (Hoffman 1995; Marmarou, Walker et al. 2005). As a result, the KSP domains on the NF-H (NF sidearms) dephosphorylate reduce the electrostatic repulsion between adjacent NFs, thus reducing interfilament distance and causing compaction of NFs (Hoffman 1995; Kumar and Hoh 2004; Marmarou, Walker et al. 2005). The mechanism of NF transport along the axon is unknown; however, it is believed that the dephosphorylation of specific KSP may retard the movement of NF (Hoffman 1995). Consequently, the NFs will accumulate at the region of increased $Ca^{2+}$ (Node). NF immunocytochemistry has been extensively used to determine TAI histologically (Povlishock 1992; Yaghmai and Povlishock 1992; Grady, McLaughlin et al. 1993; Povlishock 1993; Christman, Grady et al. 1994; Maxwell and Graham 1997; Povlishock, Marmarou et al. 1997; Okonkwo, Pettus et al. 1998; Stone, Singleton et al. 2001; Huh, Laurer et al. 2002; Smith, Meaney et al. 2003; Marmarou, Walker et

al. 2005; Pal, Toth et al. 2006; DiLeonardi, Huh et al. 2009).  The NF monoclonal antibodies RM014 specifically recognize the epitopes on the NF-M rod domain of the NF-M that becomes available after dephosphorylation and thus illuminates axonal injury.  It has been documented that within 15 minutes post-TBI, focal increase of NF-H starts to occur and, over time (30 min – 1 hour) the neurofilament misalignment becomes more prominent (Povlishock 1992; Yaghmai and Povlishock 1992; Povlishock, Marmarou et al. 1997; Stone, Singleton et al. 2001; Suehiro, Singleton et al. 2001; Huh, Laurer et al. 2002; Marmarou, Walker et al. 2005).

### *Amyloid Precursor Protein*

In addition to the NF compaction, loss of microtubular network also occurs as a result of the induced insult to the axon (Pettus and Povlishock 1996; Maxwell, Povlishock et al. 1997; Povlishock, Buki et al. 1999).  β-amyloid precursor protein (β-APP) is a member of glycoprotein normally present in the neuronal cells and it is involved in cell growth, adhesion, synaptic function, and response to injury (Nebuloni, Pellegrinelli et al. 2001; Hortobagyi and Al-Sarraj 2008).  β-APP is synthesized in the soma cytoplasm and transported via a fast anterograde transport system down the axon (McKenzie, McLellan et al. 1996; Geddes, Cargill et al. 2003; Hortobagyi and Al-Sarraj 2008).  In the event of TAI the axonal transport system is disrupted via microtubule loss and β-APP accumulates at the site of disruption; thus, β-APP is a marker for impaired axonal transport (IAT).  In addition, an increased production of APP in the soma occurs after induction of injury (Van den Heuvel, Blumbergs et al. 1999).  In a normal axon β-APP is usually undetectable; however, during transport system impairment the accumulation of β-APP becomes detectable (Gentleman, Nash et al. 1993; Blumbergs, Scott et al. 1994; Sherriff, Bridges et al. 1994; Stone, Singleton et al. 2000).  β-APP is capable of detecting TAI as early as 30 minutes in rats and 35 minutes in humans (Stone, Singleton et al. 2001; Gorrie, Oakes et al. 2002; Marmarou, Walker et al. 2005; Hortobagyi, Wise et al. 2007).  Currently, β-APP is the most widely used marker of impaired axonal transport since it is an early sensitive marker of TAI

(McKenzie, McLellan et al. 1996; Stone, Singleton et al. 2001; Suehiro, Singleton et al. 2001; Gorrie, Oakes et al. 2002; Geddes, Cargill et al. 2003; Marmarou, Walker et al. 2005; Pal, Toth et al. 2006; Hortobagyi, Wise et al. 2007; DiLeonardi, Huh et al. 2009).

# CHAPTER 3: HISTOLOGICAL ASSESSMENT OF TRAUMATIC AXONAL INJURY IN THE RATS' CORPUS CALLOSUM AND OPTIC CHIASM

## Introduction

Diffuse axonal injury (DAI), also referred to as traumatic axonal injury (TAI), is a well-recognized consequence of blunt head injury (Adams, Graham et al. 1982). TAI is considered to be a major contributor to morbidity and mortality after TBI (Adams, Doyle et al. 1989; Slazinski and Johnson 1994; Bennett, O'Brien et al. 1995; Gentleman, Roberts et al. 1995; Povlishock and Christman 1995). TAI is produced by rapid head acceleration/deceleration during a traumatic event (Kelley, Farkas et al. 2006) with consequent tension or shear on axons.

Initial studies of TAI relied on silver staining to detect axonal damage such as axonal fragmentation, degeneration, and swelling (Povlishock, Becker et al. 1983). Silver staining was found to be insensitive to detecting changes at shorter survival times; therefore, immunohistochemical markers for axonal injuries such as β-amyloid precursor protein (βAPP) and neurofilament proteins were evaluated in the 1990s (Grady, McLaughlin et al. 1993; Gultekin and Smith 1994; Sherriff, Bridges et al. 1994; Blumbergs, Scott et al. 1995; Ogata and Tsuganezawa 1999). β-APP immunostaining was found to be capable of detecting TAI as early as 30 minutes in rats and 35 minutes in humans (Stone, Singleton et al. 2001; Gorrie, Oakes et al. 2002; Marmarou, Walker et al. 2005; Hortobagyi, Wise et al. 2007). Currently, β-APP is the most widely used marker of impaired axonal transport, since it is an early sensitive marker of TAI (McKenzie, McLellan et al. 1996; Stone, Singleton et al. 2001; Suehiro, Singleton et al. 2001; Gorrie, Oakes et al. 2002; Geddes, Cargill et al. 2003; Marmarou, Walker et al. 2005; Pal, Toth et al. 2006; Hortobagyi, Wise et al. 2007; DiLeonardi, Huh et al. 2009). In addition to βAPP, neurofilaments (NF) are also immunohistochemical markers of axonal injury. The NFs

are part of the neuron's cytoskeleton that provides mechanical stability (Huh, Laurer et al. 2002). As a result of brain injury, some neurofilament compaction occurs by either phosphorylation or calpain-mediated proteolysis of sidearms (Giza and Hovda 2001; Marmarou, Walker et al. 2005). The NF monoclonal antibodies RM014 specifically recognize the epitopes on the NF-M rod domain of the NF-M that becomes available after dephosphorylation and thus illuminates axonal injury.

Animal studies on axonal injury have highlighted the complexity of TAI. TAI investigations utilizing β-APP and RMO14 immunoreactivities have revealed the existence of two distinct TAI classes (Stone, Singleton et al. 2001; Suehiro, Singleton et al. 2001; Marmarou, Walker et al. 2005). Initially the accumulation of β-APP occurs in the absence of axolemma permeability; however the transport impairment may lead to delayed membrane damage and axolemma permeability (Stone, Okonkwo et al. 2004). Conversely, horseradish peroxidase (HRP) investigations have illustrated that axons experiencing axolemma permeability will tend to exhibit NF compaction (Pettus, Christman et al. 1994; Pettus and Povlishock 1996; Povlishock, Marmarou et al. 1997; Okonkwo, Pettus et al. 1998; Povlishock, Buki et al. 1999). In addition, injury to axons can occur as NF compaction and/or impared axonal transport (IAT). Immunocytochemistry studies utilizing single or dual labeling of βAPP and RMO14 have demonstrated that NF compaction and IAT are independent injuries in some axons while they are dependent in others (Stone, Singleton et al. 2001; Suehiro, Singleton et al. 2001; Marmarou, Walker et al. 2005; Marmarou and Povlishock 2006; DiLeonardi, Huh et al. 2009). In small caliber axons focal axonal injury occurs as IAT whereas in large caliber axons NF compaction and IAT are co-localized (Stone, Singleton et al. 2001). Also axons exhibit NF compaction in the absence of IAT (Stone, Singleton et al. 2001). The profile of an injured axon with only RMO14 immuoreactivity is a thin elongation bands, sometimes expressing vacuolation with little temporal change (Stone, Singleton et al. 2001; Suehiro, Singleton et al. 2001; Marmarou and

Povlishock 2006). When NF compaction occurs in axons it is accompanied by mitochondrial dilation around the region of RMO14 positive immunoreactivity; however, no organelle pooling is present (Stone, Singleton et al. 2001). In contrast, β-APP positive immunoreactive axons display bulbous and swollen profiles with an accumulation of organelles associated with increased axonal swelling over time and possible disconnection of axons (Suehiro, Singleton et al. 2001; Marmarou and Povlishock 2006). Axons demonstrating β-APP and RMO14 positive immunoreactivity also demonstrated a linear profile capped with bulbuous swelling with a progressive accumulation of organelles associated with increased axonal swelling (Stone, Singleton et al. 2001; Marmarou and Povlishock 2006).

In comparison to other histological methods immunohistochemistry appears as the most sensitive and reliable method of detecting TAI. However, animal studies have suggested that different immunohistochemical markers detect specific subsets of axonal injury (Stone, Singleton et al. 2001; Suehiro, Singleton et al. 2001; Marmarou, Walker et al. 2005; Pal, Toth et al. 2006; DiLeonardi, Huh et al. 2009). These animal studies demonstrate the complexity of TAI and thereby the importance of utilizing multiple immunocytochemistry markers to fully represent the complexity of TAI. Hence, this study will utilize β-APP and RMO14 in order to detect TAI injury in the form of IAT and NFC.

The Marmarou impact acceleration weight-drop model has been widely used since it origination in 1994 to induce TBI in rats in order to study TAI and other pathological changes. This impact acceleration model has been reported to induce DAI particularly in the corpus callosum (CC), internal capsule, optic tracts, cerebral, and cerebellar peduncles and the long tracts in the brainstem (Foda and Marmarou 1994). However, many previous studies focused their TAI findings to the brainstem structures (Povlishock, Marmarou et al. 1997; Okonkwo, Pettus et al. 1998; Buki, Walker et al. 2000; Stone, Singleton et al. 2000; Stone, Singleton et al. 2001; Suehiro, Singleton et al. 2001; Stone, Okonkwo et al. 2004; Marmarou, Walker et al.

2005; Marmarou and Povlishock 2006).   Foda et al. have noted in 1994 in their original histological study of the impact acceleration model that TAI does occur in the brainstem as well as the cortical white matter tract however, it was reported that TAI occurs to a lesser extent in the cortical white matter.  To date,  only three histological studies utilizing the Marmarou weight-drop model have investigated TAI in the cortical white matter in a quantitative manner (Ding, Yao et al. 2001; Kallakuri, Cavanaugh et al. 2003; Li, Zhang et al. 2011).  These three studies have demonstrated it is possible to induce TAI in the CC and optic chiasm (Och) via an impact acceleration model.  However, these studies looked at only TAI at one time point via a silver staining method or β-APP immunocytochemistry.  Studies on quantification of TAI over time in cortical white matter as a result of impact acceleration induced TBI is extremely limited.  Hence, this study was performed to assess the extent of TAI in the CC and Och via impaired axonal transport (IAT) and neurofilament compaction (NFC) immunochemistry at various time points of eight hours, twenty–eight hours, seventy-six hours and hundred seventy-two hours hours  after induction of TBI.

## Methods

Twenty-four male Sprague Daley rats weighing 330-506g (Harlan, IN) were utilized.  The rats were randomly assigned to four different post-TBI survival groups (n=6), and had free access to food and water.  The rats were sacrificed at eight hours, twenty-eight hours, seventy-six hours and hundred seventy-two hours post-TBI according to their group.

### Surgical Preparation and TBI Induction

TBI was induced by impact acceleration head injury model (Foda and Marmarou 1994; Marmarou, Foda et al. 1994).  Initially all rats were anesthetised by 2-2.5% isoflurane and 0.6L/min oxygen in an anaesthesia chamber, after which they were transferred to a nose cone where they received 1-1.75% isoflurane and 0.6L/min oxygen.  When the rats became unresponsive to noxious stimulus, a midline incision was preformed to expose the periosteum

covering the vertex of the skull (Marmarou, Foda et al. 1994). The periosteum was reflected and a 10 mm diameter steel disc with a thickness of 3 mm was affixed by cranioplastic powder (Plastic One, Roanoke, VA) at the midline between the bregma and lamboid sutures. The rats were positioned in a prone position on a foam bed (12x12x43 cm) contained in a Plexiglas box and taped in place around their trunk in order prevent them from falling off the foam bed after trauma induction. The nose cone was removed from the rats and a 450g cylindrical brass weight of 18mm in diameter was dropped from a 2m height onto the vertex of the skull at the center of the steel disc to induce TBI. After impact, the steel disc was removed with caution and the skull was examined for any skull fractures. The rats who had endured no severe skull fracture had the skin opening sutured and were allowed to recover.

At the designated survival time, the injured rats were euthanized with an overdose of sodium pentobarbital and exsanguinated. The rats were then transcardially perfused with normal saline followed by cold 4% paraformaldehyde in phosphate buffered saline (0.1 M, pH 7.45). Following perfusion, the brains were carefully removed and post fixed in 4% paraformaldehyde with 20% sucrose.

The brain was cut into a block which contained the genu and the splenium of the CC. This block was embedded in Tissue-Tek® O.C.T compound and frozen at $-78.5^{o}$C via dry ice. A series of 40µm coronal frozen sections were cut from the block by Leica CM 3050 cryostat (Leica Microsystems GmbH, Heidelberg Germany) and collected in multiwell plates. To investigate the distribution of TAI in the Och and CC, twelve sections from each rat were selected. Six sections were utilized to represent TAI in Och and six sections to represent TAI in caudal end of the CC. . To represent the Och, two consecutive sections were selected from the anterior, middle and posterior of the Och ranging from 0.13 to 0.84 mm posterior to bregma. To represent the caudal of the CC, three sets of two conceccutive sections of 280 µm apart were selected. The sections selected to represent TAI in the optic chaism and the caudal of the CC

were approximalty 0.13 - 0.84 mm and 3 – 4.5 mm away from the bregma respectively.  These anatomical structures and locations were utilized because they are a part of a related imaging study.

**Immunochemistry Processing**

Of the consecutive sections selected one was utilized to stain for IAT and the other for NFC.  The Och and CC sections selected were placed in a multiwell plate for histological processing.  The brain sections were rinsed 3 x 3 min in 1XPBS and then processed for antigen retrieval by incubation in citrate butter for 1 hour at 75-80$^0$C.  Next, the tissues were cooled to room temperature for 30 min and then rinsed 3 x 3 min in 1XPBS.  Subsequently, to quench endogenous peroxidase activity the brain sections were immersed in 0.3% $H_2O_2$ for 1 hour after which they were rinsed 3 x 3 min in 1XPB.  The brain sections were incubated over night either in C-terminus specific APP primary antibody (1 µg/ml; rabbit anti-C-terminus β-APP; cat # 51-2700; Zhymed, San Francisco, CA) or RM014 primary antibody (1 µg/ml; mouse anti-NF-L; cat # 13-0400; Zhymed, San Francisco, CA).  The primary antibodies were prepared with 2% normal goat serum (Vector Laboratories, Burlingame, CA), 0.01% Triton X-100 (Fisher Scientific, Fair Lawn, NJ) and 0.1% Albumin Bovine Serum (Sigma-Aldrich, St. Louis, MO) in 1xPBS.  The following day, the brain sections incubated in β-APP or RM014 were incubated in goat anti-rabbit IgG or goat anti-mouse IgG secondary antibody (Vector Laboratories, Burlingame, CA) respectively after a 3 x 3 min rinse in 1XPBS. The secondary antibodies were prepared with 2% normal goat serum (Vector Laboratories, Burlingame, CA), 0.01% Triton X-100 (Fisher Scientific, Fair Lawn, NJ) and 0.1% Albumin Bovine Serum (Sigma-Aldrich, St. Louis, MO) in 1x PBS.  Following incubation in the secondary antibody the brain sections were rinsed 3 x 3 min in 1xPBS and then incubated for one hour in avidin biotin peroxidase complex (Vectastain ABC Standard Elite Kit, Vector), after which, the brain sections were rinsed 3 x 3 min in 1xPBS and briefly incubation in 3, 3'-diaminobenzidine and hydrogen peroxide. Lastly,

the brain sections were rinsed 3 x 5 min in 1xPBS, dehydrated and slip-covered using Permount.

## Digital Image Acquisition

Serial photomicrographs for each coronal section (20x magnification, height = 436.48 µm; length = 327.04 µm; 3.18 pixels/µm) were obtained to encompass the whole region of interest (i.e. Och or CC) by Zeiss Axio Observer Inverted Microscope (Carl Zeiss Inc.) fitted with Axio MRC digital camera. The photomicrographs were saved as jpeg files and exported into Adobe Photoshop CS2. Panoramic images of the region of interest (Figures 6 A, B) for each coronal section were composed by photomerging the serial photomicrographs in Photoshop CS2. The panoramic images of the region of interest for each coronal section were saved as jpeg files. The saved jpeg panoramic images were imported into ImageJ software (from NIH http://rsb.info.nih.gov/ij/) to quantify TAI. After importing the image in imageJ software the scale was set manually to 3.18 pixels/µm, this allows the measurements given by ImageJ to represent actual tissue dimension.

## TAI Quantification

The panoramics images of the Och and CC were viewed in imageJ on a monitor. The structurese of the Och and CC (Figure 6 C, D) were delineated. For the Och, the Och boundaries and the tissues surrounding the Och boundaries were digitally removed (Figure 6 E). For the CC the delineated area was centered on the midline (Figure 6 D). The tissues outside the delineated area on the CC were removed (Figure 6 F) and the TAI of CC computation were computed within the delineated area of the CC. These delineated areass were further amplified on the monitor via ImageJ software and the TAI was quantified by the cliking the mouse on the β-APP or RMO14 positive axonal. The cell counter feature of ImageJ counted the marked immunoreactive positive axons.
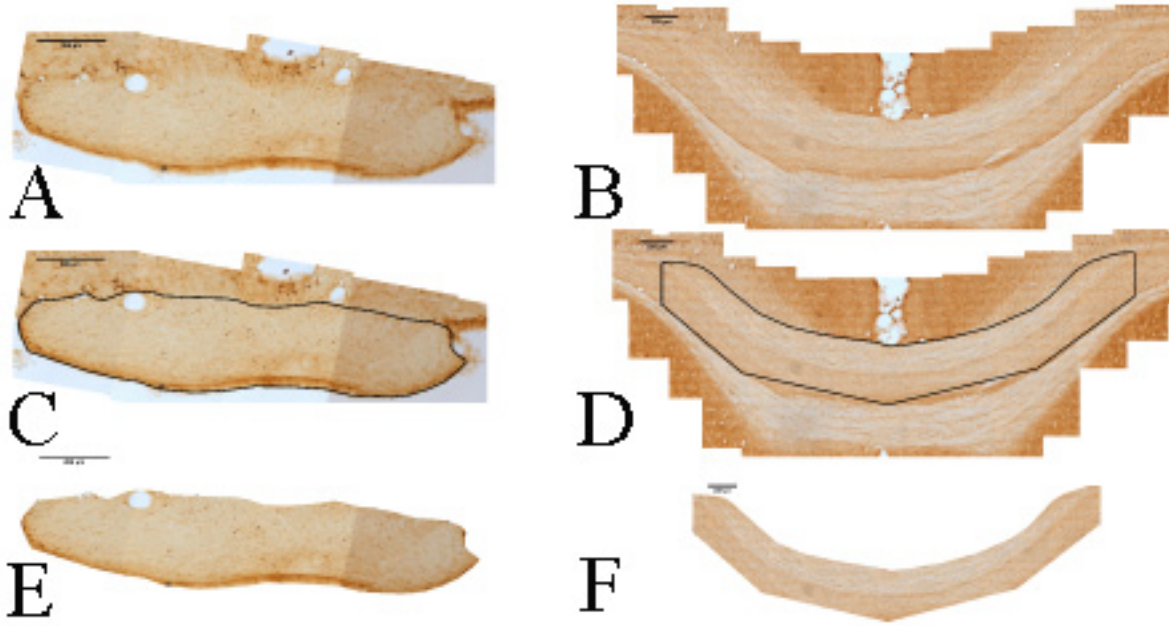
**Figure 6:** Panoramics images of the (A) Och and (B) CC.  The black outline in (C) Och and (E) CC shows outlines the boundary of the anatomical structure analysed. (E, F) represent the area within the outline of the anatomical stucuture that was analysed. (20 x magnification) Scale bar 200µm.

In order to calculate the density of axonal injury the surface area of each delineated shape was computed by ImageJ software.  ImageJ software provided the delineated surface area measurements in $mm^2$.  The injured axonal density was then computed by dividing the sum of the total number of TAI injuries in each panoramic delineated region of interest image by the sum of the corresponding delineated areas.

**Statistical Methods:**

All data were analysed using SPSS version 17 for Windows.  The numbers of injured axons were expressed as the mean value $\pm$ standard error (SEM).  The data distribution was tested by Shapiro-Wilk normality test ($p<0.05$) and by Levene's test of homogeneity of variance ($p<0.05$).  The mean values of the data set were either not normally distributed or the variances of the data set were heterogeneous.  Since Kruskal-Wallis test does not assume normality in the data set and is insensitive to outliers in the data, Kruskal-Wallis test was utilized to compare the

four time points.  If the Kruskal-Wallis test demonstrated significance (p≤0.5), then the Man-Whitney exact test was utilized for pairwise comparisons between two time points.  Statistical significance was considered to be P≤0.05.

## Results

### Qualitative Analysis

Axonal morphological changes representing IAT and NFC were present in the Och and CC (Figure 7).  The injury profiles of the IAT represented by β-APP were of swollen axons forming retraction balls (Figure 7 A, C).  The NFC profiles represented by RM014 were swollen elongated profiles (Figure 7 B, D).
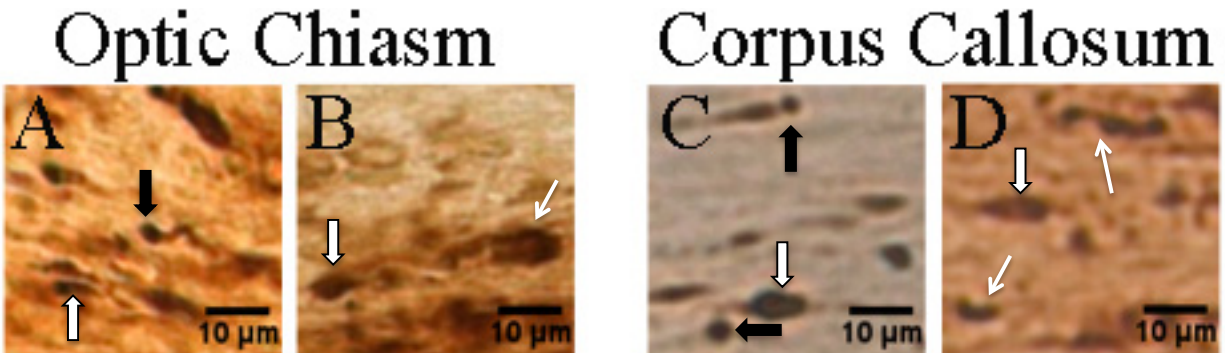


**Figure 7:** Traumatic injured axons at 28 hrs post-TBI within the Och and CC demonstrating the morphology of IAT by β-APP immunoreactivity (A, C) and morphology of NFC by RMO14 immunoreactivity (B, C).  White arrows represent swollen (thick arrow) and dense band profile (thin arrows).  Black arrows represent formation of retraction balls. Scale bar 10µm

TAI temporal morphological changes at eight hours, twenty-eight hours, seventy-six hours and hundred seventy-two hours post-injury within the Och (Figure 8) and CC (Figure 9) were present at different densities.  At eight hours post-injury IAT was present in the Och and CC; however, IAT was more prevalent in the Och (Figure 8 A, 9 A).  NFC was absent at eight hours in the Och and minimally present in the CC (Figure 8 B, 9 B).  At twenty-eight hours, NFC becomes most prominent in both CC and Och (Figure 8 C, 9 C).  At seventy-six hours and

hundred seventy-two hours post-injury the IAT and NFC were still present in the Och and CC; however, at a minor degree (Figure 7 D, 8 D).

At eight hours post-TBI positive β-APP axons within the Och and CC were punctuated and spherical in shape (Figure 8 A, 9 A). Within the Och and CC, positive β-APP axonal spherical shapes were more prominent at eight hours and twenty-eight hours post-TBI respectively and became less prominent as time elapsed (Figure 8 A-D, 9 A-D).
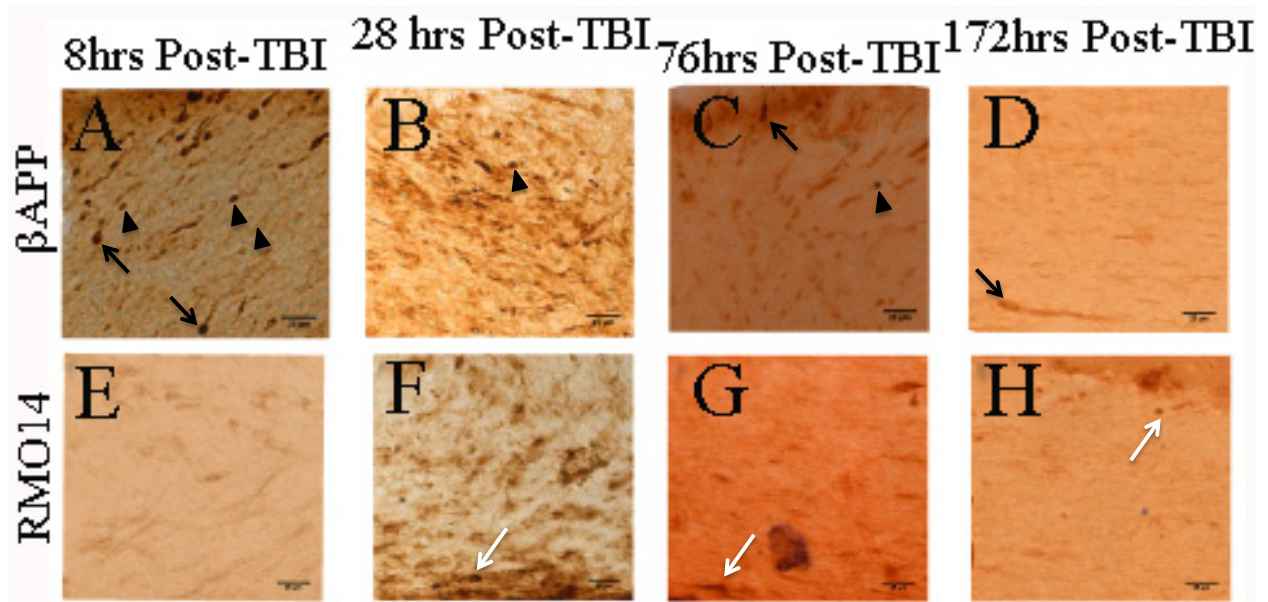


**Figure 8:** Traumatic injured axons within the Och demonstrated by β-APP immunoreactivity at (A) 8 hrs, (B) 28 hrs, (C) 76 hrs, and (D) 172 hrs Post-TBI. Neurofilament compactions in the axons within the CC demonstrated by RMO14 immunoreactivity at (E) 8 hrs, (F) 28 hrs, (G) 76 hrs, (H) 7days Posttraumatic brain injury. Black arrowheads represent the punctuated axonal profile, black arrows represent the axonal spherical shapes, and white arrows represent elongated axonal structures. Scale bar 25µm

At eight hours post-TBI positive RMO14 axons were present only within CC at a low level as dense band profile (Figure 9 E). Twenty-eight hours post-TBI the RMO14 positive axons became more prominent within the Och and CC and their morphological profiles were dense band profile (Figure 8 F, 9 F). As time progressed to seventy-six hours and hundred seventy-two hours post-TBI, the RMO14 positive axons became less prominent in the Och and CC (Figure 8 G-H, 9 G-H).
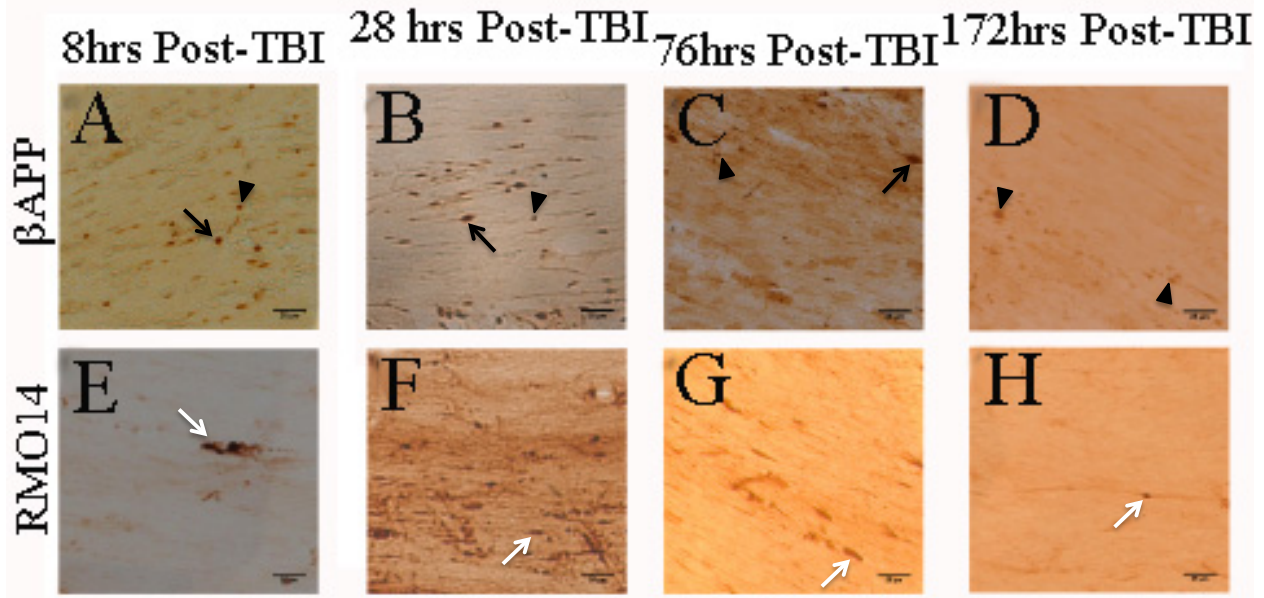
**Figure 9:** Traumatic injured axons within the CCdemonstrated by β-APP immunoreactivity at (A) 8 hrs, (B) 28hrs, (C) 76 hrs, (D) 172 hrs Posttraumatic brain injury.  Neurofilament compactions in the axons within the CC demonstrated by RMO14 immunoreactivity at (E) 8 hrs, (F) 28 hrs, (G) 76 hrs, (H) 172 hrs Posttraumatic brain injury.  Black arrowheads represent the punctuated axonal profile, black arrows represent the axonal spherical shapes, and white arrows represent elongated axonal structures. Scale bar 25μm.

Dual labelling strategy did not allow discrimination between β-APP, NFC and collocolized APP and RMO14 immunoreactive axons.  Therefore data from dual labelling represented all three types immunoreactive axons a combined population of injured axons. Dual labelling for IAT and NFC via β-APP and RMO14 within corpus callosum demonstrated that the injury profile between eight hours post-TBI and twenty-eight hours post-TBI to be similar in density.  However, at twenty-eight hours post-TBI the NFC became more prominent in comparison to eight hours post-TBI.  The single-labelled RMO14 immunoreactivity also demonstrated this injury profile.  Similar to the injury profile of the single-labelled immunoreactivity (Figure 8 and 9), as time progressed to seventy-six hours and hundred seventy-two hours post-TBI, the β-APP and RMO14 positive axons became less prominent in the CC (Figure 10 C, D).
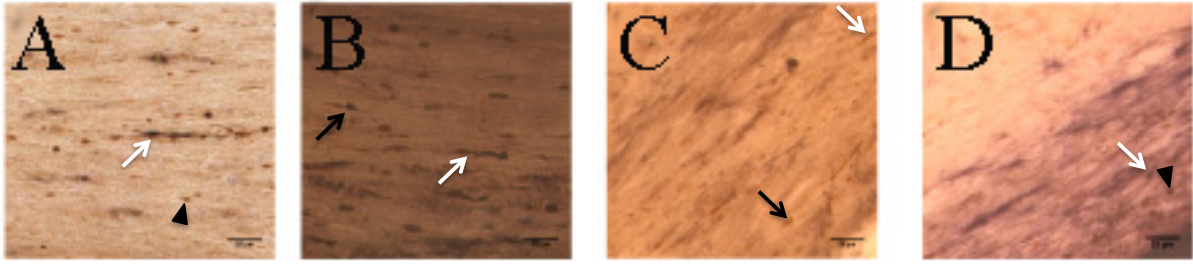
**Figure 10:**Traumatic injured axons (IAT and NFC) within the CCdemonstrated by dual β-APP and RMO14 immunoreactivity at (A) 8 hrs, (B) 28 hrs, (C) 76 hrs, (D) 172 hrs post traumatic brain injury. Black arrowheads represent the punctuated axonal profile, black arrows represent the axonal spherical shapes, and white arrows represent elongated axonal structures. Scale bar 25μm.

**Quantitative Analysis**

Quantitative analysis of β-APP and RMO14 over time demonstrated significant changes in the Och. In the Och, the β-APP positive axons were most prominent at eight hours post-TBI and significantly decreased as time elapsed (Figure 11 A). The mean number of β-APP damaged axons in the Och decreased from $109.27 \pm 14.98$ at eight hours post-TBI to $29.43 \pm 13.36$, $7.56 \pm 1.68$, and $3.3 \pm 0.84$ at twenty-eight hours, seventy-six hours and hundred seventy-two hours post-TBI respectively (Figure 11 A; $p<0.05$). However, the mean numbers of RMO14 damaged axons in the Och were most prominent at twenty-eight hours post-TBI and decreased thereafter. The mean number of RMO14 damaged axons in the Och increased from $7.44 \pm 2.70$ at eight hours post-TBI to $51.09 \pm 23.71$ at twenty-eight hours post-TBI however this increase was not statistically significant (Figure 11 B; $P = 0.052$). Following the twenty-eight hours increase significant decrease of $3.06 \pm 0.95$ and $6.11 \pm 1.11$ at seventy-six hours and hundred seventy-two hours post-TBI occured respectively (Figure 11 B; $P<0.05$).

During the observation timeline the CC, quantitative analyses demonstrated similar injury profile between β-APP and RMO14 damaged axons; however, these changes were not statistically significant. The mean number of β-APP and RMO14 damaged axons in the CC increased from $26.76 \pm 16.66$ and $14.46 \pm 6.57$ at eight hours post-TBI to $72.42 \pm 56.11$ to $61.54 \pm 43.23$ at twenty-eight hours post-TBI, respectively (Figure 11 C, D). After twenty-

eighthrs post-TBI the mean number of β-APP and RMO14 damaged axons decreased at seventy-six hours post-TBI to 28.26 $\pm$ 16.67 and 12.44 $\pm$ 10.04 and hundred seventy-two hours post-TBI to 12.00 $\pm$ 11.01 and 26.19 $\pm$ 21.45 respectively.
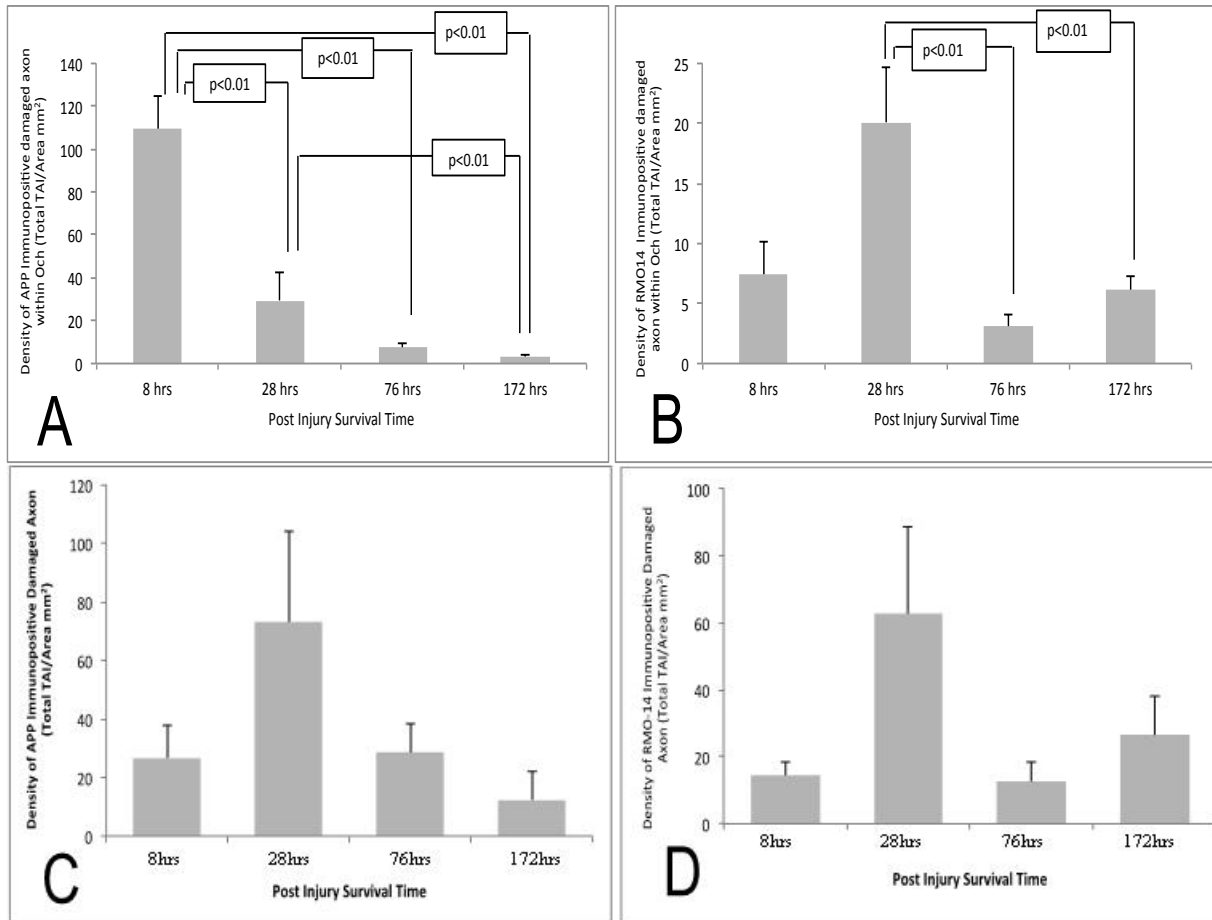


**Figure 11**: Representation of the quantified mean number of positive (A,C) β-APP and (B, D) RMO14 in the (A, B) Och and (C,D) CC at 8 hrs, 28 hrs, 76 hrs and 172 hrs post-Injury. Representation of the quantified mean number of positive (A,C) β-APP and (B, D) RMO14 in the (A, B) Och and (C,D) CC at 8 hrs, 28 hrs, 76 hrs and 172 hrs post-Injury.  (A) Within the Och β-APP damaged axons most prominent at 8 hrs post-TBI and significantly decreased as time elapsed.  (B)  RMO14 immunoreactive damaged axons within the Och were most prominent at 28 hrs post-TBI and significantly decreased as time elapsed.  (C, D)Within the CC, β-APP and RMO14 immunoreactive damaged axon were most prominent at 28 hrs.  (C, D) However, the β-APP and RMO14 immunoreactive damaged axons within the CC between each time point were not significant.  Values represent mean $\pm$ SE.  Error Bars represent standard error of the mean.

In the Och and CC, the linear relationship between the density of β-APP and RMO14 damaged axons were determined (Figure 12).  In the Och no linear relationship was present between β-APP and RMO14 damaged axons (Figure 12 A); however, in the CC a strong linear

relationship existed between β-APP and RMO14 damaged axons (Figure 12 B; $R^2$=0.861, p<0.01). This linear relationship was consistent when the data were subdivided into each survival group. For all survival time points the Och demonstrated no linear relationship between the β-APP and RMO14 damaged axons. In the CC the linear relationship between β-APP and RMO14 damage axons was strong at all survival time points. At eight hours and seventy-six hours post-TBI the Pearson correlation was 0.872 with P< 0.05 (2 tailed test) between β-APP and RMO14 damaged axons. At twenty-eight hours and hundred seventy-two hours post-TBI the Pearson correlation was 0.994 and 0.998 respectively with P<0.01 (2 tailed test) between β-APP and RMO14 damaged axons.
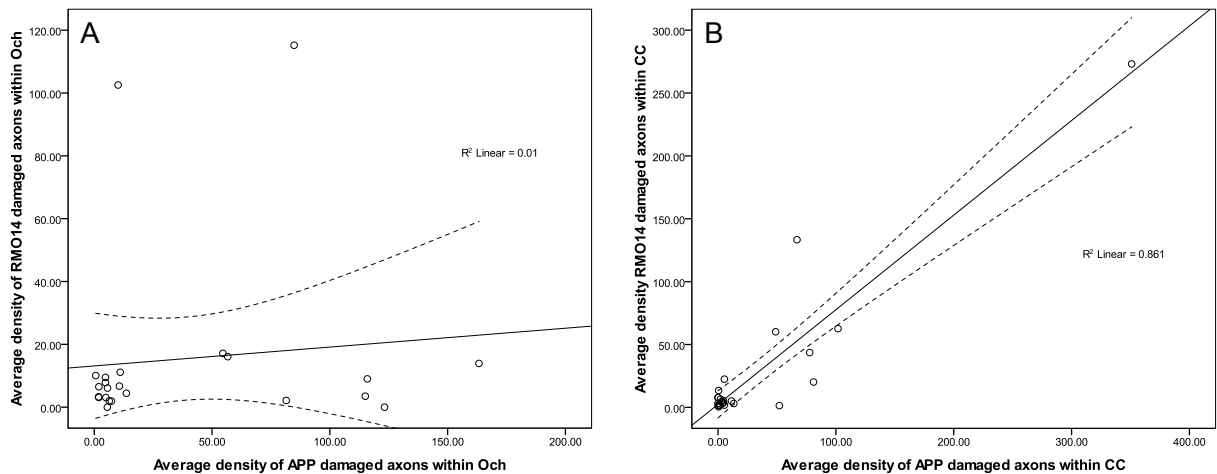


**Figure 12:** Correlation of the average density of RMO14 damaged axons with the average density of β-APP damaged axons in the (A) Och and (B) CC for all survival time points. Each circle represents one rat. (B) A strong correlation is present between RMO14 and β-APP in the CC with $R^2$ = 0.861 (p<0.001). Dashed lines represent the 95% mean confidence intervals.

## Discussion

The results of this study confirmed that TAI could be induced in the cortical white matter tract such as the CC and Och by the impact acceleration model. Axonal pathology in the CC and Och reacted for visualization of IAT using β-APP, or NFC using RMO14 to demonstrate classical morphological changes. The injury profile for IAT was swollen axons, forming retraction balls whereas NFC injury profile was dense bands. In previous literature,

morphological profiles for β-APP immunoreactive axons were described to be swollen and bulbous in shape, whereas, the morphological profile for RMO14 were described to be dense band or compact linear shapes (Povlishock, Marmarou et al. 1997; Stone, Walker et al. 1999; Stone, Singleton et al. 2000; Stone, Singleton et al. 2001; Suehiro, Singleton et al. 2001; Stone, Okonkwo et al. 2004; Marmarou, Walker et al. 2005; Marmarou and Povlishock 2006). Previous studies have demonstrated the impact acceleration model does induce TAI in CC and Och; however, these studies were limited to silver staining, 68KD neurofilament subunit, or β-APP immunochytochemsitry (Foda and Marmarou 1994; Ding, Yao et al. 2001; Kallakuri, Cavanaugh et al. 2003; Li, Zhang et al. 2011). This study was the first study utilizing β-APP and RMO14 to visualize and quantify TAI in the CC and Och up to hundred seventy-two hours after induction of TBI via impact acceleration model.

**Corpus Callosum Comparison to Optic Chiasm**

In this current investigation, the temporal TAI profile was inconsistent between the CC and Och. The variability of the TAI profile between CC and Och could be attributed to the different axonal population found within these structures. The CC is composed of unmyelinated and myelinated fiber combinations ranging from 0.1 - 0.7 µm and 0.3 – 1.0 µm diameters respectively (Waxman and Black 1988) while the optic fibers are unmyelinated at birth and become almost completely myelinated by adulthood with approximate average diameters of 1.3 or 1.7 µm (Duvdevani, Lavie et al. 1993). Smaller-caliber axons possessed proportionally greater numbers of microtubules per unit area (Malbouisson, Ghabriel et al. 1985), whereas larger-caliber axons possessed proportionally greater numbers of neurofilaments per unit area (Price, Paggi et al. 1988).

Previous studies on the Och demonstrated that the optic axons cross-section possessed some non-circular shapes (Duvdevani, Lavie et al. 1993; Sugioka, Sawai et al. 1995). Since Och axons tended to possess some non-circular cross sectional axons, the force distribution on

these axons will differ in comparison to the circular cross section area. It has been illustrated that IAT occurred independent of the axolemmal disruption, and initially IAT might be due to the force application on the axon rather than the chemical cascade that occurred as a result of axolemmal disruption (Stone, Okonkwo et al. 2004).

In this investigation, the Och exhibited the greatest density of positive β-APP axons at eight hours post-TBI and as time passed the density of positive β-APP axons decreased. However, in the CC the greatest density of positive β-APP axons occurred at twenty-eight hours post-TBI and similar to Och it decreased over time. Since the temporal profile for Och TAI injury does not exist in any current literature, the earlier peak of β-APP density in the Och might be due to the optical axons non-circular cross sectional profile compared to CC and to the anatomical location of the Och. The Och fibers are ventral to the floor of the skull unlike the CC fibers that are surrounded by cortical tissues; therefore, the Och might experience a greater amount of force in comparison to the CC. Through the finite element model of the rat brain, Kallakuri et al. have demonstrated that Och does experience a great force during impact acceleration injury (Kallakuri, Zhang et al. 2006).

**Temporal Profile of Impared Axonal Transpost**

In 2005 study of Marmarou et al similar observation was reported in the brainstem. Marmarou et al. also reported that the corticospinal tract and medial lemniscus positive β-APP density was greater in the corticospinal tract (contains primary small caliber axons) than the medial lemniscus (contains larger caliber axons). However, the corticospinal tract and medial lemniscus highest β-APP detection occurred at twenty-eight hours. It is worth noting that large calbier axons of the thoraco-lumber in the spinal cord were found to display its greatest density of positive β-APP at six hours post-injury which is earlier then described by brainstem tracts (Marmarou, Walker et al. 2005; Czeiter, Pal et al. 2008); so, peak positive β-APP may be anatomical structure dependent.

Additionaly, the temporal profile of β-APP in this study is in agreement with an electrophysiological study by Reeves, Philips et al. 2005. Reeves et al. measured compound action potential (CAP) of injured CC from three hours until 7days post-TBI (Reeves, Phillips et al. 2005). CAP wave is composed of two components N1 and N2. N1 and N2 arise from axonal populations of fast-conduction myelinated fibers and slow unmyelinated fibers respectively. Therefore, the amplitude of N1 and N2 waves is inversely related to the axonal dysfunction i.e. decreased N1 and N2 amplitude implies increased axonal dysfunction. In the Reeves et al. study it was reported that the greatest decrease of N1 and N2 waves occured at twenty-eight hours post-TBI and thereafter N1 wave amplitude increased at 3days post-TBI and further increased to a significant recovery by 7days post-TBI; however, N2 amplitude did not recover. The change in the CAP amplitude in the Reeves study mimics the temporal β-APP profile of decreased β-APP positive axons at seventy-six hours and further decreasing at hundred seventy-two hours.

During this investigation, the Och exhibited the greatest density of β-APP positive axons at eight hours post-TBI and as time elapsed the density of positive β-APP positive axons decreased. However, in the CC the greatest density of β-APP positive axons occurred at twenty-eight hours post-TBI and similarly to Och it decreased over time.

Temporal TAI changes in the CC were found to be insignificant; this might be caused by the wide variation of the CC injury density. This wide variation of the CC injury density behaviour has been observed previously in our lab (Li, Zhang et al. 2011). Therefore, inducing TAI in the CC is possible by the impact acceleration model but with a wide variation of injury tolerance. On the contrary, the Och injury density was consistent across animals and demonstrated a much lower injury density variation when compared to the CC.

**Temporal Profile of Neurofilament Compaction**

In the Och contrary to positive β-APP axons an increase of positive RMO14 axons occurred from eight hours post-TBI to twenty-eight hours post-TBI. At twenty-eight hours the Och exhibited the greatest density of positive RM014 followed by a decrease of positive RM014 axons as time elapsed. It has been reported in previous studies a strong association between foci showing altered axolemmal permeability and NFC (Pettus, Christman et al. 1994; Povlishock, Marmarou et al. 1997). When the axolemmal permeability is altered as a result of TBI, $Ca^{2+}$ influx will increase and thus cause intracellular $Ca^{2+}$ concentration to elevate (Povlishock 1992; Maxwell and Graham 1997; Giza and Hovda 2001; Smith, Meaney et al. 2003; Marmarou, Walker et al. 2005). The increase intracellular $Ca^{2+}$ activates calcineurin (calcium-activated phosphatase) (Hoffman 1995; Marmarou, Walker et al. 2005), which dephosphorylates the neurofilament sidearms making the epitopes available for RM014 binding. In a TAI ventral brainstem it was reported that as time elapsed from five minutes to sixty minutes RM014 immunoreactivity increased and NFC injuries became most prominent at twenty-eight hours post-TBI (Povlishock, Marmarou et al. 1997). This fact was also observed in this study. As time elapsed to seventy-six hours post-TBI, positive RM014 axons decreased in the CC and Och. Unlike the continuous decrease of positive β-APP at hundred seventy-two hours post-TBI, a slight increase of positive RM014 axons occurred in the CC and Och. Since NFC occurs as a result of a repertoire of chemical reactions, the slight increase of NFC at hundred seventy-two hours post-TBI may be due to a secondary chemical cascade.

**Relationship Between Impared Axonal Transport and Neurofilament Compaction**

The immunoreactive β-APP and RMO14 axons displayed a different temporal profile in the injured Och. Interestingly, even though a temporal change of IAT and NFC in the CC was not statistically significant, it was observed the temporal behaviour was very similar in IAT and NFC. To further investigate the relationship between IAT and NFC in these two anatomical

structures a linear correlation was computed.  The Och showed no linear relationship between the density of β-APP and RM014.  Therefore, one can assume that β-APP and RMO14 occur in different axonal population in the Och.  However, CC showed a strong linear correlation between β-APP and RMO14 consistent with the DiLeonardi et al. 2009 study.  DiLeonardi et al. reported that within the CC single labeled β-APP and RM014 occurred in the same anatomical location and at three days post-TBI the β-APP and RM014 positive axons were intermingeled but occurred in independent immunoreactive axons.  In addition, DiLeornardi et al. also reported other structures such as cingulum did not have co-locolized immunoreactive β-APP and RMO14 axons.

Through the observations of this study and other studies the complexity of TAI injury profile can be appreciated.  The injury profile between IAT and NFC are temporal and anatomically variable.  Thus, to map out TAI in the brain multiple immunohistochemical markers are needed and each anatomical structure needs to be studied separatelety.

# CHAPTER 4: MAGNETIC RESONANCE IMAGING

Magnetic Resonance Imaging (MRI) is a noninvasive imaging technique extensively used in the clinical and research realm of injury, disease and disorder detection. Over a quarter of a million articles are currently present in PubMed dealing with MRI. MRI utilizes powerful magnetic fields to align the magnetization of some atoms in the body. The static magnetic field of the MRI scanner is measured in units of Tesla. One Tesla unit is equivalent to 10 000 gauss, whereas the natural magnetic field on the earth's surface is approximately 0.5 gauss. Because of the abundance of hydrogen atoms in the biological tissues MRI targets hydrogen atoms during image acquisition(Hornak 1996-2011). The hydrogen atom, also referred to as proton, possesses a magnetic dipole with a corresponding south and north pole. The dipoles, also denoted as spins, are randomly distributed under normal conditions (Figure 13A). In the presence of an externally applied magnetic field such as the static externally applied magnetic field $B_0$ generated by a MRI scanner, the spins align either along or against $B_0$ (Figure 13B). However, a large excess of spins aligns along rather than against $B_0$ and thereby creates a net
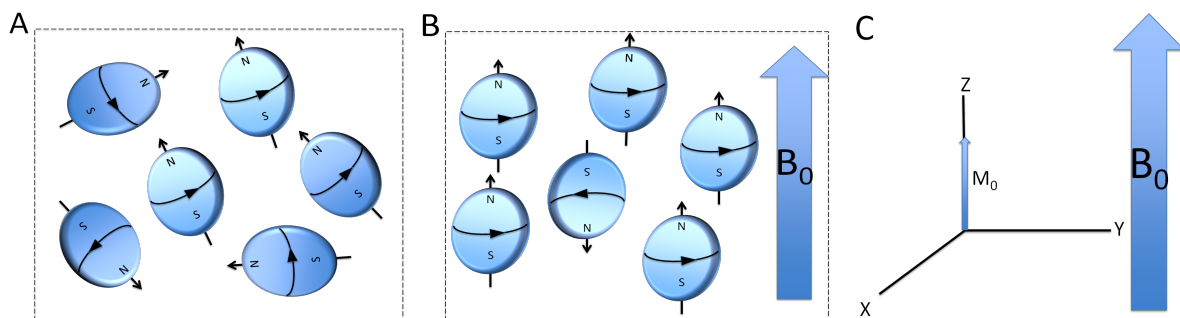


**Figure 13:** Schematic presentation of protons. (A) Represent random distributed proton sample under normal conditions. The black arrow represents the momentum the individual proton (blue sphere) possesses. N and S represent the corresponding south and north poles of the magnetic dipole of the proton. (B) The proton samples in the presence of an external magnetic field $B_0$ (wide blue arrow). The applied magnetic field forces the proton to align parallel or antiparallel to it. The protons aligned parallel to the magnetic field are in excess therefore leading to (C) a net magnetization $M_0$ (Narrow blue arrow) in the direction of the applied magnetic field.

magnetization $M_0$ in the direction of the external magnetic field (Figure 13B). As the $B_0$ values of the MRI scanner increases, the greater the excess of protons will be present thereby generating a greater MR signal. Consequently a high field MRI scanner will tend to have a higher signal to noise ratio (SNR).

As the spins are aligned to $B_0$, they precess about $B_0$ with a frequency γ represented by Larmor equation (equation 4-1). In the Larmor equation γ and B represent the gyromagnetic ratio of the atom and the magnetic field strength respectively. The gyromagnetic ratio is a constant unique to every atom. For the hydrogen atom the γ value is 42.6 MHz/Tesla (Haacke, Brown et al. 1999).

$$v = γB \hspace{3cm} \text{(equation 4-1)}$$

For only a brief duration a second magnetic field oscillating at radio frequency, hence called rf pulse, is generated by the MRI scanner. When the applied rf pulse frequency equals the Larmor frequency of the spins, the spins absorb energy and rotate away from their preferred orientation along $B_0$. By varying the rf pulse strength and duration the protons can be rotated to a specific angle i.e. by applying the rf pulse with a tip angle of $90^o$ the spin will precess perpendicular to the direction of $B_0$ (Figure 14).
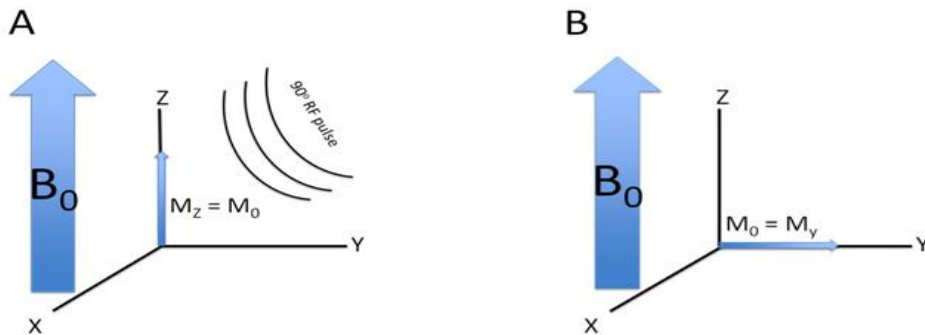


**Figure 14:** (A) An application of a 90orf pulse on the net magnetization M0. The applied 90orf pulse rotates the net magnetization away from the longitudinal Z axis (B) to the transverse XY axis.

Immediately after application of the rf pulse the $M_0$ aligns along the Y axis (Figure 14B). As time elapses the frequencies of the precessing spins of the protons cause small inhomogeneities in the magnetic field and as a result the spins lose their phase coherence in the XY plane (Figure 16 A-C). In addition to the loss of phase coherence, as time passes the precessing part of the magnetizations will exponentially decay with a time constant of T2 referred to as spin-spin relaxation time (Table 2, Figure 4-3B).

**Table 2:** Representation of various human tissue relaxation parameters, T1 and T2 in millisecond (ms) at $37^o$C and $B_0$ of 1.5T (Haacke, Brown et al. 1999)**.**

| Tissue | T1 (ms) | T2 (ms) |
|---|---|---|
| Gray Matter (GM) | 950 | 100 |
| White Matter (WM) | 600 | 80 |
| Muscle | 900 | 50 |
| Cerebrospinal Fluid | 4500 | 2200 |
| Fat | 250 | 60 |
| Blood | 1200 | 100-200 |

Since the $B_0$ is constantly present within the system, the spins realign exponentially in the direction of $B_0$ with a time constant T1 known as longitudinal relaxation time. The T2 and T1 time constants are tissue variable (Table 2) (Haacke, Brown et al. 1999). T2 and T1 will cause decay and recovery respectively to occur at various rates depending upon the tissue, resulting in different signal intensity (Figure 4-3). The signal intensity differences between tissues are utilized in imaging to achieve contrast between the different tissues.

Since the coherently precessing spins induce a rotational magnetic field, a receiving coil placed near the specimen to be imaged detects the change in the magnetic environment. According to Faraday's Law any change in the magnetic environment of a coil will cause a voltage to be induced in the coil and thus create current. This induced current is the signal used to generate MR images. The brightness intensity of each pixel in an image is a depiction on the

strength of the induced current. The current strength is dependent on the coherence of the phase of the precess spins.
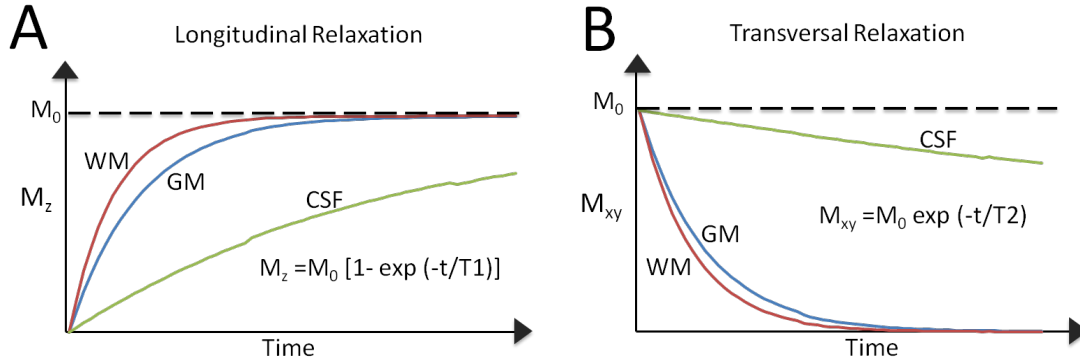


**Figure 15:** Magnetization relaxation of WM (red), GM (blue) and CSF (green) of human tissue with relaxation parameters (A) T1 and (B) T2 reported by Table 2. (A) Relaxation of the longitudinal magnetization which represents the rate of recovery $M_z$ along the longitudinal Z axis with T1 relaxation time constant. The equation on the graph represents the relationship between T1 relaxation time constant and the recovery of $M_Z$ overtime. (B) Exponential decay of the transverse magnetization MXY with T2 relaxation time constant. The equation on the graph represents the relationship between T2 relaxation time constant and the exponential decay of $M_{XY}$ over time.

In addition to the rf, the MRI scanner generates magnetic field gradients. These applied gradients create linear alterations in the main magnetic field along three orthogonal directions; therefore, the magnetic field within the scan can be represented by equation 4-2. The applied gradient along the three orthogonal directions are $G_x(t)$, $G_y(t)$, and $G_z(t)$.

$$B = B_0 + G_x(t)x + G_y(t)y + G_z(t)z \qquad \text{(equation 4-2)}$$

The three applied gradients are rapidly turned on and off during an MRI experiment and their functions are slice selection, image encoding, and diffusion weighting.

## T1 Weighted Imaging

The longitudinal relaxation time of a proton is the time required for the proton to gain its longitudinal magnetization when placed in the magnetic field and following an rf pulse. Since the hydrogen protons in the body are bound to molecules, their longitudinal relaxation time is

variable and dependent on the molecules to which they are bound. All molecules are constantly vibrating, rotating and translating. The molecules' natural motions are dependent on their molecular size; for example smaller molecules tend to move more rapidly in comparison to larger molecules thus resulting in higher natural frequencies. The T1 relaxation time is a product between the molecular motions' frequency and the Larmor frequency. After the application of the rf pulse the spins are moved away from the longitudinal axis to an angle equal to the applied rf pulse utilized. As time elapses the spins regain their longitudinal magnetization. The longitudinal magnetization recovery rate is dependent on the relationship between the molecular motion frequency and the Larmor frequency. For example, a rapid T1 recovery occurs when the two frequencies are similar, and a slow T1 recovery occurs when the two frequencies are different. As a result, the receiving coil will detect a stronger signal from the molecules possessing short T1 recovery; therefore, on a T1 weighted images these areas will appear bright.

## T2 Weighted Imaging

Spin-Echo sequence is a commonly used pulse sequence (Hornak 1996-2011) utilized to acquire T2 weighted images. As an rf pulse of $90^o$ angle is applied to spins aligned along $B_0$, the spins rotate into the XY plane (Figure 14). Immediately after the application of the rf pulse $M_0$ align along the Y ($M_0=M_Y$) and as time elapses the spins start to dephase due to magnetic field inhomogeneities and dipolar interactions (Figure 16 A-C). A second rf pulse of $180^o$ angle is applied at some time τ to the dephasing spin. The second $180^o$rf pulse flips the spins in the plane perpendicular to the $B_0$ thereby placing more rapid precessing spins behind the more slowly precessing spins (Figure 16). Over time keeping all parameters unchanged, the more rapid precessing spins accrue more phases in comparison to the slowly precessing spins. As a result all the spins will come back into phase at time TE (2τ) (Figure 16 F). Therefore, this method reverses the dephasing that has occurred as a result of magnetic field inhomogeneities.

This procedure is referred to as spin echo and, accordingly to this rephrasing procedure, the receiving coil detects signals from coherent magnetization of all spins reduced only by the T2 decay after excitation. The signal reduction caused by the T2 decay is represented by a 3D image and referred to as T2 weighted image. Each voxel of the image is associated with a gray level that encodes the relative signal intensity of the MRI
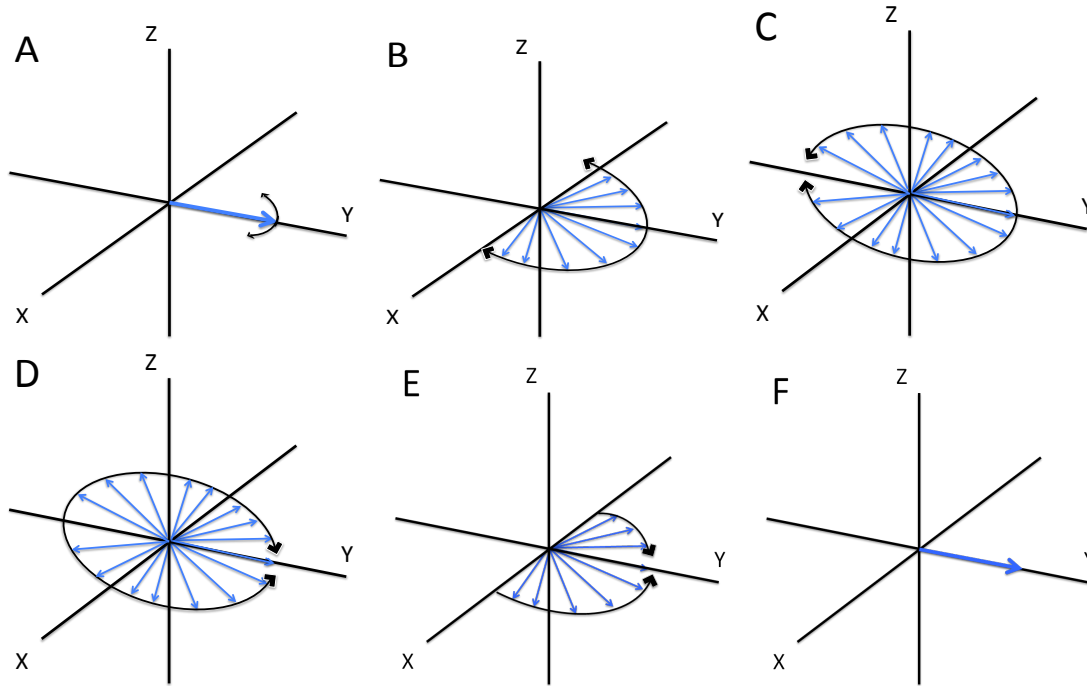


**Figure 16:** Schematic diagrams of the magnetization in spin echo sequence. (A) Immediately after the application of a 90°rf pulse the $M_0$ is rotated onto the xy plane (blue arrow). (B-C) The inhomogeneity of the magnetic field induced by the precessing of the protons causes the protons to dephase progressively over time. (D) 180°rf pulse is applied in the y direction causing a rotation of the protons around the x axis. (D-F) after the application of the 180°rf pulse the proton phase is reversed and the spins are rephased.

as a result of the tissue properties present within the voxel (refer to Table 2). The values of the measured signal are organized in a K-space coordinate system. The application of gradients in different directions and with different intensities at a specific moment of data acquisition enables the filling of the K space (Figure 17). The raw MRI data from the K space are then transformed by Fourier transform to encode a visual image.

## Diffusion

Diffusion Tensor Imaging (DTI) images the diffusion characteristics of the spins within a specimen. Since the geometric structure of the environment influences the diffusion processes, the MRI scanner can be utilized to probe the cellular structural environment noninvasively via DTI.
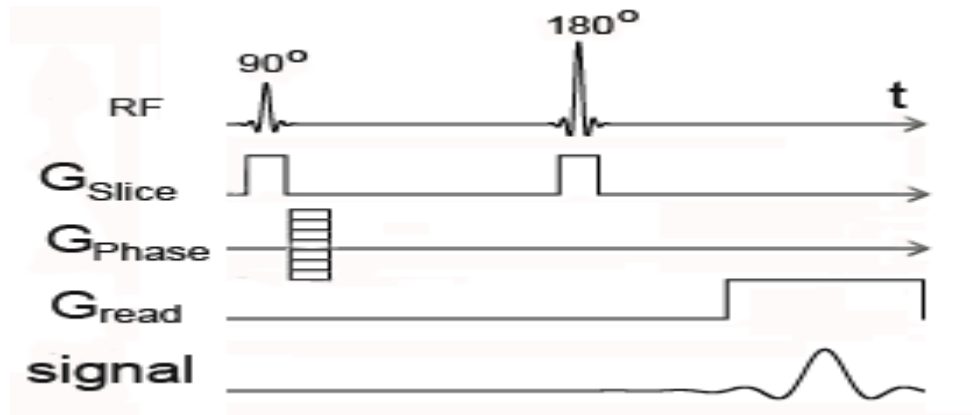


**Figure 17:** Pulse gradient spin echo sequence for T2 image.RF is the radio frequency pulses applied to move the spins. $G_{slice}$is the section selective gradient, $G_{phase}$ is the phase encoding gradient, and $G_{read}$ is the readout gradient and t represents the acquisition time.

### Diffusion Displacement Distribution

Molecules are in constant motion as a result of their thermal energy; in a liquid state these molecules collide with each other and thereby randomly displace to a new location (Beaulieu 2002; Hagmann, Jonasson et al. 2006; Johansen-Berg and Behrens 2009). In the new location, the molecule will again collide with its neighboring molecules and thus displace again and so forth. Molecular diffusion refers to the random motion of the molecules (i.e. water) driven by their thermal energy (Beaulieu 2002; Hagmann, Jonasson et al. 2006; Johansen-Berg and Behrens 2009). In diffusion space where barriers are absent the molecule will diffuse completely randomly without favoring one direction over another. This random diffusion without
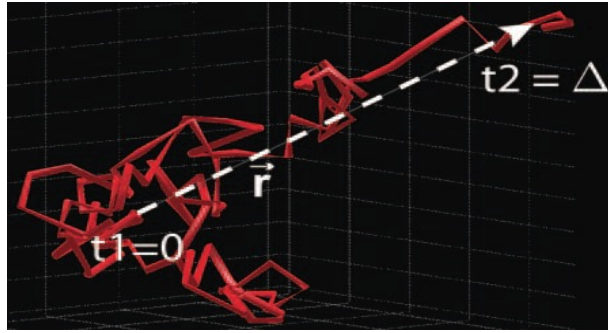
**Figure 18:** This diagram depicts a molecular path (red line) of the molecular diffusion over time interval Δ. The vector r (dotted white line) represents the molecular displacement during the diffusion time interval. (Hagmann, Jonasson et al. 2006).

discrimination between paths is referred to as isotropic diffusion (Beaulieu 2002) . In contrast, when barriers are present in the diffusion space they hinder diffusion and thereby the molecules will diffuse around the obstacles. Favoring one pathway of diffusion over another is referred to as anisotropic diffusion (Beaulieu 2002). The displacement distribution describes the amount of molecules undergoing displacement in a specific direction and distance (Figure 18). The displacement distribution is dependent on diffusion coefficient D and the diffusion time Δ (equation 4-3).

$$\langle r^2 \rangle = 2D\Delta \qquad \text{(equation 4-3)}$$
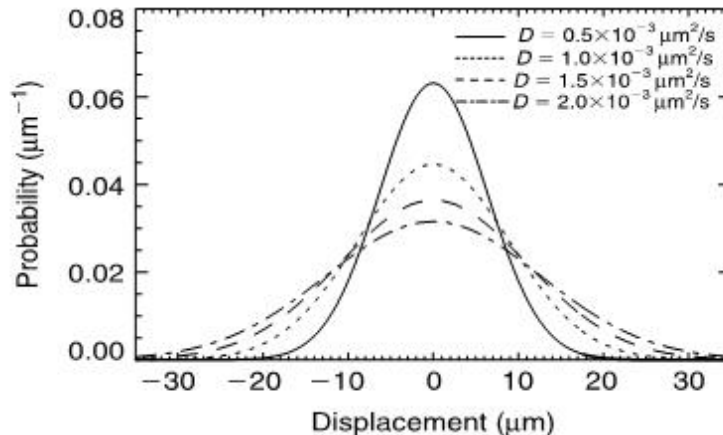


**Figure 19:** The Gaussian displacement distribution of unrestricted water diffusion with various diffusion coefficients at diffusion time of 40ms. The larger the diffusion coefficient D the greater the diffusion displacement that occurs because of increased mobility. (Johansen-Berg and Behrens 2009)

The diffusion coefficient D of a molecule is dependent on various parameters such as: the intrinsic property of the diffusion medium, the size of the diffusion molecules, the temperature of the diffusion environment, and the microstructure of the diffusion environment.

In a homogenous diffusion environment the molecular diffusion displacement can be described as having a Gaussian distribution (Figure 19). However, in a heterogeneous diffusion environment (i.e. biological tissues) the diffusion displacement distribution is more complex. In biological tissue there are a variety of compartments and barriers of different diffusivity; therefore, the water diffusion displacement is hindered by the compartmental boundaries and other molecular obstacles with the result that the diffusion distance is reduced in comparison to unrestricted diffusion (Beaulieu 2002; Hagmann, Jonasson et al. 2006; Johansen-Berg and Behrens 2009). The neuronal tissue can be divided into two different cellular environmental organizations. In GM the cellular architecture is composed of neuronal soma, dendrites, axons and glial cells. Unlike WM, the axons in the GM are randomly oriented. This random orientation of axons and cell bodies hinders the water diffusion. However, no specific preferential direction of diffusion occurs; therefore, diffusion distribution occurs as an approximate bell shaped curve (Figure 4-8 A) (Hagmann, Jonasson et al. 2006). Contrary, in WM tightly packed and coherently aligned axons are surrounded by glial cells that are often organized in bundles thus facilitates diffusion in one direction (Hagmann, Jonasson et al. 2006; Johansen-Berg and Behrens 2009). The WM cellular architecture hinders water diffusion to a greater extent in the direction perpendicular to the axonal orientation rather than parallel to it. Thus, the molecular displacement along the axonal direction will be greater than the displacement perpendicular to it (Beaulieu 2002; Hagmann, Jonasson et al. 2006; Johansen-Berg and Behrens 2009). With anisotropic diffusion the molecular displacement distribution is no longer Gaussian but rather resembles a cigar shape (Figure 20 B) (Hagmann, Jonasson et al. 2006). The axonal bundles align in two manners in the WM in which they align either along

$$\phi(x(t)) = -\omega(x(t))\tau'$$
$$= \phi(x(t)) = -\gamma(B_0 + G\,x(t))\tau'$$
$$= -\gamma(B_0 + G\,x(t))\tau'$$

the same orientation (i.e. CC) or decussate (i.e. Och).  These two-bundle orientations still

induce anisotropic diffusion; however, their molecular displacement differs from each other.  The

bundles that are oriented along the same orientation will have the cigar-like shape distribution,

whereas the decussated bundles will have a cross-like shape of displacement distribution

(Figure 20 C) (Hagmann, Jonasson et al. 2006).
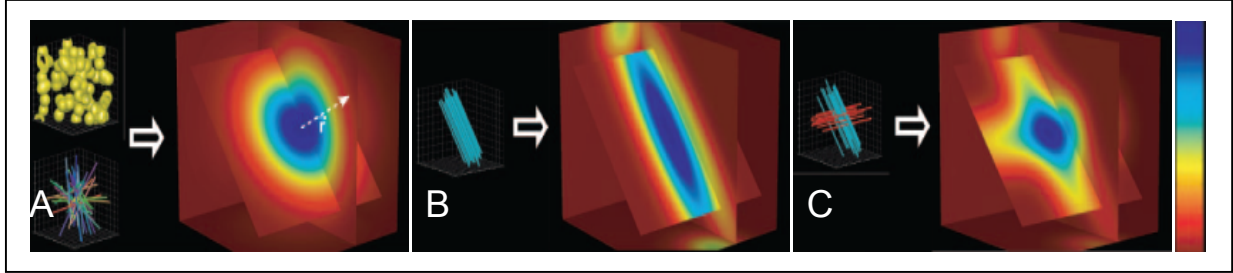


**Figure 20:** These diagrams represent diffusion displacement distribution within a single voxel. They represent a probabilistic density function in a voxel that contains (A) spherical cells (top left) or randomly oriented tubular structure such as axons (bottom left).  (B) Axon aligned in the same direction and (C) axons intersecting at an angle $90^{\circ}$.  Color bar represents the spectrum used in color-coding the distribution probability in the voxel.  Red and blue represents the lowest and highest displacement distribution probability respectively.  (Hagmann, Jonasson et al. 2006)

## Diffusion Tensor Imaging

DTI images the diffusional characteristics of the spins within a specimen.  Since the

geometric structure of the environment influences the diffusion processes, the MRI scanner can

be   utilized   to   probe   the   cellular   structural   environment   noninvasively   via   DTI.
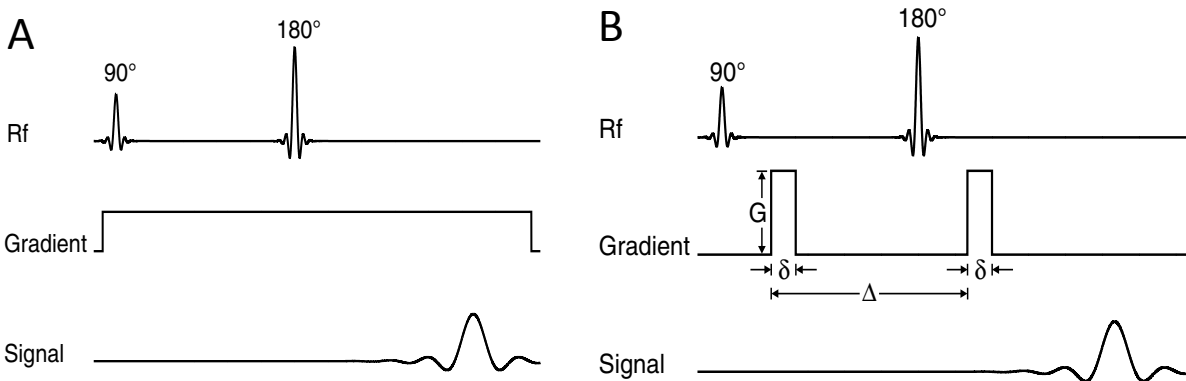


**Figure 21:** Schematic diagrams of the spin echo experiments for detecting random molecular diffusion described by (A) Carr and Purcell and (B) Stejskal and Tanner. (Johansen-Berg and Behrens 2009)

In 1950 Hahn recognized the sensitivity of the spin echo MR signal to molecular diffusion (Hahn 1950). The spin echo signal reduction was reported to decrease because of a dephasing of spins caused by the translational diffusion within inhomogeneous magnetic fields (Hahn 1950). Carr and Purcell in 1954 recognized that the echo in spin echo imaging could be sensitized exclusively to the effect of random molecular dispersing caused by diffusion (Carr and Purcell 1954). Since the spin's precession frequency is determined by the local magnetic field (equation 4-3), applying magnetic field gradient spins at different locations will experience location different magnetic fields; therefore, the spins will precess at different angular frequency. Consequently, as time elapses, the spins would have acquired different phase shifts depending on their location. Hence, to detect the random diffusion of the molecules Carr and Purcell (1954) proposed the application of a constant magnetic field gradient throughout the spin echo acquisition (Figure 21 A). A decade after Stejska and Tanner (1965) modified the constant magnetic field application proposed by Carr and Purcell. Stejska and Tanner modification of the constant magnetic field gradient has made modern diffusion measurements by MRI possible (Johansen-Berg and Behrens 2009). Stejska and Tanner replaced the Carr and Purcell's constant magnetic field with short duration gradient pulses (Figure 21 B). These short duration gradient pulses permit clear distinction between the encoding time $\delta$ and diffusion time $\Delta$. Since the diffusion gradient is applied for short duration of time, theoretically the diffusion occurring during the gradient application can be neglected. Therefore, the net phase change $\phi$ occurring after the first and second gradient application is described in Equations 4-4A and B respectively. In equation 4-4, $x_1$ and $x_2$ represent the position of the particle during application of the first and second gradient pulse of G amplitude and $\delta$ duration respectively.

$$\phi_1 = -\gamma\delta Gx_1 \qquad\qquad \text{(equation 4-4A)}$$

$$\phi_2 = -\gamma\delta Gx_2 \qquad\qquad \text{(equation 4-4B)}$$

The phase change due to $B_0$ is neglected in equation 4-4 since the phase change due to $B_0$ is constant for all the spins in the ensemble.  In between the two applied pulse gradients an rf pulse of 180 degrees is applied.  The 180 degrees rf pulse reverses the phase change prior to its application as was discussed previously and thus the total phase change the particle experiences can be represented by the following equation.

$$\phi_1 - \phi_2 = -\gamma \delta G (x_2 - x_1)$$
(equation 4-5)

Because the particles are incessantly randomly diffusing within the excited volume, the phase increment $\phi_1$ gained during the first period does not generally cancel the phase decrement $\phi_2$ the particle accumulates during the second period.  Consequently, the incoherence of the individual magnetic moments attenuates the overall MR signal.

The MR signal attenuation $E(q)$ is the ratio between the diffusion attenuated signal $S(q)$ and the signal in the absence of any gradients $S_0 = S(0)$, where $q = \gamma \delta G$ (equation 4-6) .

$$E(q) = \frac{S(q)}{S_0}$$
(equation 4-6)

Assuming free diffusion of particles within a volume the diffusion propagation will follow a Gaussian distribution and therefore the MR signal attenuation is represented by

$$E(q) = e^{-bD}$$
(equation 4-7)

where $b = (\gamma \delta G)^2 (\Delta - \delta/3)$, $\Delta$ represents the time separation between the two pulse gradients, and D represents the diffusion coefficient.  In biological MRI literature D is referred to as apparent diffusion coefficient (ADC, equation 4-8).  ADC is not a true intrinsic diffusion but rather a measure of diffusion depending on the interactions of the diffusion molecules with cellular structures over a specific diffusion time (Beaulieu 2002).

$$D = ADC = \frac{\ln(\frac{S}{S_0})}{b}$$
(equation 4-8)

For free diffusion Stejskal utilized a tensor **D** of 3 × 3 matrix to represent the natural orientation of diffusion with respect to the three axes determined by the orthogonal orientation of magnetic field gradients produced by three gradient coils (Stejskal and Tanner 1965). Therefore, a general method referred to as DTI was developed to measure the entire diffusion tensor (equation 4-9) in each voxel of the image within the orthogonal orientation of the magnetic field gradients (Basser, Mattiello et al. 1994).

$$\mathbf{D} = \begin{bmatrix} D_{xx} & D_{xy} & D_{xz} \\ D_{xy} & D_{yy} & D_{zy} \\ D_{xz} & D_{yz} & D_{zz} \end{bmatrix} \qquad \text{(equation 4-9)}$$
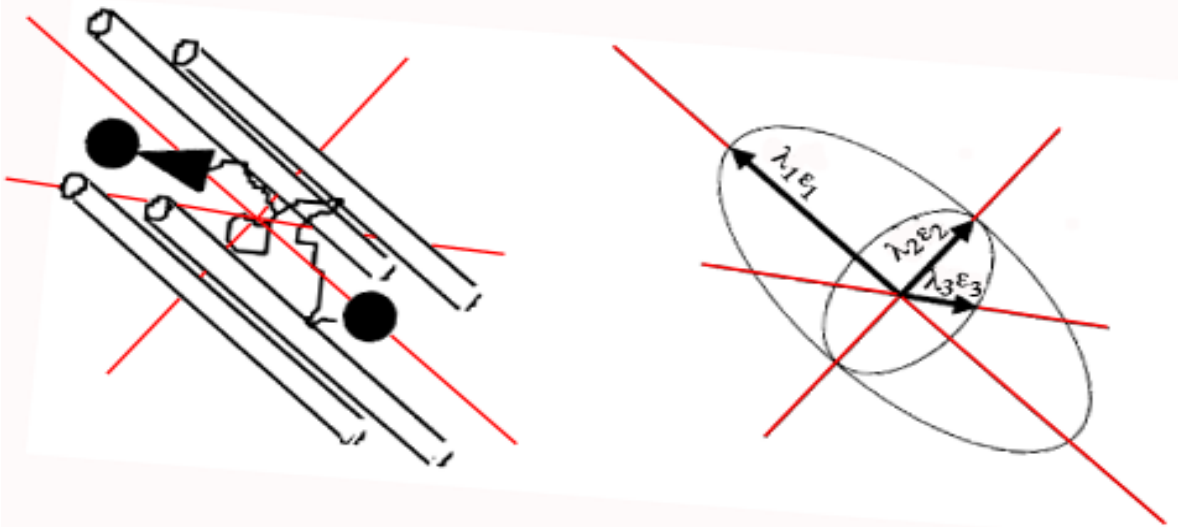


**Figure 22:** Diffusion is highly anisotropic in WM environment. Left side demonstrates the water diffusion within WM. Right hand side illustrates the diffusion ellipsoid utilized to represent diffusion (Melhem, Mori et al. 2002).

The diffusion tensor is represented by an ellipsoid and the diagonalization of the diffusion tensor matrix represents eigenvector and eigenvalues. The eigenvectors $\varepsilon_1, \varepsilon_2, \varepsilon_3$ are the representation of the major medium and minor principle axes of the ellipsoid and the eigenvalues $\lambda 1, \lambda 2, \lambda 3$ represent the molecular diffusivities in these three directions respectively (Figure 22) (Jellison, Field et al. 2004). The eigenvectors are orthogonal to each other and along with the eigenvalues they describe the tensor properties. Each eigenvalue corresponds

to one eigenvector (Figure 22).  The eigenvalue $\lambda_1$ corresponds to the principle eigenvector $\varepsilon_1$ and is the largest eigenvalue.  $\lambda_1$ represents diffusion along the least resistive path.  In WM the least resistive path is parallel to the axon and thus $\lambda_1$ is also referred to as the axial diffusivity (AD).  Orthogonal to $\lambda_1$ the second and third eigenvalues, $\lambda_2$ and $\lambda_3$, are averaged to represent the radial diffusivity (RD) (equation 4-10).

$$RD = \frac{\lambda_2 + \lambda_3}{2} \qquad \text{(equation 4-10)}$$

The three eigenvalues are ordered as $\lambda_1 \geq \lambda_2 \geq \lambda_3$ and their values indicate the diffusion shape.  If the eigenvalues are significantly different from each other, the diffusion is anisotropic.  If $\lambda_1$ is much greater than the $\lambda2$, the diffusion is cigar shaped, whereas, if $\lambda_1$ and $\lambda_2$are similar but much greater then $\lambda_3$, the diffusion is referred to as planar or disc shaped(Hagmann, Jonasson et al. 2006).  Finally, when all the eigenvalues are approximately equal, the diffusion is isotropic and is represented by a spherical shape (Westin, Maier et al. 2002).  Furthermore, the eigenvalues of the tensor matrix allow the extraction of important scalar measurement to study the cellular environment.  One of the scalar measurements derived from the eigenvalues is trace.  Trace is the mean diffusivity computed by averaging the three eigenvalues (equation 23).  These trace values are utilized to compute a trace map that represents these data as an MRI image (Figure 23 A).

$$Trace = \frac{\lambda_1 + \lambda_2 + \lambda_3}{3} \qquad \text{(equation 4-11)}$$

The most widely used scalar value to describe anisotropy is fractional anisotropy (FA), computed by the eigenvalues (Le Bihan, Mangin et al. 2001). The FA value is computed by comparing each eigenvalue to the mean of all eigenvalues <$\lambda$> (equation 4-12). In addition, the eigenvalues can also be utilized to calculate relative anisotropy (RA, equation 4-13).  FA and RA are measurements that describe the degree of anisotropic diffusion.  The FA and RA values

range from zero representing isotropic diffusion to one ($\sqrt{2}$ for RA) representing highly anisotropic diffusion. The FA and RA values are utilized to compute a FA (Figure 23 B) and RA maps that represents these data as an MRI image.

$$FA = \sqrt{\frac{3}{2}}\sqrt{\frac{(\lambda_1-<\lambda>)^2+(\lambda_2-<\lambda>)^2+(\lambda_3-<\lambda>)^2}{\lambda_1^2+\lambda_2^2+\lambda_3^2}}$$ (equation 4-12)

$$RA = \frac{\sqrt{(\lambda_1-<\lambda>)^2+(\lambda_2-<\lambda>)^2+(\lambda_3-<\lambda>)^2}}{\sqrt{\lambda_1+\lambda_2+\lambda_3}}$$ (equation 4-13)
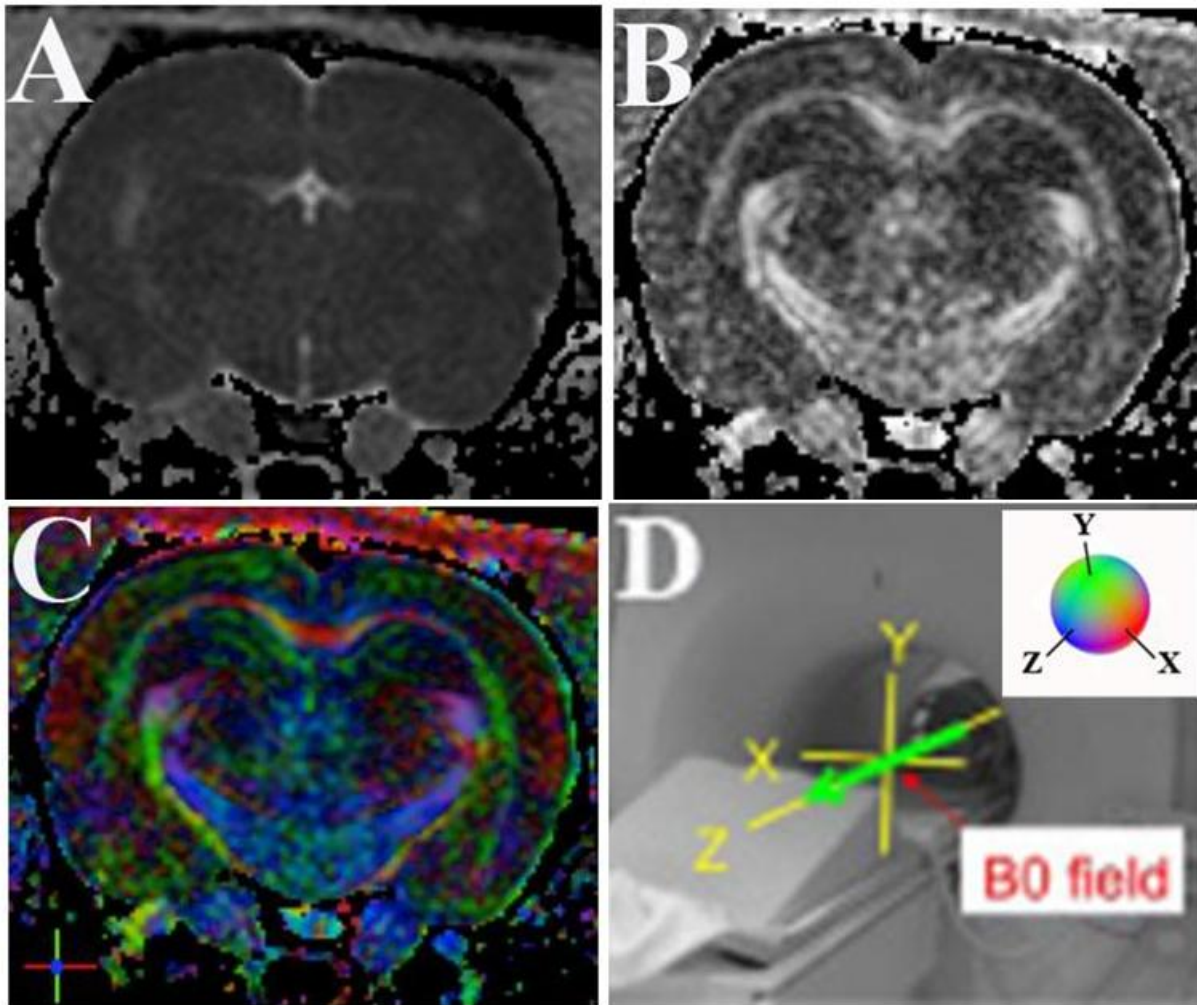


Figure 23: Diagrams (A – C) represent various DTI maps of a healthy rat's brain from this study. The following DTI image maps are(A) Diffusion trace map, (B) FA map, and (C) Principle Eigen value map with color coded direction MR image  (D)  This diagram shows the X, Y and Z magnetic field gradients corresponding to the MR magnet and the top right side insertion represents adopted colors of the fiber direcions at each voxel (Mori and Zhang 2006).  The color red, green, and blue, represent the X, Y , Z direction respectively.

The principle direction of diffusion that is considered to represent the directions of the fiber bundle is utilized to color code the diffusion data. $\lambda_1$ values are utilized to compute a $\lambda_1$ map; however, color-coding the voxels allows a representation of diffusivity along the axons and its directionality to be visualized via MR image (Figure 23 C). In order to generate these DTI parameter maps discussed previously the raw DTI data are processed in DTI Studio V2.02 (crmrm.med.jhmi.edu). Figure 23 represents diffusion trace map, FA map, and principle eigenvalue color map from a healthy Sprague Dawley rat generated by DTI Studio. The diffusion directionality color-coding system utilized in this PhD thesis is as follows: red corresponds to transverse axis(X axis), green corresponds to the inferior-superior axis (Y axis, Figure 23 D), and blue corresponds to the anterior-posterior axis (Z axis, Figure 23 D).

# CHAPTER 5 DIFFUSION TENSOR IMAGING VALUES OF THE GRAY AND WHITE MATTER

## Introduction

Diffusion Tensor Imaging (DTI) is an non-invasive MRI method which probes the cellular architecture of the tissue *in vivo* by measuring the water molecule self-diffusion driven by thermal energy (Basser, Mattiello et al. 1994; Le Bihan, Mangin et al. 2001; Beaulieu 2002; Alexander, Lee et al. 2007). Diffusion of the molecules in space can occur either as isotropic or anisotropic diffusion. Isotropic diffusion occurs when no barriers are present, therefore diffusion will be the equal in all directions (Beaulieu 2002; Alexander, Lee et al. 2007). However, in the presence of barriers in the diffusion space, the molecular diffusion tends to be hindered by the obstacle and thus the path with least restriction is selected. Taking one path of diffusion over another is known as anisotropic diffusion (Beaulieu 2002; Alexander, Lee et al. 2007). Within the tissue, water molecule diffusion is hindered by a variety of factors such as cell membranes, cytoskeleton, and macromolecules (Beaulieu 2002). In the central nervous system, gray matter (GM) and the cerebral spinal fluid (CSF) tend to have a low degree of anisotropic diffusion as water molecules tend to diffuse in an undistinguishable path. In contrast, white matter (WM) tends to attain high degree of anisotropic diffusion (Pierpaoli and Basser 1996; Pierpaoli, Jezzard et al. 1996). In WM, such as the corpus callosum (CC), cellular architecture is composed of parallel-organized colossal commissure neuronal fibers. The colossal commissure fibers are bundles of contralateral axonal projections connection the left and right cerebral hemispheres by contralateral axonal projection. Since the diffusion of water molecules tends to be less hindered along rather than perpendicular to the nerve fibers (Pierpaoli, Jezzard et al. 1996; Beaulieu 2002), the water molecule favours diffusion along the axons, thus exhibiting anisotropic diffusion.

Diffusion in the tissue is detectable in a MRI magnet via signal intensity attenuation. Through the detection of MRI signal intensity attenuation as the result of diffusion properties in the tissue, DTI provides a non–invasive method of mapping the cellular architecture of the tissue. In each voxel, DTI characterizes a 3-D spatial diffusion distribution of water molecules (Basser and Pierpaoli 1996; Conturo, McKinstry et al. 1996). The molecular diffusion is represented by a symmetric 3x3 diffusion tensor matrix, D. D is measured by detecting the initial signal and the signal intensity attenuation of the diffusion-sensitizing gradient factor (b) (Beaulieu 2002; Melhem, Mori et al. 2002; Jiang, van Zijl et al. 2006; Alexander, Lee et al. 2007). The diffusion-sensitizing gradient factor b can be determined by the sensitizing gradient scheme implemented by the MR experiment through the following parameters: the duration of the sensitizing gradient, the strength of the sensitizing pulse gradients along given directions, and the time interval between these pulsed gradients (Le Bihan, Mangin et al. 2001; Beaulieu 2002; Melhem, Mori et al. 2002; Jiang, van Zijl et al. 2006). To best describe the diffusion in the cellular environment the symmetric 3x3 diffusion tensor matrix D eigenvalues ($\lambda_1$, $\lambda_2$, $\lambda_3$) were utilized. The eigenvalues represent the diffusion of the molecules in the following manner: $\lambda_1$, also referred to as axial diffusion (AD), represents the maximal diffusivity in the tissue; therefore; it is the diffusion along the least resistive path. $\lambda_2$ and $\lambda_3$ represent the diffusion perpendicular to the maximal diffusion and their average is referred to as radial diffusivity (RD) (equation 3). In biological tissue the diffusion coefficient D is referred to as the apparent diffusion coefficient (ADC) (Le Bihan, Mangin et al. 2001; Beaulieu 2002; Jiang, van Zijl et al. 2006). The ADC is a measurement of the overall diffusivity in the tissue, and it is

calculated by averaging the principle eigenvalues in the tensor D matrix. In addition to the ADC, the eigenvalues can be utilized to calculate the fractional anisotropy (FA) and relative anisotropy (RA), which describe the degree of the anisotropic diffusion. The FA and RA values range from 0 representing isotropic diffusion to $1(\sqrt{2}$ for RA) representing infinite anisotropic diffusion (refer to chapter 4).

One of the most problematic issues in DTI is partial volume effect (PVE). PVE occurs in volumetric imaging where one voxel contains several types of tissues such as GM and WM or CSF and WM (Shimony, McKinstry et al. 1999; Alexander, Hasan et al. 2001; Papadakis, Martin et al. 2002). As a result of PVE the voxels will represent the average value of the different tissue combinations (Pierpaoli, Jezzard et al. 1996; Wiegell, Larsson et al. 2000; Tuch, Reese et al. 2003). Consequently, GM and CSF contaminates of WM voxels will lead to a decrease in FA values since GM and CSF FA values are lower than the WM FA values (Virta, Barnett et al. 1999; Pfefferbaum and Sullivan 2003; Hofer and Frahm 2006; Kim, Park et al. 2008). Since, in TBI studies, a decrease of FA value in WM is considered to be a factor related to traumatic axonal injury (TAI), DTI PVE may play a role in false positive of TAI detection. In consideration of PVE, this study investigated the voxel base distribution of a region of interest (ROI) within the CC and cortex with minimal to no PVE. The DTI parameters (FA, RA, ADC, AD and AD) distributions across the CC and cortex ROIs were computed. Since these ROIs of the CC and cortex have minimal to no PVE, their FA voxel base distributions were utilized as a template for calculating the PVE percentage in the subsequent chapter.

## Methods

### Anaesthesia:

The Wayne State University animal investigation committee has approved all animal procedures in this study. The rats (n=24) were placed in a sealed acrylic chamber and

anaesthetized by a mixture of isoflurane (2% for induction; 0.75-1.75% for maintenance) and 0.6L/min oxygen.  Any escaped or excess gas was scavenged by a vacuum system.

## MRI Acquisition:

The anaesthetized rats were positioned on a magnetic resonance compatible fixture and restrained by pointed ear and bite bars.  Anaesthesia was maintained at 0.75-1.75% isoflurane and 0.6L/min oxygen via nose cone.  The rats were placed in 4.7T Bruker horizontal-bore magnetic resonance spectrometer with a 72mm bore actively shielded gradient coil capable of producing a magnetic field gradient up to 250mT/m.  The DTI were acquired by standard 2D spin echo DTI sequence with six gradient encoding orientation uniformly distributed in space with a spin echo time (TE) of 37ms and 1.9s repetition time (TR).  Two diffusion sensitizing gradient factors of 0 and 800 $sec/mm^2$ were utilized with a diffusion gradient duration/separation of 8/20ms.  The field of view was 32 x 32 $mm^2$ with a matrix size of 128 x 128.  A total of 19 slices of 1mm thick were acquired with a spatial resolution of $0.25x0.25mm^2$ by a total imaging time of 29 minutes per rat.

### *MR Image Processing:*

The raw DTI data were processed in DTI Studio v2.02 (crmrm.med.jhmi.edu) to generate FA, RA, ADC, three directional eigenvalues, and color maps.  All generated maps were saved in analyze image format files in DTI studio.  The analysed format image files in DTI studio generate a high dynamic range (HDR) image file.  The generated maps' HDR image files were imported into signal processing in NMR (SPIN) software developed at Wayne State University for further quantitative analysis.  The images were amplified (up to eight times) in SPIN for an accurate region of interest (ROI) delineation.  After delineation of the ROI the SPIN software computed the mean value and voxel base distribution of FA, RA, ADC and the three directional eigenvalues within the ROI.

*ROI Delineation:*

In the SPIN software the midline of the coronal section of the rats' brains were identified in the DTI b0 images (Figure 24A).

Corpus Callosum ROI Delineation:

The principle eigenvalue with color coded direction map was utilized to draw the ROI. In the principle eigenvalue with color coded direction map the white matter tracts were more distinguishable, and discriminating between two adjacent white matter structures was possible since different fiber directions had different color representation. A symmetrical region of interest composed of 10 points was drawn on the CC (Figure 24B). The first point (bottom center point of the ROI) was placed on the CC midline lower boundary (Figure 24B). The ROI represented in Figure 24B was customized to fit each CC; therefore, the areas for each rat were different (area range from: 0.27-1.08 $mm^2$). Since the rostral side of each section was the caudal side of its succeeding section, by projecting the CC delineation of the preceding section onto its succeeding section, this would represent the preceding section rostral side CC delineation location. Thus the delineating ROI was projected on the proceeding coronal section for each rat to ensure no PVE had occurred along the voxel depth (Figure 24B, C).
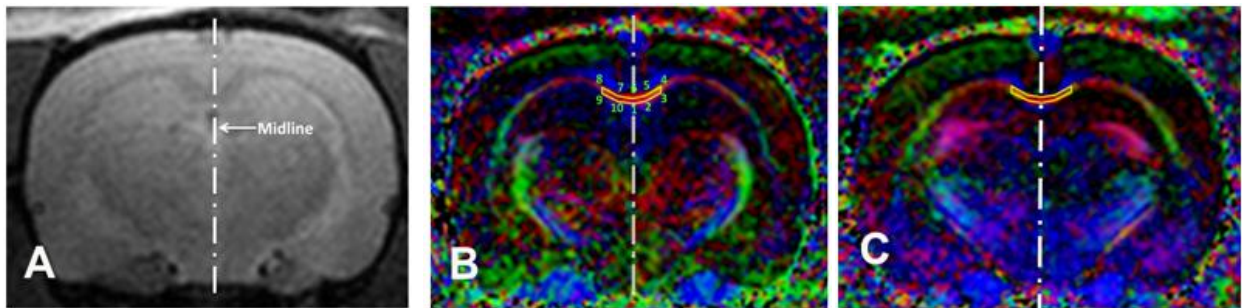


**Figure 24:** (A) The DTI b0 image with the midline. (B, C) Color map of the principle eigenvector with ROI v-like delineation (yellow lines) of CC. (B) The numbers around the yellow delineation represent the different points utilized to draw the V-like shape onto the CC. (C) The succeeding section of image B with the V-like delineation shape of image B transposed onto it.

The ROIs in the proceeding coronal image that did not include GM were assumed to be absent of PVE (GM contamination) and were utilized for further analysis. Because of the angular anatomical structure of the CC, the most posterior coronal image of the CC permitted a delineation of the CC with no PVE along the depth of the voxel. As a result, only six rats from the twenty-four rats analysed showed no PVE occurring at the voxel depth and thus only these six rats were utilized for the CC data.

Cortex ROI Delineation:

In the DTI b0 images 3.21mm from each side of the midline was identified in addition to the boundary of the cortex and cerebral spinal fluid (CSF) boundary (Figure 25 A). After identifying the cortex and the CSF boundary, the color maps of the corresponding images were opened in the SPIN software. Utilising the color maps the ROIs were delineated. The ROIs were delineated on the color map since the white matter tracts were more distinguishable in these maps and therefore eliminating white matter contamination of the ROI. On the cortex, rectangular (2.19 X 1.06 mm$^2$) ROIs' were delineated at 3.21mm away from each side of the midline and 1mm away from the cortex and CSF boundary (Figure 25B). The delineating ROI was then projected on the proceeding coronal section for each rat to ensure no PVE at the voxel depth had occurred (Figure 25C). The ROIs in the proceeding coronal image that did not include CSF or white matter tracts were assumed to be absent of PVE. All 24 of the tested rats showed no PVE for the cortex, therefore, the data for the cortex is representative of all 24 rats.

The ROIs that were assumed to have no PVE for the cortex (n=24) and for the CC (n=6) were saved and later utilized for FA, RA, ADC, AD and RD analysis of their corresponding coronal sections.
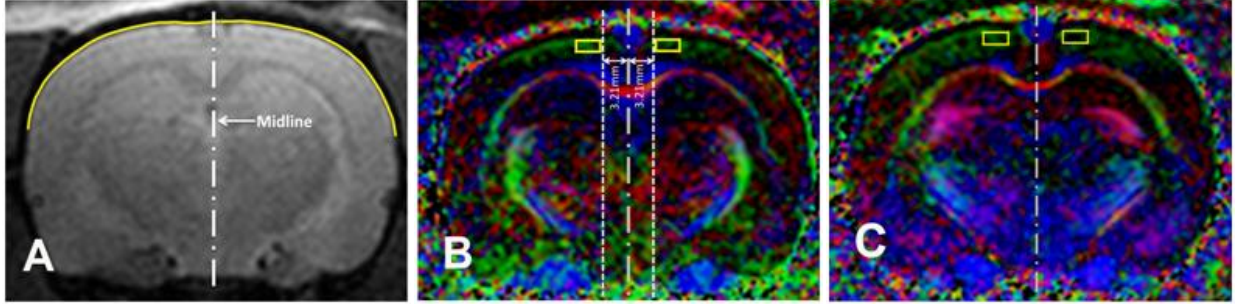
**Figure 25:** (A) The DTI b0 image with the white midline and yellow line delineating the cortex and CSF boundary. (B, C) Color map of the principle eigenvector with the rectangular ROI of the cortex. (B) Each rectangular ROI are 3.21mm away from the midline. (C) The succeeding section of image B with the rectangular ROI delineation of image B transposed on to it.

<u>DTI Histogram Analysis:</u>

In the SPIN software the DTI maps of FA, RA, ADC, and the three directional eigenvalues were uploaded. Each ROI was uploaded on its corresponding image; and the data was processed automatically for these DTI maps by SPIN software. For each DTI map, the voxel values within the ROI were generated and stored in an Excel file. In addition, the average value and standard deviation of the DTI parameters were also generated for the ROI and stored in the Excel file.

To compute the frequency of voxel distribution in the ROI each DTI data set was organized in a specific interval of 0.05 units bins in Microsoft 2007 Excel. For each bin the frequency of distribution was computed and normalized by dividing the computed frequency of each bin by the total frequency of all the bins in the ROI.

***Statistical Methods:***

All data were analysed using SPSS version 17 for Windows. The cortex and the CC DTI parameters (FA, RA, ADC, AD, and RD) values were compared by a non-parametric test (Man-Whitney U test). The Mann-Whitney U test was utilized because Kolmogorov-Smirnov normality test indicated a deviation from the normal distribution for each DTI parameter. Statistical significance threshold was defined for two sided P values of less than 0.05.

## Results and Discussion

The diffusion of the water molecule behavior in the central nervous system varies between GM and WM due to their cellular architecture. In this study, the water diffusion molecule behavior summarized by the DTI parameters was significantly different between the cortex and CC (Table 3). The cortex cellular architecture is composed of neuronal cell bodies, dendrites, glial cells, unmyelinated and myelinated axons, while WM cellular architecture is mainly composed of myelinated and unmyelinated tightly packed and coherently aligned axons that are surrounded by glial cells. This tightly organized coherently aligned axons in the WM fibres facilitates the diffusion of the water molecules along the axonal pathway (Beaulieu 2002; Nicholson 2004; Sen 2004; Alexander, Lee et al. 2007); therefore, water molecule diffusion in WM is more anisotropic in comparison to the GM (Moseley, Cohen et al. 1990; Basser and Pierpaoli 1996; Le Bihan, Mangin et al. 2001; Beaulieu 2002; Hagmann, Jonasson et al. 2006; Alexander, Lee et al. 2007). FA and RA are a measurement of the degree of anisotropic diffusion in the cellular environment. It was observed that the cortex has a significant lower average FA and RA in comparison to the CC (Table 3).

**Table 3:** The average FA, RA, ADC, AD, and RD values of the cortex and CC ROIs. The ADC, AD and RD are reported in units x $10^{-3}$ mm$^2$s$^{-1}$.

| DTI Parameters | Cortex (Average ± Std) | Min - Max | Corpus Callosum (Average ± Std) | Min - Max |
|---|---|---|---|---|
| FA | 0.334 ± 0.099 | 0.08 -0.62 | 0.760 ± 0.096 | 0.37 - 0.95 |
| RA | 0.297 ± 0.099 | 0.07 - 0.7 | 0.812 ± 0.165 | 0.31 - 1.23 |
| ADC | 0.733 ± 0.168 | 0.39 - 1.61 | 0.772 ± 0.127 | 0.53 - 1.13 |
| AD | 0.996 ± 0.241 | 0.51 - 2.22 | 1.631 ± 0.343 | 0.83 - 2.70 |
| RD | 0.602 ± 0.150 | 0.26 - 1.46 | 0.351 ± 0.119 | 0.10 - 0.71 |

Moreover, the voxel base distribution of FA and RA values were statistically different between the cortex and CC (Figure 26 and 27). The voxel base FA distributions histogram plots in this study (Figure 26) were similar to FA histogram distribution plots demonstrated by Alexander et al (Alexander, Lee et al. 2007). However, in Alexander et al (Alexander, Lee et al. 2007) white

matter FA histogram distribution was very broad, unlike this study.  Alexander et al (Alexander,

Lee et al. 2007) presented FA histogram distribution data of the whole brain; therefore, much of

the FA variation may have been caused by crossing of fibres and PVE.  However, this study

focused on a specific homogenous non-crossing fibre population of the CC, thus narrowing the

WM FA distribution.  This study demonstrated that there does exist a major difference between

the degree of anisotropic diffusion between healthy cortex and CC with a small overlap in voxel

base distribution as observed in Figure 26 and 27.  Accordingly, this distinct voxel base

distribution between GM and WM can be employed to separate GM and WM in DTI analysis

(Liu, Young et al. 2006; Liu, Li et al. 2007).
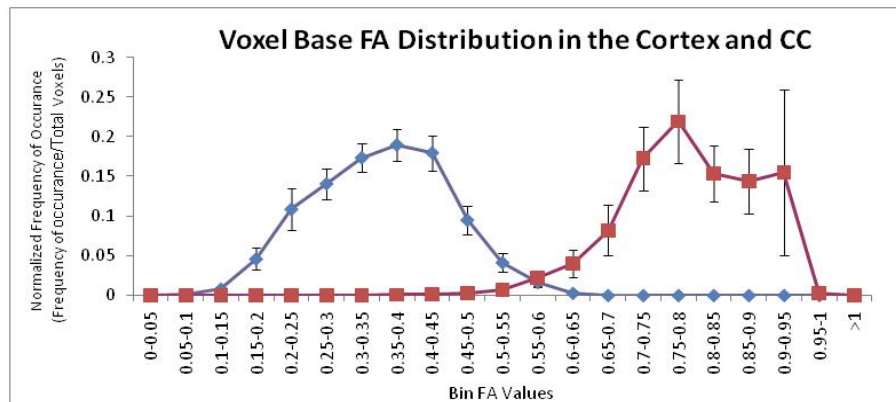


**Figure 26:** The mean normalized FA frequency of voxel base distribution for the ROI of the cortex (blue n=24) and CC (red, n=6).The mean normalized FA voxel distribution of the cortex and CC are statistically different (p<0.05).  Error bars represent standard error of the mean.
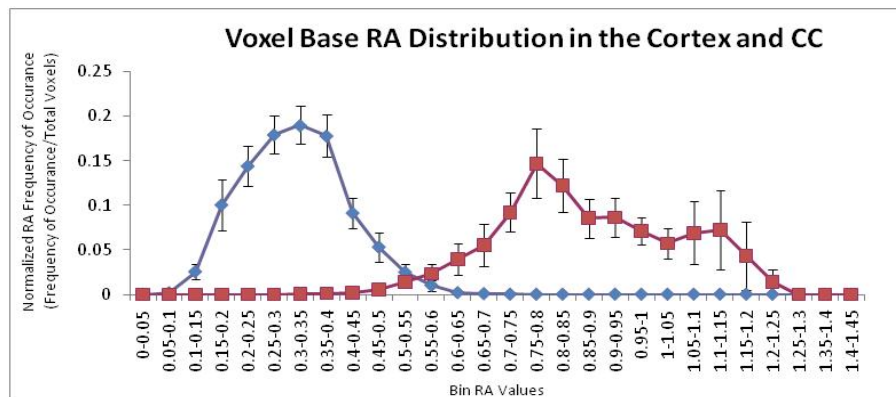


**Figure 27:** The mean normalized RA frequency of voxel base distribution for the ROI of the cortex (blue n=24) and CC (red, n=6).The mean normalized RA voxel distribution of the cortex and CC are statistically different (p<0.05).  Error bars represent standard error of the mean.

Contrary to FA and RA, the DTI parameters ADC, AD and RD described the water molecule diffusion within the cellular environment rather than the degree of anisotropy. Examination of water molecule diffusion in the cellular environment rather than the degree of anisotropic diffusion enabled further probing in the cellular environment. In the CC environment a majority of the axons are myelinated and tightly packed in a coherently aligned manner. Hindrance of the water molecule diffusion is least along the axons; thus, diffusion along these axons is favoured, resulting in a high AD value. In contrast, perpendicular diffusion (RD) is hindered by the axonal membrane and myelin surrounding the axon resulting in low RD values (Le Bihan, Mangin et al. 2001; Beaulieu 2002; Qiu, Tan et al. 2008). Unlike the CC architecture, the cortex cellular environment is more heterogeneous, composed of neuronal cell bodies, dendrites, glial cells, unmyelinated and myelinated axons that run various directions. Therefore, diffusion in the cortex is not favored along a specific diffusion path such as axonal oreintation. This diffusion behavior was presented by the results in this study which indicated that CC has a significant higher average AD value in comparison to the cortex (Table 3). Additionally, the fact that the CC had a significantly lower average RD value in comparison to the cortex (Table 3) was also demonstrated by this study.

In addition to the average AD and RD values, the voxel based distribution of the AD and RD values were significantly different in the cortex and CC (Figure 28 and 29) and were similar to AD and RD histogram distribution plots demonstrated by Alexander et al (Alexander, Lee et al. 2007). However, in this study the AD voxel base distributions values were greater than the AD histogram distribution values of the whole-brain WM presented by Alexander et al (Alexander, Lee et al. 2007). The increased AD values in this study were the effect of studying specific homogenous values within the non-crossing fibre population of the CC in comparison to the heterogeneous crossing fibres of the whole-brain white matter studied by Alexander et al (Alexander, Lee et al. 2007). The RD and AD voxel based distribution displayed a wider

overlapping region between the cortex and CC in comparison the FA and RA voxel based
distribution of the cortex and CC (Figure 26 and 27).
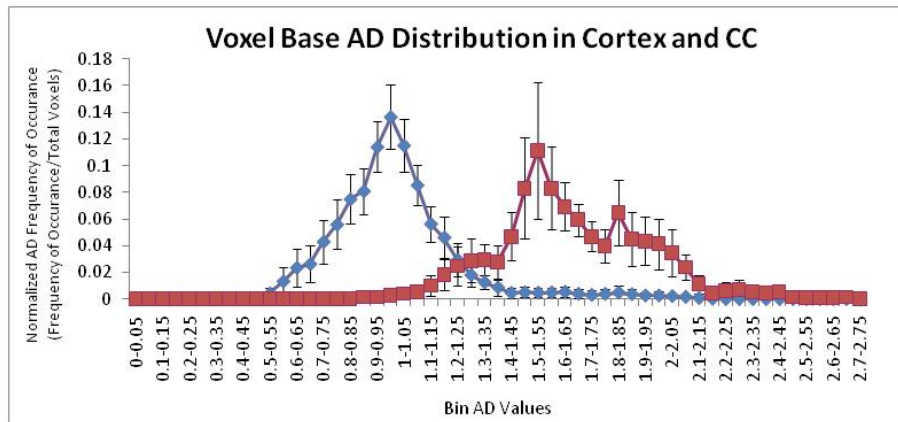


**Figure 28:** The mean normalized AD frequency of voxel base distribution for the ROI of the
cortex (blue n=24) and CC (red, n=6).The mean normalized AD voxel distribution of the cortex
and CC are statistically different (p<0.05).  Error bars represent standard error of the mean.
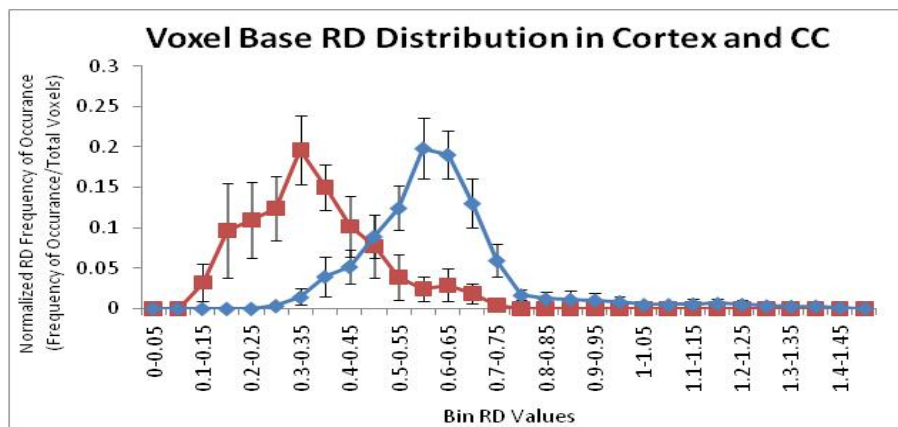


**Figure 29:** The mean normalized RD frequency of voxel base distribution for the ROI of the
cortex (blue n=24) and CC (red, n=6).The mean normalized RD voxel distribution of the cortex
and CC are statistically different (p<0.05).  Error bars represent standard error of the mean.

The other DTI parameter ADC had a significantly lower average value in the cortex in

comparison to the CC (Table 3).  However, the ADC voxel base distribution between the cortex

and CC overlapped frequently (Figure 30). This frequent overlapping of the ADC value was also

demonstrated by Alexander et al (Alexander, Lee et al. 2007).  Despite the fact that voxels ADC

values distribution were statistically different between the cortex and CC the range of voxels

values that was present only in either the cortex or CC was undefined. Likewise, an undefined

ADC boundary between the GM and WM was documented by Liu et al (Liu, Young et al. 2006).
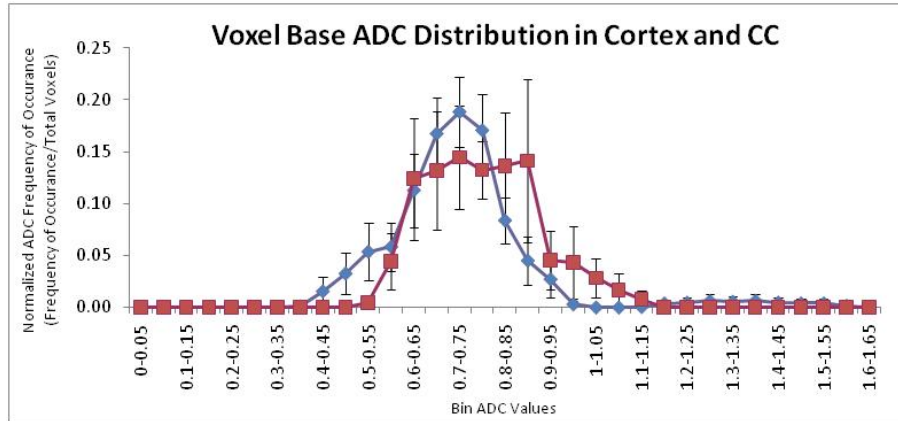


**Figure 30:** The mean normalized ADC frequency of voxel base distribution for the ROI of the cortex (blue n=24) and CC (red, n=6).The mean normalized ADC voxel distribution of the cortex and CC are statistically different (p<0.05).  Error bars represent standard error of the mean.

The above results have demonstrated that from DTI parameters (FA, RA, AD, RD and

ADC) the FA and RA were the best candidates for differentiating between WM and GM values.

The FA and RA voxel base distribution possessed the least overlapping values between the

cortex and CC.  As a result the FA or RA voxel base distribution values could be utilized as a

template for determining PVE (cortex contamination) across the CC.

# CHAPTER 6 FRACTIONAL ANISOTROPY A DISTRIBUTION ACROSS THE CORPUS CALLOUSM TO TEST PARTIAL VOLUME EFFECT

## Introduction

The corpus callosum (CC) is a broad bundle of neuronal fibers that spans from the rostral to the caudal part of the brain interconnecting the neocortical portion of the two hemispheres. It is divided into three parts: a curved rostral part referred to as the genu; a large middle part referred to as the body or truncus; and a thickened caudal part referred to as the splenium. Numerous studies have focused on the CC to study development, disorder, disease and injuries (Downhill, Buchsbaum et al. 2000; Keshavan, Diwadkar et al. 2002; Murray, Viehman et al. 2006; Wilde, Chu et al. 2006). The CC is the largest subcortical white matter fibers and can be directly identified by conventional MRI (Hofer and Frahm 2006). With advancements in diffusion tensor MRI methods the CC has been investigate noninvasively using DTI (Agartz, Andersson et al. 2001; Hofer and Frahm 2006; Wilde, Chu et al. 2006; Medina and Gaviria 2008; Rutgers, Fillard et al. 2008; Hoare, Fouche et al. 2010).

Diffusion tensor imaging (DTI) is a volumetric imaging technique that constructs an image by utilizing signal intensity within voxels. Voxels are volume elements defined in 3D space whose spatial resolutions determine the clarity of an image whereas the depth of the voxels determines the slice thickness. Since DTI involves volumetric imaging, the structural characteristics of the CC, such as its angulation, produce partial volume effect (PVE) along its length. Since the CC is composed of non-crossing fiber populations, the PVE of the voxels within this structure may arise from contamination of gray matter (GM), cerebral spinal fluid (CSF) or other white matter (WM) tracts along the voxels' depth.

PVE of voxels within WM structures can be problematic when trying to detect WM tract injuries since voxel contamination of GM or CSF will lead to a decrease in DTI parameters such as fractional anisotropy (FA).  If healthy WM is exhibiting high anisotropic diffusion, the FA value is large (Beaulieu 2002; Assaf and Pasternak 2008). During injury in WM tracts the anisotropic diffusion decreases, subsequently decreasing the FA values (Arfanakis, Haughton et al. 2002; Huisman, Schwamm et al. 2004; Inglese, Makani et al. 2005; Benson, Meda et al. 2007; Kraus, Susmaras et al. 2007; Xu, Rasmussen et al. 2007; Rutgers, Fillard et al. 2008; Sidaros, Engberg et al. 2008; Lipton, Gulko et al. 2009; Kumar, Saksena et al. 2010; Kinnunen, Greenwood et al. 2011). Contrary to WM, GM and CSF diffusion is more isotropic, thus possessing a low FA value (Beaulieu 2002; Assaf and Pasternak 2008).  When voxels representing a WM structure contain GM or CSF contamination along their depth (invisible along 2D image), the average FA voxel value will decrease.  Since a decrease of DTI FA parameter is a hallmark of white matter injuries; PVE may result in  a false positive indication  of injured white matter tracts.

In Chapter 5 the eigenvector images that contained the most caudal part of the CC were utilized to delineate ROIs within the CC and cortex.  These sections permitted the delineation of ROI with no PVE along the voxel depth.  The average voxel based distributions of the different DTI parameters were computed.  From all the DTI parameters it was concluded that FA and relative anisotropy (RA) are the best candidates for differentiating between WM and GM values. As a result the FA voxel based distribution values from Chapter 5 can be utilized as a template for determining PVE (cortex contamination) across the full length of the CC.  The purpose of the current study was to determine the PVE across the full length CC (splenium to genu) of healthy Sprague Dawley rats in order to determine the area of the CC with the lowest PVE.  The CC area with the lowest PVE was further studied in chapter 7 to investigate the relationship between DTI parameters and diffuse axonal injury.

## Methods

All procedures involving animals in this study were reviewed and approved by the Wayne State University Animal Investigation Committee. Eighteen adult male Sprague Dawley rats weighing (323-506g, Harlan, IN) were utilized. All animals had free access to food and water.

## Anaesthesia

All rats (n=18) were placed in a sealed acrylic chamber and anaesthetized by a mixture of isoflurane (2% for induction; 0.75-1.75% for maintenance) and 0.6 L/min of oxygen. Any escaped or excess gas was scavenged by a vacuum system.

## MRI Acquisition

The anaesthetized rats were positioned on a magnetic resonance compatible fixture and restrained by pointed ear bars and bite bar. Anaesthesia was maintained at 0.75-1.75% Isoflurane and 0.6L/min oxygen via nose cone. The rats were placed in 4.7T Bruker horizontal-bore magnetic resonance spectrometer with a 72mm bore actively shielded gradient coil capable of producing magnetic field gradient up to 250mT/m.

Sagittal T2 weighted imaging was acquired via standard 2D spin echo sequence with echo time (TE) of 46.83 ms and 1573.136 ms repetition time (TR). The field of view was $32 \times 32 mm^2$ and a matrix size of 256x256. A total of 16 slices of 1mm thick were acquired with a spatial resolution of $0.125 \times 0.125 mm^2$ and a total imaging time of 1min and 40s per rat.

The DTI were acquired by standard 2D spin echo DTI sequence with six gradient encoding orientation uniformly distributed in space with a TE of 37 ms and 1.9 s TR. Two diffusion sensitizing gradient factors of 0 and 800 $sec/mm^2$ were utilized, with a diffusion gradient duration/separation of 8/20ms. The field of view was $32 \times 32 mm^2$ and a matrix size of

128 x 128. A total of 19 slices of 1mm thick were acquired with a spatial resolution of 0.25x0.25mm$^2$ and a total imaging time of 29 minutes per rat.

## Image Processing

To calculate the CC angulations from the splenium to its genu, the T2 weighted sagittal images were utilized. T2 weighted images were opened and amplified four times in signal processing in NMR (SPIN) software developed at Wayne State University. On the amplified mid-sagittal T2 image the CC boundaries were delineated manually (Figure 31 A). The T2 weighted images with the delineation were saved as TIF files and exported to ImageJ software (from NIH http://rsb.info.nih.gov/ij/). The body of the CC in the sagittal plane had a uniform linear slope with dorsal and ventral sides of the body of the CC parallel to each other. Therefore, a line parallel to the dorsal and ventral side of the CC was created (Figure 31 B). The angle of the created line was computed by ImageJ software and it was considered to be the angulation of the CC in this study. In addition to the angulation of the CC, the length of the CC spanning from rostral (genu) to caudal (splenium) was also computed by surrounding the dorsal, ventral, rostral and caudal boundaries of the CC with a rectangular selection. The width and height of the rectangle (Figure 31 C) was computed using ImageJ software. Since the T2 weighted images were sagittal, the width of the rectangle represented the rostral to caudal length of the CC and thus represented the length of the CC that would be present in the coronal sections.

In order to generate the coronal FA and color maps, the raw DTI data were processed in DTI studio v2.02 (crmrm.med.jhmi.edu) and saved as high dynamic range (HDR) image files. The HDR image files of FA and color maps were imported into SPIN software and amplified eight times for an accurate region of interest (ROI) delineation. The principle eigenvalue with color coded direction map was utilized to draw the ROI. In the principle eigenvalue with color coded direction map the white matter tracts were more distinguishable and discriminatory between two adjacent white matter structures compared to the FA map. This difference was

possible since different fibre directions had different color representation.  Every coronal section containing the CC were analysed and  the CC structure was delineated (Figure 32).  After delineation of the ROI the SPIN software was used to compute the average FA in addition to the voxel base distribution of FA value within the ROI.
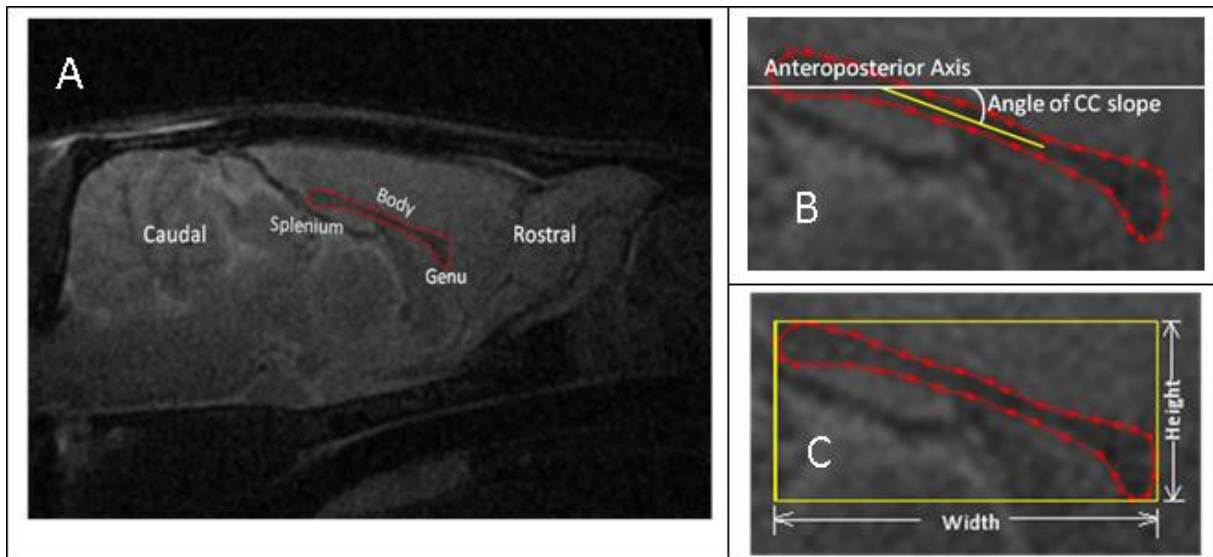


**Figure 31:** (A) T2 weighted image of the mid sagittal section of the rat brain. The red delineates the CC boundaries. (B) The yellow line is an approximation of the CC body slope and the angle of the CC slope calculated from the anteroposterior axis. (C) The yellow rectangle borders the outer boundary of the CC whereas the width of the rectangle represents the rostral to caudal extent of CC.

### Statistical Methods:

All data were analysed using SPSS version 17 for Windows.  The FA value for each MRI section was expressed as the mean value $\pm$standard error (SEM).  The data distribution was tested by Shapiro-Wilk normality test (p<0.05) and by Levene's test of homogeneity of variance (p<0.05).  The mean values of the data set were normally distributed with homogeneous variance.  The one-way analysis of variance Bonferoni test was preformed to compare the various MRI sections spanning the CC to each other.  Statistical significance was considered to be P<0.05.
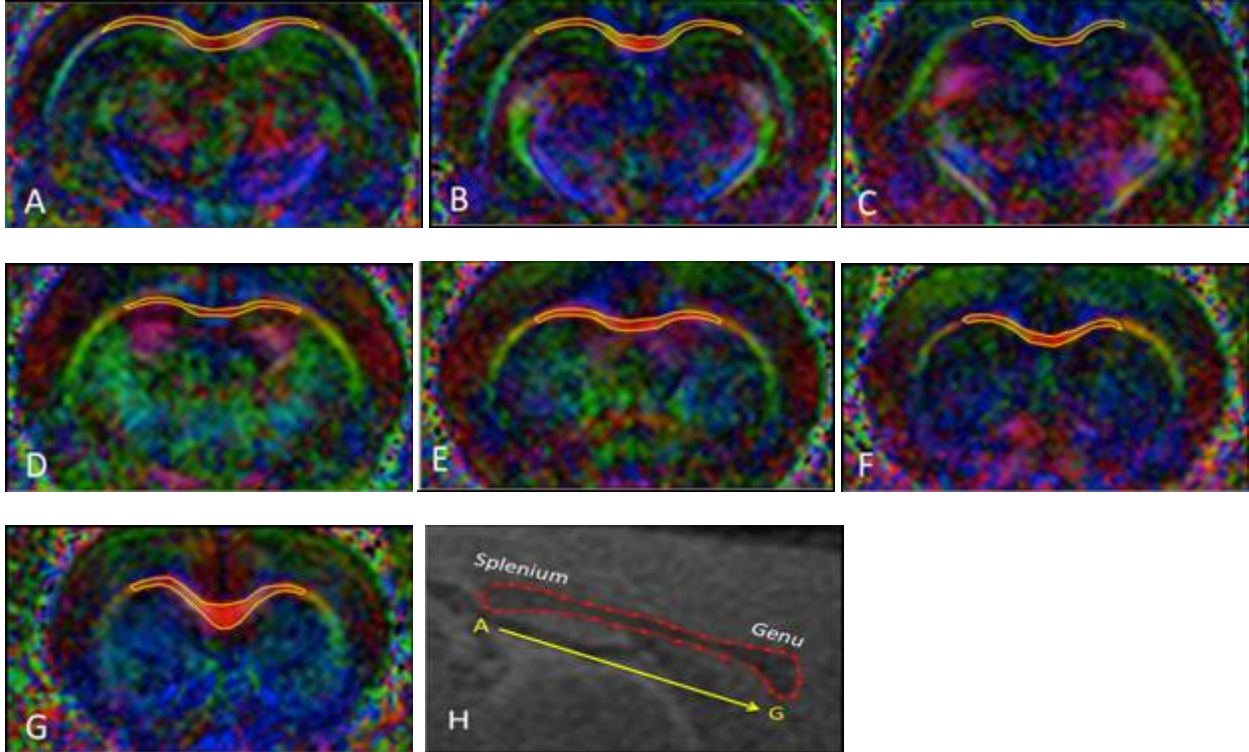
**Figure 32:** (A-G) Color principle eigenvector maps of the MRI coronal sections containing the CC.  (A-G) Yellow lines delineate the boundaries of the CC.  (H) Sagittal T2 weighted image of the corpus callosum displaying the location of the coronal color maps A through G on the sagittal plane.  Color Maps A and G represent the most caudal and rostral sections of the CC, respectively.

## Results

The average CC angulation at the mid-sagittal section as computed by ImageJ was 18.11$^O$ $\pm$11.28 (average angle $\pm$ SEM).  In addition, the average width and length of the rectangular surrounding the outer boundary of the CC in the mid-sagittal plane was 6.68 mm $\pm$ 0.06   and 2.93mm $\pm$ 0.09 (average $\pm$ SEM) respectively.  According to the length of the rectangle in the mid-sagittal plane the corpus callosum should have been present in six to seven coronal MRI images, since the MRI slice thickness is 1mm.  For each rat, the length of the rectangular was consistent with the number of coronal MRI slices that featured the CC.  The CC angulation and the length were found to be uncorrelated to the weight of the animal; therefore, the size of the animal was not a determining factor of the angle and size of the CC.

The average CC FA values across the full length of the corpus callosum (Table 4) were not consistent from one coronal section to the other. The most caudal and rostral section of the CC (Section A and G) possessed the highest FA value of 0.671 $\pm$ 0.011 and 0.645 $\pm$ 0.017 respectively. Sections B through Section F possessed a lower average CC FA value, ranging from 0.603 $\pm$ 0.016 to 0.475 $\pm$ 0.023 (Table 4). Section A average FA value was statistically different from sections C, D and E average FA values. Section B average FA value was statistically different from sections C, and D FA average values. Section C average FA value was statistically different from sections E, F and G average FA values. Section D average FA value was statistically different from sections G average FA value.

**Table 4:** Average CC FA value and SEM for each coronal section as outlined in Figure 31 and 32. For each coronal section the percentage of the FA voxel distribution less than 0.55 (GM FA values) and greater than 0.6 (WM FA values) are represented.

|  | Section A | Section B | Section C | Section D | Section E | Section F | Section G |
|---|---|---|---|---|---|---|---|
| Average FA | 0.671 | 0.603 | 0.475 | 0.516 | 0.569 | 0.569 | 0.645 |
| SEM | 0.011 | 0.016 | 0.023 | 0.024 | 0.018 | 0.018 | 0.017 |
| FA<0.55 | 15% | 28% | 67% | 58% | 35% | 31% | 23% |
| FA>0.6 | 76% | 61% | 23% | 29% | 46% | 55% | 66% |

In addition to the inconsistency of the average FA value across the full length of the CC the voxel based FA distribution demonstrated a similar behaviour. In Figure 33 the voxel based FA distribution of each coronal section of the CC possessed a different distribution profile. In Figure 33 the blue and red lines represent the FA voxel distribution of grey matter (GM, cortex) and white matter (WM, CC) with no PVE as it was determined in Chapter 7. The black line in Figure 33 A-G represents the FA voxel based distribution profile of the delineated CC in Figure 32 A-G respectively. The most caudal section (Section A) of the CC possessed the least and most overlapping FA voxel distribution of the GM and WM, respectively (Figure 33 A). Note that

Section C and D (body of the CC) possessed the most and least overlapping FA voxel distribution of the GM and WM, respectively (Figure 33 C, D). The mid- sagittal section of the CC (Figure 33H) demonstrated that the depth of CC ROI selection in Sections C and D tended to have the highest PVE, whereas half of the ROI selection was contained within the CC and the other half within the cortex.  In addition, Sections B, E and F tended to have similar grey matter contamination within their CC ROI depth as seen in the mid-sagittal section; however, their ROI contained more WM (CC) area than GM (cortex) (Figure 33H).  This PVE behaviour of sections B, E and F could also be seen in their voxel based distribution graphs (Figures 33B, E and F). Note that the calculated length of the CC from its most caudal to its most rostral part was 6.68 mm $\pm$ 0.06; therefore, the last MRI CC coronal section (Section G) would tend to have the CC present in approximately 68% of its depth (Figure 33H).

In addition to the FA voxel based distribution profile across the CC, Figure 34 presents a pictorial demonstration of PVE at each coronal section of the CC.  Since the MRI imaging acquisition began at the caudal end of the brain the first coronal section of the CC would be section A followed by section B and henceforth.  Consequently, the backside of each section was the forepart of its succeeding section; thus, by projecting the CC delineation of a preceding section onto its succeeding section, the preceding section's backside CC delineation location of the preceding section could be visualized.  Figure 34 A-G represents the caudal side of each coronal section of the CC from its most caudal section (Figure 34A) to its most rostral section (Figure 34G) whereas Figure 34 A'-G' represent the rostral side of coronal sections A-G (Figure 34 A-G) of the CC respectively.  Similar to the FA voxel based CC distribution results it was observed that Section A (Figure 34 A) had the least PVE since CC delineation of the caudal side  projection had a good match to the rostral side (Figure 34 A') of section A.  When the CC delineation of the caudal side  of Sections C and D (Figure C and D) was projected to the rostral side  of these sections (Figure C', D'), the CC regions were excluded completely by
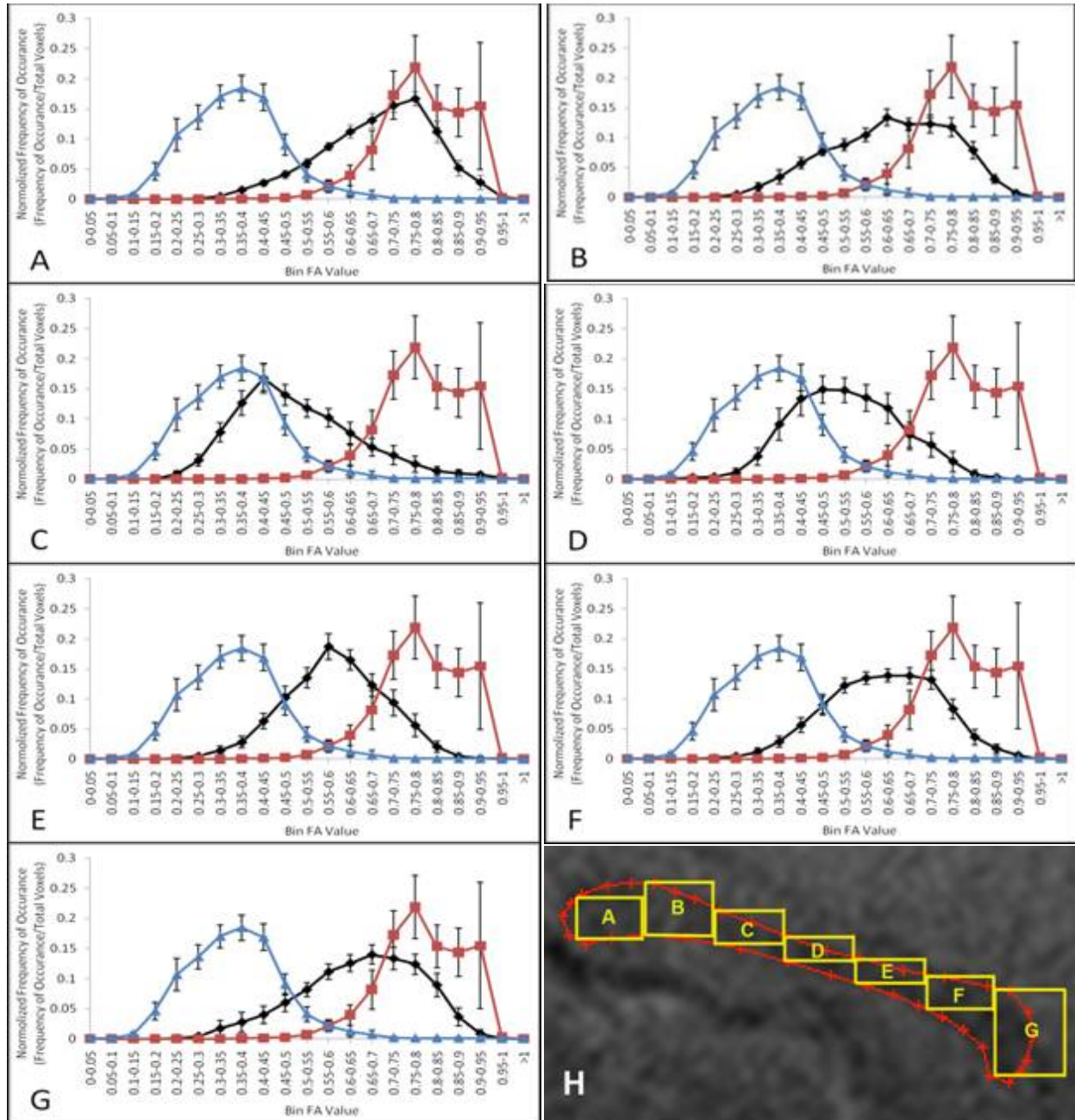
**Figure 33:** (A-G) Represents the FA voxel base distribution within the CC across its full length.Graph A represents the most caudal section and graph G represent the most rostral section of the CC.The blue and red lines represent the FA voxel based distribution within the cortex and CC, of minimal PVE respectively, as described in Chapter 5. The black graph line represents the voxel based distribution within the CC across its full length. The black lines in graph A through G represent the FA voxel based distribution as it is delineated in Figure 32 A through G, respectively. (A-G) The markers on the graph lines repesent the average FA distribution across all rats (Black n=18, Blue n=24, Red n=6) and the error bars represent the standard error of the mean. (H) T2 weighted image of the mid-sagittal section of the brain with the CC sagittal profile delineated by the red line. (H) The yellow rectangles demonstrate approximate locationthe coronal CC delineation depth (rectangular width of A-G) in section A-G respectively and it is for visualiztion purpose only.

the delineation. However, when the CC delineations of the caudal side of Section B, C and D (Figure C and D) were projected to the rostral side of these sections (Figure B', C', D') a small amount of the CC was contained within the delineation.  Since the full length of the CC was not divided evenly into 1mm coronal sections, the last section (Section G) did not fully contain the CC structure within its volume.  Figure 34G' is the rostral side of the last coronal section and it can be seen the CC was absent in this section.
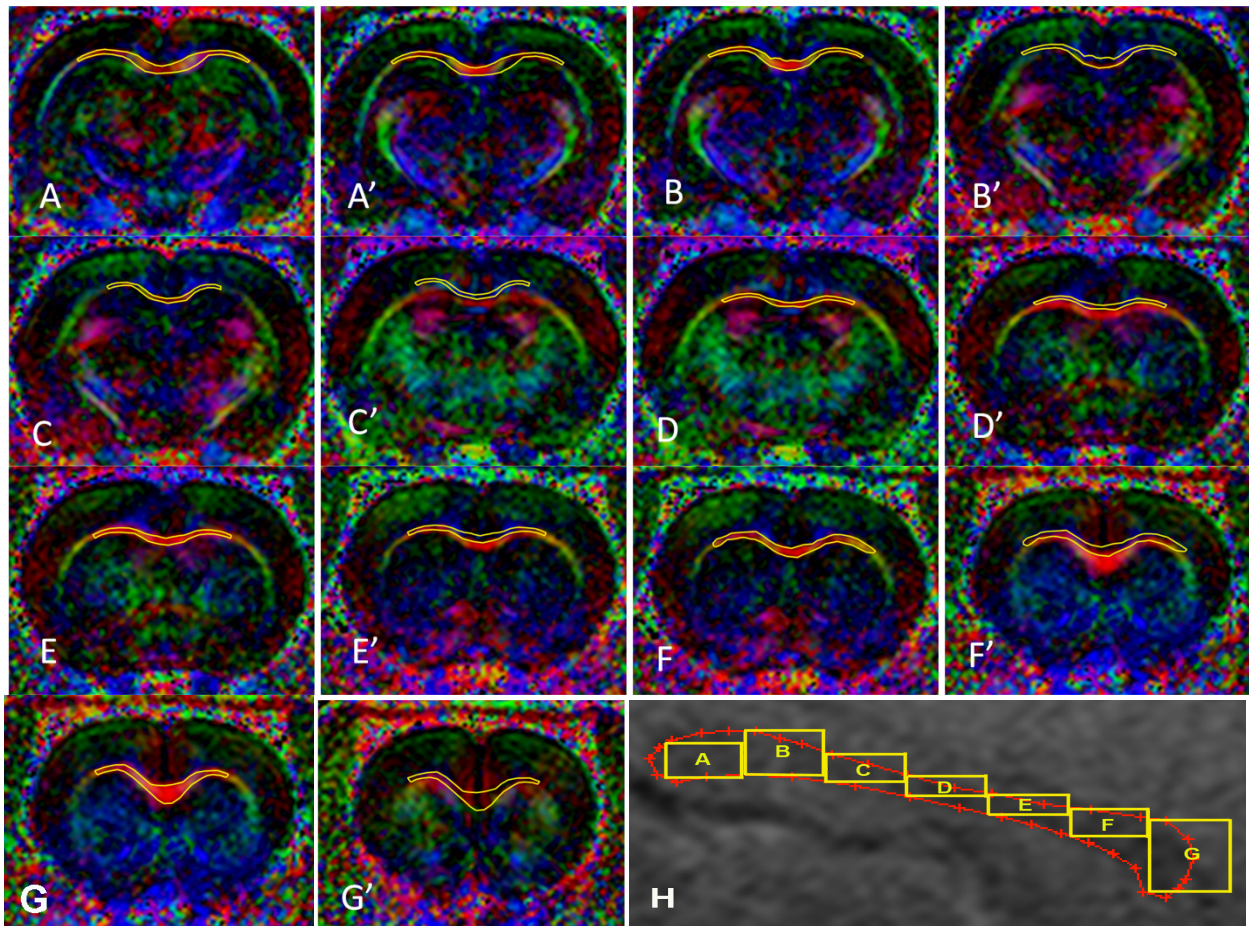


**Figure 34:** (A-H) Color principle eigenvector maps of the MRI coronal sections containing the CC.  (A-H) Yellow delineates are the boundaries of the CC.  (A'-G') Yellow delineation is the delineated boundaries of the previous section superimposed onto these succeeding sections. (H) T2 weighted image of the mid-sagittal section of the brain with the CC sagittal profile delineated by the red line.   (H) The yellow rectangles on the CC represent the depth (rectangular width of A-G) of the coronal CC delineation in sections A-G respectively and it is for visualiztion purpose only.  .

## Discussion

In this study, the highest FA value in the CC was found in the most posterior aspect at the splenium (Section A).  These results agree with studies carried out on human subjects (Hofer and Frahm 2006; Kim, Park et al. 2008; Seoung, Kim et al. 2009; Kochumov, Williamson et al. 2010).  No study on the rat brain has been carried out to investigate the FA values across the full length of CC.  Two studies  carried out on humans  investigated the CC FA values in five regions of the CC (Hofer and Frahm 2006; Kim, Park et al. 2008).  The five regions along the CC that were investigated by Hofer et al in 2006 and Kim et al in 2008 were region I, representing the genu of the CC; region II-IV, representing the body of the CC; and region V, representing the splenium of CC.  In the Hofer et al 2006 study, two FA maps were analysed with spatial resolution either in the mid-sagittal or axial plane. Region V (splenium) was found to have the highest FA value at both spatial resolutions.  The region I-IV of the CC FA value increased when it was analysed in the mid-sagittal plane in comparison to the axial plane.  The discrepancy in the FA values of CC body between the spatial resolutions in the mid-sagittal and the axial plane were thought to be caused by PVE.  In the study by Kim et al (2008), the FA maps were analysed only in the transverse plane.  It was also concluded that region V had the highest FA value and the lowest FA value was present in region III and IV.  In these two studies PVE was referred to as one of the causes of decreased FA value across the CC.  The highest FA values present in the splenium most caudal part of CC demonstrate lowest PVE and the lowest FA values present in the middle regions (body) of the CC demonstrate high PVE.

Visualization of the depth of the voxel by assuming that the backside of each section was the forepart of its succeeding section was revealed by this investigation.  As can be seen from the coronal images representing the CC body (Figure 34 C-F), the ROI delineation was above the CC structure at the backside of these images.  The error in the delineation of the CC at the backside was the PVE occurring along the depth of the voxel.   This pictorial

demonstration of PVE was in agreement with the average of FA values and the voxel based FA distributions across the CC (Table 4, Figure 33).  One method to minimize PVE is  to decrease the voxel size during image acquisition; however, a decrease in the voxel size would lead to a decrease in signal to noise ratio (SNR) (Alexander, Hasan et al. 2001).

DTI makes two assumptions that lead to PVE because of the limitations of voxel size relative to changes at the cellular level.  One of the assumptions that the DTI method makes is the probable displacement of water molecule is Gaussian (Basser 1995); however, restricted and compartmentalization diffusion such as the diffusion in the brain leads to a non-Gaussian distribution (Assaf and Cohen 2000; Beaulieu 2002; Cohen and Assaf 2002).  The second underlying assumption made is that a single diffusion tensor is sufficient to characterize each voxel.  However, in a DTI experiment a voxel in WM contained thousands of axons and glial cells surrounded by extracellular matrix; thus, a single diffusion tensor representation in a voxel is over simplified.  Currently many methods such as composite hindered and restricted model of diffusion (CHARMED) MRI, q-Space MRI, and persistent angular structure (PAS) MRI are being developed to better represent the complexity of the diffusion within the brain tissue; however, these methods are still problematic and time consuming and require strong computational power (Assaf and Cohen 2000; Assaf, Ben-Bashat et al. 2002; Tuch, Reese et al. 2002; Jansons and Alexander 2003; Tuch, Reese et al. 2003; Assaf and Basser 2005).

Despite the shortcomings related to PVE in the traditional development of DTI, this imaging method does supply information unavailable via conventional imaging methods.  A recent PubMed search has indicated that DTI has been utilized in 231 TBI studies.  Since the general purpose of this overall study was to assess the traditional DTI ability in predicting axonal injury induced by TBI, an effort was made to minimize PVE in this study in order to minimize false positive findings.  Accordingly, the most caudal part of the CC rather the full length was studied because that region contains the least PVE.

# CHAPTER 7: Comparison of Traumatic Axonal Injury with Histology and Diffusion Tensor Imaging

## Introduction

A great deal of understanding of traumatic brain injury (TBI) and diffuse axonal injury (DAI) pathomechanisms has been accomplished through research; however, clinical and neuroimaging assessment of TBI, especially DAI, still remains a great challenge to clinicians. Conventional neuroimaging techniques underestimate or fail to recognize the extent of TBI (Gentry, Godersky et al. 1988; Kelly, Zimmerman et al. 1988; Rugg-Gunn, Symms et al. 2001). As a result, clinicians are ill equipped to order additional diagnostic testing or prescribe adequate treatments that could address the long-term functional deficits, often observed. In the past decade diffusion tensor imaging (DTI), a magnetic resonance imaging modality, has been used successfully in clinical research to show changes in the injured brain where conventional imaging has failed to detect any changes (Arfanakis, Haughton et al. 2002; Xu, Rasmussen et al. 2007).

As described in the previous chapter, DTI utilizes water molecule diffusion-driven displacements to map out tissue structures at a microscopic scale well beyond the usual image resolution (Le Bihan, Mangin et al. 2001). During the diffusion-driven displacement the water molecules bounce, cross, or interact with many tissue components i.e. cell membranes, fibers or macromolecules with the result of mapping out a diffusion path (Le Bihan, Mangin et al. 2001). During diseased or injured states the cellular architecture and behavior are modified, leading to an alteration of the water diffusion-driven displacement. For example, during TBI various cellular pathologies occur (as discussed in Chapter 2), thus altering the water diffusion driven displacement.

## White Matter Morphological Alteration

During traumatic insult, rotational forces are exerted on the brain within the cranial cavity, thus contributing to stretching and shearing of white matter (WM) (Gennarelli, Thibault et al. 1982). The stretching and shearing of WM leading to injury to the axons is referred to as DAI or traumatic axonal injury (TAI). TAI severity is directly related to the magnitude of applied forces on the axons (Gennarelli and Thibault 1985). The forces exerted onto the axons can lead to either primary axotomy (immediate tearing of the axons) or secondary axotomy (delayed injury) of the axons (Povlishock, Becker et al. 1983; Povlishock and Christman 1995; Pettus and Povlishock 1996). Secondary axotomy is more prevalent and comprises a sequence of morphological changes in the axons. The secondary axotomy of TAI is difficult to diagnose via conventional imaging but is evident via post-mortem examination (Adams 1988).

TAI morphological changes begin with focal perturbation of axolemma and cytoskeleton misalignment (Povlishock and Christman 1995). The misalignment of the cytoskeleton impairs the axonal transport system resulting in an accumulation of organelles, and thus leading to local swelling and expansion of the axon (Suehiro, Singleton et al. 2001; Marmarou and Povlishock 2006). As time progresses, lobulation of axonal swelling occurs that leads to axonal disconnection (Suehiro, Singleton et al. 2001; Marmarou and Povlishock 2006). After axon disconnection, the proximal and distal segments become caped by continuous axolemma with a progressive accumulation of organelles associated with increased axonal swellings (Stone, Singleton et al. 2001; Marmarou and Povlishock 2006). In a laboratory setting the Marmarou's impact acceleration weight model is capable of inducing these injuries on a rat brain with an intact skull. For that reason Marmarou's weight drop model is utilized in this study to induce TAI (for more details on the Marmarou's weight drop model refer to Chapter 2).

**Diffusion Tensor Imaging Representation of Cellular Environment**

DTI describes the diffusion in the cellular environment by a symmetric 3x3 diffusion tensor matrix D.  In biological tissue the diffusion coefficient D is referred to as apparent diffusion coefficient (ADC) (Le Bihan, Mangin et al. 2001; Beaulieu 2002; Jiang, van Zijl et al. 2006). The eigenvalues and vectors of the tensor matrix represent the diffusion of the molecules in the three principle directions.  The first eigenvalue $\lambda_1$, also referred to as axial diffusion (AD), represents the maximal diffusivity in the tissue; therefore; it is the diffusion along the least resistive path parallel to the axon's orientation.  One TAI characteristic is the pooling of organelles at the site of axonal transport dysfunction.  This pooling of organelles will hinder the diffusion along the injured axon, therefore decreasing AD.  Orthogonal to AD are the second and third eigenvalues $\lambda_2$ and $\lambda_3$.  The average of $\lambda_2$ and $\lambda_3$ represents a plane perpendicular to AD and is denoted by radial diffusivity (RD).  In the presence of TAI axolemmal permeability increases and axonal swelling occur, thus rendering an increase in diffusivity across the axon and resulting in an increase of RD.  Other scalar measurements of water molecule diffusion utilized to describe the cellular environment are diffusion trace and fractional anisotropy (FA).  Trace is a measurement of the overall diffusivity in the tissue, and it is calculated by averaging the principle eigenvalues in the tensor D matrix.  In addition the eigenvalues are utilized to calculate the FA, which describes the degree of the anisotropic diffusion.  The FA values range from 0 to 1 representing isotropic and anisotropic diffusion respectively.  In WM the axons are coherently aligned and, therefore, water will diffuse along the axons more easily than perpendicular to it, resulting in a large FA value.  In the presence of TAI axonal structures are modified by swellings, pooling of organelles and axolemmal permeability.  These pathological features of WM will cause facilitation in RD and hindrance of AD thus decreasing the degree of anisotropy and resulting in decreasing the FA value.

**Findings of Clinical Diffusion Tensor Imaging Studies**

Many clinical investigations have utilized the above described scalar DTI values to investigate how these different parameters can detect pathological changes in TBI patients. Some researchers have further investigated how these changes can be a predictor of outcome in these patients. Clinically, DTI is capable of detecting changes in areas that were found to be normal by conventional imaging. However, the changes to the DTI parameters were found to be inconsistent between studies. The clinical studies have reported an increase (Kraus, Susmaras et al. 2007; Sidaros, Engberg et al. 2008; Kinnunen, Greenwood et al. 2011), a decrease (Arfanakis, Haughton et al. 2002; Sidaros, Engberg et al. 2008), and no significant change (Benson, Meda et al. 2007; Chu, Wilde et al. 2010; Kumar, Saksena et al. 2010; Mayer, Ling et al. 2010) in AD values of TBI patients in comparison to control. In addition, the RD also had a reported increase (Arfanakis, Haughton et al. 2002; Benson, Meda et al. 2007; Kraus, Susmaras et al. 2007; Sidaros, Engberg et al. 2008; Kumar, Saksena et al. 2010; Kinnunen, Greenwood et al. 2011), decrease (Wilde, McCauley et al. 2008; Chu, Wilde et al. 2010; Mayer, Ling et al. 2010) and a non-statistical significant change (Kraus, Susmaras et al. 2007) in TBI patients compared to control. Interestingly, RD decreased only in mild TBI cases and did not show a decrease in moderate to sever TBI cases. In addition, the trace value also demonstrated a variable change of increase (Inglese, Makani et al. 2005; Xu, Rasmussen et al. 2007; Rutgers, Fillard et al. 2008; Sidaros, Engberg et al. 2008; Lipton, Gulko et al. 2009; Kumar, Saksena et al. 2010; Kinnunen, Greenwood et al. 2011), decrease (Huisman, Schwamm et al. 2004; Benson, Meda et al. 2007; Sidaros, Engberg et al. 2008; Wilde, McCauley et al. 2008; Chu, Wilde et al. 2010) and non-statistical significant change (Arfanakis, Haughton et al. 2002) in the TBI group. Furthermore the FA change also varied between studies; however, a majority of the studies demonstrated a decrease in FA in TBI patients (Arfanakis, Haughton et al. 2002; Huisman, Schwamm et al. 2004; Inglese, Makani et al. 2005; Benson, Meda et al. 2007; Kraus, Susmaras et al. 2007; Xu, Rasmussen et al. 2007; Rutgers,

Fillard et al. 2008; Sidaros, Engberg et al. 2008; Lipton, Gulko et al. 2009; Kumar, Saksena et al. 2010).  In addition to a clinically reported decrease in FA values in TBI patients, four mild TBI studies carried out by three independent research teams have demonstrated a clinical increase in the FA value in mild-TBI patients (Bazarian, Zhong et al. 2007; Wilde, McCauley et al. 2008; Chu, Wilde et al. 2010; Mayer, Ling et al. 2010).

The changes in the FA value in TBI patients were found to correlate with the Glasgow Coma Scale (GCS), the Rankin score, post-concussive symptoms, cognition and post-traumatic amnesia (Huisman, Schwamm et al. 2004; Bazarian, Zhong et al. 2007; Benson, Meda et al. 2007; Kraus, Susmaras et al. 2007; Sidaros, Engberg et al. 2008).  However, a limitation of clinical studies is that histological assessment is unavailable in these studies, and therefore the cellular basis for changes in the DTI parameters remains a speculation of TAI.

**Laboratory Diffusion Tensor Imaging Findings**

To date only one animal study has attempted to validate that TAI causes the change in DTI parameters after TBI.  MacDonald et al. utilized a cortical impact injury model in mice to evaluate the changes in DTI parameters over time (Mac Donald, Dikranian et al. 2007; Mac Donald, Dikranian et al. 2007).  MacDonald et al reported a significant reduction of AD and relative anisotropy (RA) in injured, pericontusional corpus callosum (CC) and external capsule, while no significant changes were seen in the conventional MRI T2 weighted images in these regions (Mac Donald, Dikranian et al. 2007).  Similar to FA, RA describes the degree of the anisotropic diffusion and it values range from zero, representing isotropic diffusion, to square root of two, representing infinite anisotropic diffusion.  A decrease RA represents a decrease in the degree of anisotropic diffusion.

In addition, it was reported by MacDonald et al. that DTI parameter changes over time depending on the pathological profile of injury (Mac Donald, Dikranian et al. 2007).  Significant

correlations were found between changes in relative anisotropy and the density of β-APP stained axons across mice and across subregions spanning the spatial gradient of injury (Mac Donald, Dikranian et al. 2007). Also, it was reported by MacDonald et al that a decrease in AD occurred at acute time points (4hrs, 24hrs, 4 days post-TBI) whereas, the AD became comparable to control at subacute time points (7days and 1month post-TBI)(Mac Donald, Dikranian et al. 2007). In addition, the RD appeared normal during acute time point and increased during the subacute time points; however, the relative anisotropy decreased throughout the acute and subacute time points (Mac Donald, Dikranian et al. 2007).

No other animal study has been carried out to validate Mac Donald et al findings. MacDonald et al utilized a cortical impact model, which is a penetrating brain injury model that requires a craniotomy. The cortical impact model replicates clinical brain injury with skull deformation and related cortical compression (Cernak 2005); however, it is not a true representation of the closed head injury which results in diffused axonal injury. In the cortical impact model the opening of the cranial vault to induce the TBI and then placing a plastic skull over the cranial opening with adhesion induces such variables as immune responses which are unrelated to TBI. In addition, the open cortical impact model induces contusion. Since an increased applied force to the cortex will cause an increase in contusion and TAI, thus the degree of TAI and contusion may be linked. Thus cellular and extracellular changes induced by the choice of injury model may disguise as TAI.

DTI parameter changes as a result of TAI need further laboratory study, especially as contradictory FA parameter changes are immerging via clinical studies. Only one group of researchers have attempted to validate the DTI changes as a result of TBI; however, the injury model is a penetrating injury model and may have introduced various variables to the cellular injury as a result of TBI. Therefore, further laboratory study for validating DTI is crucially needed. For that reason this study has been carried out to further evaluate DTI measurements

as an indication of TAI.  In this study a non-penetrating weight drop injury model was utilized to induce TBI in order to minimize variables that are present in the cortical impact model.

## Specific Aims and Hypothesis

*Specific Aim 1:* To demonstrate if DTI parameters of FA, trace, AD, and RD are significantly correlated with traumatic axonal injury in the CC and optic chiasm (Och) at four time points (4 hrs, 24 hrs, 3 days, and 7 days) post-impact, in adult male Sprague Dawley rats subjected to severe TBI via an acceleration impact model.

Method:  In selected regions of interest (ROI), that is, CC and Och, the FA, diffusion trace, RD and AD histogram distributions were measured.  Beta-amyloid precursor protein (β-APP) and neurofilament immunocytochemistry were carried out in the corresponding tissue and the number of retraction balls (RB) and axonal swellings were quantified in the same ROIs.  The RB and axonal swelling quantification were compared to the DTI parameters of the corresponding region at each time interval (4 hrs, 24 hrs, 3 days, and 7 days).  Additionally, the relationship between the location of injury and the ability of DTI to detect TAI at different time points were investigated.

*Hypothesis 1:* The severity of axonal injury is characterized by the retraction ball and axonal swelling count.  Therefore, the severity of TAI will correlate with the DTI parameters (FA, trace, AD and RD).  The changes in retraction ball and swollen axon counts will correlate with the DTI parameter changes over time, since DTI parameter changes are dependent on the axonal integrity.

*Specific Aim 2:*  To determine if the DTI parameters can effectively trace the TAI injury profile as time progresses.

Method:  The progression of TAI was monitored by DTI at 4, 24, 3 days, and 7 days.  At each time point, a group of animals (n = 6) was sacrificed and histological analyses were carried out

to quantify axonal swellings/retraction balls by β-APP and neurofilament immunocytochemistry. The DTI parameters variations were compared to the pathological changes of the tissue over time.

*Hypothesis 2:* TAI is a secondary injury of TBI; therefore, as time progresses the injury will become more prominent and more damage will become evident. Thus the early detection of DTI parameter changes should be a good indicator of axonal injury progression as time increases. As time progresses, after induction of TBI, the pathology profile changes where some recovery of axons will take place while other axons will become disconnected from their distal end. This pathological profile should influence the DTI parameter changes over time.

## Experimental Methods

All surgical procedures in these experiments were approved by Wayne State University Animal Investigation Committee.. Twenty-four male Sprague Daley rats weighing (330-506g, Harlan, IN) were utilized. The rats were randomly assigned to four different post-TBI survival groups (n=6); they had free access to food and water. The rats were sacrificed at eight hours (group 1), twenty-four hours (group 2), three days (group 3) and seven days (group 4) post-TBI according to the group to which they belonged.

### Surgical Preparation and TBI induction

TBI was induced by impact acceleration weight drop head injury model (Foda and Marmarou 1994; Marmarou, Foda et al. 1994). All rats were initially anesthetised by 2-2.5% isoflurane and 0.6L/min oxygen in an anaesthesia chamber after which they were transferred to a nose cone. Through the nose cone the rats received 1-1.75% isoflurane and 0.6L/min oxygen. When the rats become unresponsive to noxious stimulus, a midline incision was preformed to expose the periosteum covering the vertex of the skull (Marmarou, Foda et al. 1994). The periosteum was reflected and a 10 mm diameter steel disc with a thickness of 3mm

was affixed by cranioplastic powder (Plastic One, Roanoke, VA) at the middle between bregma and lamboid sutures.  The rats were positioned in a prone position on a foam bed (12x12x43 cm) contained in a Plexiglas box and secured in place with tape.  The nose cone was removed from the rats and a 450g cylindrical brass weight of 18mm in diameter was dropped from a 2m height onto the vertex of the skull at the center of the steel disc to induce TBI.  After impact, the steel disc was removed with caution and the skull was examined for any skull fractures.  Rats without any severe skull fracture had their skin sutured and were allowed to recover.

## MRI Acquisition

**Table 5:** Time line for imaging and tissue harvesting of the rats in each group.

| Time Line | MR Acquisition | | | | Sacrifice |
|---|---|---|---|---|---|
| | Group 1 (n=6) | Group 2 (n=6) | Group 3(n=6) | Group 4 (n=6) | |
| Pre TBI | X | X | X | X | |
| 4 hrs Post-TBI | X | X | X | X | Group 1 |
| 24 hrs Post-TBI | | X | X | X | Group 2 |
| 3days Post-TBI | | | X | X | Group 3 |
| 7 days Post-TBI | | | | X | Group 4 |

All rats (n=24) were placed in a sealed acrylic chamber and anaesthetized by a mixture of isoflurane (2% for induction; 0.75-1.75% for maintenance) and 0.6 L/min of oxygen.  Any escaped or excess gas was scavenged by a vacuum system.  The anaesthetized rats were positioned on a magnetic resonance compatible fixture and restrained by pointed ear bars and bite bar.  Anaesthesia was maintained at 0.75-1.75% Isoflurane and 0.6L/min oxygen via a nose cone.  The rats were placed in 4.7T Bruker horizontal-bore magnetic resonance spectrometer with a 72mm bore actively shielded gradient coil capable of producing a magnetic field gradient up to 250mT/m.  All rats were imaged before TBI; in addition, the rats were imaged at four hours, twenty-four hours, three days and seven days post-TBI according to the group to which they belonged (Table5).  The DTI were acquired by standard 2D spin echo DTI sequence with six gradient encoding orientation uniformly distributed in space with a spin echo time (TE) of

37ms and 1.9s repetition time (TR). Two diffusion sensitizing gradient factors of 0 and 800 sec/mm$^2$ were utilized with a diffusion gradient duration/separation of 8/20ms. The field of view was 32 x 32 mm$^2$ with a matrix size of 128 x 128. A total of 19 slices of 1mm thick were acquired with a spatial resolution of 0.25x0.25mm$^2$ by a total imaging time of 29 minutes per rat.

**Sectioning and Storing of the Harvested Brain Tissue**

At the designated survival time, the injured rats were euthanized with an overdose of sodium pentobarbital and exsanguinated. The rats were then transcardially perfused with normal saline followed by cold 4% paraformaldehyde in phosphate buffered saline (0.1 M, pH 7.45). Following perfusion, the brains were carefully removed and post fixed in 4% paraformaldehyde with 20% sucrose. The harvested brains that were post fixed in 4% paraformaldehyde with 20% sucrose were cut into blocks containing the genu and the splenium of the CC (Figure 35 A). These blocks were embedded in Tissue-Tek® O.C.T compound and frozen at -78.5$^o$C via dry ice. A series of 40μm coronal frozen slices were cut from each block by Leica CM 3050 cryostat (Leica Microsystems GmbH, Heidelberg Germany) and collected in anatomical order in 96 multiwell plates. Two 96 multiwell plate were used for each rat to collect and store all the slices within the block. Each well within the plate contained one brain slice in anatomical order in phosphate buffer solution (Figure 35 B). The anatomical order of the slices was preserved by collecting and storing the first rostral section of the block in plate one A1 (row A, column 1) and its succeeding section was stored in A2 and so forth. After each row was full the subsequent row was used until all rows were full. After plate one was filled plate two was utilized in the same method as plate one.
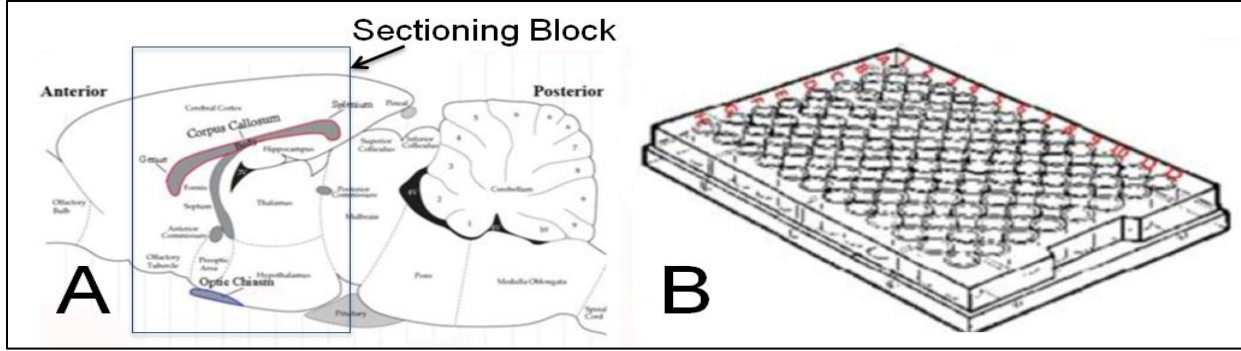
**Figure 35:** (A) Schematic depiction of the brain sectioning block containing the genu and the splenium of the CC that was further cut into 40 µm thick coronal slices and stored in the 96 multiwell plates (Paxinos and Watson 2005). (B) The 96 multiwell plate that was utilized to collect and store all the brain slices within the brain block of each rat. Letters and numbers represent each row and column of the multiwell plate respectively.

## MR Image Processing:

The raw DTI data were processed in DTI Studio v2.02 (crmrm.med.jhmi.edu) to generate FA, diffusion trace, three directional eigenvalues, and color maps. All generated maps were saved as high dynamic range (HDR) image files. The HDR image files were imported into SPIN software developed at Wayne State University for further quantitative analysis. The images were amplified (up to eight times) in SPIN for an accurate region of interest (ROI) delineation. After delineation of the ROI the SPIN software computed the mean value and voxel-based distribution of FA, diffusion trace, and the three directional eigenvalues within the ROI. In addition, in SPIN software the same ROI was placed on T2 weighted image and the voxel-based distribution of the T2 signal intensity was computed. The T2 signal intensity was normalized by dividing the T2 signal intensity by the average cerebral spinal fluid signal intensity of the corresponding rat and imaging time.

## ROI Delineation on DTI

The principle eigenvalue with color coded direction maps were utilized to draw the ROI. In the principle eigenvalue with color coded direction map the white matter tracts are more distinguishable and discrimination between two adjacent white matter structures was possible since different fibre directions have different color representation.

### *Optic Chiasm of Interest*

On the principal eigenvalue with color coded direction maps the sections containing the optic chiasm (Och) were utilized for Och analysis. An ROI was delineated around the boundary of the Och and saved in the SPIN software (Figure 36 A).  The ROI delineations were imported onto the FA maps (Figure 36 B) and modification to the ROI was carried out if deemed necessary.  The modified ROI were saved and utilized for further analysis.
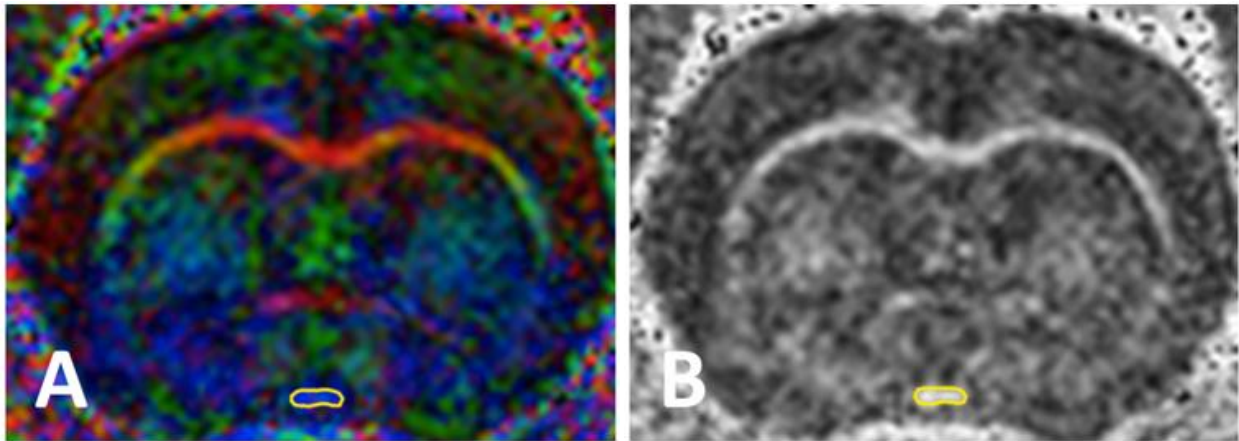


**Figure 36:** (A) The principle eigenvalue with color coded direction map of the section that contains the Och, the yellow delineation delineates the Och.  (B) FA map corresponding to the principle eigenvalue with color coded direction map section in A, the yellow delineation is the Och delineation from A superimposed onto the FA map.

### *Corpus Callosum Region of Interest*

Since the CC is a large cortical white matter tract it permits selection of the structure where partial volume effect (PVE) is minimized, as has been discussed in the previous chapter. Accordingly, only the most caudal section of the CC was investigated in this study since it demonstrated the lowest PVE along the depth of the voxel (refer to Chapter 6).  Utilizing the principal eigenvalue with color coded direction maps the pre and post-TBI sections were matched by utilizing anatomical markers such as optic tract, cerebral peduncle, medial lemniscus, and the hippocampus.  After matching the pre and post-TBI sections the full volume of sections in pre and post-TBI were scanned to ensure accuracy of the match throughout the

brain volume.  Further, on the DTI b0 images the midline of the coronal sections for each rat brain was identified (Figure 37 A).  After the identification of the midline of the coronal sections on the pre-TBI principal eigenvalue with color coded direction maps a symmetrical V-like ROI shape composed of 10 points was drawn on the CC (Figure 37 B).  The first point (bottom center point of the ROI) was placed on the CC midline lower boundary (Figure 37 B).  The ROI represented in Figure 37 B was customized to fit each CC; therefore, the areas for each rat were different. Since the backside of each section is the forepart of its succeeding section, by projecting the CC delineation of the preceding section onto its succeeding section the preceding section backside CC delineation location was represented.  Therefore, the delineating ROI was projected onto the proceeding coronal section for each rat to ensure minimal partial PVE had occurred along the voxel depth.   The delineated ROI on the pre-TBI CC was saved and imported onto the corresponding post-TBI images.
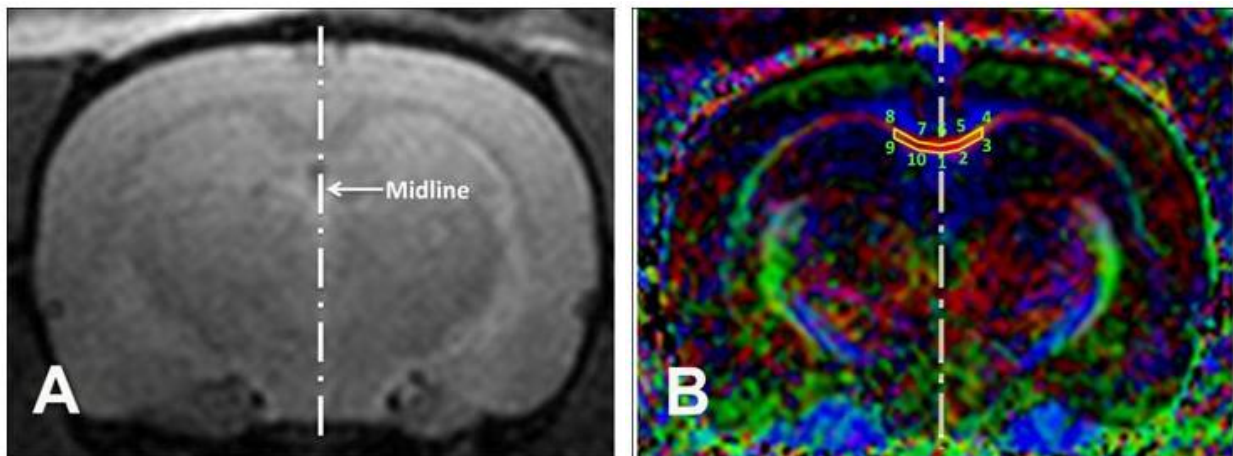


**Figure 37:** (A) The DTI b0 image with the midline. (B) Color map of the principle eigenvector with ROI v-like delineation (yellow lines) of CC.  (B) The numbers around the yellow delineation represent the different points utilized to draw the V-like shape onto the CC.

## Selection of Brain Slices to Represent Och and CC

To represent the Och, three consecutive brain slices were selected from the anterior, middle and posterior areas of the optic chiasm that ranged from 0.13 to 0.84mm posterior to bregma for histological analysis.

Unlike the small anatomical structure of the Och the CC is a large cortical WM tract; therefore, a more precise matching between the harvested brain slices and the analysed CC DTI sections were carried out. In view of the fact that the white matter tracts are more distinguishable in the principle eigenvalue with color coded direction map, these maps were utilized to anatomically match the DTI section with the harvested brain slices. The anatomical landmarks utilized to match between the coronal DTI sections and the coronal harvested brain slices were the otpic tract, cereberal peduncle, medial lemniscus, and the hippocampus (Figures 38).
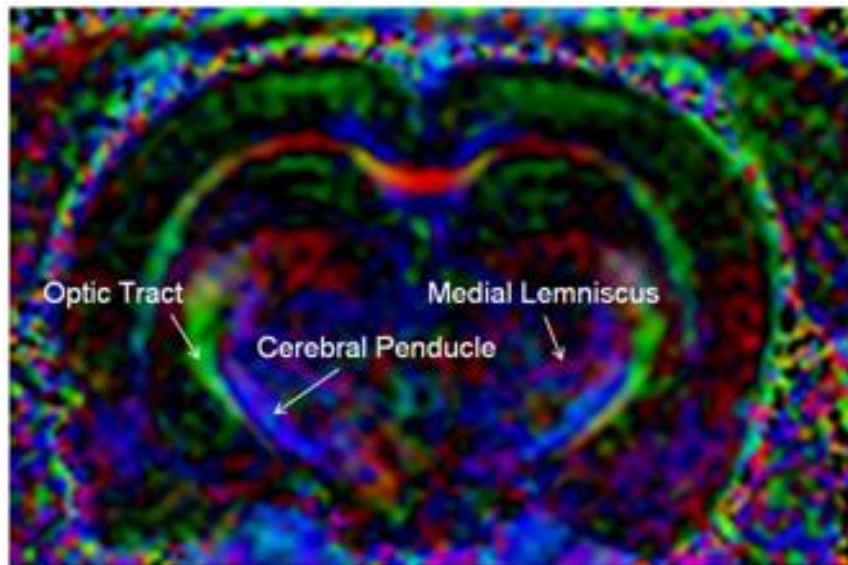


**Figure 38:** The principle eigenvalue with color coded direction map of the section with the anatomical landmarks utilized to match coronal DTI section with coronal harvested brain slices.

Since the voxel size for the MRI is 0.25 ×0.25 × 1 mm$^3$, the thickness of each coronal section is one milimeter in depth. Therefore, the harvested brain slices choosen to represent the MRI coronal image were acquired within a one millimeter volume from the matched brain slice. The harvested brain slices are 40 μm thick therefore, twenty-five consecutive wells represent the one millimetre volume in which the brain slices are choosen from. Since the DTI acquisition begins caudally and ends rostrally along the brain volume, after matching the coronal DTI section with the harvested brain slice, three sets of the harvested brain slices were

collected from the matched DTI preceding wells for histological analysis (Figure 39).  Preceding

the DTI matched well the sixth, seventh and eighth wells, and the twelfth, thirteenth and

fourteen wells, and finally the eighteenth, nineteenth and twentieth wells were utilized to

represent the first, second and third histological sets (Figure 39).  This method of slicing the

brain selections permitted the tissues to be selected across the voxel depth of the DTI section

with a 240µm and 160µm error buffer from the forepart and backside of the voxel respectively.
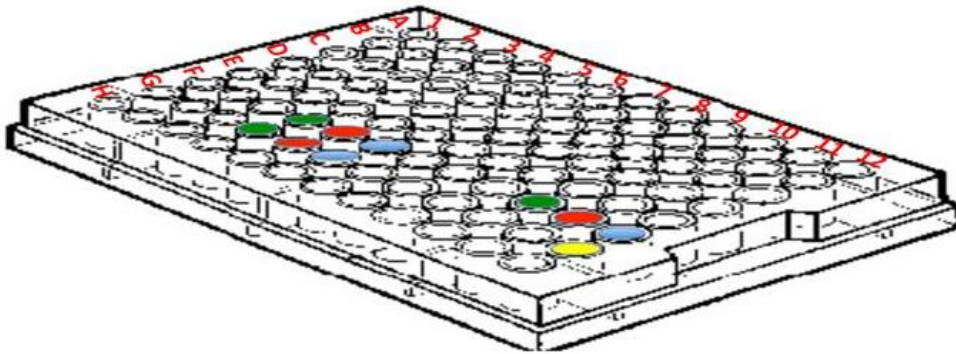


**Figure 39:** An example of the harvested brain slice selections from multiwell plate for the CC histological analysis.The yellow well represents the well storing the brain slice matched to the DTI section.  The three consecutive blue, red and green-marked wells represent one histological data set.  To represent the full voxel depth three histological data sets were utilized.  Within each histological set three different immunostainings were carried out.  The brain slices in the green- and red-marked wells were utilized for IAT and NFC staining respectively.  In addition, the brain slices in the blue-marked wells were utilized for IAT and NFC dual staining.

**Immunochemistry Processing**

The three consecutive brain slices selected were utilized to stain for single labeling IAT

and NFC and dual labeling of IAT and NFC (Figure 39).  The brain slices selected for Och and

CC analysis were placed in a twenty-four multiwell plate for histological processing.  The brain

slices were rinsed 3 x 3 min in 1XPBS, then processed for antigen retrieval by incubation in

citrate butter for 1 hour at $75\text{-}80^0$C.  Next, the tissues were cooled to room temperature for

30min and then were rinsed 3 x 3 min in 1XPBS.  Subsequently, to quench endogenous

peroxidase activity the brain slices were immersed in 0.3% $H_2O_2$ for one hour and then were

rinsed 3x3min in 1XPB.  For single labeling of IAT and NFC the brain slices were incubated

overnight in either C-terminus specific β-APP primary antibody (1μg/ml; rabbit anti-C-terminus β-APP; cat # 51-2700; Zhymed, San Francisco, CA) or RM014 primary antibody (1μg/ml; mouse anti-NF-L; cat # 13-0400; Zhymed, San Francisco, CA) respectively.  For dual labeling of IAT and NFC the brain slices were incubated overnight in both C-terminus specific β-APP primary antibody (1μg/ml; rabbit anti-C-terminus β-APP; cat # 51-2700; Zhymed, San Francisco, CA) and RM014 primary antibody (1μg/ml; mouse anti-NF-L; cat # 13-0400; Zhymed, San Francisco, CA).  The primary antibodies were prepared with 2% normal goat serum (Vector Laboratories, Burlingame, CA), 0.01% Triton X-100 (Fisher Scientific, Fair Lawn, NJ) and 0.1% Albumin Bovine Serum (Sigma-Aldrich, St. Louis, MO) in 1xPBS.  The following day, the brain slices were rinsed three times in 1XPBS for three minutes each rinse.  Following the rinse the brain slices that were incubated overnight in either β-APP or β-APP and RMO14 were incubated in goat anti-rabbit IgG secondary antibody (Vector Laboratories, Burlingame, CA) In addition, the brain slices incubated in RMO14 were incubated in goat anti-mouse IgG secondary antibody (Vector Laboratories, Burlingame, CA).  The secondary antibodies were prepared with 2% normal goat serum (Vector Laboratories, Burlingame, CA), 0.01% Triton X-100 (Fisher Scientific, Fair Lawn, NJ) and 0.1% Albumin Bovine Serum (Sigma-Aldrich, St. Louis, MO) in 1x PBS.  Following the 90-minute incubation in secondary antibody the brain slices were rinsed 3x3 min in 1xPBS, and then incubated for one hour in avidin biotin peroxidase complex (Vectastain ABC Standard Elite Kit, Vector).  Afterward, the brain slices were rinsed 3x3 min in 1xPBS and briefly incubation in 3, 3'-diaminobenzidine and hydrogen peroxide.  The brain slices were rinsed 3x5 min in 1x PBS.  The singled β-APP- and RMO14-labeled brain slices were dehydrated and slip covered using Permount.  The brain slices that were dual labeled with β-APP and RMO14 were incubated for 90 minutes in goat anti-mouse IgG secondary antibody (Vector Laboratories, Burlingame, CA).  The secondary antibodies were prepared with 2% normal goat serum (Vector Laboratories, Burlingame, CA), 0.01% Triton X-100 (Fisher Scientific, Fair Lawn, NJ) and 0.1% Albumin Bovine Serum (Sigma-Aldrich, St. Louis, MO) in 1x

PBS. Following the 90-minute incubation in secondary antibody the brain slices were rinsed 3x3 min in 1xPBS, and then incubated for one hour in avidin biotin peroxidase complex (Vectastain ABC Standard Elite Kit, Vector). Afterward, the brain slices were rinsed 3x3 min in 1xPBS and briefly incubation in 3, 3'-diaminobenzidine nickel and hydrogen peroxide. Finaly, the dual labelled brain slices were rinsed 3x5 min in 1x PBS, dehydrated and slip covered using Permount.

## Digital Image Acquisition

Serial photomicrographs for each coronal section (20x magnification, height = 436.48 µm; length = 327.04 µm; 3.18 pixels/µm) were obtained to encompass a whole region of interest (i.e. Och or CC) by Zeiss Axio Observer Inverted Microscope (Carl Zeiss Inc.) fitted with Axio MRC Digital Camera. The photomicrographs were saved as jpeg files and exported into Adobe Photoshop CS2. Panoramic images of the anatomical region of interest (Figure 40 A and B) for each coronal section were composed by photomerging the serial photomicrographs into Photoshop CS2. The panoramic images of the region of interest for each coronal section were saved as jpeg files. The saved jpeg panoramic images were imported into ImageJ software (from NIH http://rsb.info.nih.gov/ij/) to quantify TAI. After importing the image in imageJ software the scale was set manually to 3.18pixels/µm, allowing the measurements given by ImageJ to represent actual tissue dimensions.

## ROI Delineation on Harvested Brain Slices

The panoramics images of the Och and CC were viewed on a monitor in ImageJ. The structure of the Och and CC were delineated by the following methods.

*Optic Chiasm*

By utilizing ImageJ software the Och boundaries were delineated and any of the tissues present outside the delineated boundary were removed (Figures 7C and E).  Therefore, all Och analyses included only injuries within the Och and excluded injuries to surrounding structures.

*Corpus Callosum*

Since the corpus callosum anatomical size allows for an accurate matching between DTI sections and the harvested brain slices a more detailed ROI delineation was carried out to ensure an identical ROI was delineated on the brain slices as it was on the DTI sections.  First, in order to account for tissue shrinkage for each rat, the width and height for the DTI section to be analyzed were calculated for all time points in the SPIN software (Figure 41 A) and the average width and height for each rat was utilized to represent its true tissue dimension.  In addition, each rat's histologically processed brain slices were digitally imaged.  The width and height of all the histologically processed brain slices for each rat (3 sections/staining method) were measured in ImageJ (Figure 41 B).  The width and height for each staining method were calculated by averaging the sections stained with the corresponding staining method.
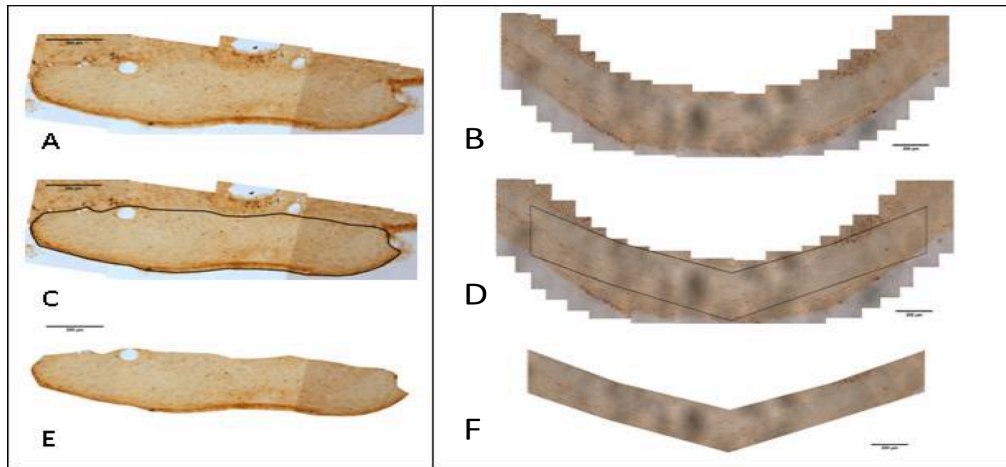


**Figure 40:** The panoramic images of (A) the Och and (B) the CC. The black delineation on the (C) Och and (E) CC images outlines the boundaries of the anatomical structures analysed. (E, F) represent the area within the delineation of the anatomical structures that were analysed. (20x magnification) Scale bar 200μm.

The ratio of the tissue shrinkage was calculated for the width and the height of the tissue and utilized in the calculation of the width and height of the ROI for the brain tissues respectively. For each rat the ratio of the width shrinkage was calculated by dividing the difference between the average DTI width measurements and the average histological width measurements divided by the average DTI width measurements. Similarly, for each rat the ratio of the height shrinkage was calculated by dividing the difference between the average DTI height measurements and the average histological height measurements divided by the average DTI height measurements. For each rat the computed shrinkage width and height ratio was further multiplied by the width and height of the ROI drawn on its colored map respectively in order to compute the new dimension of the ROI on the brain slice. For each rat the width and height of shrinkage ratio was computed for every histological method (β-APP, RMO14, β-APP and RMO14) and was applied to it corresponding histologically processed brain slices. After the computation of the new ROI dimensions the V-like shape and center of the midline of the CC (Figure 40 D) were delineated. The tissues outside the delineated V-like shape on the CC were removed (Figure 40 F) and the TAI counts were computed within the V-like CC delineation shape.
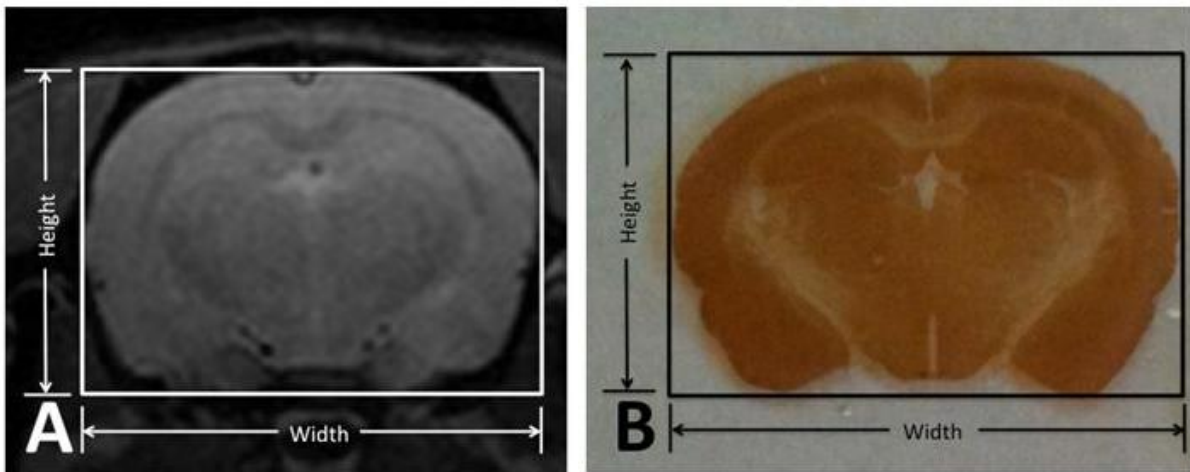


**Figure 41:** (A) DTI b0 image was utilized to compute the original dimensions of the rat brain prior to any tissue shrinkage as a result of histological processing. (B) Histologically processed brain slice corresponding to the DTI b0 Section A. The dimensions of this slice represent the dimension of the tissue after shrinkage due to histological processing.

**Quantification of Axonal injury**

The delineated area within the Och and CC were further amplified on the monitor via ImageJ software and the TAI was quantified by clicking the mouse on the axons stained positively for β-APP and RMO14. When clicking the mouse on the β-APP and the RMO14 positive axons the ImageJ software highlights this selection (Figure 42); therefore, duplicate counting of the axonal injury was avoided. Finally, the cell counter feature in ImageJ counted the marked immunoreactive positive axons that were chosen by the investigator. In order to calculate the density of axonal injury the surface area of each delineated shape was computed by ImageJ software. ImageJ software provided the delineated surface area measurements in $mm^2$. The injured axonal density was then computed by dividing the sum of the total number of TAI injuries in each panoramic delineated region of interest by the sum of the corresponding delineated areas.
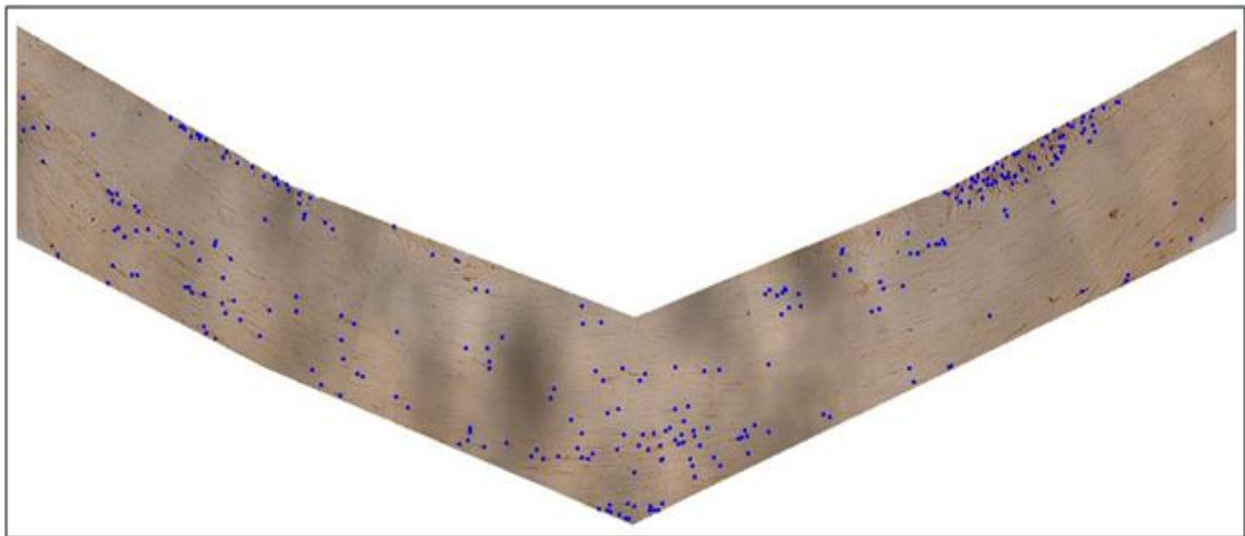


**Figure 42:** V-like shape of the CC panoramic images with blue highlights representing the quantified TAI via ImageJ software.

**Statistical Methods:**

All data were analysed using SPSS version 17 for Windows and statistical significance was considered to be $P \leq 0.05$. To assess the relationships between measured DTI parameters (FA, diffusion trace, AD and RD) and quantified histological TAI measurements or the

relationships between measured DTI parameters (FA, diffusion trace, AD and RD) and T2 weighted images at different time points after TBI Bivariate Pearson Correlation was utilized.

The MRI and DTI parameters voxel-based data distribution were tested by Shapiro-Wilk normality test (p<0.05) and by Levene's test of homogeneity of variance (p<0.05). The voxel-based data distributions were skewed and heterogeneous. Since the mean value was not a robust measurement in skewed distribution, the data analyses were carried out on the voxel-based distribution rather than on the average values.

A nested mixed model was utilized to analyse the differences in the MRI and DTI parameters between pre-TBI and post-TBI. The mean difference of the DTI and MRI parameters was estimated marginal means (unweighted means) at different time points. The estimated marginal means were group means that were estimated from the fitted model. In this nested mixed model the MRI and DTI voxel-based analysis data were the dependent variables nested within the imaging time, and the imaging time were nested within the rats. The fixed effects between the rats and imaging time were found to be significant; therefore the main or simple effect for the rats and image time was not analysed further. Bonferroni test was utilized to detect significant differences in the MRI and DTI parameters between pre-TBI and post-TBI.

To analyze the shapes of the FA voxel base distribution between pre and post-TBI the kurtosis and the skewness of the distribution was computed (tables 9-16). Kurtosis measures if the data distribution is either peaked or flat relative to a normal distribution. Normally distributed data distribution will have a kurtosis value of about zero, and this type of distribution is referred to as mesokurtic distribution (DeCarlo 1997; Bai and Ng 2005). A kurtosis value greater than zero indicates the data distribution is a leptokurtic distribution (higher peak than normal distribution with heavier tails) (DeCarlo 1997; Bai and Ng 2005). A kurtosis value less than zero indicate the data distribution is a platykurtic distribution (lower peak than normal distribution and

lighter tails) (DeCarlo 1997; Bai and Ng 2005). If the standard error of kurtosis is two times greater than the absolute mean kurtosis then the data distribution differs from the normal distribution to a significant degree (SPSS 2007). In addition to the kurtosis measurement the skewness of the data distribution was computed. Skewness of the distribution measures the degree of asymmetry around the mean. A mean skewness of zero indicates the data distribution is symmetrical around the mean (Bai and Ng 2005). A mean skewness greater than zero indicates the data distribution is positively skewed (right tail is more pronounced than the left tail) and the bulk of the values lie to the left of the mean (Bai and Ng 2005). A mean skewness less than zero indicates the data distribution is negatively skewed (left tail is more pronounced than the right tail) and the bulk of the values lie to the right of the mean (Bai and Ng 2005). Similar to kKurtosis, if the standard error of the skew is two times greater than the absolute mean the skew than the data distribution differ from the normal distribution to a significant degree (SPSS 2007). Benson et al. has also utilized kurtosis and skewness measurements to compare voxel base FA distribution in TBI patients and controls (Benson, Meda et al. 2007).

To test for significances in the MRI alteration in individual rats the voxel-based data distribution were utilized and compared to each other across time for each individual rat. The data distribution was tested by Shapiro-Wilk normality test ($p < 0.05$) and by Levene's test of homogeneity of variance ($p < 0.05$). The mean values of the data set were either not normally distributed or the variances of the data set were heterogeneous. Since Kruskal-Wallis test does not assume normality in the data set and is insensitive to outliers in the data, Kruskal-Wallis test was utilized to compare pre-TBI with post-TBI points. If the Kruskal-Wallis test demonstrated significance ($p \leq 0.5$), then the Man-Whitney exact test was utilized for pairwise comparisons between the two time points. Statistical significance was considered to be $P \leq 0.05$.

## Specific Aim 1 Results

**Specific Aim 1:** To demonstrate if DTI parameters of FA, trace, AD, and RD are significantly correlated with TAI in the CC and Och at four time points (4, 24, 3 days, and 7 day) post-impact, in adult male Sprague Dawley rats subjected to severe TBI via an acceleration impact model.

### *Fractional Anisotropy Correlation to Traumatic Axonal Injury*

The change in FA mean value between pre-TBI and all time points (4 hours, 24 hours, 3 days, and 7 days) post-TBI demonstrated an insignificant linear relationship with quantified TAI expressed by an impaired axonal transport system and/or neurofilament compaction within the CC ROI and Och (Figures 43 –Figures 46).

Since there were insignificant differences in the MRI or histological parameters of the CC between four hours and twenty-four hours post-TBI, the CC four hours and twenty-four hours post-TBI data were pooled together to represent acute injury time.  By pooling the acute injury time points together the sample size increased to twelve for the CC, since the lack of correlation may be related to the small sample size.  However, pooling Och data for four hours post-TBI and twenty-four hours post-TBI was not carried out since significant differences were observed in the histological data between these two time points.  The chronic data from three days post-TBI and seven days post-TBI were pooled together since no significant difference was found in any of the MRI and histological parameters within the CC and Och between these time points.  By combining the data from three days post-TBI and seven days post-TBI the sample size increased to twelve for the CC and Och.  By pooling data and increasing the sample size a significant linear relationship between the change of FA and TAI density represented by RMO14 immunopositive axons became evident.  At the chronic time point a significant linear relationship ($R^2$=0.357, p<0.05) was present between the change of FA and RMO14 immunopositive axonal density within the CC (Figures 48 B).
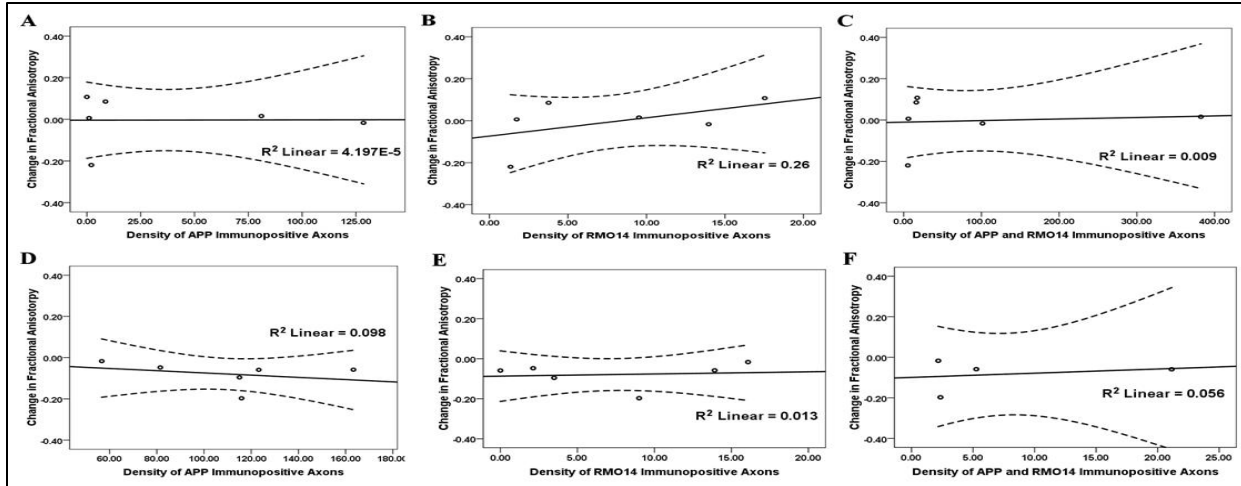
**Figure 43:** These graphs represent the relationship between the change in fractional anisotropy and TAI at four hours post-TBI in the (A-C) CC (n=6) and (D-F) Och (n=6); note that for Figure F, n = 4 because two rats did not have an available Och tissue for dual labelling of β-APP and RMO14 immunostaining). The change in fractional anisotropy (y axis) is represented by the mean FA value at four hours post-TBI minus its corresponding mean pre-TBI FA value. The standard error of the mean FA difference is approximately 5% and 10% of CC and Och FA mean difference respectively (Table B-1 and B-2). Density of TAI (x axis) is computed by quantifying the amount of (A, D) β-APP, (B, E) RMO14, or (C, F) β-APP and RMO14 immunopositive axons per mm$^2$ within the ROI. Each circle represents the data from one rat. No significant correlation was found between FA and TAI. Dashed lines represent the 95% confidence intervals.
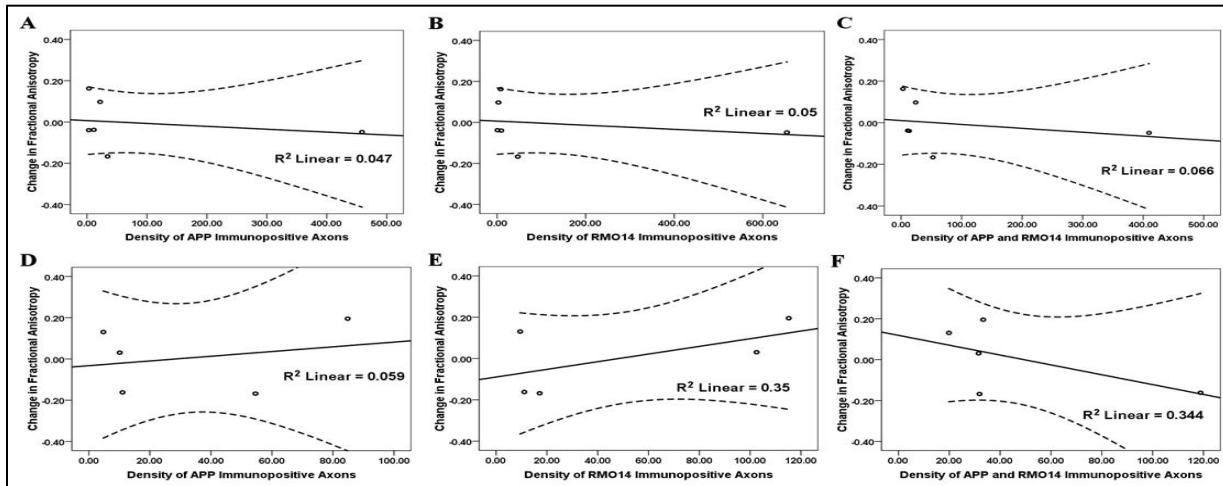


**Figure 44:** The graphs represent the relationship between the change in fractional anisotropy and TAI at twenty-four hours post-TBI within the (A-C) CC (n=6) and (D-F) Och (n=5, in one animal the Och was lost during histological processing). The change in fractional anisotropy (y axis) is represented by the mean FA value at twenty-four hours post-TBI minus its corresponding pre-TBI mean FA value. The standard error of the mean FA difference is approximately 3% and 1% of CC and Och FA mean difference respectively (Table B-3 and B-4). Density of TAI (x axis) is computed by quantifying the amount of (A, D) β-APP, (B, E) RMO14, or (C, F) β-APP and RMO14 immunopositive axons per mm$^2$ within the ROI. Each circle represents the data from one rat. No significant correlation was found between FA and TAI. Dashed lines represent the 95% confidence intervals.
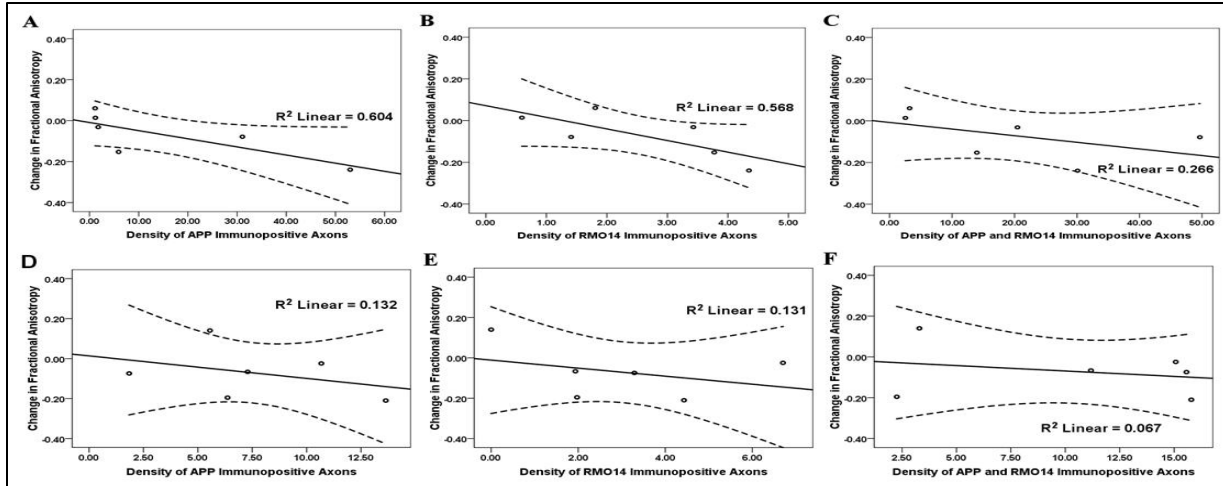
**Figure 45:** The graphs represent the relationship between the change in fractional anisotropy and TAI at three days post-TBI within the (A-C) CC (n=6) and (D-F) Och (n=6). ). The change in fractional anisotropy (y axis) is represented by the mean FA value at three days post-TBI minus its corresponding pre-TBI mean FA value. The standard error of the mean FA difference is approximately 0.5% and 5% of CC and Och FA mean difference respectively (Table B-5 and B-6). Density of TAI (x axis) is computed by quantifying the amount of (A, D) β-APP, (B, E) RMO14, or (C, F) β-APP and RMO14 immunopositive axons per mm$^2$ within the ROI. Each circle represents the data from one rat. No significant correlation was found between FA and TAI. Dashed lines represent the 95% confidence intervals.
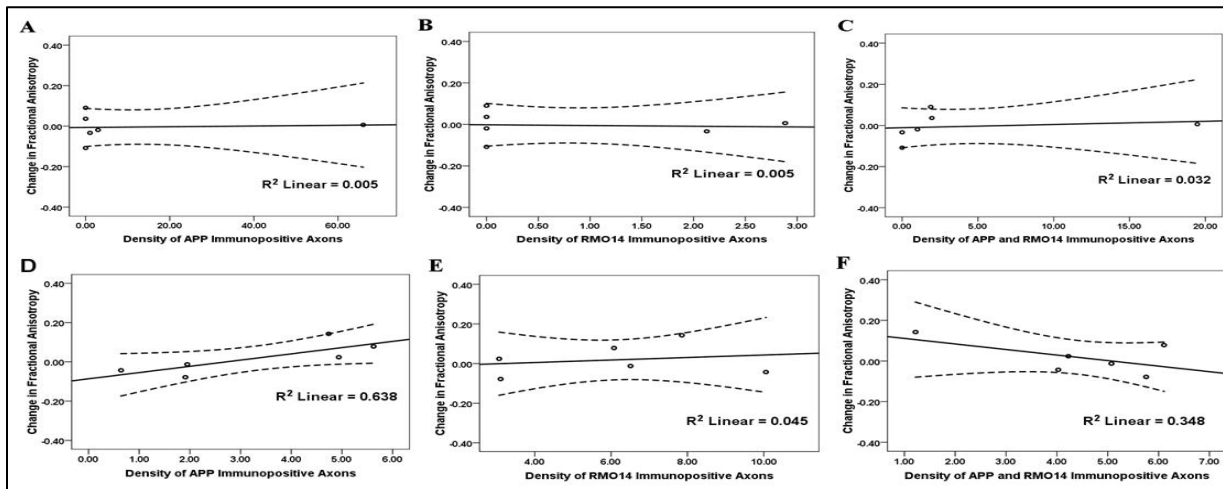


**Figure 46:** The graphs represent the relationship between the change in fractional anisotropy and TAI at seven days post-TBI within the (A-C) CC (n=6) and (D-F) Och (n=6). The change in fractional anisotropy (y axis) is represented by the mean FA value at seven days post-TBI minus its corresponding pre-TBI mean FA value. The standard error of the mean FA difference is approximately 9% and 3% of CC and Och FA mean difference respectively (Table B-7 and B-8). Density of TAI (x axis) is computed by quantifying the amount of (A, D) β-APP, (B, E) RMO14, or (C, F) β-APP and RMO14 immunopositive axons per mm$^2$ within the ROI. Each circle represents the data from one rat. No significant correlation was found between FA and TAI. Dashed lines represent the 95% confidence intervals.
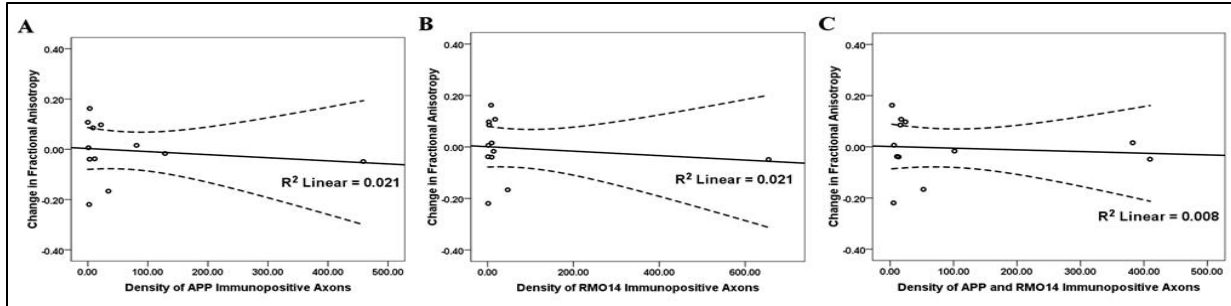
**Figure 47:** The graphs represent combined acute fractional anisotropy and TAI data from four hours and twenty-four hours post-TBI. The change occurring in the fractional anisotropy and TAI at both of these two particular time points are represented within the CC (n=12). The change in fractional anisotropy (y axis) is represented by the mean FA value at post-TBI minus its corresponding pre-TBI mean FA value. The standard error of the mean FA difference is approximately 5% of CC FA mean difference (Table B-1 and B-3). Density of TAI (x axis) is computed by quantifying the amount of (A) β-APP, (B) RMO14, or (C) β-APP and RMO14 immunopositive axons per mm$^2$ within the ROI. Each circle represents the data from one rat. No significant correlation was found between FA and TAI. Dashed lines represent the 95% confidence intervals.
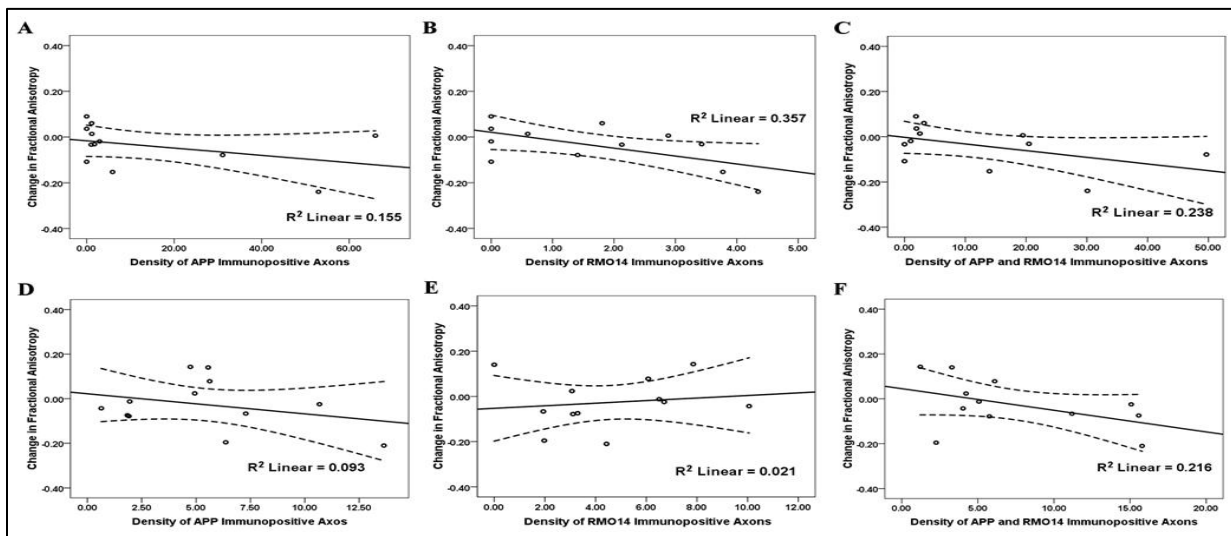


**Figure 48:** These graphs represent combined fractional anisotropy and TAI data from three days and seven days post-TBI. The changes in the fractional anisotropy and TAI at these time points are represented within the (A-C) CC (n=12) and (D-F) Och (n=12). The change in fractional anisotropy (y axis) is represented by the mean FA value at post-TBI minus its corresponding pre-TBI mean FA value. The standard error of the mean FA difference is approximately 9% and 5% of CC and Och FA mean difference respectively (Table B-1 to B4). Density of TAI (x axis) is computed by quantifying the amount of (A, D) β-APP, (B, E) RMO14, or (C, F) β-APP and RMO14 immunopositive axons per mm2 within the ROI. Each circle represents the data from one rat. No significant correlation was found between FA and TAI except in (B) where a negative correlation between fractional anisotropy change and RMO14 immunopositive axons density occurred within the CC with R2= 0.357 (p<0.05). Dashed lines represent the 95% confidence intervals.

### *Diffusion Trace Correlation to Traumatic Axonal Injury*

The average diffusion trace difference between four hours post-TBI and pre-TBI demonstrated an insignificant relationship with quantified TAI expressed by impaired axonal transport system or neurofilament compaction within the CC ROI (Figures 49 A-C). Within the Och, the average diffusion trace difference between pre-TBI and four hours post-TBI demonstrated a linear association ($R^2$ = 0.796, p<0.05) with the impaired axonal transport system density (Figures 49 D). However, within the Och at four hours post-TBI the change in the average diffusion trace demonstrated an insignificant relationship with neurofilament compaction (Figures 49 E and F).
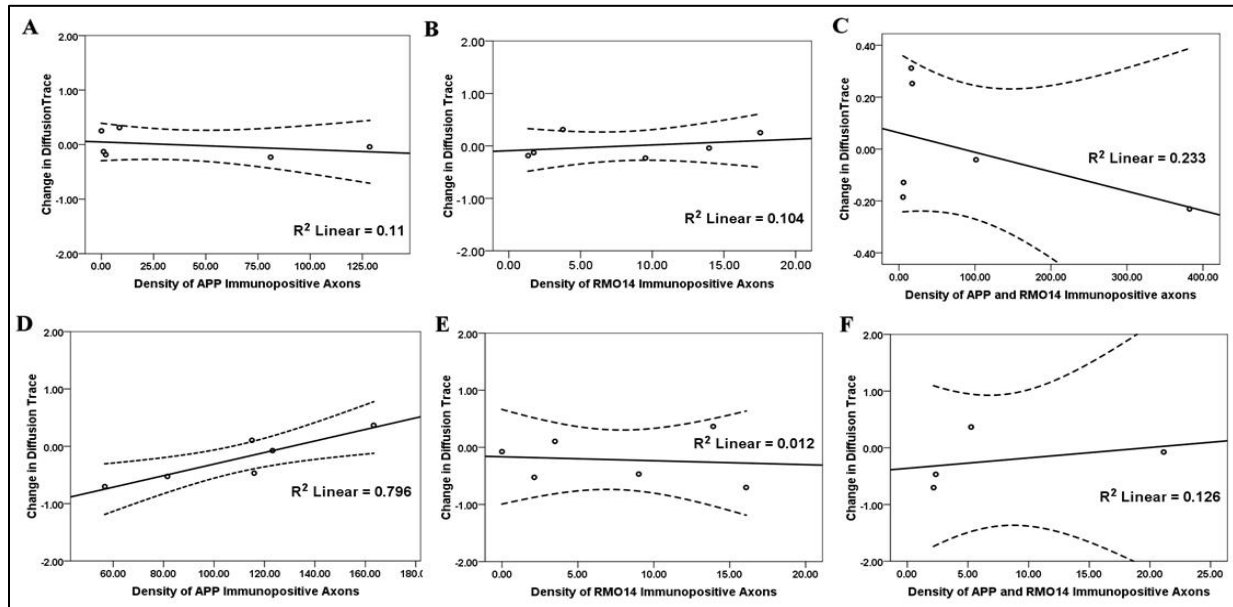


**Figure 49:** The graphs represent the relationship between the change in diffusion trace and TAI at four hours post-TBI within the (A-C) CC (n=6) and (D-F) Och (n=6; note that for Figure F n = 4 because two rats did not have an available Och tissue for dual labelling of β-APP and RMO14 immunostaining). The change in diffusion trace (y axis) is represented by the mean diffusion trace value at four hours post-TBI minus its corresponding pre-TBI mean diffusion trace value (diffusivity × $10^{-3}$mm$^2$/s). The standard error of the mean diffusion trace difference is approximately 5% and 3% of CC and Och diffusion trace mean difference respectively (Table B-1 and B-2). Density of TAI (x axis) is computed by quantifying the amount of (A, D) β-APP, (B, E) RMO14, or (C, F) β-APP and RMO14 immunopositive axons per mm$^2$ within the ROI. Each circle represents the data from one rat. No significant correlation was found between diffusion trace and TAI except for (D), a positive linear correlation present between diffusion trace change and β-APP immunopositive axons within the Och with $R^2$ = 0.796 (p<0.05). Dashed lines represent the 95% confidence intervals.

The change in the diffusion trace mean value between pre-TBI and twenty-four hours post-TBI (Figures 50), or pre-TBI and three days post-TBI (Figures 51) demonstrated an insignificant linear relationship with quantified TAI expressed by impaired axonal transport system and/or neurofilament compaction within the CC ROI and Och.

The diffusion trace mean difference between seven days post-TBI and pre-TBI demonstrated an insignificant relationship with quantified TAI expressed only by neurofilament compaction within the CC ROI (Figures 52 A-B). TAI expressed by impaired axonal transport system demonstrated a significant inverse linear relationship ($R^2$ = 0.75, p<0.05) with the change in the diffusion trace mean within the CC ROI (Figures 52 A). In addition, the combined quantification of impaired axonal transport system and neurofilament compaction density within the CC ROI demonstrated a significant inverse linear relationship ($R^2$ = 0.779, p<0.05) with the diffusion trace difference between seven days post-TBI and pre-TBI (Figures 52 C). Within the Och, the diffusion trace mean difference between seven days post-TBI and pre-TBI demonstrated an insignificant linear relationship with impaired axonal transport system or neurofilament compaction densities (Figures 52 D-F).

In addition, since the various plots suggested a statistical significance (i.e. Figures 50 D, E) but did not attain significance with the sample size, the acute data from four hours post-TBI and twenty-four hours post-TBI were pooled together. The chronic data from three days post-TBI and seven days post-TBI were pooled together as well. When the data was pooled together the linear relationship between the change in the diffusion trace mean values and density of TAI were no longer statistically significant. At the acute and chronic stage no linear relationship was present between diffusion trace and TAI after pooling the data.
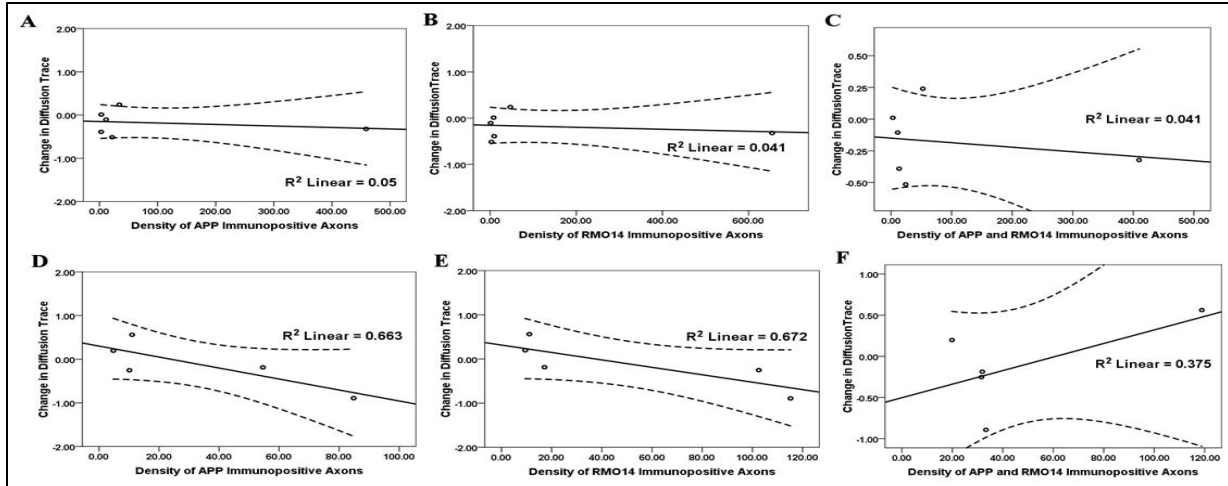
Figure 50: The graphs represent the relationship between the change in diffusion trace and TAI at twenty-four hours post-TBI within the (A-C) CC (n=6) and (D-F) Och (n=5; in one animal the Och was lost during histological processing). The change in diffusion trace (y axis) is represented by the mean diffusion trace value at twenty-four hours post-TBI minus its corresponding pre-TBI mean diffusion trace value (diffusivity × $10^{-3}$mm$^2$/s). The standard error of the mean diffusion trace difference is approximately 1% and 2% of CC and Och diffusion trace mean difference respectively (Table B-3 and B-4). Density of TAI (x axis) is computed by quantifying the amount of (A, D) β-APP, (B, E) RMO14, or (C, F) β-APP and RMO14 immunopositive axons per mm$^2$ within the ROI. Each circle represents the data from one rat. No significant correlation was found between diffusion trace and TAI. Dashed lines represent the 95% confidence intervals.
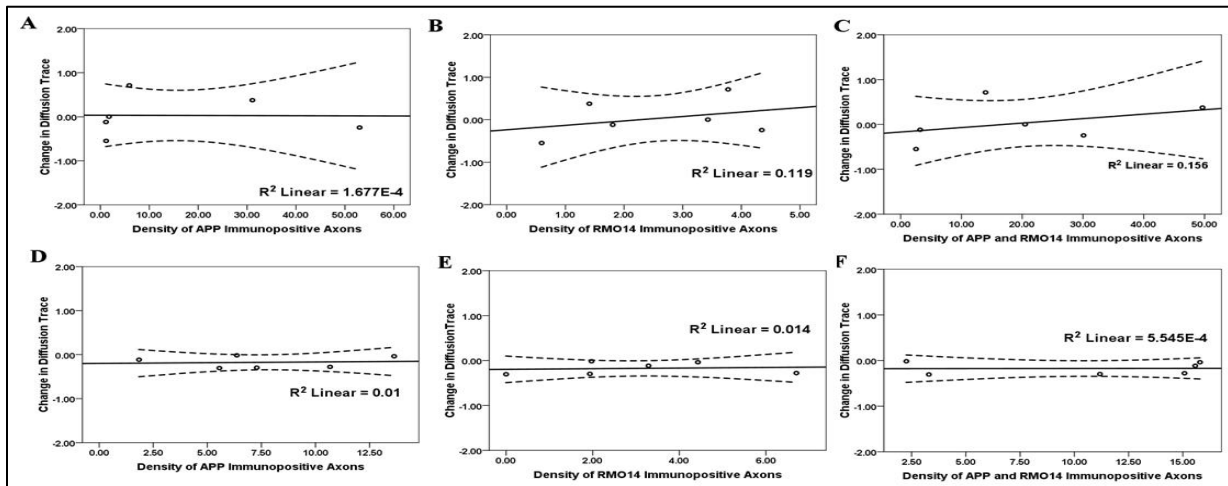


**Figure 51:** The graphs represent the relationship between the change in diffusion trace and TAI at three days post-TBI within the (A-C) CC (n=6) and (D-F) Och (n=6). The change in diffusion trace (y axis) is represented by the mean diffusion trace value at three days post-TBI minus its corresponding pre-TBI mean diffusion trace value (diffusivity × $10^{-3}$mm$^2$/s). The standard error of the mean diffusion trace difference is approximately 1% and 20% of CC and Och diffusion trace mean difference respectively (Table B-5 and B-6). Density of TAI (x axis) is computed by quantifying the amount of (A, D) β-APP, (B, E) RMO14, or (C, F) β-APP and RMO14 immunopositive axons per mm$^2$ within the ROI. Each circle represents the data from one rat. No significant correlation was found between diffusion trace and TAI. Dashed lines represent the 95% confidence intervals.
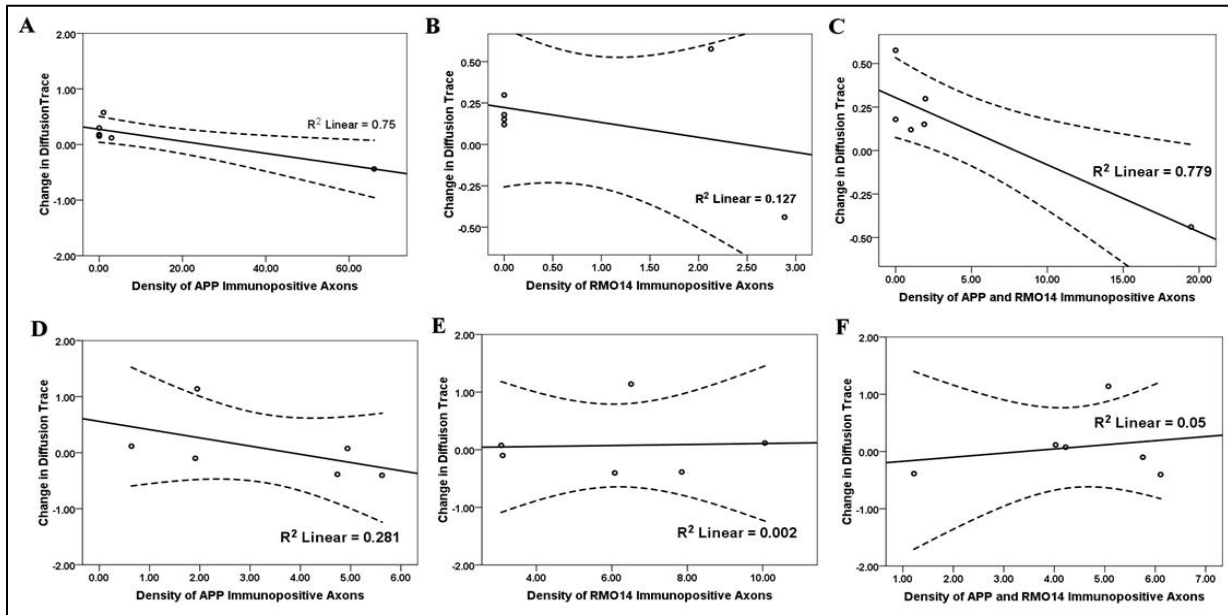
**Figure 52:** The graphs represent the relationship between the change in diffusion trace and TAI at seven days post-TBI within the (A-C) CC (n=6) and (D-F) Och (n=6). The change in diffusion trace (y axis) is represented by the mean diffusion trace value at seven days post-TBI minus its corresponding pre-TBI mean diffusion trace value (diffusivity $\times$ $10^{-3}$mm$^2$/s). The standard error of the mean diffusion trace difference is approximately 5% and 6% of CC and Och diffusion trace mean difference respectively (Table B-7 and B-8). Density of TAI (x axis) is computed by quantifying the amount of (A, D) β-APP, (B, E) RMO14, or (C, F) β-APP and RMO14 immunopositive axons per mm$^2$ within the ROI. Each circle represents the data from one rat. No significant correlation was found between diffusion trace and TAI except for a negative linear correlation present between (A) diffusion trace change and β-APP immunopositive axons within the CC with $R^2$ = 0.75 (p<0.05) and (C) diffusion trace change and β-APP and RMO14 immunopositive axons within the CC with $R^2$ = 0.779 (p<0.05). Dashed lines represent the 95% confidence intervals.

### *Axial Diffusivity Correlation to Traumatic Axonal Injury*

The change of AD post-TBI within the CC ROI and Och at four hours, twenty-four hours, three days, and seven days post-TBI demonstrated an insignificant linear relationship with TAI expressed by impaired axonal transport system or neurofilament compaction (Figures 53 – Figures 56). Additionally, when the data were pooled into acute data (four hours post-TBI and twenty-four hours post-TBI) and chronic data (three days post-TBI and seven days post-TBI) the linear relationship remained insignificant between AD and TAI density.
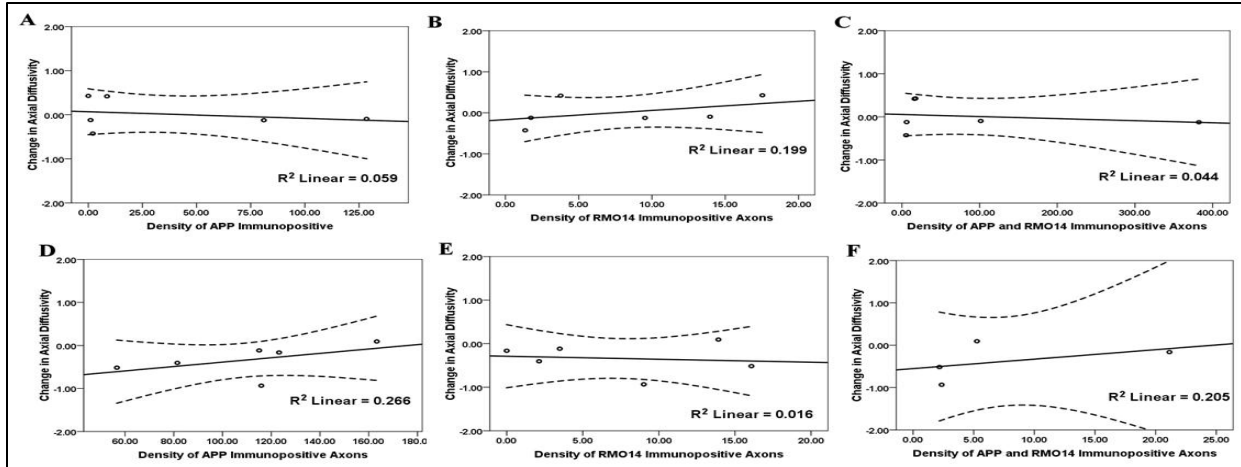
**Figure 53:** The graphs represent the relationship between the change in axial diffusivity and TAI at four hours post-TBI within the (A-C) CC (n=6) and (D-F) Och (n=6, note that for Figure F n = 4 because two rats did not have an available Och tissue for dual labelling of β-APP and RMO14 immunostaining). The change in axial diffusivity (y axis) is represented by the mean axial diffusivity value at four hours post-TBI minus its corresponding pre-TBI mean axial diffusivity value (diffusivity × $10^{-3}$mm$^2$/s). The standard error of the mean diffusion trace difference is approximately 3% and 2% of CC and Och axial diffusivity mean difference respectively (Table B-1 and B-2). Density of TAI (x axis) is computed by quantifying the amount of (A, D) β-APP, (B, E) RMO14, or (C, F) β-APP and RMO14 immunopositive axons per mm$^2$ within the ROI. Each circle represents the data from one rat. No significant correlation was found between axial diffusivity change and TAI. Dashed lines represent the 95% mean confidence intervals.
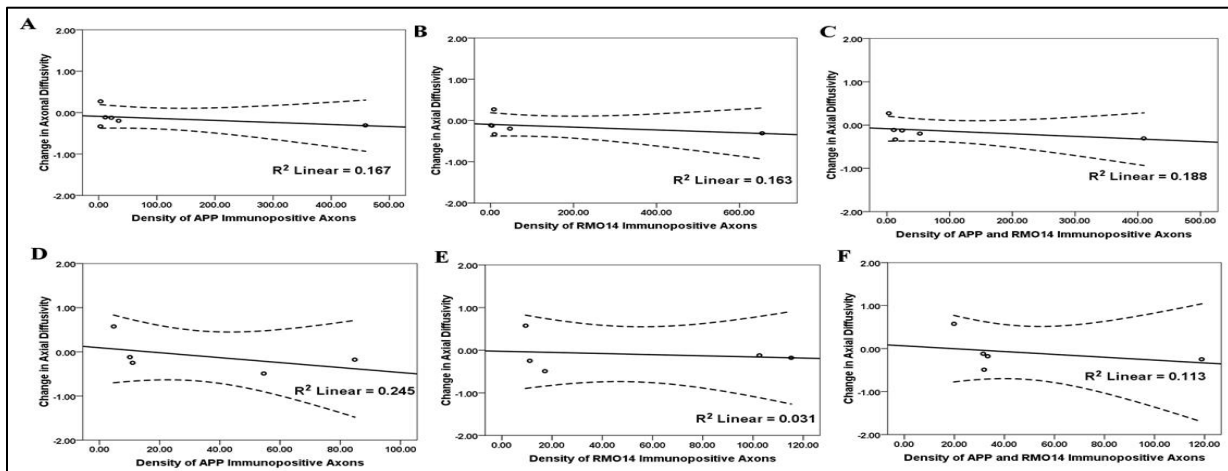


**Figure 54:** The graphs represent the relationship between the change in axial diffusivity and TAI at twenty-four hours post-TBI within the (A-C) CC (n=6) and (D-F) Och (n=5; in one animal the Och was lost during histological processing. The change in axial diffusivity (y axis) is represented by the mean axial diffusivity value at twenty-four hours post-TBI minus its corresponding pre-TBI mean axial diffusivity value (diffusivity × $10^{-3}$mm$^2$/s). The standard error of the mean diffusion trace difference is approximately 3% and 7% of CC and Och axial diffusivity mean difference respectively (Table B-3 and B-4). Density of TAI (x axis) is computed by quantifying the amount of (A, D) β-APP, (B, E) RMO14, or (C, F) β-APP and RMO14 immunopositive axons per mm2 within the ROI. Each circle represents the data from one rat. No significant correlation was found between axial diffusivity change and TAI. Dashed lines represent the 95% mean confidence intervals.
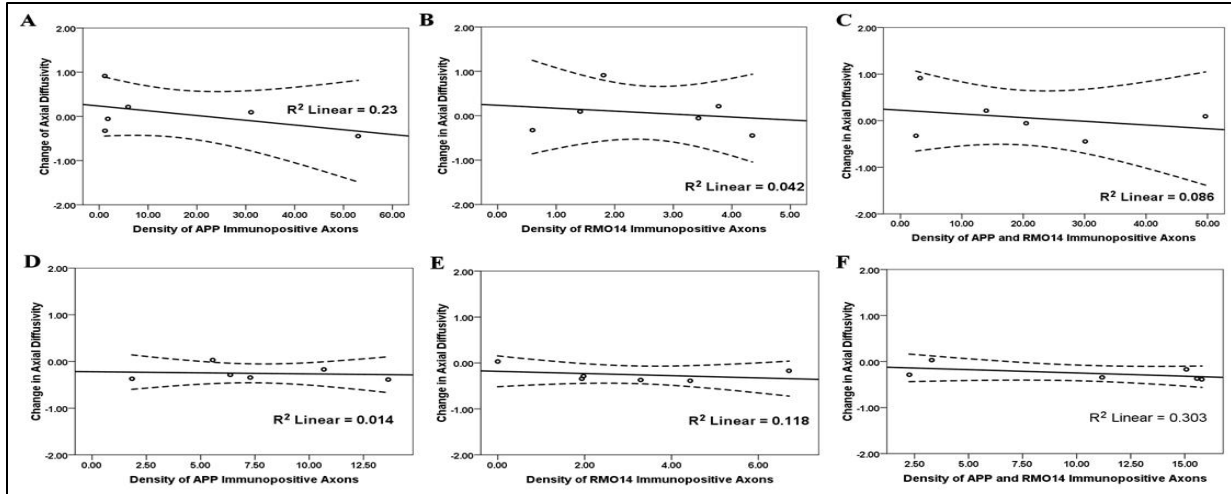
**Figure 55:** The graphs represent the relationship between the change in axial diffusivity and TAI at three days post-TBI within the (A-C) CC (n=6) and (D-F) Och (n=6). The change in axial diffusivity (y axis) is represented by the mean axial diffusivity value at three days post-TBI minus its corresponding pre-TBI mean axial diffusivity value (diffusivity $\times$ $10^{-3}$mm$^2$/s). The standard error of the mean diffusion trace difference is approximately 0.5% and 17% of CC and Och axial diffusivity mean difference respectively (Table B-5 and B-6). Density of TAI (x axis) is computed by quantifying the amount of (A, D) β-APP, (B, E) RMO14, or (C, F) β-APP and RMO14 immunopositive axons per mm$^2$ within the ROI. Each circle represents the data from one rat. No significant correlation was found between axial diffusivity change and TAI. Dashed lines represent the 95% mean confidence intervals.
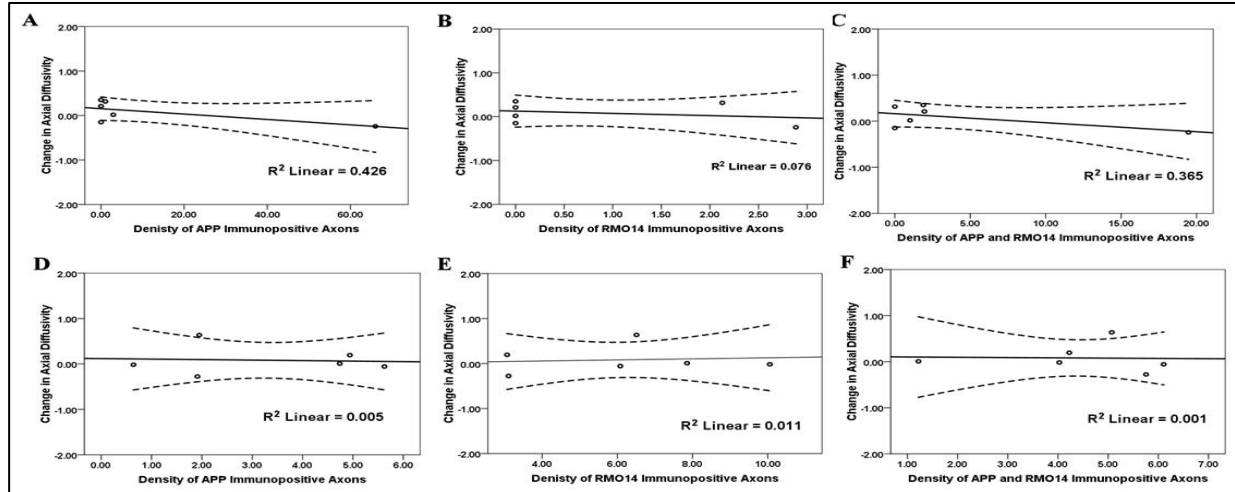


**Figure 56:** The graphs represent the relationship between the change in axial diffusivity and TAI at seven days post-TBI within the (A-C) CC (n=6) and (D-F) Och (n=6). The change in axial diffusivity (y axis) is represented by the mean axial diffusivity value at seven days post-TBI minus its corresponding pre-TBI mean axial diffusivity value (diffusivity $\times$ $10^{-3}$mm$^2$/s). The standard error of the mean axial diffusivity difference is approximately 9% and 17% of CC and Och axial diffusivity mean difference respectively (Table B-7 and B-8). Density of TAI (x axis) is computed by quantifying the amount of (A, D) β-APP, (B, E) RMO14, or (C, F) β-APP and RMO14 immunopositive axons per mm$^2$ within the ROI. Each circle represents the data from one rat. No significant correlation was found between axial diffusivity change and TAI. Dashed lines represent the 95% mean confidence intervals.

### *Radial Diffusivity Correlation to Traumatic Axonal Injury*

The average RD change between four hours post-TBI and pre-TBI demonstrated an insignificant relationship with quantified TAI expressed by impaired axonal transport system or neurofilament compaction within the CC ROI (Figures 57 A-C).   Within the Och, the average RD change between four hours post-TBI and pre-TBI demonstrated a positive linear relationship ($R^2$ = 0.89, p<0.01) with impaired axonal transport density (Figures 57 D).  However, within the Och at four hours post-TBI the average RD demonstrated an insignificant relationship with neurofilament compaction density (Figures 57 E and F).
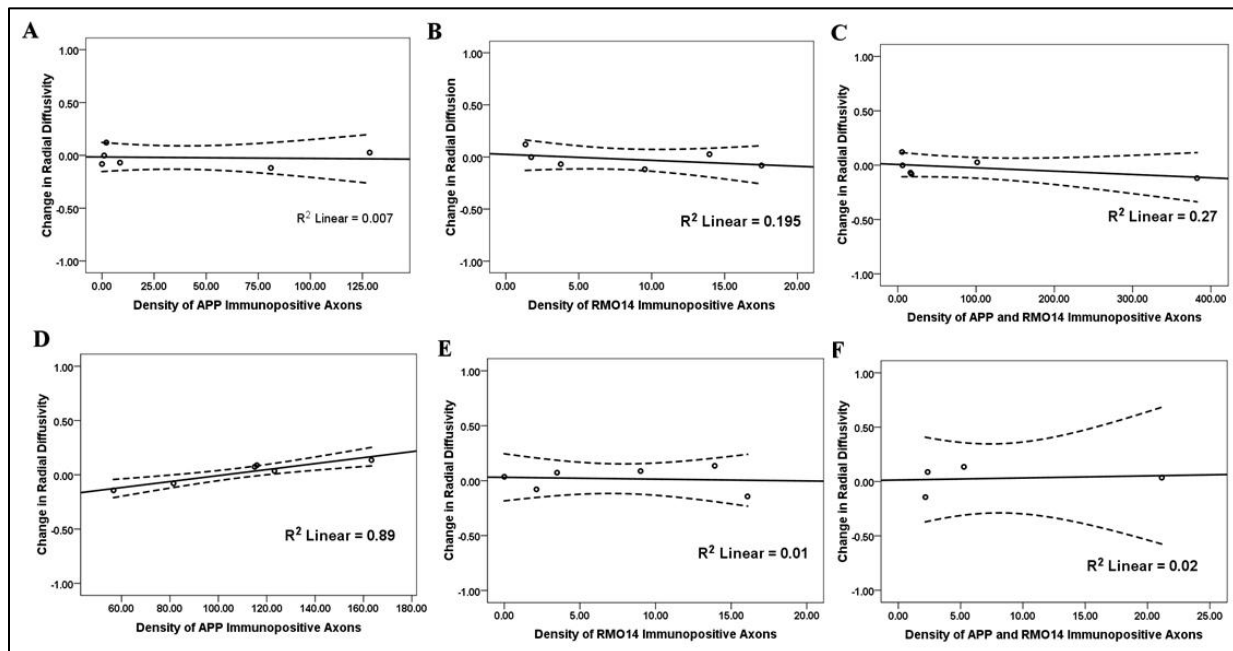


**Figure 57**: The graphs represent the relationship between the change in radial diffusivity and TAI at four hours post-TBI within the (A-C) CC (n=6) and (D-F) Och (n=6; note that for Figure F n = 4 because two rats did not have an available Och tissue for dual labelling of β-APP and RMO14 immunostaining).  The change in radial diffusivity (y axis) is represented by the mean radial diffusivity value at four hours post-TBI minus its corresponding pre-TBI mean radial diffusivity value (diffusivity × $10^{-3}$mm$^2$/s).   The standard error of the mean radial diffusivity difference is approximately 2% and 4% of CC and Och radial diffusivity mean difference respectively (Table B-1 and B-2).  Density of TAI (x axis) is computed by quantifying the amount of (A, D) β-APP, (B, E) RMO14, or (C, F) β-APP and RMO14 immunopositive axons per mm$^2$ within the ROI.  Each circle represents the data from one rat.  No significant correlation was found between radial diffusivity and TAI except for (D) a positive linear correlation present between radial diffusivity change and β-APP immunopositive axons within the Och with $R^2$ = 0.89 (p<0.01).  Dashed lines represent the 95% mean confidence intervals.

The average RD difference between pre-TBI and the following time points: twenty-four hours post-TBI, three days post-TBI, and seven days post-TBI demonstrated an insignificant linear relationship with the quantified TAI expressed by impaired axonal transport system or neurofilament compaction within the CC ROI and Och (Figures 58 – Figures 60).  In addition, since Figures 60 D suggested a statistical significance but did not attain significance with the sample size, the acute data from four hours post-TBI and twenty-four hours post-TBI were pooled together, and the chronic data from three days post-TBI and seven days post-TBI also were pooled together.  When the data were pooled together the linear relationships between the changes in the RD mean values and density of TAI was insignificant.
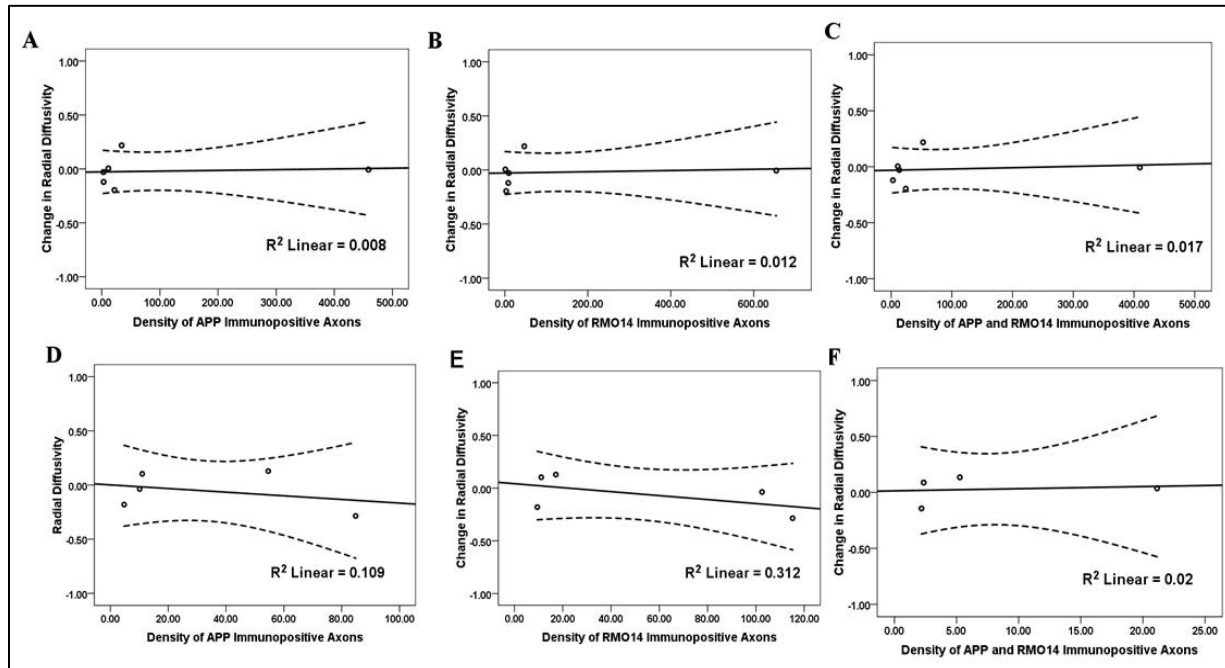


**Figure 58:** The graphs represent the relationship between the change in radial diffusivity and TAI at twenty-four hours post-TBI within the (A-C) CC (n=6) and (D-F) Och (n=5; in one animal the Och was lost during histological processing).  The change in radial diffusivity (y axis) is represented by the mean radial diffusivity value at twenty-four hours post-TBI minus its corresponding pre-TBI mean radial diffusivity value (diffusivity × $10^{-3}$ mm$^2$/s).  The standard error of the mean radial diffusivity difference is approximately 3% and 1% of CC and Och radial diffusivity mean difference respectively (Table B-3 and B-4).  Density of TAI (x axis) is computed by quantifying the amount of (A, D) β-APP, (B, E) RMO14, or (C, F) β-APP and RMO14 immunopositive axons per mm$^2$ within the ROI.  Each circle represents the data from one rat.  No significant correlation was found between radial diffusivity and TAI.  Dashed lines represent the 95% mean confidence intervals.

**Figure 59:** The graphs represent the relationship between the change in radial diffusivity and TAI at three days post-TBI within the (A-C) CC (n=6) and (D-F) Och (n=6). The change in radial diffusivity (y axis) is represented by the mean radial diffusivity value at three days post-TBI minus its corresponding pre-TBI mean radial diffusivity value (diffusivity × $10^{-3}mm^2$/s). The standard error of the mean radial diffusivity difference is approximately 6% of CC and Och radial diffusivity mean difference (Table B-5 and B-6). Density of TAI (x axis) is computed by quantifying the amount of (A, D) β-APP, (B, E) RMO14, or (C, F) β-APP and RMO14 immunopositive axons per $mm^2$ within the ROI. Each circle represents the data from one rat. No significant correlation was found between radial diffusivity and TAI. Dashed lines represent the 95% mean confidence intervals.
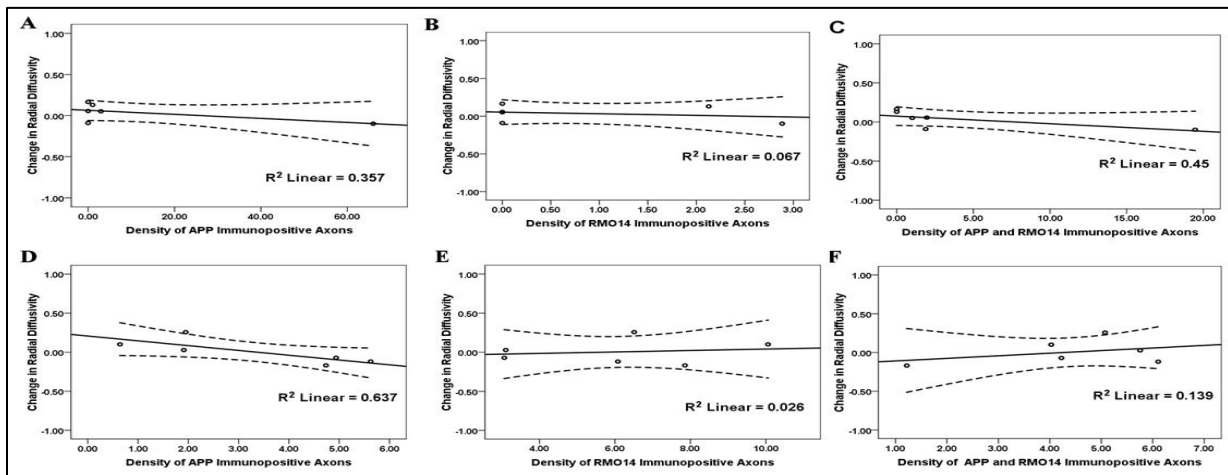


**Figure 60:** The graphs represent the relationship between the change in radial diffusivity and TAI at seven days post-TBI within the (A-C) CC (n=6) and (D-F) Och (n=6). The change in radial diffusivity (y axis) is represented by the mean radial diffusivity value at seven days post-TBI minus its corresponding pre-TBI mean radial diffusivity value (diffusivity × $10^{-3}mm^2$/s). The standard error of the mean radial diffusivity difference is approximately 3% and 6% of CC and Och radial diffusivity mean difference respectively (Table B-7 and B-8). Density of TAI (x axis) is computed by quantifying the amount of (A, D) β-APP, (B, E) RMO14, or (C, F) β-APP and RMO14 immunopositive axons per $mm^2$ within the ROI. Each circle represents the data from one rat. No significant correlation was found between radial diffusivity and TAI except for (D) a positive linear correlation present between radial diffusivity change and β-APP immunopositive axons within the Och with $R^2$ = 0.735 (p<0.05). Dashed lines represent the 95% mean confidence intervals.

*Data Pooling To Increase Sample Size*

Since insignificant correlation may be related to the small sample size the data across all time points were pooled together increasing the sample size from n=6 to n=24. After pooling the data together all the relationships between DTI parameters (FA, diffusion trace, AD, and RD) and TAI density (β-APP density, RMO14 density and β-APP and RMO14 density) was insignificant in the CC and Och. In addition further increase to the sample size was attained by pooling the data of the CC and Och across all time points together further increasing the sample size to n= 48. Even with a sample size of forty-eight the relationship between DTI parameters and TAI still remained insignificant.

## Specific Aim 1 Discussion

Hypothesis 1: The severity of axonal injury is characterized by the retraction ball and axonal swelling count. Therefore, the severity of DAI will correlate with the DTI parameters (FA, ADC, AD and RD). The changes in retraction ball and swollen axons counts will correlate with the DTI parameter changes over time, since DTI parameter changes are dependent on the axonal integrity.

### Fractional Anisotropy and Traumatic Axonal Injury

This study was unable to demonstrate any linear relationship between FA and the histological quantification TAI injury at the various time points of four hours, twenty-four hours, three days and seven days post-TBI (Figures 40 – Figures 46). The lack of linear relationship between TAI and FA is in opposition to our hypothesis, one that states that the changes in retraction ball and swollen axons counts (TAI density) will correlate with the DTI parameter changes over time, since DTI parameter changes are dependent on the axonal integrity.

At the acute stage of the injury at four hours and twenty-four hours no relationship was found between FA and TAI density, which is contradictory to the MacDonald et al study (Mac

Donald, Dikranian et al. 2007).  Mac Donald et al demonstrated that a linear relationship exists between relative anisotropy (RA) and TAI density (density of β-APP positive axons) within the CC at acute time point (four hrs and twenty-four hours combined).  RA is similar to FA in that it describes the degree of anisotropic diffusion in the tissue.  The MacDonald et al study utilized a controlled cortical impact (CCI) injury model (penetrating injury model) to induce moderately severe TBI in ten male and female mice.  These mice were imaged at four to six hours post-TBI and/or at twenty-four hours post-TBI.  The mice data from four hours and twenty-four were pooled together and compared with histology.  This study utilized Marmarou weight-drop model (non-penetrating injury model) to induce sever TBI in twenty-four Sprague Dawley rats (n=6 for each survival time, refer to table 5).  These rats were imaged at four hours, twenty-four hours, three days and seven days post-TBI.  The imaging results for each time point were compared with histology.  The main difference between these two studies is the type of impact model utilized.  The CCI model utilized by MacDonald et al requires a craniotomy to be performed in order to induce TBI by a tip of an impactor pressing down onto the brain dura.  The Marmarou weight drop model utilized in this study is a closed head injury model and, thereby, the skull remains intact during induction of TBI.  One of the noticeable differences between the two injury models is that the brain injured with the weight drop model has tissue that appears to be normal and intact; however, the brain injured by the CCI model has brain tissue which appears to be distorted by the injury induction (Figure 61).  MacDonald et al reported that part of the injuries produced by the CCI in their study was contusion in the cortex, hippocampus directly underlying the impactor tip, and pericontusional WM injuries in surrounding the regions of CC and external capsule.  In the control cortical injury model, the disruption to the brain was most prominent at the epicenter of the injury at the cortex, white matter tracts, and hippocampus and was apparent in all imaging modalities (Mac Donald, Dikranian et al. 2007).  Mac Donald et al omitted the epicenter from the ROI of the study and analysed only areas with intact white matter.  Even though the epicenter was eliminated from the analysis, the sections that were further analysed

by Mac Donald et al still demonstrated a slight distortion between the gray and white matter due to the injury induction (Figures 61).  In contrast, in this study all the tissues demonstrated no distortion and were similar to the control by visual inspection (Figure 40 and Figure 41 B), with the only difference between the control and injured brain being the presence of TAI as it was observed under the microscope.
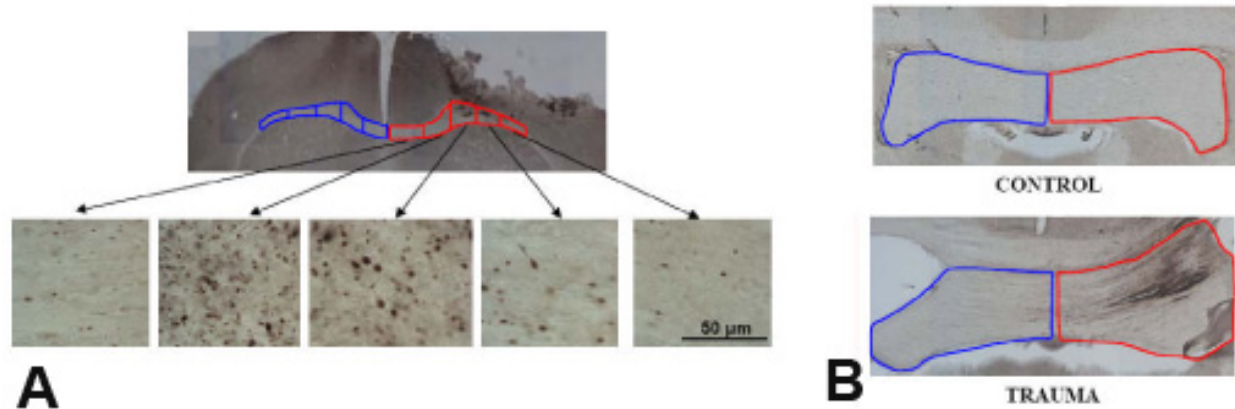


**Figure 61:**This is a representation of injured mice brain tissue from the MacDonald et al study. (A) Represents the ROI within the CC analysed.  Note on the right side of the CC outlined in red (injury induction side) the tissue is distorted.  (B) Represents the ROI within the hippocampal commissure analysed.  Note on the right side of the hippocampal commissure outlined in red that the tissue is distorted. (Mac Donald, Dikranian et al. 2007).

Additionally, another inconsistency between this study and the Mac Donald et al study is the fact that Mac Donald et al reported a constant decrease in the RA value across all injured animals.  This study on the other hand has detected both increase and decrease of the FA value in the injured rats.  Previous clinical research has reported a decrease in FA in mild and in moderate to severe TBI patients in comparison to the control (Arfanakis, Haughton et al. 2002; Inglese, Makani et al. 2005; Benson, Meda et al. 2007; Kraus, Susmaras et al. 2007; Xu, Rasmussen et al. 2007; Rutgers, Fillard et al. 2008; Sidaros, Engberg et al. 2008; Lipton, Gulko et al. 2009; Kumar, Saksena et al. 2010; Kinnunen, Greenwood et al. 2011).  In 2007, Bazarian et al  first  reported an increase in the FA value in mild TBI patients (Bazarian, Zhong et al. 2007).  Bazarian et al reported an increase FA value in the fiftieth percentile of the FA quantile

analysis. Another clinical study by Wilde et al in 2008 also reported an increase of the CC FA in eight mild TBI patients and a decrease of the CC FA in two of the mild TBI cases (Wilde, McCauley et al. 2008). In addition, in 2010 two studies by Mayer et al and Chu et al also reported an increase in FA value in mild TBI patients (Chu, Wilde et al. 2010; Mayer, Ling et al. 2010). It is worth noting that all the studies that have reported an increase in FA were of mild TBI clinical cases.

In this study the animals were injured from a two meters drop height in order to induce severe TBI; however the CC TAI injuries in this study were widely variable (refer to Chapter 3). Note, many previous studies focused their TAI findings to the brainstem structures since TAI density is greater in the brainstem in comparison to cortical WM (Povlishock, Marmarou et al. 1997; Okonkwo, Pettus et al. 1998; Buki, Walker et al. 2000; Stone, Singleton et al. 2000; Stone, Singleton et al. 2001; Suehiro, Singleton et al. 2001; Stone, Okonkwo et al. 2004; Marmarou, Walker et al. 2005; Marmarou and Povlishock 2006). In comparison to the Mac Donald et al paper, this study's TAI density appears less severe. Thus the Mac Donald CC TAI densities are representative of severe TAI whereas in this study the TAI densities are more comparable to mild TAI. Since the TAI density profiles in these rats are more comparable to mild TAI, the variations (increase and decrease) in the FA change post injuries are similar to the variations found clinically (Arfanakis, Haughton et al. 2002; Bazarian, Zhong et al. 2007; Kraus, Susmaras et al. 2007; Rutgers, Fillard et al. 2008; Wilde, McCauley et al. 2008; Chu, Wilde et al. 2010; Mayer, Ling et al. 2010; Kinnunen, Greenwood et al. 2011).

## Diffusion Trace and Traumatic Axonal Injury

Diffusion trace is another DTI parameter that was studied while its linear relationship to the density of TAI in the CC and Och was investigated. A significant linear correlation was found between the diffusion trace and TAI density at four hours post-TBI and seven days post-TBI. At four hours post-TBI the Och demonstrated a positive linear relationship between TAI

densities represented by β-APP positive axons and the change in diffusion trace after TBI (Figures 49 D).  In addition, at seven days post-TBI within the CC a negative linear relationship was found between diffusion trace and TAI densities represented by positive immunolabeled β-APP axons or dual immunolabeled β-APP and RMO14 (Figures 52 A and C).  Unlike the positive linear correlation within the Och at four hours post-TBI, the negative linear relationship within the CC at seven days post-TBI occurs due to an outlier in the data.  To further investigate the impact of this outlier to this linear relationship a non-parameteric test (Pearson's rank order correlation) was carried out since non-parametric testing is much less sensitive to outliers.  The Pearson's rank order correlation test demonstrated that the linear relationship at seven days post-TBI within the CC is not significant and thus the original linear significance was due to the outlier.

## Axial and Radial Diffusivity and Traumatic Axonal Injury

Axial diffusivity changes after TBI demonstrated insignificant linear relationship with TAI.  On the other hand, the radial diffusivity changes after TBI demonstrated a significant linear relationship within the Och at four hours and seven days post-TBI.  A negative linear relationship was present between change radial diffusivity at four hours post-TBI and TAI densities represented by immunopositive β-APP axons (Figures 57).

This study is the first study to look at the various DTI parameter (trace, AD, RD) and TAI density relationships.  The Mac Donald et al study only determined the linear relationship between RA and TAI (Mac Donald, Dikranian et al. 2007).  The lack of linear relationship within the corpus callosum may be due to the fact that CC TAI density is widely variable whereas the Och TAI density are less variable (refer to Chapter 3).

## Water Diffusion and the b Value

The lack of correlation between TAI densities of DTI parameters may stem from the b value utilized in acquiring the DTI images. Water diffusion within neuronal tissue as it is detected by DTI can be subdivided into compartments in relationship to its diffusion rate. Water diffusion can be assigned to either a fast diffusion compartment or a slow diffusion compartment (Assaf and Cohen 1996; Clark and Le Bihan 2000; Inglis, Bossart et al. 2001; Le Bihan, Mangin et al. 2001). The fast diffusion compartment is thought to be the extracellular space, and the slow diffusion compartment is thought to be the intracellular space (Clark and Le Bihan 2000; Inglis, Bossart et al. 2001; Le Bihan, Mangin et al. 2001). In DTI the range of b value utilized during image acquisition can depict water diffusion within either the extracellular space or the intracellular space. A low b value range up to approximately 1500 $s/mm^2$ describes the fast water diffusion and thus represents diffusion within the extracellular space (Clark and Le Bihan 2000). On the other hand, a large b value greater than 1500 $s/mm^2$ describes the slow water diffusion and thereby depicts restricted diffusion within the intracellular space (Clark and Le Bihan 2000). Clinical and experimental studies usually utilize a low b value (less than 1500 $sec/mm^2$) when acquiring DTI (Clark and Le Bihan 2000). The TBI clinical and experimental studies described in the introduction have utilized a low b value in their DTI acquisition. These studies have utilized DTI to study TAI; however; utilizing a low b value in these studies is problematic because TAI is an intracellular injury. However, these studies have suggested that the changes detected by DTI are suggestive of TAI.

Similar to the described studies, this study also utilized a low b value of 800 $sec/mm^2$ and attempted to correlate the changes in the DTI parameters with TAI density. Our original hypothesis based on previous clinical and laboratory research described in the introductory section was found to be unsupported by the lack of relationships between DTI parameters and TAI density. The most critical point that has been overlooked by the other studies in relating the

TAI with DTI changes is the b value. When utilizing a small b value it is the anisotropic tortuosity of the extracellular spaces between aligned fibers that are being examined rather than the restricted diffusion inside the axons (Clark and Le Bihan 2000; Le Bihan, Mangin et al. 2001). Thereby, any change detected as a result of TBI may be a result of an indirect relationship between the extracellular and intracellular environment during TAI such as, increased membrane permeability (Pettus, Christman et al. 1994; Pettus and Povlishock 1996; Povlishock, Marmarou et al. 1997; Okonkwo, Pettus et al. 1998; Stone, Okonkwo et al. 2004).

## Specific Aim 2 Results

**Specific Aim 2:** Determining if the DTI parameters can effectively trace the injury profile as time progresses.

**Table 6:** MRI analysis is divided into four groups (groups A-D). Group A represents pre-TBI and 4hrs post-TBI MRI data from all survival groups (group 1-4). Group B represents pre-TBI, 4 hrs and 24 hrs post-TBI MRI data from survival groups 2-4. Group C represents pre-TBI, 4hrs, 24 hrs and 3days post-TBI MRI data from survival group 3-4. Group D represents pre-TBI, 4hrs, 24 hrs, 3 days and 7days post-TBI MRI data from survival group 4.

| MR Analysis Groups | Survival Groups (Table 1) | | | |
|---|---|---|---|---|
| | Group 1 (n=6) | Group 2 (n=6) | Group 3 (n=6) | Group 4 (n=6) |
| **Group A (n=24)** | Pre-TBI MRI<br>4hrs post-TBI MRI | Pre-TBI MRI<br>4hrs post-TBI MRI | Pre-TBI MRI<br>4hrs post-TBI MRI | Pre-TBI MRI<br>4hrs post-TBI MRI |
| **Group B (n=18)** | | Pre-TBI MRI<br>4hrs post-TBI MRI<br>24hrs post-TBI MRI | Pre-TBI MRI<br>4hrs post-TBI MRI<br>24hrs post-TBI MRI | Pre-TBI MRI<br>4hrs post-TBI MRI<br>24hrs post-TBI MRI |
| **Group C (n=12)** | | | Pre-TBI MRI<br>4hrs post-TBI MRI<br>24hrs post-TBI MRI<br>3days post-TBI MRI | Pre-TBI MRI<br>4hrs post-TBI MRI<br>24hrs post-TBI MRI<br>3days post-TBI MRI |
| **Group D (n=6)** | | | | Pre-TBI MRI<br>4hrs post-TBI MRI<br>24hrs post-TBI MRI<br>3days post-TBI MRI<br>7days post-TBI MRI |

The rats were organized into four groups for imaging analyses. The imaging groups are denoted as group A thorough D (Table 6). Group A represents MRI data of all rats imaged at four hours post-TBI and their corresponding pre-TBI MRI data (n=24). Group B represents data

from rats imaged at twenty-four hours post-TBI and their corresponding pre-TBI and four hours post-TBI MRI data (n = 18).  Group C represents data from rats imaged at three days post-TBI and their corresponding pre-TBI four hours and twenty-four hours post-TBI MRI data (n = 12). Group C represents data from rats imaged at seven days post-TBI and their corresponding pre-TBI, four hours, twenty-four hours, and 3days post-TBI MRI data (n = 6).

Table 7 and 8 summarizes the DTI parameters (FA, AD, RD, diffusion trace) values and the normalized T2 values for group A – D.  For detailed explanation of the DTI parameters and T2 refer to chapter 3.  Table 7 and 8 represents the central tendency of the DTI parameters and normalized T2 within each group by the median rather than mean. The median was utilized because the data distribution within each group (group A – D) was not normally distributed.

**Table 7:** CC DTI parameters values and Normalized T2 values (median $\pm$ std) across all survival time.

| | | Group A (n=24) | Group B (n=18) | Gropu C (n=12) | Group D (n=6) |
|---|---|---|---|---|---|
| **FA** | Pre-TBI | 0.7439 $\pm$ 0.0543 | 0.7428 $\pm$ 0.0595 | 0.7453 $\pm$ 0.0602 | 0.7300 $\pm$ 0.0374 |
| | 4hrs Post-TBI | 0.7231 $\pm$ 0.0981 | 0.7162 $\pm$ 0.0979 | 0.7226 $\pm$ 0.0995 | 0.6684 $\pm$ 0.0946 |
| | 24hrs Post-TBI | | 0.7327 $\pm$ 0.0952 | 0.7464 $\pm$ 0.0973 | 0.7297 $\pm$ 0.0386 |
| | 3days Post-TBI | | | 0.7582 $\pm$ 0.1071 | 0.7765 $\pm$ 0.0509 |
| | 7days Post-TBI | | | | 0.7217 $\pm$ 0.0482 |
| **AD** | Pre-TBI | 1.5822 $\pm$ 0.2349 | 1.6753 $\pm$ 0.2504 | 1.6213 $\pm$ 0.2176 | 1.7007 $\pm$ 0.1970 |
| | 4hrs Post-TBI | 1.6307 $\pm$ 0.2887 | 1.6307 $\pm$ 0.2686 | 1.7493 $\pm$ 0.3100 | 1.8757 $\pm$ 0.1402 |
| | 24hrs Post-TBI | | 1.627 $\pm$ 0.3024 | 1.7181 $\pm$ 0.3322 | 1.7639 $\pm$ 0.2708 |
| | 3days Post-TBI | | | 1.7302 $\pm$ 0.3749 | 1.9601 $\pm$ 0.1909 |
| | 7days Post-TBI | | | | 1.9387 $\pm$ 0.1501 |
| **RD** | Pre-TBI | 0.3818 $\pm$ 0.0995 | 0.3909 $\pm$ 0.1123 | 0.3699 $\pm$ 0.1087 | 0.4321 $\pm$ 0.0934 |
| | 4hrs Post-TBI | 0.4080 $\pm$ 0.1610 | 0.4250 $\pm$ 0.1760 | 0.4250 $\pm$ 0.1816 | 0.5190 $\pm$ 0.1548 |
| | 24hrs Post-TBI | | 0.4201 $\pm$ 0.1587 | 0.4166 $\pm$ 0.1709 | 0.4287 $\pm$ 0.0256 |
| | 3days Post-TBI | | | 0.3650 $\pm$ 0.1835 | 0.3721 $\pm$ 0.0965 |
| | 7days Post-TBI | | | | 0.4958 $\pm$ 0.0776 |
| **Trace** | Pre-TBI | 2.3436 $\pm$ 0.3943 | 2.4776 $\pm$ 0.4366 | 2.4000 $\pm$ 0.3969 | 2.5758 $\pm$ 0.3475 |
| | 4hrs Post-TBI | 2.4937 $\pm$ 0.4652 | 2.5014 $\pm$ 0.4907 | 2.5199 $\pm$ 0.5167 | 2.8816 $\pm$ 0.3780 |
| | 24hrs Post-TBI | | 2.3712 $\pm$ 0.3591 | 2.3495 $\pm$ 0.3328 | 2.6265 $\pm$ 0.2965 |
| | 3days Post-TBI | | | 2.5123 $\pm$ 0.4715 | 2.7207 $\pm$ 0.2894 |
| | 7days Post-TBI | | | | 2.8290 $\pm$ 0.1901 |
| **Normalized T2** | Pre-TBI | 0.8023 $\pm$ 0.1149 | 0.8286 $\pm$ 0.1130 | 0.8023 $\pm$ 0.1166 | 0.8178 $\pm$ 0.1438 |
| | 4hrs Post-TBI | 0.7714 $\pm$ 0.0920 | 0.8028 $\pm$ 0.0926 | 0.7883 $\pm$ 0.0854 | 0.8205 $\pm$ 0.0888 |
| | 24hrs Post-TBI | | 0.7845 $\pm$ 0.0908 | 0.7851 $\pm$ 0.0883 | 0.7358 $\pm$ 0.0741 |
| | 3days Post-TBI | | | 0.8234 $\pm$ 0.1149 | 0.8760 $\pm$ 0.1444 |
| | 7days Post-TBI | | | | 0.7813 $\pm$ 0.0649 |

**Table 8:** Och DTI parameters values and Normalized T2 values (median ± std) across all survival time.

| | | Group A (n=24) | Group B (n=18) | Gropu C (n=12) | Group D (n=6) |
|---|---|---|---|---|---|
| **FA** | Pre-TBI | 0.7307 ± 0.0583 | 0.7431 ± 0.0602 | 0.7447 ± 0.5645 | 0.7300 ± 0.0374 |
| | 4hrs Post-TBI | 0.6846 ± 0.0812 | 0.6957 ± 0.0796 | 0.6846 ± 0.8649 | 0.6684 ± 0.0946 |
| | 24hrs Post-TBI | | 0.7391 ± 0.0895 | 0.7321 ± 0.0569 | 0.7297 ± 0.0386 |
| | 3days Post-TBI | | | 0.7582 ± 0.0871 | 0.7765 ± 0.0509 |
| | 7days Post-TBI | | | | 0.7438 ± 0.0587 |
| **AD** | Pre-TBI | 1.6215 ± 0.3494 | 1.5584 ± 0.2947 | 1.5732 ± 0.2536 | 1.7007 ± 0.1970 |
| | 4hrs Post-TBI | 1.7614 ± 0.3299 | 1.8545 ± 0.3504 | 1.8545 ± 0.3308 | 1.8757 ± 0.1402 |
| | 24hrs Post-TBI | | 1.5529 ± 0.2937 | 1.6167 ± 0.2672 | 1.7639 ± 0.2708 |
| | 3days Post-TBI | | | 1.4879 ± 0.4292 | 1.9601 ± 0.1909 |
| | 7days Post-TBI | | | | 1.7960 ± 0.4893 |
| **RD** | Pre-TBI | 0.4573 ± 0.1096 | 0.4218 ± 0.1095 | 0.3889 ± 0.1096 | 0.4321 ± 0.0934 |
| | 4hrs Post-TBI | 0.4823 ± 0.1396 | 0.4636 ± 0.1517 | 0.4487 ± 0.1570 | 0.5190 ± 0.1548 |
| | 24hrs Post-TBI | | 0.4047 ± 0.1237 | 0.4047 ± 0.0940 | 0.4287 ± 0.0256 |
| | 3days Post-TBI | | | 0.3721 ± 0.1007 | 0.3721 ± 0.0965 |
| | 7days Post-TBI | | | | 0.4910 ± 0.2260 |
| **Trace** | Pre-TBI | 2.5558 ± 0.4960 | 2.2724 ± 0.4600 | 2.2577 ± 0.4038 | 2.5758 ± 0.3475 |
| | 4hrs Post-TBI | 2.6671 ± 0.5010 | 2.6671 ± 0.5501 | 2.6186 ± 0.5023 | 2.8816 ± 0.3780 |
| | 24hrs Post-TBI | | 2.4582 ± 0.4470 | 2.4322 ± 0.4047 | 2.6265 ± 0.2965 |
| | 3days Post-TBI | | | 2.3299 ± 0.5347 | 2.7207 ± 0.2894 |
| | 7days Post-TBI | | | | 2.8321 ± 0.9509 |
| **Normalized T2** | Pre-TBI | 0.4494 ± 0.0396 | 0.4492 ± 0.0408 | 0.4492 ± 0.0395 | 0.4605 ± 0.0413 |
| | 4hrs Post-TBI | 0.4349 ± 0.0433 | 0.4347 ± 0.0418 | 0.4347 ± 0.0300 | 0.4427 ± 0.0351 |
| | 24hrs Post-TBI | | 0.4710 ± 0.0480 | 0.4710 ± 0.0478 | 0.4701 ± 0.0540 |
| | 3days Post-TBI | | | 0.4408 ± 0.0460 | 0.4421 ± 0.0641 |
| | 7days Post-TBI | | | | 0.4143 ± 0.0429 |

### *Group A*

For this group (n=24) MRI data were acquired at pre-TBI and four hours post induction of TBI. The MRI changes detected between pre-TBI and four hours post-TBI in this group were statistically significant (Figure 62).

Corpus Callosum

Refer to Table 8 for the summary of the CC median values of the DTI parameters and normalized T2 across survival time.

*Fractional Anisotropy*

After induction of TBI the FA decreased from 0.7439±0.0543 (median ± std) pre-TBI to 0.7231± 0.0982 four hours post-TBI (Figure 62 A). In addition to the decrease of central

tendency of the FA values, the FA distribution became more spread out at four hours post-TBI (Figure 62 A). At four hours post-TBI the interquartile range (IQR) of the FA distribution increased from 0.0744 pre-TBI (25th percentile = 0.6966, 75th percentile = 0.7710) to 0.1328 four hours post-TBI (25th percentile = 0.6507, 75th percentile = 0.7835). IQR is a measurement of variability between the 25th and 75th percentile and it is not affected by outliers or extreme values. The range of the FA distribution increased from 0.18 ($FA_{min}$ = 0.65, $FA_{max}$ = 0.83) pre-TBI to 0.37 ($FA_{min}$ = 0.51, $FA_{max}$ = 0.88) four hours post-TBI.

*Axial Diffusivity*

After induction of TBI the AD increased from 1.5822$\pm$0.2350 (median $\pm$ std) pre-TBI to 1.6307$\pm$ 0.2887 four hours post-TBI (Figure 62 C). In addition to the increase of central tendency of the AD values, the AD distribution became less spread out at four hours post-TBI (Figure 62 C). At four hours post-TBI the IQR of the AD distribution decreased from 0.4089 pre-TBI (25th percentile = 1.4675, 75th percentile = 1.8764) to 0.3290 four hours post-TBI (25th percentile = 1.5619, 75th percentile = 1.8909). On the other hand, the range of the AD distribution increased from 0.93 ($AD_{min}$ = 1.15, $AD_{max}$ = 2.03) pre-TBI to 1.41 ($AD_{min}$ = 1.09, $AD_{max}$ = 2.49) four hours post-TBI. The maximum value in the AD distribution at four hours post-TBI was a mild outlier (mild outliers lie between 1.5 and 3 IQR) of the data. Furthermore, the AD distribution became negatively skewed at four hours post-TBI in comparison to the pre-TBI AD distribution.

*Radial Diffusivity*

After induction of TBI the RD increased from 0.3818$\pm$0.0995 (median $\pm$ std) pre-TBI to 0.4080$\pm$ 0.1610 four hours post-TBI (Figure 62 E). In addition to the increase of central tendency of the RD values, the RD distribution became more spread out at four hours post-TBI (Figure 62 E). At four hours post-TBI the IQR of the RD distribution increased from 0.1132 pre-TBI (25th percentile = 0.3277, 75th percentile = 0.3818) to 0.1754 four hours post-TBI (25th

percentile = 0.3029, 75$^{th}$ percentile = 0.4783).  As well, the range of the RD distribution increased from 0.41 (RD$_{min}$ = 0.22, RD$_{max}$= 0.63) pre-TBI to 0.64 (RD$_{min}$ = 0.15, RD$_{max}$= 0.79) four hours post-TBI.  Two values in the RD distribution at pre-TBI and two values in the RD distribution at four hours post-TBI demonstrated mild outliers in the data sets.

*Trace Diffusion*

After induction of TBI the trace of the diffusion increased from 2.3436$\pm$0.3943 (median $\pm$ std) pre-TBI to 2.4937$\pm$ 0.4652 four hours post-TBI (Figure 62 G).  In addition to the increase of central tendency of the trace values, the trace distribution became more spread out at four hours post-TBI (Figure 62 G).  At four hours post-TBI the IQR of the trace distribution increased from 0.5495 pre-TBI (25$^{th}$ percentile = 2.1256, 75$^{th}$ percentile = 2.6751) to 0.5865 four hours post-TBI (25$^{th}$ percentile = 2.1273, 75$^{th}$ percentile = 2.7138).  As well, the range of the trace distribution increased from 1.51 (Trace$_{min}$ = 1.78, Trace$_{max}$= 3.29) pre-TBI to 1.60 (Trace$_{min}$ = 1.83, Trace$_{max}$= 3.44) four hours post-TBI.

*Normalized T2*

After induction of TBI the normalized T2 decreased from 0.8023$\pm$0.1149 (median $\pm$ std) pre-TBI to 0.7714$\pm$ 0.0920 four hours post-TBI (Figure 62 I).  In addition to the decrease of central tendency of the normalized T2 values, the normalized T2 distribution became less spread out at four hours post-TBI (Figure 62 I).  At four hours post-TBI the IQR of the normalized T2 distribution decreased from 0.1662 pre-TBI (25$^{th}$ percentile = 0.7212, 75$^{th}$ percentile = 0.8874) to 0.1601 four hours post-TBI (25$^{th}$ percentile = 0.6998, 75$^{th}$ percentile = 0.8599).  As well, the range of the normalized T2 distribution decreased from 0.42 (T2 $_{min}$ = 0.62, T2$_{max}$= 1.04) pre-TBI to 0.28 (T2$_{min}$ = 0.68, T2$_{max}$= 0.96) four hours post-TBI.  Additionally, the normalized T2 distribution became positively skewed at four hours post-TBI in comparison to the pre-TBI normalized T2 distribution.

<u>Optic Chiasm</u>

*Fractional Anisotropy*

After induction of TBI the FA decreased from $0.7307\pm0.05833$ (median $\pm$ std) pre-TBI to $0.6846\pm$ 0.08125 four hours post-TBI (Figure 62 B). In addition to the decrease of central tendency of the FA values, the FA distribution became more spread out at four hours post-TBI (Figure 62 B). At four hours post-TBI the IQR of the FA distribution increased from 0.0865 pre-TBI ($25^{th}$percentile = 0.6667, $75^{th}$ percentile = 0.7532) to 0.1016 four hours post-TBI ($25^{th}$ percentile = 0.6361, $75^{th}$ percentile = 0.7376). As well, the range of the FA distribution increased from 0.21 ($FA_{min}$ = 0.62, $FA_{max}$= 0.83) pre-TBI to 0.34 ($FA_{min}$ = 0.51, $FA_{max}$= 0.85) four hours post-TBI.

*Axial Diffusivity*

After induction of TBI the AD increased from $1.6215\pm0.3495$ (median $\pm$ std) pre-TBI to $1.7614\pm$ 0.3299 four hours post-TBI (Figure 62 D). In addition to the increase of central tendency of the AD values, the AD distribution became more spread out at four hours post-TBI (Figure 62 D). At four hours post-TBI the IQR of the AD distribution increased from 0.4378 pre-TBI ($25^{th}$ percentile = 1.4947, $75^{th}$ percentile = 1.9325) to 0.4844 four hours post-TBI ($25^{th}$ percentile = 1.5241, $75^{th}$ percentile = 2.0085). In addition, the range of the AD distribution increased from 1.25 ($AD_{min}$ = 1.19, $AD_{max}$= 2.44) pre-TBI to 1.38 ($AD_{min}$ = 1.15, $AD_{max}$= 2.52) four hours post-TBI.

*Radial Diffusivity*

After induction of TBI the RD increased from $0.4573\pm$ 0.1096 (median $\pm$ std) pre-TBI to $0.4823\pm$ 0.1396 four hours post-TBI (Figure 62 F). In addition to the increase of central tendency of the RD values, the RD distribution became less spread out at four hours post-TBI (Figure 62 F). At four hours post-TBI the IQR of the RD distribution increased from 0.1861 pre-

TBI (25$^{th}$ percentile = 0.3529, 75$^{th}$ percentile = 0.5390) to 0.1369 four hours post-TBI (25$^{th}$ percentile = 0.4209, 75$^{th}$ percentile = 0.5578). However, the range of the RD distribution increased from 0.37 (RD$_{min}$ = 0.30, RD$_{max}$= 0.67) pre-TBI to 0.59 (RD$_{min}$ = 0.19, RD$_{max}$= 0.79) four hours post-TBI. The increase in the range of the RD distribution at four hours post-TBI occurred as a result of two mild outlier, one outlier at each end of the data distribution.

*Trace Diffusion*

After induction of TBI the trace of the diffusion increased from 2.5558$\pm$ 0.4960 (median $\pm$ std) pre-TBI to 2.6671$\pm$ 0.5010 four hours post-TBI (Figure 62 H). In addition to the increase of central tendency of the trace values, the trace distribution became less spread out at four hours post-TBI (Figure 62 H). At four hours post-TBI the IQR of the trace distribution decreased from 0.8728 pre-TBI (25$^{th}$ percentile = 2.0632, 75$^{th}$ percentile = 2.9360) to 0.7629 four hours post-TBI (25$^{th}$ percentile = 2.3402, 75$^{th}$ percentile = 3.1031). On the other hand, the range of the trace distribution increased from 1.74 (Trace$_{min}$ = 1.88, Trace$_{max}$= 3.62) pre-TBI to 1.78 (Trace$_{min}$ = 1.79, Trace$_{max}$= 3.57) four hours post-TBI.

*Normalized T2*

After induction of TBI the normalized T2 decreased from 0.4492$\pm$0.0396 (median $\pm$ std) pre-TBI to 0.4349$\pm$ 0.0433 four hours post-TBI (Figure 62 J). In addition to the decrease of central tendency of the normalized T2 values, the normalized T2 distribution became less spread out at four hours post-TBI (Figure 62 J). At four hours post-TBI the IQR of the normalized T2 distribution decreased from 0.0678 pre-TBI (25$^{th}$ percentile = 0.4295, 75$^{th}$ percentile = 0.4973) to 0.0580 four hours post-TBI (25$^{th}$ percentile = 0.4128, 75$^{th}$ percentile = 0.4707). However, the range of the normalized T2 distribution increased from 0.15 (T2 $_{min}$ = 0.39, T2$_{max}$= 0.54) pre-TBI to 0.18 (T2$_{min}$ = 0.38, T2$_{max}$= 0.56) four hours post-TBI. The increase in the range of the normalized distribution at four hours post-TBI occurred as a result of mild outliers at the maximum value of the data distribution.
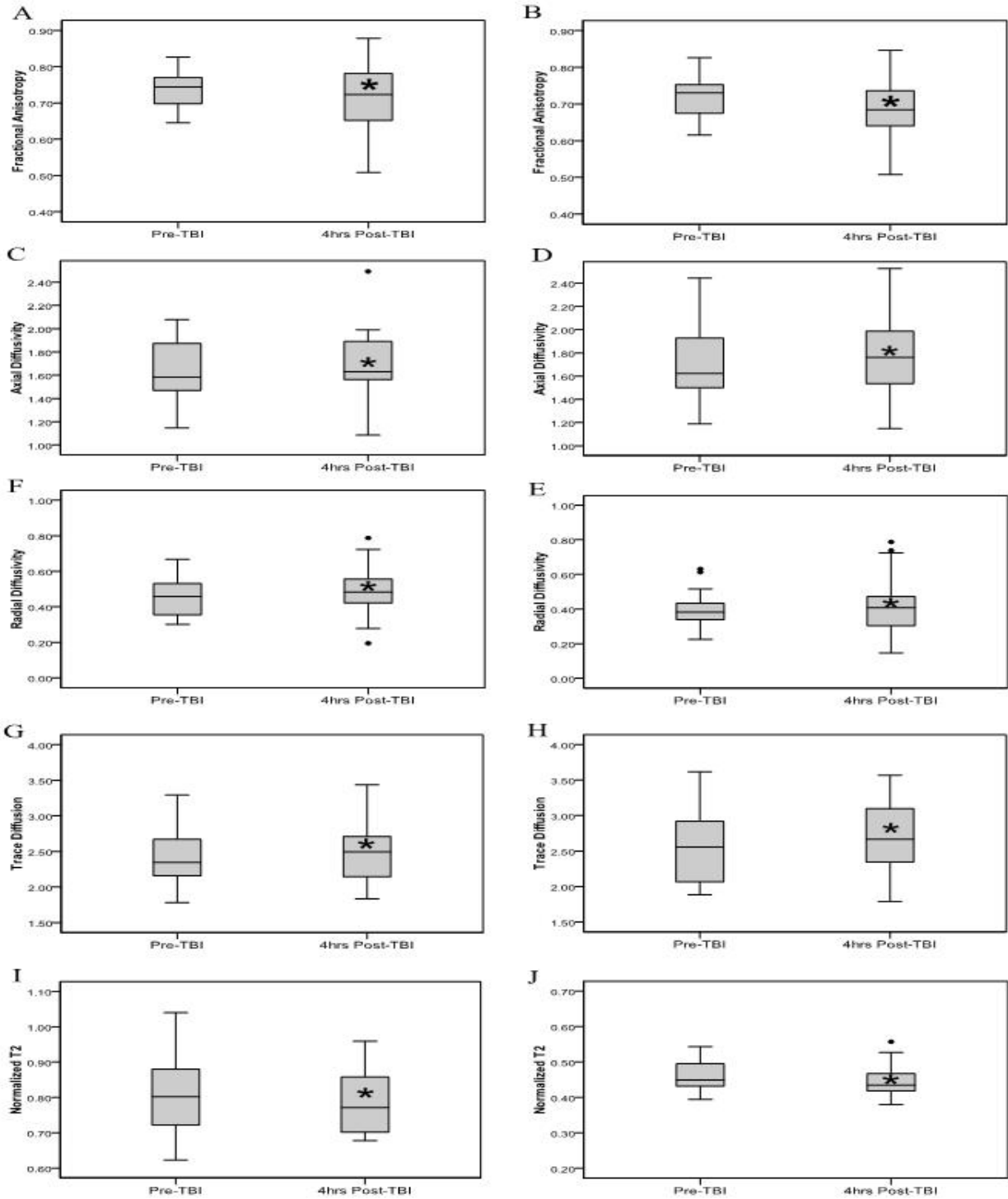
**Figure 62**: Group A's average(n=24)  (A, B) FA, (C, D) AD, (E, F) RD, (G, H) diffusion trace, and (I, J) T2 values at pre-TBI and four hours post-TBI within the CC (left column) and Och (right column). Diffusivity unit of measurement is $10^{-3}$ mm$^2$/s. The · represent the mild outliers in the data set.  * represents statistical significance ($p<0.05$) between pre-TBI and post-TBI rats.
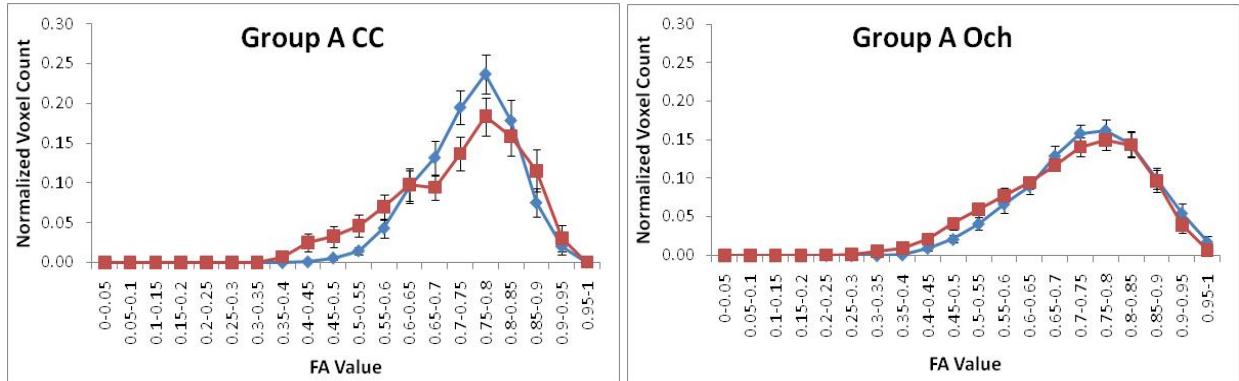
**Figure 63:** FA histograms of the CC V-like shape ROI (left) and Och (right) for all rats (n=24) in group A. The histograms are group average histograms at pre-TBI (blue, diamond) and four hours post-TBI (red, square). The FA total range (x-axis) was divided into twenty equally spaced bins of 0.05 with marker (diamond or square) representing each bin. Error bars represent the standard error.

**Table 9:** Comparison of the CC FA histogram shape parameters.

| CC | Pre-TBI | | 4hrs Post-TBI | | Difference |
|---|---|---|---|---|---|
| Parameter | Mean | Std Error | Mean | Std Error | Post - Pre |
| Skewness | -0.534 | 0.013 | -0.631 | 0.013 | -0.097 |
| Kurtosis | 0.131 | 0.027 | -0.362 | 0.026 | -0.493 |
| FA Mean | 0.7341 | 0.0049 | 0.7148 | 0.00069 | -0.0193 |

**Table 10:** Comparison of the Och FA histogram shape parameters.

| Och | Pre-TBI | | 4hrs Post-TBI | | Difference |
|---|---|---|---|---|---|
| Parameter | Mean | Std Error | Mean | Std Error | Post - Pre |
| Skewness | -0.283 | 0.013 | -0.233 | 0.012 | 0.05 |
| Kurtosis | -0.45 | 0.026 | -0.608 | 0.025 | -0.158 |
| FA Mean | 0.7281 | 0.00065 | 0.6776 | 0.00069 | -0.0505 |

At four hours post-TBI the FA histograms (Figure 63) revealed a widening of the voxel base distribution. A small shift to the left, which represents voxel base distribution FA value decrease, is present within the CC and Och. However, within the CC at four hours post-TBI a small amount of voxels did demonstrate an increase in their FA value (Figure 63). In addition, other shape changes also occurred at four hours post-TBI compared to pre-TBI (Tables 9-10). These shape changes included negative kurtosis in CC and Och and skewness (negative in CC and positive in Och). FA histogram of the four hours post-TBI data is also more variable

compared to the pre-TBI histogram.  At four hours post-TBI the FA data distribution is more platykurtic (less peaked about its mean than the normal distribution) in comparison to pre-TBI (Tables 9 and 10).

<u>TBI outcome Detected in MRI Alteration in Individual Rats</u>

The data distributions discussed above, group A were derived from twenty-four rats imaged at pre-TBI and four hours post-TBI.  The MRI changes detected within these animals' pre-TBI and four hours post-TBI were not uniform across all rats (Figure 64).  Within the CC ROI eleven rats demonstrated a significant decrease in their FA values, ten rats demonstrated a significant increase in their FA values, whereas three rats demonstrated insignificant changes in their FA values at four hours post-TBI in comparison to pre-TBI (Figure 64 A).  Within the Och sixteen rats demonstrated a significant decrease in their FA values, seven rats demonstrated a significant increase in their FA values, but only one rat demonstrated insignificant changes in its FA values at four hours post-TBI in comparison to pre-TBI (Figure 64 B).On average both CC and Och illustrated a decrease in the FA values at four hours post-TBI in comparison to pre-TBI. The Och demonstrated a greater decrease in the FA values at four hours post-TBI in comparison to the CC.  In addition, the FA changes at four hours post-TBI were not consistent in each rat between the two (CC and Och) ROI (Figure 64 A, B).  For the FA voxel base distribution of each rat refer to appendix C.

Additionally, the diffusivitybehaviors across the individual rats were as follows.  Within the CC ROI twelve rats demonstrated a significant decrease in their AD values, ten rats demonstrated a significant increase in their AD values, while two rats demonstrated insignificant changes in their FA values at four hours post-TBI in comparison to pre-TBI (Figure 64 C). Within the Och fifteen rats demonstrated a significant decrease in their AD values, eight rats demonstrated a significant increase in their AD values, but only one rat demonstrated insignificant changes in its AD values at four hours post-TBI in comparison to pre-TBI (Figure 64

D).Conversely, more rats demonstrated RD increase rather than decrease at four hours post-TBI within the CC and Och (Figure 64 E and F).  Within the CC ROI eleven rats demonstrated a significant decrease in the RD value while thirteen rats demonstrated a significant increase in the RD value at four hours post-TBI in comparison to pre-TBI (Figure 64 E).  Within the Och seven rats demonstrated a significant decrease in their RD values, sixteen rats demonstrated a significant increase in their RD values, and only one rat demonstrated insignificant changes in its RD values at four hours post-TBI in comparison to pre-TBI (Figure 64 F).On average, the CC illustrated an increase in the AD values at four hours post-TBI in comparison to pre-TBI whereas the Och illustrated a decrease in the AD values at four hours post-TBI in comparison to pre-TBI. The RD on average demonstrated an increase in both the CC and Och; however, the Och illustrated a greater increase in RD in comparison to CC at four hours post-TBI.  Within the CC, the diffusion trace decreased in eight rats and increased in fourteen rats at four hours post-TBI in comparison to pre-TBI (Figure 64 G).  Two rats demonstrated no significant change in the diffusion trace within the CC at four hours post-TBI in comparison to pre-TBI (Figure 64 G). Within the Och, the diffusion trace decreased and increased in an equal number of rats (Figure 64 H).  Eleven rats illustrated a decrease in the trace and eleven rats illustrated an increase in the trace at four hours post-TBI in comparison to pre-TBI (Figure 64 G).  Two rats demonstrated no significant change in the diffusion trace within the Och at four hours post-TBI in comparison to pre-TBI (Figure 64 H).  On average, the diffusion trace increased in both the CC and Och; however, the CC demonstrated a greater increase from pre-TBI to four hours post-TBI of the average trace compared to the Och.

The normalized T2 values of these rats also demonstrated various changes at four hours post-TBI within the CC and Och.  Compared to the pre-TBI values, at four hours post TBI the normalized T2 values within the CC decreased in fourteen rats and increased in nine rats (Figure 64 I).Within the Och sixteen rats demonstrated a decrease in their normalized T2 value

while six rats demonstrated an increase in their normalized T2 values at four hours post-TBI in comparison to pre-TBI (Figure 64 J). Only one rat demonstrated a non-significant change in its normalized T2 value within the Och at four hours post-TBI in comparison to its pre-TBI normalized T2 value (Figure 64 J). For the normalized T2 data n=23 because the four hours post-TBI data for one rat was not available.
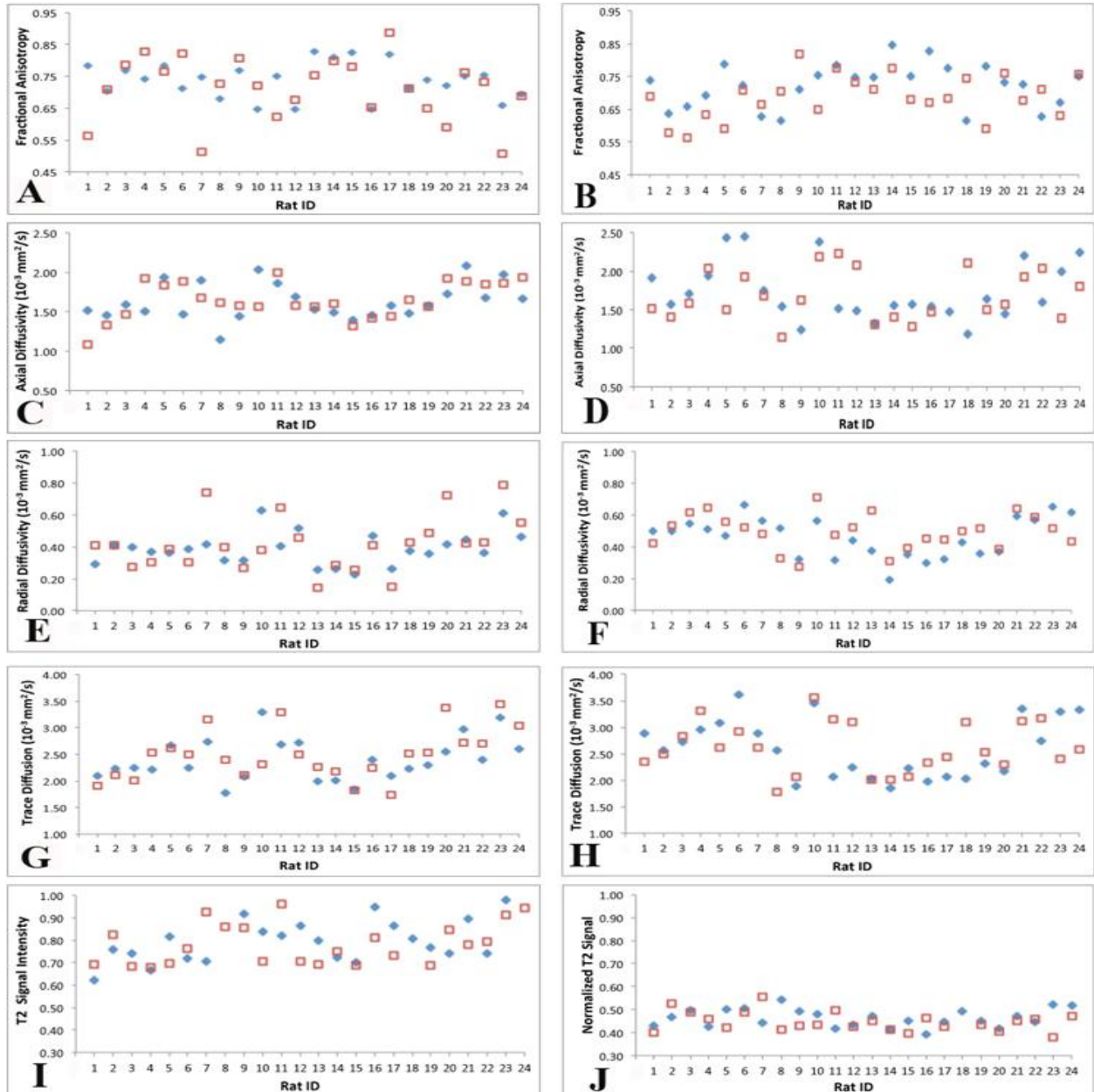


**Figure 64:** Group A's (A, B) FA, (C, D) AD, (E, F) RD, (G, H) diffusion trace, and (I, J) T2 values at pre-TBI (blue diamond) and four hours post-TBI (red square) for each rat within the CC (left column) and Och (right column).

### *Group B*

For this group (n=18) MRI data were acquired at pre-TBI, four hours and twenty-four hours post induction of TBI.  The MRI changes detected between pre-TBI and four hours post-TBI in this group were statistically significant (Figure 65).  The MRI changes detected between pre-TBI and twenty-four hours post-TBI were statistically significant in the CC.  In the optic chiasm the MRI change detected between pre-TBI and twenty-four hours post-TBI were statistically significant except for the RD and trace. Corpus Callosum

### *Fractional Anisotropy*

After induction of TBI the FA decreased from $0.7428 \pm 0.0595$ (median $\pm$ std) pre-TBI to $0.7162 \pm 0.0979$ four hours post-TBI (Figure 65 A). At twenty-four hours post-TBI the FA median increased to $0.7327 \pm 0.0952$ in comparison to four hours post-TBI; however, the FA median remained decreased in comparison to the pre-TBI value.  In addition to the decrease of central tendency of the FA values, the FA distribution became more spread out at four hours and twenty-four hours post-TBI in comparison to pre-TBI FA distribution (Figure 65 A).  At post-TBI the IQR of the FA distribution increased from 0.0944 pre-TBI ($25^{th}$ percentile = 0.6739, $75^{th}$ percentile = 0.7684) to 0.1233 four hours post-TBI ($25^{th}$ percentile = 0.6433, $75^{th}$ percentile = 0.7666) and then to 0.1372 twenty-four hours post-TBI ($25^{th}$ percentile = 0.6593, $75^{th}$ percentile = 0.7965).  As well, the range of the FA distribution increased from 0.18 ($FA_{min}$ = 0.65, $FA_{max}$ = 0.83) pre-TBI to 0.37 ($FA_{min}$ = 0.51, $FA_{max}$ = 0.88) at four hours and at twenty-four hours post-TBI.

### *Axial Diffusivity*

After induction of TBI the AD decreased from $1.6753 \pm 0.2504$ (median $\pm$ std) pre-TBI to $1.6307 \pm 0.2685$ four hours post-TBI and further decreased to $1.6271 \pm 0.3024$ twenty-four hours post-TBI (Figure 65 C).  In addition to the decrease of central tendency of the AD values, the AD distribution became less spread out at four hours post-TBI but then became more

spread out at twenty-four hours post-TBI (Figure 65 C). At four hours post-TBI the IQR of the AD distribution decreased from 0.4107 pre-TBI ($25^{th}$ percentile = 1.4720, $75^{th}$ percentile = 1.8827) to 0.3306 four hours post-TBI ($25^{th}$ percentile = 1.5677, $75^{th}$ percentile = 1.8983) and then increased to 0.5097 twenty-four hours post-TBI ($25^{th}$ percentile = 1.3843, $75^{th}$ percentile = 1.8940). On the other hand, the range of the AD distribution increased from 0.93 ($AD_{min}$ = 1.15, $AD_{max}$ = 2.08) pre-TBI to 1.18 ($AD_{min}$ = 1.31, $AD_{max}$ = 2.49) four hours post-TBI. The maximum value in the AD distribution at four hours post-TBI demonstrated a mild outlier of the data. Furthermore, the AD distribution range increased to 1.07 ($AD_{min}$ = 1.13, $AD_{max}$ = 2.20) at twenty-four hours post-TBI.

*Radial Diffusivity*

After induction of TBI the RD increased from 0.3909$\pm$ 0.1123 (median $\pm$ std) pre-TBI to 0.4250$\pm$ 0.1760 four hours post-TBI (Figure 65 E). At twenty-four hours post-TBI the RD slightly decreased in comparison to four hours post-TBI to 0.4201 $\pm$ 0.1587 (median $\pm$ Std); however, it remained greater than the pre-TBI value (Figure 65 E). In addition to the increase of central tendency of the RD values in comparison to pre-TBI, the RD distribution became more spread out at four hours post-TBI (Figure 65 E). At four hours post-TBI the IQR of the RD distribution increased from 0.1504 pre-TBI ($25^{th}$ percentile = 0.3166, $75^{th}$ percentile = 0.4669) to 0.2225 four hours post-TBI ($25^{th}$ percentile = 0.3548, $75^{th}$ percentile = 0.5774).After four hours post-TBI, the IQR of the RD distribution decreased to 0.1540 at twenty-four hours post-TBI ($25^{th}$ percentile = 0.3048, $75^{th}$ percentile = 0.4589); however, the interquartile ranges at twenty-four hours post-TBI remained larger in comparison to pre-TBI interquartile range. As well, the range of the RD distribution increased from 0.41 ($RD_{min}$ = 0.22, $RD_{max}$ = 0.63) pre-TBI to 0.64 ($RD_{min}$ = 0.15, $RD_{max}$ = 0.79) four hours post-TBI. The range of RD distributions increased after four hours post-TBI to 0.70 ($RD_{min}$ = 0.20, $RD_{max}$ = 0.90). This further increase in the range at twenty-four

hours post TBI occurred due to a maximum extreme outlier (extreme outliers are greater than 3 IQR) in the data at twenty-four hours post-TBI.

*Trace Diffusion*

After induction of TBI the trace of the diffusion increased from 2.477$\pm$ 0.4366 (median $\pm$ std) pre-TBI to 2.501$\pm$ 0.49073four hours post-TBI (Figure 65 G). This increase of trace diffusion is followed by a decrease at twenty-four hours post-TBI where the trace became 2.3712 $\pm$ 0.3591 (Figure 65 G). In addition to the increase at four hours and decrease at twenty-four hours post TBI of the central tendencies, the trace distribution became more spread out at four hours post-TBI and less dispersed at twenty-four hours post-TBI in comparison to the pre-TBI trace distribution (Figure 65 G).At four hours post-TBI the IQR of the trace distribution increased from 0.6700 pre-TBI (25$^{th}$ percentile = 2.0570, 75$^{th}$ percentile = 2.7270) to 0.8522 four hours post-TBI (25$^{th}$ percentile =2.2218, 75$^{th}$ percentile = 3.0739). After four hours post-TBI, the IQR of the trace distribution decreased to 0.5534 at twenty-four hours post TBI (25$^{th}$ percentile = 2.1440, 75$^{th}$ percentile = 2.6975). The IQR of the trace distribution was lower than that of the pre-TBI interquartile range. Similar to the interquartile range, the trace distribution range increased from 1.51 (Trace$_{min}$ = 1.78, Trace$_{max}$= 3.29) pre-TBI to 1.60 (Trace$_{min}$ = 1.83, Trace$_{max}$= 3.44) four hours post-TBI and then decreased to 1.25 twenty-four hours post-TBI (Trace$_{min}$ = 1.79, Trace$_{max}$= 3.05)

*Normalized T2*

After induction of TBI the normalized T2 decreased from 0.8286$\pm$ 0.1130 (median $\pm$ std) pre-TBI to 0.8028$\pm$0.0926 (median $\pm$ Std) four hours post-TBI and further decreased to 0.7845 $\pm$ 0.0908 (median $\pm$ Std) twenty-four hours post-TBI (Figure 65 I).In addition to the decrease of central tendency of the normalized T2 values post-TBI, the normalized T2 distribution became less spread out at four hours and twenty-four hours post-TBI (Figure 65 I). At four hours post-TBI the IQR of the normalized T2 distribution decreased from 0.1900 pre-TBI (25$^{th}$ percentile =

0.7356, 75<sup>th</sup> percentile = 0.9255) to 0.1719 four hours post-TBI (25<sup>th</sup> percentile = 0.7057, 75<sup>th</sup> percentile = 0.8776) and further decreased at twenty-four hours post TBI to 0.1334 (25<sup>th</sup> percentile = 0.6923, 75<sup>th</sup> percentile = 0.8258). As well, the range of the normalized T2 distribution decreased from 0.35 (T2 $_{min}$ = 0.69, T2$_{max}$= 1.04) pre-TBI to 0.27 (T2$_{min}$ = 0.69, T2$_{max}$= 0.96) four hours post-TBI and to 0.3 (T2$_{min}$ = 0.65, T2$_{max}$= 0.95) twenty-four hours post-TBI.

## Optic Chiasm

### *Fractional Anisotropy*

After induction of TBI the FA decreased from 0.7431$\pm$ 0.0602 (median $\pm$ std) pre-TBI to 0.6957$\pm$ 0.0797 four hours post-TBI (Figure 65 B). At twenty-four hours post-TBI the FA median increased to 0.7321$\pm$ 0.0952 in comparison to four hours post-TBI; however, the FA median remained decreased in comparison to the pre-TBI value.   In addition to the decrease of central tendency of the FA values, the FA distribution became more spread out at four hours and twenty-four hours post-TBI in comparison to pre-TBI FA distribution (Figure 65 B).  At post-TBI the IQR of the FA distribution increased from 0.0732 pre-TBI (25<sup>th</sup> percentile = 0.6856, 75<sup>th</sup> percentile = 0.7588) to 0.0881 four hours post-TBI (25<sup>th</sup> percentile = 0.6605, 75<sup>th</sup> percentile = 0.7486) and then to 0.1272 twenty-four hours post-TBI (25<sup>th</sup> percentile = 0.6547, 75<sup>th</sup> percentile = 0.7819).  As well, the range of the FA distribution increased from 0.21 (FA$_{min}$ = 0.62, FA$_{max}$= 0.83) pre-TBI to 0.34 (FA$_{min}$ = 0.51, FA$_{max}$= 0.85) four hours and to 0.34 (FA$_{min}$ = 0.53, FA$_{max}$= 0.88) twenty-four hours post-TBI.  Note that, at four hours post-TBI a mild outlier was present at the lower values of the FA distribution.

### *Axial Diffusivity*

After induction of TBI the AD increased from 1.5584$\pm$ 0.2947 (median $\pm$std) pre-TBI to 1.8545$\pm$ 0.3504 four hours post-TBI and was followed by a decrease to 1.5529$\pm$ 0.2937 twenty-

four hours post-TBI (Figure 65 D). In addition to the increase of the AD values of central tendency at four hours post-TBI followed by a decrease of central tendency at twenty-four hour post-TBI, the AD distribution became more spread out at four hours post-TBI and twenty-four hours post-TBI (Figure 65 D). At four hours post-TBI the IQR of the AD distribution increased from 0.2714 pre-TBI (25$^{th}$ percentile = 1.4572, 75$^{th}$ percentile = 1.7285) to 0.5203 four hours post-TBI (25$^{th}$ percentile = 1.5609, 75$^{th}$ percentile = 2.0812). Then at twenty-four hours post-TBI the AD IQR distribution decreased to 0.4239 (25$^{th}$ percentile = 1.3928, 75$^{th}$ percentile = 1.8167). The twenty-four hours IQR remained greater than the pre-TBI range. On the other hand, the range of the AD distribution increased from 1.19 (AD$_{min}$ = 1.19, AD$_{max}$= 2.38) pre-TBI to 1.38 (AD$_{min}$ = 1.15, AD$_{max}$= 2.52) four hours post-TBI. The maximum value in the AD distribution at pre-TBI demonstrated a mild outlier of the data. Furthermore, the AD distribution range decreased to 1.07 (AD$_{min}$= 1.12, AD$_{max}$ = 2.20) at twenty-four hours.

*Radial Diffusivity*

After induction of TBI the RD increased from 0.4218$\pm$ 0.10951 (median $\pm$ std) pre-TBI to 0.4636$\pm$ 0.12372 four hours post-TBI (Figure 65 F). At twenty-four hours post-TBI the RD decreased in comparison to pre-TBI and four hours post-TBI to 0.4047$\pm$ 0.12372 (Figure 65 F). In addition, the RD distribution became less dispersed at four hours and twenty-four hours post-TBI (Figure 65 F). At four hours post-TBI the IQR of the RD distribution decreased from 0.2058 pre-TBI (25$^{th}$ percentile = 0.3216, 75$^{th}$ percentile = 0.5274) to 0.1481 four hours post-TBI (25$^{th}$ percentile = 0.3839, 75$^{th}$ percentile = 0.5320). After four hours post-TBI, the IQR of the RD distribution increased to 0.1605 at twenty-four hours post-TBI (25$^{th}$ percentile = 0.2825, 75$^{th}$ percentile = 0.4431); however, the IQR at twenty-four hours post-TBI remained less than the pre-TBI interquartile range. On the other hand, the range of the RD distribution increased from 0.33 (RD$_{min}$ = 0.30, RD$_{max}$= 0.63) pre-TBI to 0.59 (RD$_{min}$ = 0.19, RD$_{max}$= 0.79) four hours post-TBI and then to 0.43 (RD$_{min}$ = 0.26, RD$_{max}$= 0.69) twenty-four hours post-TBI. This discrepancy

between the IQR and the full data distribution range was due to a maximum mild outlier in the data at four hours and twenty-four hours post-TBI.  In addition, the data distribution at pre-TBI and twenty-four hours post-TBI were positively skewed.  Note, the data distribution difference between pre-TBI and twenty-four hours post-TBI were statistically insignificant.

*Trace Diffusion*

After induction of TBI the trace of the diffusion increased from $2.2724\pm 0.4600$ (median $\pm$ std) pre-TBI to $2.667\pm 0.5501$ four hours post-TBI (Figure 65 H).  This increase of trace diffusion was followed by a decrease at twenty-four hours post-TBI where the trace became $2.4582\pm 0.4470$ (Figure 65 H).  The trace distribution became more spread out at four hours post-TBI and less dispersed at twenty-four hours post-TBI in comparison to the pre-TBI trace distribution (Figure 65 H).  At four hours post-TBI the IQR of the trace distribution increased from 0.6433 pre-TBI ($25^{th}$ percentile = 2.0292, $75^{th}$ percentile = 2.6724) to 0.8798 four hours post-TBI ($25^{th}$ percentile =2.2378, $75^{th}$ percentile = 3.1176).  After four hours post-TBI, the IQR of the trace distribution decreased to 0.6260 at twenty-four hours post TBI ($25^{th}$ percentile = 2.0533, $75^{th}$ percentile = 2.6793).  The IQR of the trace distribution was lower than that of pre-TBI interquartile range.  The trace distribution range increased from 1.58 ($Trace_{min}$ = 1.88, $Trace_{max}$= 3.46) pre-TBI to 1.78 ($Trace_{min}$ = 1.79, $Trace_{max}$= 3.57) four hours post-TBI and then decreased to 1.64 twenty-four hours post-TBI ($Trace_{min}$ = 1.63, $Trace_{max}$= 3.27).  Furthermore, the pre-TBI data distribution was positively skewed with a maximum mild outlier in the data.  Note, the data distribution difference between pre-TBI and twenty-four hours post-TBI was statistically insignificant.

*Normalized T2*

After induction of TBI the normalized T2 decreased from $0.4492\pm 0.0408$ (median $\pm$ std) pre-TBI to $0.4347\pm0.0418$ four hours post-TBI and then was followed by an increase to $0.4710 \pm0.04802$ twenty-four hours post-TBI (Figure 65 J).  In addition, the normalized T2 distribution became

less dispersed at four hours and was followed by a wide spread of the data distribution at twenty-four hours post-TBI in comparison to pre-TBI (Figure 65 J). At four hours post-TBI the IQR of the normalized T2 distribution decreased from 0.0624 pre-TBI (25$^{th}$ percentile = 0.4299, 75$^{th}$ percentile = 0.4923) to 0.0499 four hours post-TBI (25$^{th}$ percentile = 0.4122, 75$^{th}$ percentile = 0.4621) and further decreased at twenty-four hours post TBI to 0.0648 (25$^{th}$ percentile = 0.4147, 75$^{th}$ percentile = 0.4795). However, the range of the normalized T2 distribution increased from 0.15 (T2 $_{min}$ = 0.39, T2$_{max}$= 0.54) pre-TBI to 0.18 (T2$_{min}$ = 0.38, T2$_{max}$= 0.56) four hours post-TBI and to 0.16 (T2$_{min}$ = 0.37, T2$_{max}$= 0.52) twenty-four hours post-TBI. At four hours post-TBI a positive mild outlier was present within the data set.
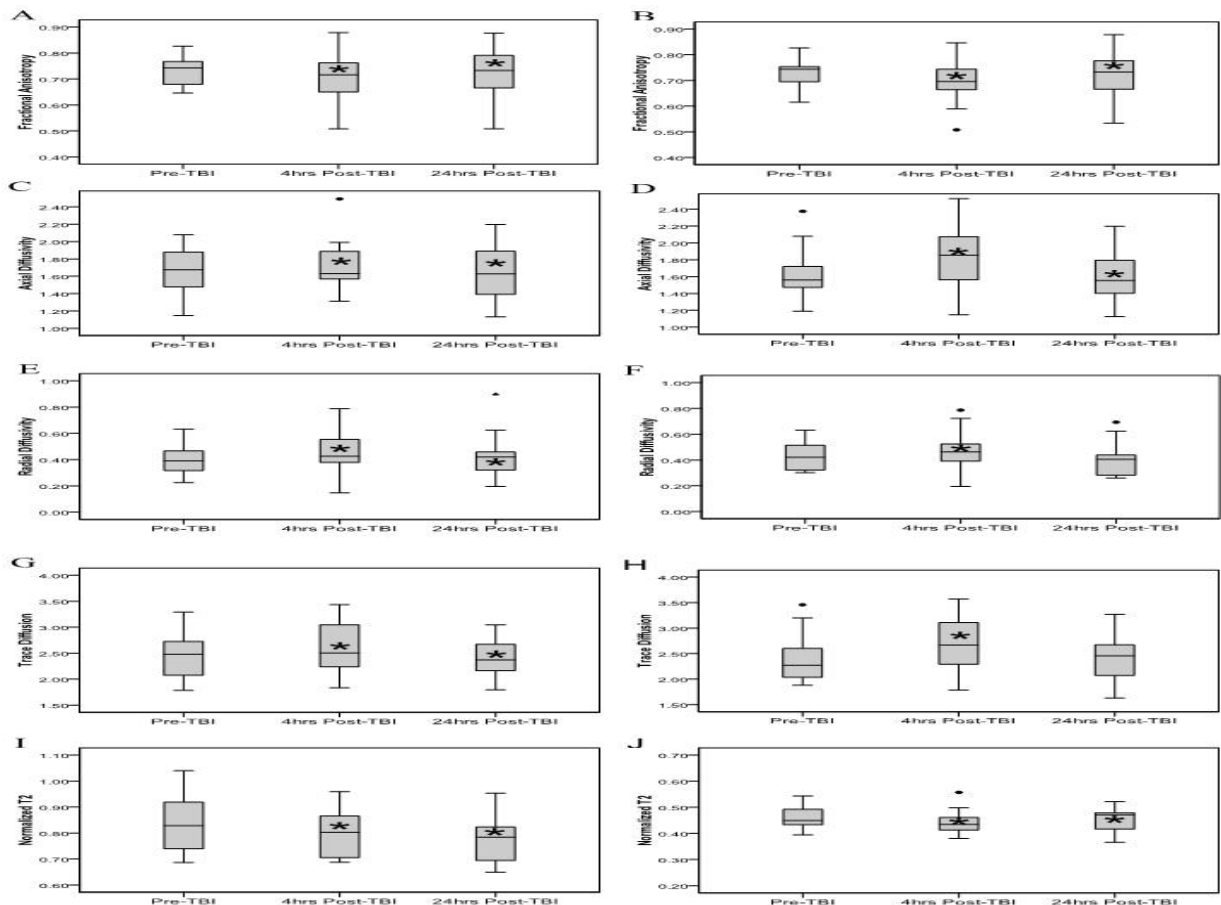


**Figure 65:** Group B's average (n=18)  (A, B) FA, (C, D) AD, (E, F) RD, (G, H) diffusion trace, and (I, J) T2 values at pre-TBI, four hours and twenty-four hours post-TBI within the CC (left column) and Och (right column). Diffusivity unit of measurement is 10$^{-3}$ mm$^2$/s. The ˙ and ▲ represents mild and extreme outliers in the data set respectively.  * represents statistical significance (p<0.05) between pre-TBI and post-TBI.
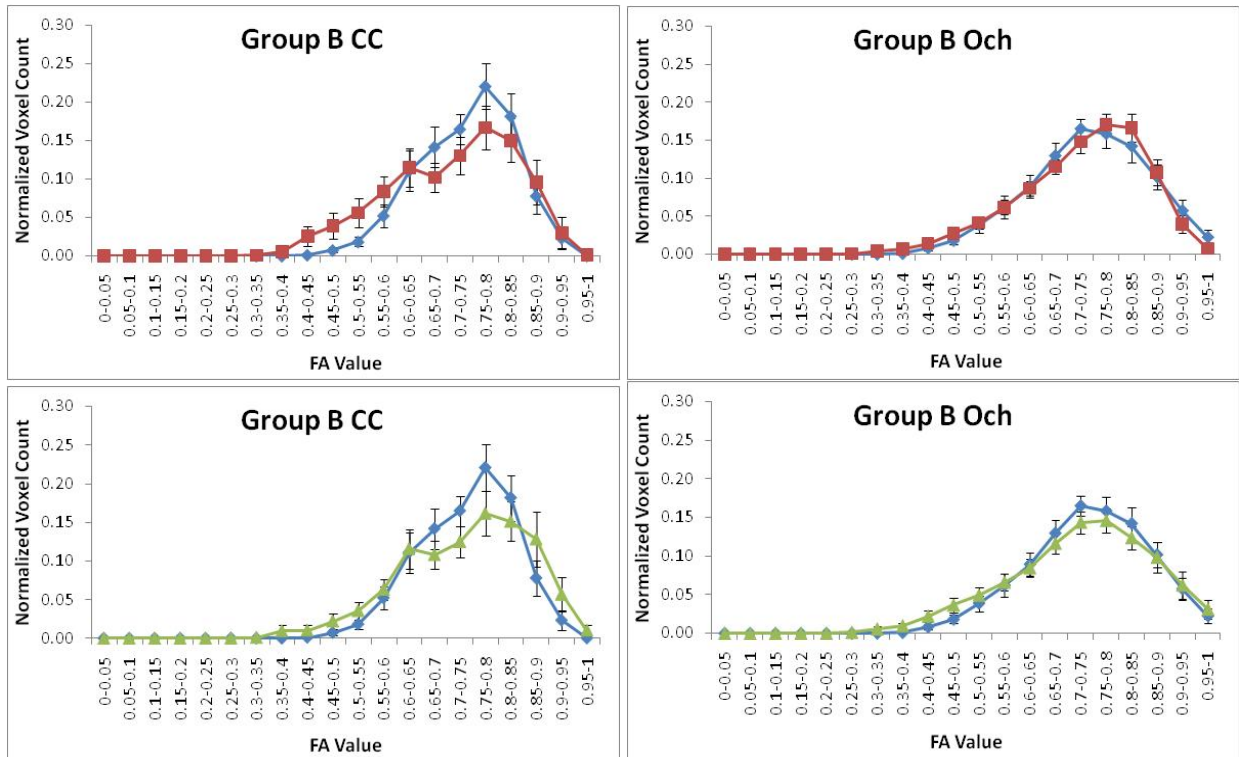
**Figure 66:** FA histograms of the CC V-like shape ROI (left) and Och (right) for all rats (n=18) in group B. The histograms are group average histograms at pre-TBI (blue, diamond), four hours post-TBI (red, square) and twenty-four hours post-TBI (green, triangle). The FA total range (x-axis) was divided into twenty equally spaced bins of 0.05 with marker (diamond, square, or triangle) representing each bin. Error bars represent the standard error.

**Table 11:** Comparison of the CC FA histogram shape parameters.

| CC | Pre-TBI | | 4hrs Post-TBI | | Difference | 24hrs Post-TBI | | Difference |
|---|---|---|---|---|---|---|---|---|
| Parameter | Mean | Std Error | Mean | Std Error | Post - Pre | Mean | Std Error | Post - Pre |
| Skewness | -0.41 | 0.016 | -0.433 | 0.015 | -0.023 | -0.528 | 0.015 | -0.118 |
| Kurtosis | -0.264 | 0.032 | -0.664 | 0.031 | -0.4 | -0.198 | 0.031 | 0.066 |
| FA Mean | 0.7286 | 0.0006 | 0.7035 | 0.00084 | -0.0251 | 0.7252 | 0.00082 | -0.0034 |

**Table 12:** Comparison of the Och FA histogram shape parameters.

| Och | Pre-TBI | | 4hrs Post-TBI | | Difference | 24hrs Post-TBI | | Difference |
|---|---|---|---|---|---|---|---|---|
| Parameter | Mean | Std Error | Mean | Std Error | Post - Pre | Mean | Std Error | Post - Pre |
| Skewness | -0.237 | 0.016 | -0.426 | 0.016 | -0.189 | 0.7174 | 0.0009 | 0.9544 |
| Kurtosis | -0.309 | 0.032 | -0.324 | 0.031 | -0.015 | -0.563 | 0.016 | -0.254 |
| FA Mean | 0.7285 | 0.0076 | 0.7012 | 0.00079 | -0.0273 | -0.096 | 0.031 | -0.8245 |

At four hours post-TBI a small shift to the left, which represents voxel base distribution FA value decrease occurred in the CC (Figure 66). At twenty-four hours post-TBI in the CC and

Och a small shift to the left which represents voxel base distribution FA value decrease occurred; however, at this time point some of the CC voxels also demonstrated an increase in their FA value (Figure 66). In addition, other shape changes also occurred at four hours and twenty-four hours post-TBI compared to pre-TBI (table 11-12). At four hours post-TBI compared to pre-TBI these shape changes included negative kurtosis in CC and Och and skewness (negative in CC and Och). At twenty-four hours post-TBI compared to pre-TBI the shape changes included positive kurtosis in the CC and negative kurtosis in the Och and skewness (negative in CC and positive in Och). FA histogram in the CC post-TBI is more variable compared to the pre-TBI histogram. The FA data distributions are more platykurtic at four post-TBI in the CC and Och and at twenty-four hours post-TBI in the Och in comparison to pre-TBI since their post-TBI mean kurtosis values are less than their pre-TBI mean kurtosis values (Tables 11 and 12).

**TBI Outcome Detected in MRI Alteration in Individual Rats**

The data distributions discussed above of group B were derived from eighteen rats imaged at pre-TBI, four hours and twenty-four hours post-TBI. The MRI changes detected within these animals between pre-TBI and four hours post-TBI, also between pre-TBI and twenty-four hours post-TBI,were not uniform across all rats (Figure 67). Within the CC ROI nine rats demonstrated a significant decrease in their FA values, seven rats demonstrated a significant increase in their FA values, and two rats demonstrated insignificant changes in their FA values at four hours and twenty-four hours post-TBI in comparison to pre-TBI (Figure 67 A). Even though the increase, decrease and status quo number of rats remained the same at four hours and twenty-four hours post-TBI in comparison to pre-TBI, these rats that experienced these changes were not identical between the two time points (Figure 67 A). Within the Och,ten rats demonstrated a significant decrease in their FA values, seven rats demonstrated a significant increase in their FA values, and only one rat demonstrated insignificant changes in its

FA values at four hours post-TBI in comparison to pre-TBI (Figure 67 B).  At twenty-four hours post-TBI within the Och ten rats demonstrated a significant decrease in their FA values, six rats demonstrated a significant increase in their FA values, and two rats demonstrated insignificant changes in their FA values in comparison to pre-TBI (Figure 67 B). On average both CC and Och illustrated a decrease in the FA values at four hours and twenty-four hours post-TBI in comparison to pre-TBI.  The Och demonstrated a greater decrease in the average FA at twenty-four hours post-TBI compared to four hours post-TBI.  Contrary, the CC demonstrated a greater decrease in the average FA at four hours post-TBI compared to twenty-four hours post-TBI. Also, the rats FA changes at four hours and twenty-four hours post-TBI were not consistent in each rat between the two (CC and Och) ROI (Figure 67 A, B).  For the FA voxel base distribution of each rat refer to appendix c.

Additionally, the diffusivity behaviors across the individual rats were as follows.  Within the CC ROI twelve rats demonstrated a significant decrease in their AD values, ten rats demonstrated a significant increase in their AD values, and two rats demonstrated insignificant changes in their FA values at four hours post-TBI in comparison to pre-TBI (Figure 67 C).  At twenty-four hours post-TBI within the CC ten rats demonstrated a significant decrease in their AD values, and eight rats demonstrated a significant increase in their AD values in comparison to pre-TBI (Figure 67 C).  Within the Och ten rats demonstrated a significant decrease in their AD values, seven rats demonstrated a significant increase in their AD values, and only one rat demonstrated insignificant changes in its AD values at four hours and twenty-four hours post-TBI in comparison to pre-TBI (Figure 67 D). Even though the increase, decrease and status quo number of rats remained the same at four hours and twenty-four hours post-TBI in comparison to pre-TBI, these rats that experienced these changes were not identical between the two time points (Figure 67 D).  Conversely, more rats illustrated a RD increase rather than a decrease post-TBI within the CC and Och (Figure 67 E and F).  Within the CC ROI seven rats

demonstrated a significant decrease in their RD values while eleven rats demonstrated a significant increase in their RD value at four hours post-TBI in comparison to pre-TBI (Figure 67 E). At twenty-four hours post-TBI within the CC seven rats demonstrated a significant decrease in their RD values, eight rats demonstrated a significant increase in their RD values, and three rats demonstrated insignificant changes in their RD values in comparison to pre-TBI (Figure 67 E). Within the Och five rats demonstrated a significant decrease in their RD values, and thirteen rats demonstrated a significant increase in their RD values at four hours post-TBI in comparison to pre-TBI (Figure 67 F). At twenty-four hours post-TBI within the Och seven rats demonstrated a significant decrease in their RD values, ten rats demonstrated a significant increase in their RD values, and only one rat demonstrated insignificant changes in its RD values in comparison to pre-TBI (Figure 67 F). On average, the CC illustrated an increase in the AD values at four hours and twenty-four hours post-TBI in comparison to pre-TBI whereas, the Och illustrated an increase and a decrease of the AD values at four hours and twenty four post-TBI respectively compared to pre-TBI. The RD on average demonstrated an increase in both the CC and Och at four hours and twenty-four hours post-TBI compared to pre-TBI. Within the CC and Och the greater increase in RD occurred at four hours post-TBI in comparison to twenty-four hours post-TBI. Another diffusion value measured was the diffusion trace. Within the CC, the diffusion trace decreased in five rats and increased in twelve rats at four hours post-TBI in comparison to pre-TBI (Figure 67 G). One rat demonstrated no significant change in the diffusion trace within the CC at four hours post-TBI in comparison to pre-TBI (Figure 67 G). At twenty-four hours post-TBI within the CC, the diffusion trace decreased in six rats and increased in ten rats, but in two rats there was no significant change in their diffusion trace values in comparison to pre-TBI (Figure 67 G). Within the Och, the diffusion trace decreased in seven rats and increased in nine rats at four hours and twenty-four hours post-TBI in comparison to pre-TBI (Figure 67 H). Two rats demonstrated no significant change in their diffusion trace within the Och at four hours and twenty-four hours post-TBI in comparison to pre-TBI (Figure 67 H).Even though the increase,

decrease and status quo number of rats remained the same at four hours and twenty-four hours post-TBI in comparison to pre-TBI, these rats that experienced these changes were not identical between the two time points (Figure 67 H).  On average, within the CC and Och the diffusion trace increased at four hours post-TBI and decreased at twenty-four hours post-TBI in comparison to pre-TBI.

The normalized T2 values of these rats also demonstrated various changes at four hours and twenty-four hours post-TBI within the CC and Och.  Compared to the pre-TBI values, at four hours post TBI the normalized T2 values within the CC decreased in twelve rats and increased in five rats (Figure 67 I, note: for the normalized T2 data n=17 at four hour post-TBI because one rat's four hours post-TBI data was not available).  At twenty-four hours post-TBI the normalized T2 values within the CC decreased in twelve rats and increased in six rats in comparison to pre-TBI (Figure 67 I).  For ten out of twelve rats the T2 values stayed at the decreased value at twenty-four hours post-TBI while two new rats had decreased values at twenty-four hours post-TBI.  Within the Och twelve rats demonstrated a decrease in their normalized T2 values, and three rats demonstrated an increase in their normalized T2 values at four hours post-TBI in comparison to pre-TBI (Figure 67 J).  Only one rat demonstrated a non-significant change in its normalized T2 value within the Och at four hours post-TBI in comparison to its pre-TBI normalized T2 value (Figure 65 J, note: for the normalized T2 data n=23 because one rat's four hours post-TBI data was not available).  At twenty-four hours post-TBI more rats demonstrated a significant T2 increase in comparison to four hours post-TBI. Within the Och at twenty-four hours post-TBI ten rats demonstrated a decrease in their normalized T2 values and eight rats demonstrated an increase in their normalized T2 values. On average, within the CC and Och the normalized T2 values remained decreased at four hours and twenty-four hours post-TBI in comparison to pre-TBI.  However, the average normalized T2

decrease within the Och became less prominent at twenty-four hours post-TBI in comparison to
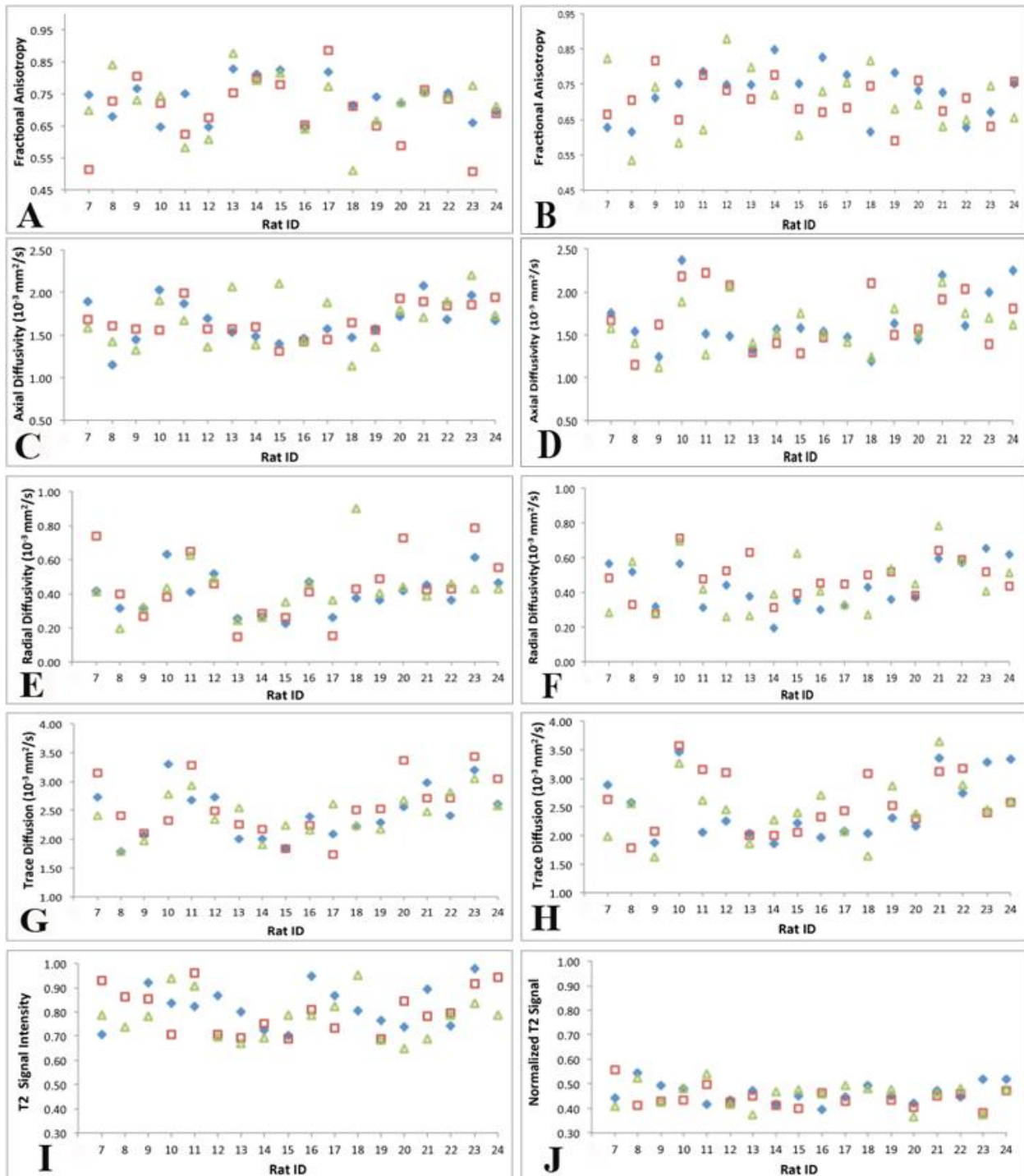
four hours post-TBI.



**Figure 67:** Group B's (A, B) FA, (C, D) AD, (E, F) RD, (G, H) diffusion trace, and (I, J) T2 values at pre-TBI (blue, diamond), four hours post-TBI (red, square), and twenty four hours post-TBI (green, triangle) for each rat within the CC (left column) and Och (right column).

*Group C*

For this group (n=12) MRI data were acquired at pre-TBI, four hours, twenty-four hours and three days post induction of TBI. The MRI changes detected between pre-TBI and post-TBI in this group were statistically significant except for the change in the diffusion trace at three days post-TBI in the CC (Figure 68).

<u>Corpus Callosum</u>

*Fractional Anisotropy*

After induction of TBI the FA decreased from $0.7453\pm 0.0602$ (median $\pm$ Std) pre-TBI to $0.7226\pm 0.0995$ four hours post-TBI (Figure 68 A). At twenty-four hours post-TBI the FA median increased to $0.7464\pm 0.0973$ and continued to increase to $0.7582 + 0.1071$ at three days post TBI (Figure 68 A). In addition, the FA distribution became more spread out at four hours, twenty-four hours and three days post-TBI in comparison to pre-TBI FA distribution (Figure 68 A). At post-TBI the IQR of the FA distribution increased from 0.1017 pre-TBI ($25^{th}$ percentile = 0.6994, $75^{th}$ percentile = 0.8012) to 0.1239 four hours post-TBI ($25^{th}$ percentile = 0.6507, $75^{th}$ percentile = 0.7747) then to 0.1311 twenty-four hours post-TBI ($25^{th}$ percentile = 0.6771, $75^{th}$ percentile = 0.8082) and finally to 0.1375 three days post-TBI ($25^{th}$ percentile = 0.6641, $75^{th}$ percentile = 0.8016). As well, the range of the FA distribution increased from 0.18 ($FA_{min}$ = 0.65, $FA_{max}$= 0.83) pre-TBI to 0.37 ($FA_{min}$ = 0.51, $FA_{max}$= 0.88) four hours and twenty-four hours post-TBI and then further increased to 0.41 ($FA_{min}$ = 0.47, $FA_{max}$= 0.89) at three days post-TBI. The FA distribution at twenty-four hours post-TBI, its minimum value, was a mild outlier in the data set .For three days post-TBI the FA distribution was negatively skewed.

*Axial Diffusivity*

After induction of TBI the AD increased from $1.6213\pm 0.2176$ (median $\pm$ std) pre-TBI to $1.7493\pm0.3100$ four hours post-TBI and then decreased to $1.7181\pm 0.33221$ twenty-four hours

post-TBI followed by an increase to 1.7302 $\pm$ 0.3749. The AD central tendency was increased post-TBI across all time points in comparison to the pre-TBI AD central tendency (Figure66 C). In addition to the increase of central tendency of the AD values post-TBI, the AD distribution became less spread out at four hours post-TBI and then became more spread out at twenty-four hours and three days post-TBI (Figure 68 C). At four hours post-TBI the IQR of the AD distribution decreased from 0.3597 pre-TBI ($25^{th}$ percentile = 1.4801, $75^{th}$ percentile = 1.8398) to 0.3542 four hours post-TBI ($25^{th}$ percentile = 1.5632, $75^{th}$ percentile = 1.9174) and then increased to 0.6260 twenty-four hours post-TBI ($25^{th}$ percentile = 1.4014, $75^{th}$ percentile = 2.0274). At three days post-TBI the IQR decreased to 0.5528 ($25^{th}$ percentile = 1.45515, $75^{th}$ percentile = 2.0043) in comparison to twenty-four hours post TBI; however, the three days post-TBI IQR remained greater than the pre-TBI and the four hours post-TBI interquartile range. The AD distribution range increased from 0.68 ($AD_{min}$ = 1.40, $AD_{max}$= 2.08) pre-TBI to 1.18 ($AD_{min}$ = 1.31, $AD_{max}$= 2.49) four hours post-TBI. The maximum value in the AD distribution at four hours post-TBI demonstrated a mild outlier of the data. Furthermore, the AD distribution range increased to 1.07 ($AD_{min}$ = 1.13, $AD_{max}$ = 2.20) at twenty-four hours post-TBI followed by another increase at three days post-TBI to 1.16 ($AD_{min}$ = 1.03, $AD_{max}$ = 2.19). Note that the AD data distribution at pre-TBI was positively skewed whereas at four days post-TBI the data distribution was negatively skewed.

*Radial Diffusivity*

After induction of TBI the RD increased from 0.3699$\pm$ 0.1087 (median $\pm$ std) pre-TBI to 0.4250 $\pm$ 0.1817 four hours post-TBI (Figure 68 E). At twenty-four hours post-TBI the RD slightly decreased in comparison to four hours post-TBI to 0.4166$\pm$ 0.1709; however, it remained greater than the pre-TBI values until three days post-TBI where RD became 0.3650 $\pm$ 0.1835 (Figure 68 E). In addition, the RD distribution became more spread out at four hours post-TBI followed by a decrease in the data spread at twenty-four hours and three days post-

TBI (Figure 68 E). At four hours post-TBI the IQR of the RD distribution increased from 0.1741 pre-TBI (25th percentile = 0.2877, 75th percentile = 0.4618) to 0.2267 four hours post-TBI (25th percentile = 0.3096, 75th percentile = 0.5363). After four hours post-TBI, the IQR of the RD distribution decreased to 0.1701 at twenty-four hours post-TBI (25th percentile = 0.2830, 75th percentile = 0.4531) and further decreased to 0.1225 at three days post-TBI (25th percentile = 0.3367, 75th percentile = 0.4592). On the other hand, the range of the RD distribution constantly increased post- TBI. The RD distribution range increased from 0.39 ($RD_{min}$ = 0.22, $RD_{max}$= 0.61) pre-TBI to 0.64 ($RD_{min}$ = 0.15, $RD_{max}$= 0.79) four hours post-TBI and continued to increase to 0.66 ($RD_{min}$ = 0.24, $RD_{max}$= 0.90) twenty-four hours post-TBI and to 0.74 ($RD_{min}$ = 0.15, $RD_{max}$= 0.89) three days post-TBI. These further increases in the range of the RD data distribution at twenty-four hours post TBI and three days post-TBI occurred as a result of outliers. At twenty-four hours post-TBI and three days post-TBI the maximum values in the data sets were extreme outliers. At three days post-TBI the minimum value of the data set was a mild outlier. Note that the RD distribution was negatively skewed at twenty-four hours post-TBI, and at three days the data was positively skewed.

*Trace Diffusion*

After induction of TBI the trace of the diffusion increased from 2.4000$\pm$ 0.3969 (median $\pm$ std) pre-TBI to 2.5199$\pm$0.51668 four hours post-TBI (Figure 68 G). This increase of trace diffusion was followed by a decrease at twenty-four hours post-TBI where the trace became 2.3495$\pm$ 0.3328 (Figure 68 G). At three days post-TBI the RD increased from its previous twenty-four-hour post-TBI value to 2.5123 $\pm$ 0.4715 In comparison to the pre –TBI trace distribution, the trace distribution became more spread out at four hours post-TBI and less dispersed at twenty-four hours post-TBI followed by a wide spread at three days post-TBI (Figure 68 G). At four hours post-TBI the IQR of the trace distribution increased from 0.5425 pre-TBI (25th percentile = 2.0639, 75th percentile = 2.6064) to 0.7762 four hours post-TBI (25th

percentile =2.1882, 75$^{th}$ percentile = 2.9645).  After four hours post-TBI, the IQR of the trace distribution decreased to 0.4841 at twenty-four hours post TBI (25$^{th}$ percentile = 2.1646, 75$^{th}$ percentile = 2.6486) followed by an increase at three days post-TBI to 0.8366 (25$^{th}$ percentile = 1.9886, 75$^{th}$ percentile = 2.8252).  Similarly, the trace distribution range increased from 1.36 (Trace$_{min}$ = 1.84, Trace$_{max}$= 3.20) pre-TBI to 1.60 (Trace$_{min}$ = 1.83, Trace$_{max}$= 3.44) four hours post-TBI then decreased to 1.15 twenty-four hours post-TBI (Trace$_{min}$ = 1.90, Trace$_{max}$= 3.05), followed by an increase to 1.50 (Trace$_{min}$ = 1.74, Trace$_{max}$= 3.24) three days post-TBI.  Note that the change in trace at three days post TBI was statistically insignificant to pre-TBI.

*Normalized T2*

After induction of TBI the normalized T2 decreased from 0.8023$\pm$ 0.1166 (median $\pm$ std) pre-TBI to 0.7883 $\pm$0.0854 four hours post-TBI and further decreased to 0.7851$\pm$0.08831 twenty-four hours post-TBI, which was followed by an increase to 0.8234 $\pm$ 0.11488 three days post TBI (Figure 68 I).  In comparison to pre-TBI, the normalized T2 distribution became less dispersed at four hours and twenty-four hours post-TBI then became more spread out at three days post-TBI (Figure 68 I).  At four hours post-TBI the IQR of the normalized T2 distribution decreased from 0.2059 pre-TBI (25$^{th}$ percentile = 0.7278, 75$^{th}$ percentile = 0.9337) to 0.1488 four hours post-TBI (25$^{th}$ percentile = 0.7120, 75$^{th}$ percentile = 0.8608) and further decreased to at twenty-four hours post TBI to 0.1306 (25$^{th}$ percentile = 0.6832, 75$^{th}$ percentile = 0.8138).After twenty- four hours post-TBI, the IQR of the normalized T2 distribution increased to 0.2114 at three days post TBI (25$^{th}$ percentile = 0.6961, 75$^{th}$ percentile = 0.9075).  At three days post-TBI the IQR became greater than the pre-TBI interquartile range.  In addition, the range of the normalized T2 distribution decreased from 0.35 (T2 $_{min}$ = 0.69, T2$_{max}$= 1.04) pre-TBI to 0.26 (T2$_{min}$ = 0.69, T2$_{max}$= 0.94) four hours post-TBI and to 0.30 (T2$_{min}$ = 0.65, T2$_{max}$= 0.95) twenty-four hours post-TBI.  At three days post-TBI the range of normalized T2 increased to 0.37 (T2$_{min}$ = 0.61, T2$_{max}$= 0.97), which was greater than that of pre-TBI.

<u>Optic Chiasm</u>

*Fractional Anisotropy*

After induction of TBI the FA decreased from $0.7447\underline{+}$ 0.0565 (median $\underline{+}$ std) pre-TBI to $0.6846\underline{+}$ 0.0865 four hours post-TBI (Figure 68 B). At twenty-four hours post-TBI the FA median increased from its previous value at four days post-TBI to $0.7321\underline{+}$ 0.0568; however, the FA median at twenty-four hours post-TBI remained less than the pre-TBI median (Figure 68 B). At three days post-TBI the FA further increased to $0.7582 \underline{+} 0.0871$ (median $\underline{+}$ std), which then became greater than the pre-TBI value (Figure 68B). In comparison to the pre-TBI FA distribution, the FA distribution became more spread out at four hours and three days post-TBI, and became less dispersed at twenty-four hours post-TBI (Figure 68B). At post-TBI the IQR of the FA distribution increased from 0.0711 pre-TBI ($25^{th}$ percentile = 0.6984, $75^{th}$ percentile = 0.7695) to 0.0875 four hours post-TBI ($25^{th}$ percentile = 0.6552, $75^{th}$ percentile = 0.7427), then decreased to 0.0571 twenty-four hours post-TBI ($25^{th}$ percentile = 0.7146, $75^{th}$ percentile = 0.7718) and then increased again to 0.990 three days post-TBI ($25^{th}$ percentile = 0.6889, $75^{th}$ percentile = 0.7879). Additionally, the range of the FA distribution increased from 0.21 ($FA_{min}$ = 0.62, $FA_{max}$= 0.83) pre-TBI to 0.34 ($FA_{min}$ = 0.51, $FA_{max}$= 0.85) four hours and then decreased back to 21 ($FA_{min}$ = 0.61, $FA_{max}$= 0.82) twenty-four hours post-TBI. This was followed by an increase in the FA distribution range to 0.28 ($FA_{min}$ = 0.54, $FA_{max}$= 0.82) three days post-TBI. At four hours, twenty-four hours, and three days post-TBI the FA distributions' minimum values were a mild outlier in the data set. Note that at three days post-TBI the FA distribution was negatively skewed.

*Axial Diffusivity*

After induction of TBI the AD increased from $1.5732\underline{+}$ 0.2536 (median $\underline{+}$ std) pre-TBI to $1.8545\underline{+}$ 0.3308 four hours post-TBI and then decreased to $1.6167\underline{+}$ 0.2672 twenty-four hours post-TBI and further decreased to $1.4879\underline{+}$ 0.4292 three days post-TBI In addition, the AD

distribution became more spread out at post-TBI (Figure 68D).  At four hours post-TBI the IQR of the AD distribution increased from 0.2842 pre-TBI ($25^{th}$ percentile = 1.4264, $75^{th}$ percentile = 1.7106) to 0.3769 four hours post-TBI ($25^{th}$ percentile = 1.5601, $75^{th}$ percentile = 1.9371) and then to 0.3764 twenty-four hours post-TBI ($25^{th}$ percentile = 1.4064, $75^{th}$ percentile = 1.7828). At three days post-TBI the IQR further increased to 0.8176 ($25^{th}$ percentile = 1.1867, $75^{th}$ percentile = 2.0043).  The AD distribution range increased from 0.89 ($AD_{min}$ = 1.19, $AD_{max}$= 2.08) pre-TBI to 1.24 ($AD_{min}$ = 1.29, $AD_{max}$= 2.52) four hours post-TBI.  The maximum value in the AD distribution at four hours post-TBI demonstrated a mild outlier of the data.  Furthermore, the AD distribution range increased to .95 ($AD_{min}$ = 1.24, $AD_{max}$ = 2.20) at twenty-four hours post-TBI followed by another increase at three days post-TBI to 1.04 ($AD_{min}$ = 1.15, $AD_{max}$ = 2.19).  Note that the AD data distribution at four hours post-TBI was negatively skewed whereas at twenty-four and three days post-TBI the data distribution was positively skewed.

*Radial Diffusivity*

After induction of TBI the RD increased from 0.3889$\pm$ 0.10959 (median $\pm$ std) pre-TBI to 0.4487$\pm$ 0.1570 four hours post-TBI (Figure 68F).  At twenty-four hours post-TBI the RD slightly decreased in comparison to four hours post-TBI to 0.4047$\pm$ 0.0940 (median $\pm$ Std); however, it remained greater than the pre-TBI values until three days post-TBI where RD became 0.3721$\pm$ 0.1007 (Figure 68F).  In addition, the RD distribution became more spread out at four hours post-TBI followed by a decrease in the data spread at twenty-four hours post-TBI and by three days post-TBI the data spread increased once again (Figure 68F).  At four hours post-TBI the IQR of the RD distribution increased from 0.1325 pre-TBI ($25^{th}$ percentile = 0.3293, $75^{th}$ percentile = 0.4618) to 0.1414 four hours post-TBI ($25^{th}$ percentile = 0.3992, $75^{th}$ percentile = 0.5406).  After four hours post-TBI, the IQR of the RD distribution decreased to 0.0904 at twenty-four hours post-TBI ($25^{th}$ percentile = 0.3454, $75^{th}$ percentile = 0.4358) and then was followed by an increase to 0.1643 three days post-TBI ($25^{th}$ percentile = 0.3191, $75^{th}$ percentile

= 0.4834).  On the other hand, the range of the RD distribution increased at four hours and twenty-four hours post- TBI in comparison to the pre-TBI RD distribution range.  At three days post-TBI the RD distribution range was equal to the pre-TBI RD distribution range.  The RD distribution range increased from 0.33 ($RD_{min}$ = 0.30, $RD_{max}$= 0.63) pre-TBI to 0.59 ($RD_{min}$ = 0.19, $RD_{max}$= 0.79) four hours post-TBI and continued to increase to 0.66 ($RD_{min}$ = 0.24, $RD_{max}$= 0.90).  At twenty-four hours post-TBI the RD range decreased to 0.36 ($RD_{min}$ = 0.26, $RD_{max}$= 0.62) in comparison to the four hours pre-TBI RD range; however; it remained greater than the pre TBI RD range.  At three days post-TBI the RD range returned to its original distribution range of 0.33 ($RD_{min}$ = 0.27, $RD_{max}$= 0.59).  Various mild outliers were present in the data set at four hours and twenty-four hours post-TBI.  Two maximum mild outliers and one minimum mild outlier were present in the four hours post-TBI data set.  At twenty-four hours post TBI one maximum mild outlier was present in the data set.  Note that for pre-TBI and three days post-TBI the data distribution was positively skewed whereas the twenty-four hours post-TBI data distribution was negatively skewed.

*Trace Diffusion*

After induction of TBI the trace of the diffusion increased from 2.2577$\pm$ 0.4038 (median $\pm$ std) pre-TBI to 2.6186$\pm$ 0.5023 four hours post-TBI (Figure 68H).  This increase of trace diffusion was followed by a decrease at twenty-four hours post-TBI where the trace became 2.4322$\pm$ 0.40470 and further decreased to 2.3299 $\pm$ 0.5347 three days post-TBI (Figure 68 H).  However, the trace median at twenty-four hours and three days post-TBI remained greater pre-TBI trace median.  In comparison to the pre –TBI, the trace distribution became more spread out post-TBI (Figure 68 G).  At four hours post-TBI the IQR of the trace distribution increased from 0.5750 pre-TBI (25th percentile = 2.0136, 75th percentile = 2.5886) to 0.7762 four hours post-TBI (25th percentile =2.3032, 75th percentile = 3.0801).  After four hours post-TBI, the IQR of the trace distribution decreased to 0.5976 at twenty-four hours post TBI (25th percentile =

2.0988, 75$^{th}$ percentile = 2.6964), followed by an increase at three days post-TBI to 1.0488 (25$^{th}$ percentile = 1.7411, 75$^{th}$ percentile = 2.7899). Similarly, the trace distribution range increased from 1.22 (Trace$_{min}$ = 1.97, Trace$_{max}$= 3.20) pre-TBI to 1.59 (Trace$_{min}$ = 1.85, Trace$_{max}$= 3.44) four hours post-TBI and then decreased to 1.40 twenty-four hours post-TBI (Trace$_{min}$ = 1.65, Trace$_{max}$= 3.05), followed by an increase to 1.56 three days post-TBI (Trace$_{min}$ = 1.68, Trace$_{max}$= 3.24). Note that at pre-TBI and three days post-TBI the trace distribution was positively skewed.

*Normalized T2*

After induction of TBI the normalized T2 decreased from 0.4492$\pm$ 0.03945 (median $\pm$ std) pre-TBI to 0.4347$\pm$ 0.0300 four hours post-TBI (Figure 68 J). At twenty-four hours the normalized T2 increased to 0.4710$\pm$ 0.0478 followed by a decrease to 0.4408$\pm$0.0460 three days post TBI (Figure 68 J). In comparison to pre-TBI, the normalized T2 distribution became less dispersed at four hours and three days post-TBI whereas, at twenty-four hours post-TBI, the normalized T2 distribution became more spread out (Figure 68 I). At four hours post-TBI the IQR of the normalized T2 distribution decreased from 0.0622 pre-TBI (25$^{th}$ percentile = 0.4259, 75$^{th}$ percentile = 0.4880) to 0.0574 four hours post-TBI (25$^{th}$ percentile = 0.4033, 75$^{th}$ percentile = 0.4608). At four hours post-TBI the IQR of the normalized T2 increased to 0.0827 (25$^{th}$ percentile = 0.3956, 75$^{th}$ percentile = 0.4783). After twenty- four hours post-TBI, the IQR of the normalized T2 distribution decreased to 0.0537 at three days post TBI (25$^{th}$ percentile = 0.4136, 75$^{th}$ percentile = 0.4673). In addition, the range of the normalized T2 distribution decreased from 0.13 (T2 $_{min}$ = 0.39, T2$_{max}$= 0.52) pre-TBI to 0.09 (T2$_{min}$ = 0.38, T2$_{max}$= 0.47) four hours post-TBI and increased back to 0.13 (T2$_{min}$ = 0.37, T2$_{max}$= 0.49) twenty-four hours post-TBI. At three days post-TBI the range of normalized T2 increased to 0.16 (T2$_{min}$ = 0.37, T2$_{max}$= 0.53), which was greater than that of pre-TBI. Note that, at three days post-TBI the maximum value of the data was a mild outlier of the distribution. In addition, the normalized T2 distribution was negatively skewed at twenty-four hours post-TBI.

153



**Figure 68:** Group C average(n=12) (A, B) FA, (C, D) AD, (E, F) RD, (G, H) diffusion trace, and (I, J) T2 values at pre-TBI, four hours, twenty-four hours and three days post-TBI within the CC (left column) and Och (right column). Diffusivity unit of measurement is 10-3 mm$^2$/s. The • and ▲ represents mild and extreme outliers in the data set respectively. * represents statistical significance ($p < 0.05$) between pre-TBI and post-TBI.
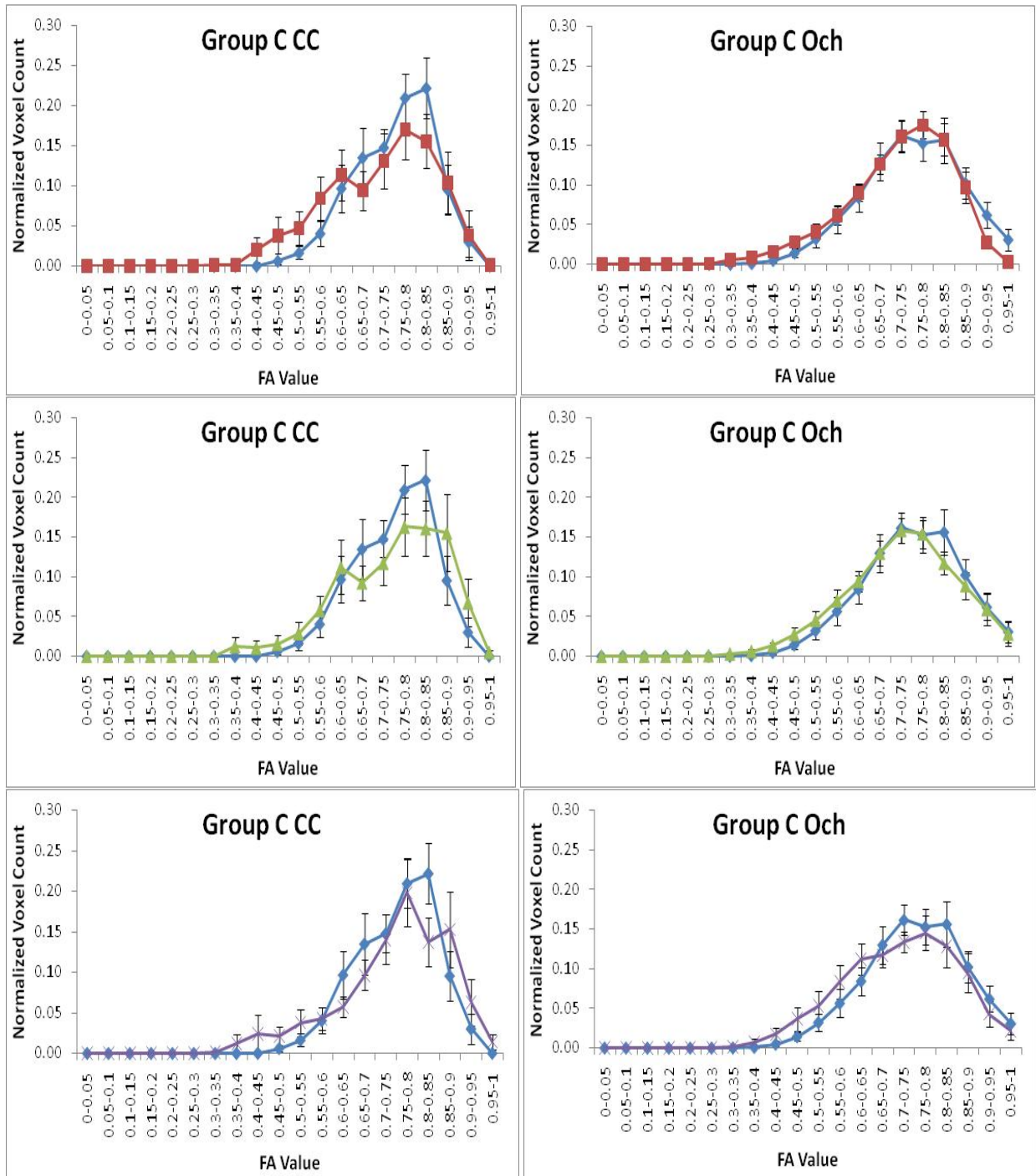
**Figure 69:** FA histograms of the CC V-like shape ROI (left) and Och (right) for all rats (n=12) in group C. The histograms are group average histograms at pre-TBI (blue, diamond), four hours post-TBI (red, square), twenty-four hours post-TBI (green, triangle), and three days post-TBI (purple, x). The FA total range (x-axis) was divided into twenty equally spaced bins of 0.05 with marker (diamond, square, triangle, or x) representing each bin. Error bars represent the standard error.

**Table 13:** Comparison of the CC FA histogram shape parameters.

| CC | Pre-TBI | | 4hrs Post-TBI | | Difference | 24hrs Post-TBI | | Difference | 3days Post-TBI | | Difference |
|---|---|---|---|---|---|---|---|---|---|---|---|
| Parameter | Mean | Std Error | Mean | Std Error | Post - Pre | Mean | Std Error | Post - Pre | Mean | Std Error | Post - Pre |
| Skewness | -0.455 | 0.02 | -0.48 | 0.02 | -0.025 | -0.648 | 0.02 | -0.193 | -0.706 | 0.019 | -0.251 |
| Kurtosis | -0.349 | 0.04 | -0.536 | 0.039 | -0.187 | -0.116 | 0.039 | 0.233 | 0.001 | 0.039 | 0.35 |
| FA Mean | 0.7386 | 0.00078 | 0.7207 | 0.00103 | -0.0179 | 0.7394 | 0.00103 | 0.0008 | 0.7364 | 0.00106 | -0.0022 |

**Table 14:** Comparison of the Och FA histogram shape parameters.

| Och | Pre-TBI | | 4hrs Post-TBI | | Difference | 24hrs Post-TBI | | Difference | 3days Post-TBI | | Difference |
|---|---|---|---|---|---|---|---|---|---|---|---|
| Parameter | Mean | Std Error | Mean | Std Error | Post - Pre | Mean | Std Error | Post - Pre | Mean | Std Error | Post - Pre |
| Skewness | -0.174 | 0.041 | -0.344 | 0.02 | -0.17 | -0.478 | 0.02 | -0.304 | -0.495 | 0.02 | -0.321 |
| Kurtosis | -0.264 | 0.021 | -0.644 | 0.04 | -0.38 | 0.27 | 0.04 | 0.534 | -0.424 | 0.04 | -0.16 |
| FA Mean | 0.7413 | 0.00097 | 0.687 | 0.00094 | -0.0543 | 0.7334 | 0.00098 | -0.0079 | 0.7181 | 0.0012 | -0.0232 |

At four hours post-TBI a small shift to the left which represents voxel base distribution FA value decrease occurs in the CC and Och (Figure 69). At twenty-four hours and three days post-TBI in the CC and Och a small shift to the left which represents voxel base distribution FA value decrease occurs, however, at these time points some of the CC voxels also demonstrate an increase in their FA value (Figure 69). In addition, other shape changes also occurred at four hours, twenty-four hours and three days post-TBI compared to pre-TBI (Table 13-14). At four hours post-TBI compared to pre-TBI these shape changes included negative kurtosis in CC and Och and skewness (negative in CC and Och). At twenty-four hours post-TBI compared to pre-TBI the shape changes included positive kurtosis in the CC and Och and skewness (negative in CC and Och). At three days post-TBI compared to pre-TBI the shape changes included positive kurtosis in the CC and negative kurtosis in the Och and skewness (negative in CC and Och). FA histogram in the CC post-TBI is more variable compared to the pre-TBI histogram. The FA data distributions are more platykurtic at four post-TBI in the CC and Och and at three days post-TBI in the Och in comparison to pre-TBI since their post-TBI mean kurtosis values are less than their pre-TBI mean kurtosis values (Tables 13 and 14).

TBI Outcome Detected in MRI Alteration in Individual Rat's

The data distribution discussed for group C was derived from twelve rats imaged at pre-TBI, four hours, twenty-four hours, and three days post-TBI. The MRI changes detected within these animals' between pre-TBI and four hours post-TBI, between pre-TBI and twenty-four hours post-TBI, and between pre-TBI and three days post-TBI were not uniform across all rats (Figure 70). Within the CC ROI seven rats demonstrated a significant decrease in their FA values, three rats demonstrated a significant increase in their FA values, and two rats demonstrated insignificant changes in their FA values at four hours in comparison to pre-TBI (Figure 70 A). At twenty-four hours post-TBI within the CC five rats demonstrated a significant decrease and five rats demonstrated a significant increase in their FA values, and two rats demonstrated no significant change to their FA values compared to pre-TBI (Figure 70 A). At three days post-TBI within the CC five rats demonstrated a significant decrease in their FA values, and seven rats demonstrated a significant increase in their FA values compared to pre-TBI (Figure 70 A). Within the Och, eight rats demonstrated a significant decrease in their FA values, and four rats demonstrated a significant increase in their FA value compared to pre-TBI (Figure 70 B). At twenty-four hours post-TBI within the Och seven rats demonstrated a significant decrease in their FA values, three rats demonstrated a significant increase in their FA values, and two rats demonstrated insignificant changes in their FA values in comparison to pre-TBI (Figure 70 B). At three days post-TBI within the Och seven rats demonstrated a significant decrease in their FA values, and five rats demonstrated a significant increase in their FA values compared to pre-TBI (Figure 70 B).On average both CC and Och illustrated a decrease in the FA values at four hours, twenty-four hours and three days post-TBI in comparison to pre-TBI. The Och demonstrated a greater decrease in the average FA compared to CC at all time points. Also, the rats FA changes at four hours, twenty-four hours and three days post-TBI were not consistent in each rat between the two (CC and Och) ROI (Figure 70 A, B). For the FA voxel base distribution of each rat refer to appendix C.

Additionally, the diffusivity behaviors across the individual rats were as follows. Within the CC ROI five rats demonstrated a significant decrease in their AD values, five rats demonstrated a significant increase in their AD values, and two rats demonstrated insignificant changes in their FA values at four hours post-TBI in comparison to pre-TBI (Figure 70 C). At twenty-four hours post-TBI within the CC five rats demonstrated a significant decrease in their AD values, and seven rats demonstrated a significant increase in their AD values in comparison to pre-TBI (Figure 70 C).At three days post-TBI within the CC four rats demonstrated a significant decrease in their AD values, and eight rats demonstrated a significant increase in their AD values in comparison to pre-TBI (Figure 70 C). Within the Och seven rats demonstrated a significant decrease in their AD values, four rats demonstrated a significant increase in their AD values, and only one rat demonstrated insignificant changes in its AD values at four hours post-TBI in comparison to pre-TBI (Figure 70 D). At twenty-four hours post-TBI within the Och five rats demonstrated a significant decrease in their AD values, six rats demonstrated a significant increase in their AD values, and only one rat demonstrated no significant change in its AD values in comparison to pre-TBI (Figure 70D).At three days post-TBI within the Och ten rats demonstrated a significant decrease in their AD values, and two rats demonstrated a significant increase in their AD values in comparison to pre-TBI (Figure 70D).Within the CC ROI four rats demonstrated a significant decrease in their RD values, and eight rats demonstrated a significant increase in their RD value at four hours post-TBI in comparison to pre-TBI (Figure 70 E). At twenty-four hours post-TBI within the CC three rats demonstrated a significant decrease in their RD values, six rats demonstrated a significant increase in their RD values, and three rats demonstrated insignificant changes in their RD values in comparison to pre-TBI (Figure 70E). At three days post-TBI within the CC five rats demonstrated a significant decrease in their RD values, and seven rats demonstrated a significant increase in their RD values in comparison to pre-TBI (Figure 70E). Within the Och two rats demonstrated a significant decrease in their RD values, and ten rats demonstrated a

significant increase in their RD values at four hours post-TBI in comparison to pre-TBI (Figure 70 F).  At twenty-four hours post-TBI within the Och four rats demonstrated a significant decrease in their RD values, seven rats demonstrated a significant increase in their RD values, and only one rat demonstrated insignificant changes in its RD values in comparison to pre-TBI (Figure 70 F).  On average, the CC illustrated an increase in the AD values at four hours, twenty-four hours and three days post-TBI in comparison to pre-TBI whereas the Och illustrated an increase at four hours post-TBI and a decrease of the AD values at twenty-four hours and three days post-TBI compared to pre-TBI. The RD on average demonstrated an increase in both the CC and Och at four hours and twenty-four hours post-TBI compared to pre-TBI.  At three days post-TBI on average the RD demonstrated an increase within the CC and a decrease within the Och compared to pre-TBI.  Of the other diffusion values measured is the diffusion trace and within the CC, the diffusion trace decreased in three rats and increased in eight rats at four hours and twenty-four hours post-TBI in comparison to pre-TBI (Figure 70 G). One rat demonstrated no significant change in the diffusion trace within the CC at four hours and twenty-four hours post-TBI in comparison to pre-TBI (Figure 70 G).At three days post-TBI within the CC the diffusion trace decreased in six rats, increased in five rats, and remained statistically the same in one rat compared to pre-TBI (Figure 70 G).Within the Och the diffusion trace decreased in five rats, and increased in six rats at four hours post-TBI in comparison to pre-TBI (Figure 70 H).  One rat demonstrated no significant change in the diffusion trace within the Och at four hours post-TBI in comparison to pre-TBI (Figure 70 H).  At twenty-four hours post-TBI within the Och the diffusion trace decreased in three rats and increased in seven rats, while two rats had no significant change in their diffusion trace values in comparison to pre-TBI (Figure 70 H).At three days post-TBI within the Och the diffusion trace decreased in eleven rats, and increased in only one rat in comparison to pre-TBI (Figure 70 H). On average, within the CC and Och the diffusion trace increased at four hours and twenty-four hours post-TBI compared to

159

pre-TBI. At three days post-TBI the average trace increased within the CC and decreased within the Och compared to pre-TBI.

The normalized T2 values of these rats also demonstrated various changes at four hours, twenty-four hours and three days post-TBI within the CC and Och. Compared to the pre-TBI values, at four hours post-TBI the normalized T2 values within the CC decreased in eight rats and increased in three rats (Figure 70 I, note: for the normalized T2 data n=11at four hours post-TBI because one rat's four-hours post-TBI data was not available). At twenty-four hours post-TBI the normalized T2 values within the CC decreased in nine rats and increased in three rats in comparison to pre-TBI (Figure 70 I). At three days post-TBI the normalized T2 values within the CC decreased in eight rats and increased in four rats in comparison to pre-TBI (Figure 70 I). Within the Och eight rats demonstrated a decrease in their normalized T2 values, and two rats demonstrated an increase in their normalized T2 values at four hours post-TBI in comparison to pre-TBI (Figure 70 J). Only one rat demonstrated a non-significant change in its normalized T2 value within the Och at four hours post-TBI in comparison to its pre-TBI normalized T2 value (Figure 70 J, note: for the normalized T2 data n=11 at four-hour post-TBI because one rat's four hours post-TBI data was not available). At twenty-four hours post-TBI more rats demonstrated a significant T2 increase in comparison to four hours post-TBI. Within the Och at twenty-four hours post-TBI six rats demonstrated a decrease in their normalized T2 values and six rats demonstrated an increase in their normalized T2 values (Figure 70 J). At three days post-TBI within the Och six rats demonstrated a decrease in their normalized T2 values, four rats demonstrated an increase in their normalized T2 values, and two rats demonstrated no significant change in their normalized T2 values compared to pre-TBI (Figure 70 J). On average, within the CC and Och the normalized T2 values remained decreased at four hours, twenty-four hours, and three days post-TBI in comparison to pre-TBI.
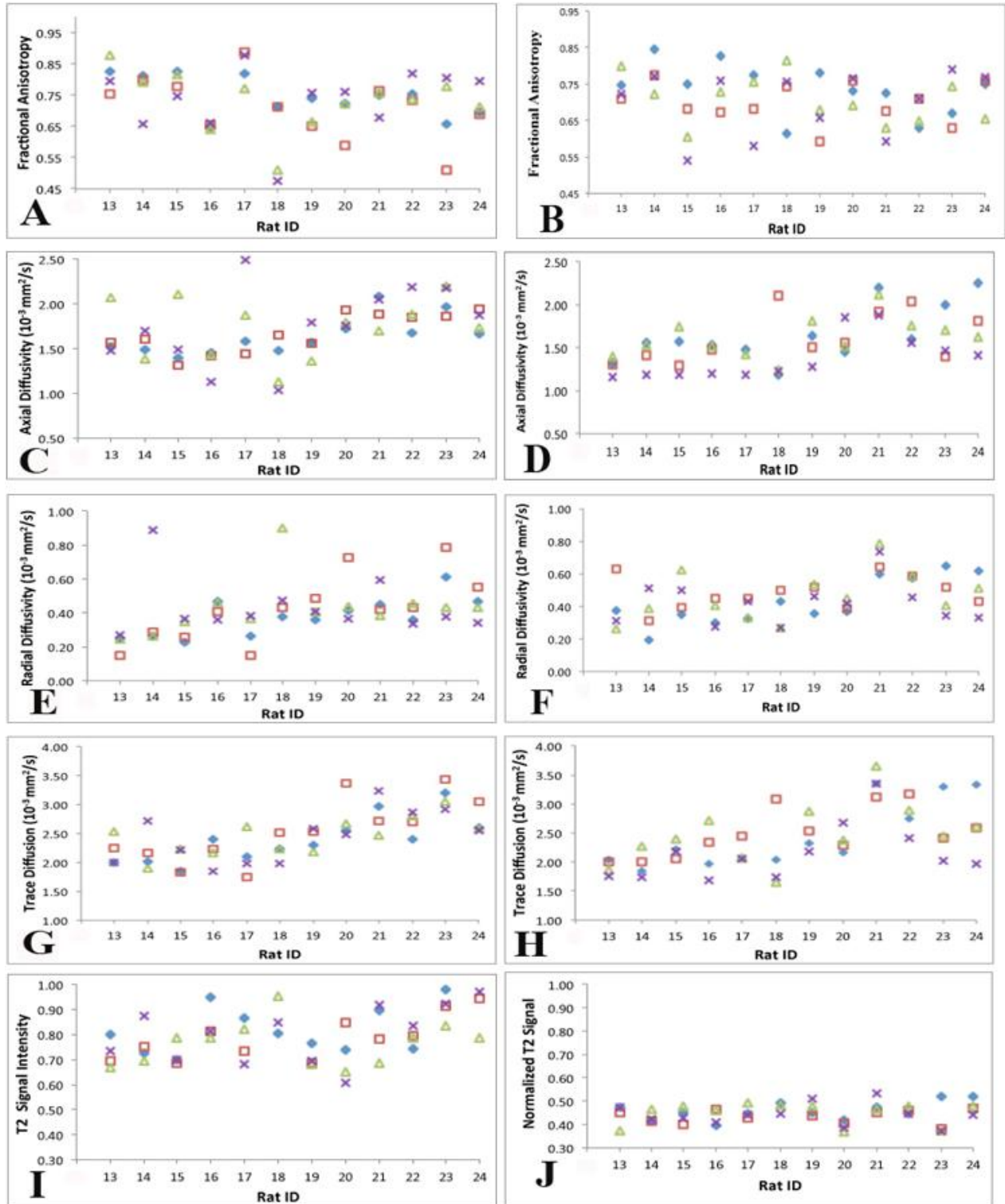
**Figure 70:** Group C's (A, B) FA, (C, D) AD, (E, F) RD, (G, H) diffusion trace, and (I, J) T2 values at pre-TBI (blue, diamond), four hours post-TBI (red, square), twenty four hours post-TBI (green, triangle) and three days post-TBI (purple, x) for each rat within the CC (left column) and Och (right column).

*Group D*

For this group (n=6) MRI data were acquired at pre-TBI, four hours, twenty-four hours three days and seven days post induction of TBI. The MRI changes detected between pre-TBI and post-TBI in this group were statistically significant except for the change in the AD at twenty-four hours post-TBTI within the CC and the FA and RD changes at three days and seven days post-TBI respectively within the Och (Figure 71).

<u>Corpus Callosum</u>

*Fractional Anisotropy*

After induction of TBI the FA decreased from $0.7300 \pm 0.0374$ (median $\pm$ std) pre-TBI to $0.6684 \pm 0.0946$ four hours post-TBI (Figure 71 A). At twenty four hours post-TBI the FA median increased to $0.7297 \pm 0.03861$ and continued increasing to $0.7765 \pm 0.0509$ at three days post TBI,but then decreasedto $0.7317 \pm 0.4815$ (Figure 71A) seven days post-TBI (Figure 71 A).Compared to pre-TBI, the FA distribution became more spread out at four hours and three days post-TBI whereas the FA distribution became less spread out at twenty-four hours and seven days post-TBI (Figure 71 A). At post-TBI the IQR of the FA distribution increased from 0.0665 pre-TBI (25$^{th}$ percentile = 0.6856, 75$^{th}$ percentile = 0.7520) to 0.1719 four hours post-TBI (25$^{th}$ percentile = 0.5688, 75$^{th}$ percentile = 0.7407) than decreasing to 0.0613 twenty-four hours post-TBI (25$^{th}$ percentile = 0.7005, 75$^{th}$ percentile = 0.7619). This decrease was followed by an FA IQR increase to 0.0709 three days post-TBI (25$^{th}$ percentile = 0.7368, 75$^{th}$ percentile = 0.8077) while on the seventh day post-TBI the FA IQR decreased to 0.643 (25$^{th}$ percentile = 0.7059, 75$^{th}$ percentile = 0.7702). The range of the FA distribution increased from 0.10 ($FA_{min}$ = 0.66, $FA_{max}$ = 0.75) pre-TBI to 0.25 ($FA_{min}$ = 0.51, $FA_{max}$ = 0.76) four hours post-TBI, followed by a decrease to 0.11 ($FA_{min}$ = 0.67, $FA_{max}$ = 0.78) twenty-four hours post-TB. After twenty-four hours post-TBI the FA distribution range began to increase to 0.14 ($FA_{min}$ = 0.68, $FA_{max}$ = 0.82) three days post-TBI and continued to increase to 15 ($FA_{min}$ = 0.66, $FA_{max}$ = 0.81) seven days post-TBI.

The minimum data points for three days and seven days post-TBI were mild outliers of the data. Note that at pre-TBI, four hours and twenty-four hours post-TBI the FA distribution was negatively skewed whereas at three days and seven days post-TBI the FA distribution was positively skewed.

*Axial Diffusivity*

After induction of TBI the AD increased from $1.7007 \pm 0.1970$ (median $\pm$ std) pre-TBI to $1.8757 \pm 0.1402$ four hours post-TBI and then decreased to $1.7639 \pm 0.27079$ twenty-four hours post-TBI (Figure 71 C).After twenty-four hours post-TBI the FA median increased to $1.9601 \pm 0.1909$ three days post-TBI and to $1.937 \pm 0.1501$ seven days post-TBI (Figure 71 C). The AD central tendency was increased post-TBI across all time points in comparison to the pre-TBI AD central tendency (Figure 71C). In addition, the AD distribution became less spread out at four hours, twenty-four hours, and seven days post-TBI but became more spread out at three days post-TBI (Figure 71 C). At four hours post-TBI the IQR of the AD distribution decreased from 0.3534 pre-TBI ($25^{th}$ percentile = 1.6454, $75^{th}$ percentile = 1.9989) to 0.1554 four hours post-TBI ($25^{th}$ percentile = 1.7751, $75^{th}$ percentile = 1.9304) and then increased to 0.3481 twenty-four hours post-TBI ($25^{th}$ percentile = 1.6185, $75^{th}$ percentile = 1.9666). At three days post-TBI the IQR increased to 0.3920 ($25^{th}$ percentile = 1.7839, $75^{th}$ percentile = 2.1759) and then was followed by a decrease to 0.2987 seven days post-TBI ($25^{th}$ percentile = 1.7774, $75^{th}$ percentile = 2.0761).The AD distribution range decreased from 0.50 ($AD_{min}$ = 1.57, $AD_{max}$= 2.08) pre-TBI to 0.38 ($AD_{min}$ = 1.56, $AD_{max}$= 1.94) four hours post-TBI. The minimum value in the AD distribution at four hours post-TBI demonstrated an extreme outlier of the data. Furthermore, the AD distribution range increased to 0.83 ($AD_{min}$ = 1.37, $AD_{max}$ = 2.20) at twenty-four hours post-TBI. The minimum and maximum value in the AD distribution at twenty-four hours post-TBI demonstrated mild outliers of the data. After twenty-four hours post-TBI the FA range decreased to 44 ($AD_{min}$ = 1.76, $AD_{max}$ = 2.19) three days post-TBI and it continued to decrease

to 0.37 ($AD_{min}$ = 1.73, $AD_{max}$ = 2.10) seven days post-TBI.  Note that no statistical significant was present between pre-TBI and twenty-four hours post-TBI.

*Radial Diffusivity*

After induction of TBI the RD increased from 0.4321$\pm$ 0.09342 (median $\pm$ std) pre-TBI to 0.5190$\pm$ 0.15483 four hours post-TBI (Figure 71 E).  At twenty-four hours post-TBI the RD decreased to 0.4287$\pm$ 0.0256 and then further decreased to 0.3721 $\pm$ 0.0965 three days post-TBI (Figure 71 E).  At seven hours post-TBI the FA increased to 0.4958 $\pm$ 0.0776 to become greater than the pre-TBI value.  In addition, the RD distribution became more spread out at four hours post-TBI followed by a decrease in the data spread at twenty-four hours, three days, and seven days post-TBI (Figure 71 E).  At four hours post-TBI the IQR of the RD distribution increased from 0.1414 pre-TBI (25$^{th}$ percentile = 0.3615, 75$^{th}$ percentile = 0.5029) to 0.3113 four hours post-TBI (25$^{th}$ percentile = 0.4281, 75$^{th}$ percentile = 0.7394).  After four hours post-TBI, the IQR of the RD distribution decreased to 0.0432 at twenty-four hours post-TBI (25$^{th}$ percentile = 0.3998, 75$^{th}$ percentile = 0.4431).  This decrease was followed by a slight increase to 0.1134 three days post-TBI (25$^{th}$ percentile = 0.3415, 75$^{th}$ percentile = 0.4549) and further increased to 0.1280 seven days post-TBI (25$^{th}$ percentile = 0.3879, 75$^{th}$ percentile = 0.5158).  The RD distribution range increased from 0.25 ($RD_{min}$ = 0.36, $RD_{max}$= 0.61) pre-TBI to 0.37 ($RD_{min}$ = 0.42, $RD_{max}$= 0.79) four hours post-TBI.  At twenty-four hours post-TBI the RD distribution range decreased to 0.07 ($RD_{min}$ = 0.39, $RD_{max}$= 0.46) after which the RD range increased to 0.26 ($RD_{min}$ = 0.33, $RD_{max}$= 0.59) three days post-TBI.  At three days post-TBI the RD distribution had a maximum mild outlier in the data set.  At seven days post-TBI the RD distribution range decreased to 0.20 ($RD_{min}$ = 0.33, $RD_{max}$= 0.52), which was less than the pre-TBI RD range.  Note that the RD distribution was negatively skewed at seven days post-TBI and positively skewed at pre-TBI and four hours post-TBI.
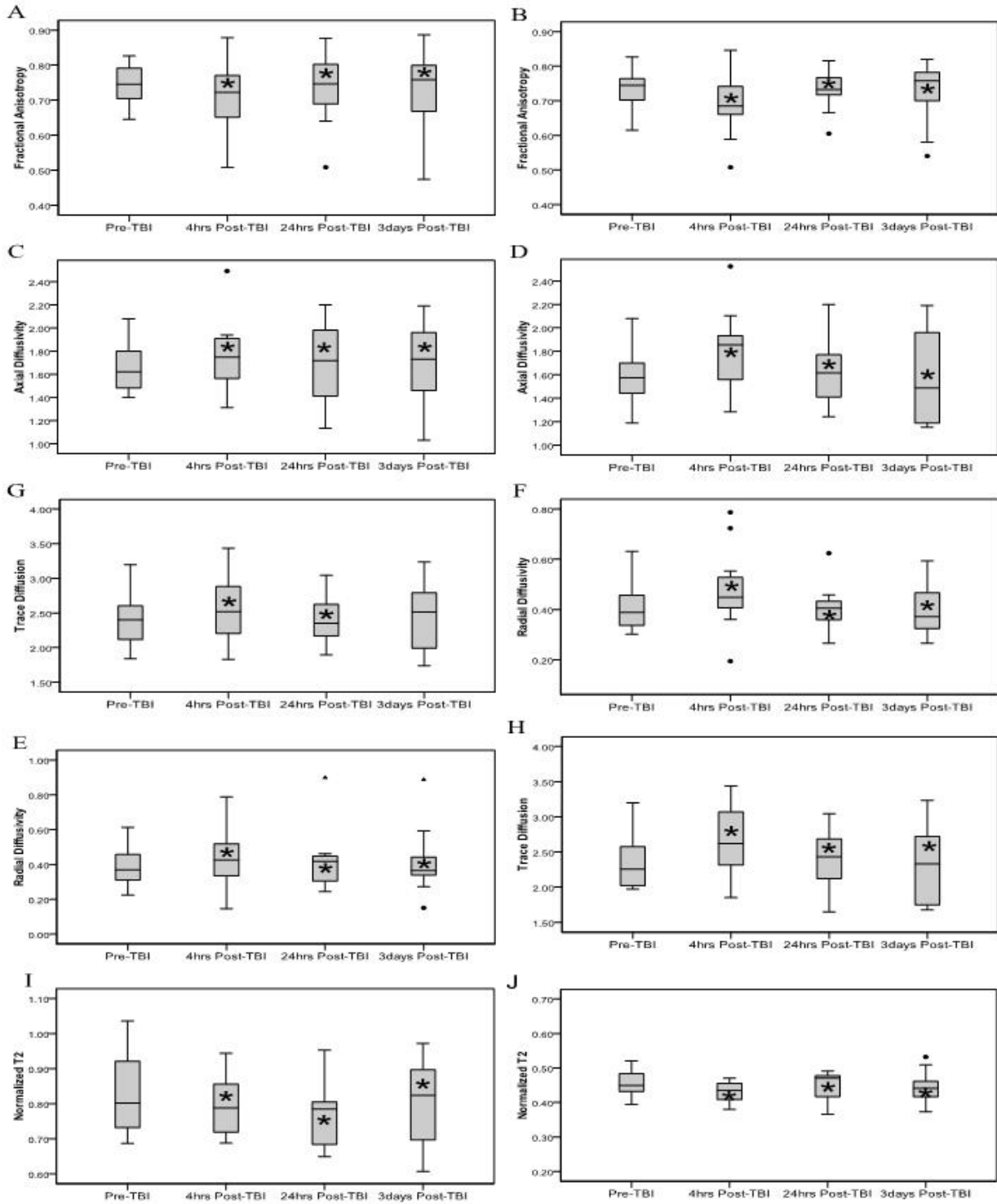
*Trace Diffusion*

After induction of TBI the trace of the diffusion increased from 2.5758$\pm$ 0.3475 (median $\pm$ std) pre-TBI to 2.8816$\pm$ 0.3780 four hours post-TBI (Figure 71 G). This increase of trace diffusion was followed by a decrease at twenty-four hours post-TBI where the trace became 2.6265$\pm$ 0.2965 (Figure 71 G). At three days post-TBI the RD increased from its previous twenty-four-hour post-TBI value to 2.7207$\pm$ 0.2894 and continued to increase to 2.8290$\pm$ 0.1901 seven days post-TBI (Figure 71 G). In comparison to the pre–TBI trace distribution, the trace distribution became more spread out at four hours post-TBI and less dispersed at twenty-four hours, three days and seven days post-TBI (Figure 71 G). At four hours post-TBI the IQR of the trace distribution increased from 0.6539 pre-TBI ($25^{th}$ percentile = 2.3768, $75^{th}$ percentile = 3.0307) to 0.7267 four hours post-TBI ($25^{th}$ percentile =2.6630, $75^{th}$ percentile = 3.397). After four hours post-TBI, the IQR of the trace distribution decreased to 0.4695 at twenty-four hours post TBI ($25^{th}$ percentile = 2.3940, $75^{th}$ percentile = 2.8635), followed by a decrease at three days post-TBI to 0.4688 ($25^{th}$ percentile = 2.5314, $75^{th}$ percentile = 3.0002). At seven days post-TBI the IQR further decreased to 0.3381 ($25^{th}$ percentile = 2.6715, $75^{th}$ percentile = 3.0096). The trace distribution range remained the same from 0.91 ($Trace_{min}$ = 2.29, $Trace_{max}$= 3.20) pre-TBI to 0.91 ($Trace_{min}$ = 2.53, $Trace_{max}$= 3.44) four hours post-TBI. At twenty-four hours post-TBI the trace distribution range decreased to 0.87 ($Trace_{min}$ = 2.18, $Trace_{max}$= 3.05) followed by a further decrease to 0.76 ($Trace_{min}$ = 2.47, $Trace_{max}$= 3.24)three days post-TBI. At seven days post-TBI the trace range continued to decrease to 0.51 ($Trace_{min}$ = 2.58, $Trace_{max}$= 3.09). Note that the trace distribution at pre-TBI and four hours post-TBI were positively skewed, and the trace distribution at seven days post-TBI was negatively skewed.

*Normalized T2*

After induction of TBI the normalized T2 increased from 0.8178$\pm$ 0.14383 (median $\pm$ std) pre-TBI to 0.8205$\pm$ 0.0888 four hours post-TBI and further decreased to 0.7358$\pm$ 0.07412

twenty-four hours post-TBI (Figure 71 I).At three days post-TBI the normalized T2 increased to 0.8760$\pm$ 0.1444 three days post TBI followed by a decrease to0.7813 $\pm$ 0.0649 seven days post-TBI (Figure 71 I). In comparison to pre-TBI, the normalized T2 distribution became less dispersed post-TBI (Figure 71I). At four hours post-TBI the IQR of the normalized T2 distribution decreased from 0.2660 pre-TBI ($25^{th}$ percentile = 0.7263, $75^{th}$ percentile = 0.9923) to 0.1586 four hours post-TBI ($25^{th}$ percentile = 0.7625, $75^{th}$ percentile = 0.9211) and further decreased at twenty-four hours post TBI to 0.1239 ($25^{th}$ percentile = 0.6740, $75^{th}$ percentile = 0.7978). After twenty-four hours post-TBI, the IQR of the normalized T2 distribution increased to 0.2612 at three days post TBI ($25^{th}$ percentile = 0.6733, $75^{th}$ percentile = 0.9345) and was followed by the normalized T2 distribution decrease to 0.1265 seven days post TBI ($25^{th}$ percentile = 0.7247, $75^{th}$ percentile = 0.8512). In addition, the range of the normalized T2 distribution decreased from 0.35 (T2 $_{min}$ = 0.69, $T2_{max}$= 1.04) pre-TBI to 0.24 ($T2_{min}$ = 0.70, $T2_{max}$= 0.94) four hours post-TBI and further decreased to 0.18 ($T2_{min}$ = 0.65, $T2_{max}$= 0.83) twenty-four hours post-TBI. At three days post-TBI the range of normalized T2 increased to 0.37 ($T2_{min}$ = 0.61, $T2_{max}$= 0.97), which decreased at seven days post-TBI to 0.15 ($T2_{min}$ = 0.72, $T2_{max}$= 0.87). Note that the normalized T2 distribution was negatively skewed at four hours and three days post-TBI and positively skewed at seven days post-TBI.

Optic Chiasm

*Fractional Anisotropy*

After induction of TBI the FA decreased from 0.7295$\pm$0.0557 (median $\pm$ std) pre-TBI to 0.6925$\pm$ 0.0685 four hours post-TBI and continued to decrease to 0.6675$\pm$ 0.0401 twenty-four hours post-TBI (Figure 71 B). This FA median decrease was followed by an increase to 0.7377$\pm$ 0.0767 three days post TBI and it continued to increase to 0.7438$\pm$ 0.0587 (Figure 71 B) seven days post-TBI (Figure 71 B). Compared to pre-TBI, the FA distribution became more spread out at four hours, three days, and seven days post-TBI whereas the FA distribution

became less spread out at twenty-four hours post-TBI (Figure 71 B).  At post-TBI the IQR of the FA distribution increased from 0.0982 pre-TBI (25th percentile = 0.6599, 75th percentile = 0.7581) to 0.1383 four hours post-TBI (25th percentile = 0.6201, 75th percentile = 0.7584) and then decreased to 0.0599 twenty-four hours post-TBI (25th percentile = 0.6449, 75th percentile = 0.7048).  This decrease was followed by an FA IQR increase to 0.1323 three days post-TBI (25th percentile = 0.6420, 75th percentile = 0.7743).  The FA interquartile range continued to increase at seventh day post-TBI at 0.1125 (25th percentile = 0.6686, 75th percentile = 0.7811). The range of the FA distribution increased from 0.15 ($FA_{min}$ = 0.63, $FA_{max}$= 0.78) pre-TBI to 0.17 ($FA_{min}$ = 0.59, $FA_{max}$= 0.76) four hours post-TBI, followed by a decrease to 0.11 ($FA_{min}$ = 0.63, $FA_{max}$= 0.74) twenty-four hours post-TB.  After twenty-four hours post-TBI the FA distribution range began to increase to 0.20 ($FA_{min}$ = 0.59, $FA_{max}$= 0.79) three days post-TBI.  At seven days post-TBI the FA range decreased to 15 ($FA_{min}$ = 0.66, $FA_{max}$= 0.81).  Note that at four hours and three days post-TBI the FA distribution was negatively skewed whereas at twenty-four hours and seven day post-TBI the FA distribution was positively skewed.  No statistical significance was found between pre-TBI and three days post-TBI data set.

*Axial Diffusivity*

After induction of TBI the AD decreased from 1.8156$\pm$ 0.3379 (median $\pm$ std) pre-TBI to 1.6852$\pm$ 0.2546 four hours post-TBI and then increased to 1.7296$\pm$ 0.2055 twenty-four hours post-TBI (Figure 71D). After twenty-four hours post-TBI the FA median decreased to 1.5106$\pm$ 0.2430 three days post-TBI and then increased to 1.7960$\pm$ 0.4893 seven days post-TBI (Figure 71D). The AD central tendency was decreased post-TBI across all time points in comparison to the pre-TBI AD central tendency (Figure 71D).  In addition, the AD distribution became less spread out at four hours, twenty-four hours, and three days post-TBI and became more spread out at seven days post-TBI (Figure 71D).  At four hours post-TBI the IQR of the AD distribution decreased from 0.6502 pre-TBI (25th percentile = 1.5631, 75th percentile = 2.2133) to 0.2644

four hours post-TBI ($25^{th}$ percentile = 1.4754, $75^{th}$ percentile = 1.9496) and then increased to 0.2894 twenty-four hours post-TBI ($25^{th}$ percentile = 1.5945, $75^{th}$ percentile = 1.8839). At three days post-TBI the IQR increased to 0.4807 ($25^{th}$ percentile = 1.3753, $75^{th}$ percentile =1.8560) and then further increased to 0.8998 seven days post-TBI ($25^{th}$ percentile = 1.5547, $75^{th}$ percentile = 2.4545). The AD distribution range decreased from 0.80 ($AD_{min}$ = 1.45, $AD_{max}$= 2.25) pre-TBI to 0.64 ($AD_{min}$ = 1.39, $AD_{max}$= 2.04) four hours post-TBI. In addition, the AD distribution range decreased to 0.60 ($AD_{min}$ = 1.52, $AD_{max}$ = 2.12) twenty-four hours post-TBI. The maximum value in the AD distribution at twenty-four hours post-TBI demonstrated mild outliers of the data. After twenty-four hours post-TBI the FA range remained at 60 ($AD_{min}$ = 1.27, $AD_{max}$ = 1.87) three days post-TBI and was then followed by an increase to 1.24 ($AD_{min}$ = 1.39, $AD_{max}$ = 2.63) seven days post-TBI. Note that at twenty-four hours and three days post-TBI the AD data distribution was negatively skewed.

*Radial Diffusivity*

After induction of TBI the RD decreased from 0.5836$\pm$ 0.1297 (median $\pm$ std) pre-TBI to 0.5155$\pm$ 0.0945 four hours post-TBI (Figure 71F). At twenty-four hours post-TBI the RD increased to 0.5251$\pm$ 0.1321 followed by a decrease to 0.4360$\pm$ 0.14674 three days post-TBI (Figure 71F). At seven hours post-TBI the FA increased to 0.4910$\pm$ 0.2260, which was less than the pre-TBI value. In addition, the RD distribution became less dispersed at four hours, twenty-four hours, and three days post-TBI followed by an increase in the data spread at seven days post-TBI in comparison to pre-TBI (Figure 71 F). At four hours post-TBI the IQR of the RD distribution decreased from 0.2593 pre-TBI ($25^{th}$ percentile = 0.3663, $75^{th}$ percentile = 0.6256) to 0.1797 four hours post-TBI ($25^{th}$ percentile = 0.4209, $75^{th}$ percentile = 0.6006). After four hours post-TBI, the IQR of the RD distribution increased to 0.1942 at twenty-four hours post-TBI ($25^{th}$ percentile = 0.4390, $75^{th}$ percentile = 0.6332). This increase was followed by a slight decrease to 0.1934 three days post-TBI ($25^{th}$ percentile = 0.3381, $75^{th}$ percentile = 0.5315) and a further

increase to 0.3461 seven days post-TBI ($25^{th}$ percentile = 0.3641, $75^{th}$ percentile = 0.7102). The RD distribution range decreased from 0.29 ($RD_{min}$ = 0.36, $RD_{max}$= 0.65) pre-TBI to 0.26 ($RD_{min}$ = 0.38, $RD_{max}$= 0.64) four hours post-TBI. At twenty-four hours post-TBI the RD distribution range increased to 0.38 ($RD_{min}$ = 0.41, $RD_{max}$= 0.78) and further increased to 0.40 ($RD_{min}$ = 0.33, $RD_{max}$= 0.73) three days post-TBI. At three days post-TBI the RD distribution had a maximum mild outlier in the data set. At seven days post-TBI the RD distribution range increased to 0.66 ($RD_{min}$ = 0.25, $RD_{max}$= 0.91). Note that the RD distribution was positively skewed at twenty-four hours post-TBI.

*Trace Diffusion*

After induction of TBI the trace of the diffusion decreased from 3.0156$\pm$ 0.5365 (median $\pm$ std) pre-TBI to 2.5585$\pm$ 0.3727 four hours post-TBI (Figure 71 H). This decrease of trace diffusion was followed by an increase at twenty-four hours post-TBI where the trace became2.7352$\pm$ 0.4637 (Figure 71H). At three days post-TBI the RD decreased to 2.3000$\pm$ 0.5170 after which it increased to 2.8320$\pm$ 0.9509 seven days post-TBI (Figure 71H). In comparison to the pre-TBI trace distribution, the trace distribution became less dispersed at four hours, twenty-four hours, and three days post-TBI and became more spread out at seven days post-TBI (Figure 71H). At four hours post-TBI the IQR of the trace distribution decreased from 1.0565 pre-TBI ($25^{th}$ percentile = 2.2801, $75^{th}$ percentile = 3.3366) to 0.7581 four hours post-TBI ($25^{th}$ percentile =2.3793, $75^{th}$ percentile = 3.1374). After four hours post-TBI, the IQR of the trace distribution decreased to 0.6465 twenty-four hours post TBI ($25^{th}$ percentile = 2.4352, $75^{th}$ percentile = 3.0817),followed by an increase at three days post-TBI to 0.8410 ($25^{th}$ percentile = 2.0060, $75^{th}$ percentile = 2.8470). At seven days post-TBI the IQR further increased to 1.4739 ($25^{th}$ percentile = 2.2081, $75^{th}$ percentile = 3.6820). The trace distribution range decreased from 1.19 ($Trace_{min}$ = 2.17, $Trace_{max}$= 3.36) pre-TBI to 0.88 ($Trace_{min}$ = 2.29, $Trace_{max}$= 3.17) four hours post-TBI. This decrease was followed by an increase in the trace distribution range to

1.27 (Trace$_{min}$ = 2.38, Trace$_{max}$= 3.65) twenty-four hours post-TBI.  At twenty-four hours post-TBI the trace distribution had a maximum mild outlier present in the data set.  After twenty-four hours post-TBI the trace distribution range continued to increase to 1.37 (Trace$_{min}$ = 1.97, Trace$_{max}$= 3.34) three days post-TBI.  At seven days post TBI the trace distribution range further increased to 2.66 (Trace$_{min}$ = 1.76, Trace$_{max}$= 4.43).  Note that the trace distribution at pre-TBI and twenty-four hours post-TBI were negatively skewed, and the trace distribution at three days post-TBI was positively skewed.

*Normalized T2*

After induction of TBI the normalized T2 decreased from 0.4605 $\pm$ 0.04133 (median $\pm$ std) pre-TBI to 0.4427 $\pm$ 0.03513 four hours post-TBI and increased to 0.4701 $\pm$ 0.0540 twenty-four hours post-TBI (Figure 71 J). At three days post-TBI the normalized T2 decreased to 0.4421 $\pm$ 0.0641 three days post TBI followed by a further decrease to 0.4143 $\pm$ 0.04289 seven days post-TBI (Figure 71 J).  In comparison to pre-TBI, the normalized T2 distribution became less dispersed at four hours and seven days post-TBI and became more spread out at twenty-four hours and three days post-TBI (Figure 71J).  At four hours post-TBI the IQR of the normalized T2 distribution decreased from 0.0810 pre-TBI (25$^{th}$ percentile = 0.4385, 75$^{th}$ percentile = 0.5195) to 0.0657 four hours post-TBI (25$^{th}$ percentile = 0.3976, 75$^{th}$ percentile = 0.4633), then increased at twenty-four hours post TBI to 0.1058 (25$^{th}$ percentile = 0.3721, 75$^{th}$ percentile = 0.4779).  After the twenty-four-hour post-TBI, the IQR of the normalized T2 distribution further increased to 0.1333 at three days post TBI (25$^{th}$ percentile = 0.3813, 75$^{th}$ percentile = 0.5146) and then decreased to 0.0443 seven days post TBI (25$^{th}$ percentile = 0.4114, 75$^{th}$ percentile = 0.4557).  In addition, the range of the normalized T2 distribution decreased from 0.10 (T2 $_{min}$ = 0.42, T2$_{max}$= 0.52) pre-TBI to 0.09 (T2$_{min}$ = 0.38, T2$_{max}$= 0.47) four hours post-TBI and then increased to 0.11 (T2$_{min}$ = 0.37, T2$_{max}$= 0.48) twenty-four hours post-TBI.  At three days post-TBI the range of normalized T2 increased to 0.16 (T2$_{min}$ = 0.37, T2$_{max}$=

0.53), afterwhich it decreased at seven days post-TBI to 0.11 (T2$_{min}$ = 0.41, T2$_{max}$= 0.52). At seven days post-TBI the normalized T2 distribution had a maximum extreme outlier present in the data set. Note that the normalized T2 distribution was negatively skewed at pre-TBI, four hours, and twenty-four hours post-TBI and positively skewed at three days post-TBI.
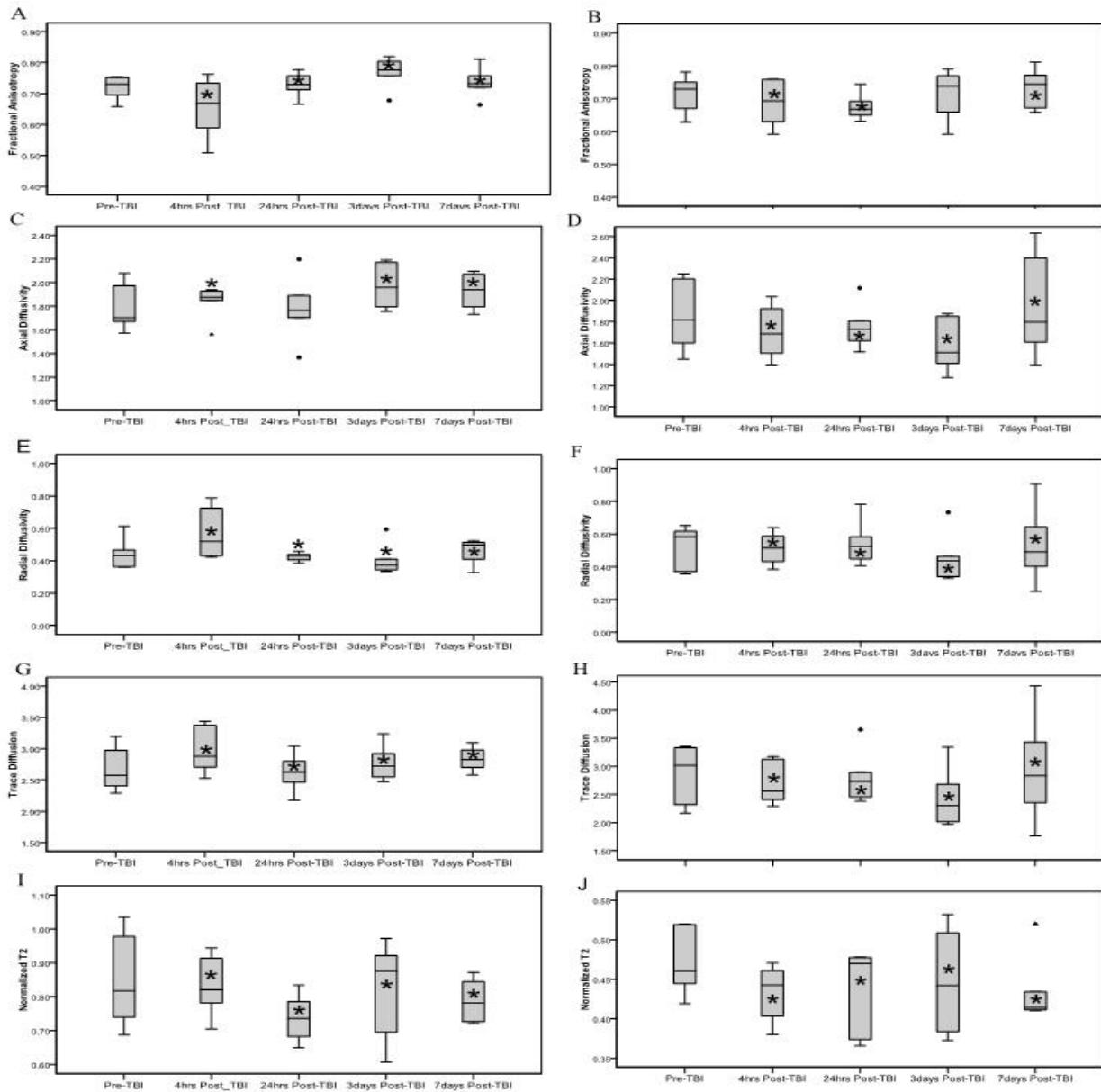


**Figure 71:** Group D average (n=6) (A, B) FA, (C, D) AD, (E, F) RD, (G, H) diffusion trace, and (I, J) T2 values at pre-TBI, four hours and twenty-four hours, three days and seven days post-TBI within the CC (left column) and Och (right column). Diffusivity unit of measurement is 10-3 mm2/s. The • and ▲ represents mild and extreme outlier in the data set respectively. * represents statistical significance (p<0.05) between pre-TBI and post-TBI.
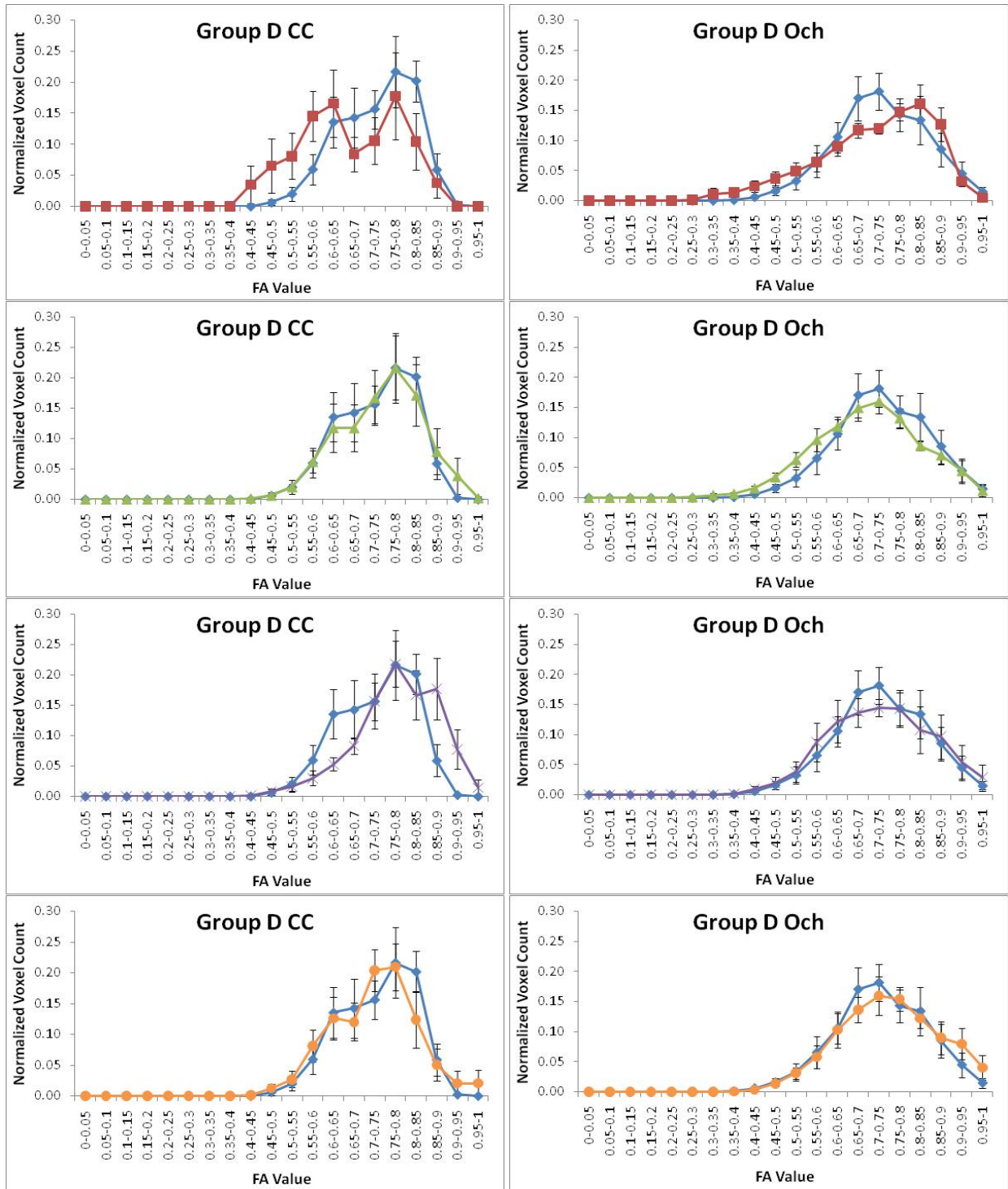
**Figure 72:** FA histograms of the CC V-like shape ROI (left) and Och (right) for all rats (n=6) in group D. The histograms are group average histograms at pre-TBI (blue, diamond), four hours post-TBI (red, square), twenty-four hours post-TBI (green, triangle), three days post-TBI (purple, x), and seven days post-TBI (orange, circle). The FA total range (x-axis) was divided into twenty equally spaced bins of 0.05 with marker (diamond, square, triangle, x, or circle) representing each bin. Error bars represent the standard error.

**Table 15:** Comparison of the CC FA histogram shape parameters.

| CC | Pre-TBI | | 4hrs Post-TBI | | Difference | 24hrs Post-TBI | | Difference | 3days Post-TBI | | Difference | 7days Post-TBI | | Difference |
|---|---|---|---|---|---|---|---|---|---|---|---|---|---|---|
| Parameter | Mean | Std Error | Mean | Std Error | Post - Pre | Mean | Std Error | Post - Pre | Mean | Std Error | Post - Pre | Mean | Std Error | Post - Pre |
| Skewness | -0.336 | 0.031 | -0.034 | 0.031 | 0.302 | -0.256 | 0.031 | 0.08 | -0.574 | 0.031 | -0.238 | -0.107 | 0.033 | 0.229 |
| Kurtosis | -0.703 | 0.062 | -1.053 | 0.062 | -0.35 | -0.447 | 0.062 | 0.256 | 0.078 | 0.062 | 0.781 | -0.175 | 0.067 | 0.528 |
| FA Mean | 0.7192 | 0.00115 | 0.6551 | 0.0015 | -0.0641 | 0.7296 | 0.00128 | 0.0104 | 0.7687 | 0.00132 | 0.0495 | 0.7246 | 0.0014 | 0.0054 |

**Table 16:** Comparison of the Och FA histogram shape parameters.

| Och | Pre-TBI | | 4hrs Post-TBI | | Difference | 24hrs Post-TBI | | Difference | 3days Post-TBI | | Difference | 7days Post-TBI | | Difference |
|---|---|---|---|---|---|---|---|---|---|---|---|---|---|---|
| Parameter | Mean | Std Error | Mean | Std Error | Post - Pre | Mean | Std Error | Post - Pre | Mean | Std Error | Post - Pre | Mean | Std Error | Post - Pre |
| Skewness | -0.11 | 0.024 | -0.524 | 0.24 | -0.414 | -0.148 | 0.024 | -0.038 | -0.053 | 0.026 | 0.057 | -0.102 | 0.026 | 0.008 |
| Kurtosis | -0.234 | 0.049 | -0.456 | 0.049 | -0.222 | -0.153 | 0.047 | 0.081 | -0.494 | 0.051 | -0.26 | -0.466 | 0.052 | -0.232 |
| FA Mean | 0.7099 | 0.00113 | 0.6863 | 0.00146 | -0.0236 | 0.674 | 0.00129 | -0.0359 | 0.7227 | 0.00133 | 0.0128 | 0.7441 | 0.0013 | 0.0342 |

At four hours post-TBI a small shift to the left which represents voxel base distribution FA value decrease occurs in the CC (Figure 72).The FA voxel base distribution of the CC is a bimodal distribution at four hours post-TBI. At twenty-four hours and three days post-TBI in the Och a small shift to the left which represents voxel base distribution FA value decrease occurs (Figure 72). Unlike the Och, at twenty-four hours and three days post-TBI the FA voxel base distribution is shifted to the right in the CC indicating an increase in the FA voxel values (Figure 72). At seven days post-TBI the FA voxel base distribution is shifted to the right in the Och indicating an increase in the FA voxel values (Figure 72). In the CC at seven days post-TBI the FA voxel base distribution is shifted back and resembles the pre-TBI distribution (Figure 72).

In addition, other shape changes also occurred at four hours, twenty-four hours, three days and seven days post-TBI compared to pre-TBI (Tables 15-16). At four hours post-TBI compared to pre-TBI these shape changes included negative kurtosis in CC and Och and skewness (positive in CC and negative in Och). At twenty-four hours post-TBI compared to pre-TBI the shape changes included positive kurtosis in the CC and Och and skewness (positive in CC and negative in Och). At three days post-TBI compared to pre-TBI the shape changes

included positive kurtosis in the CC and negative kurtosis Och and skewness (negative in CC and positive in Och). At seven days post-TBI compared to pre-TBI the shape changes included positive kurtosis in the CC and negative kurtosis Och and skewness (positive in CC and Och).

The FA data distributions are more platykurtic at four post-TBI in the CC and Och and at three days and seven days post-TBI in the Och in comparison to pre-TBI since their post-TBI mean kurtosis values are less than their pre-TBI mean kurtosis values (Tables 15 and 16).

TBI Outcome detected in MRI Alteration in Individual Rat's

The data distribution discussed above in group D was derived from six rats imaged at pre-TBI, four hours, twenty-four hours, three days, and seven days post-TBI. The MRI changes detected within these animals between pre-TBI and four hours post-TBI, between pre-TBI and twenty-four hours post-TBI, between pre-TBI and three days post-TBI, and between pre-TBI and seven days post-TBI were not uniform across all rats (Figure 73). Within the CC ROI five of the rats demonstrated a significant decrease in their FA values, and one rat demonstrated a significant increase in its FA values in comparison to pre-TBI (Figure 73 A). At twenty-four hours post-TBI within the CC one rat demonstrated a significant decrease in its FA values, three rats demonstrated an increase in their FA values, and two rats demonstrated no significant change to their FA values compared to pre-TBI (Figure 73 A). At three days post-TBI within the CC one demonstrated a significant decrease in its FA values while five rats demonstrated a significant increase in their FA values compared to pre-TBI (Figure 73 A). Finally, at seven days post-TBI within the CC three demonstrated a significant decrease in their FA values and three rats demonstrated a significant increase in their FA values compared to pre-TBI (Figure 73 A). Within the Och, three rats demonstrated a significant decrease in their FA values while three rats demonstrated a significant increase in their FA value compared to pre-TBI (Figure 73 B). At twenty-four hours post-TBI within the Och three rats demonstrated a significant decrease in their FA values, one rat demonstrated a significant increase in its FA values, and two rats

demonstrated insignificant changes in their FA values in comparison to pre-TBI (Figure 73 B). At three days post-TBI within the Och two rats demonstrated a significant decrease in their FA values, and four rats demonstrated a significant increase in their FA values compared to pre-TBI (Figure 73 B). Lastly, at seven days post TBI within the Och three rats demonstrated a significant decrease in their FA values, and three rats demonstrated a significant increase in their FA values compared to pre-TBI (Figure 73 B).On average both CC and Och illustrated a decrease in the FA values at four hours. At twenty-four hours and three days post-TBI the average FA increased and decreased in the CC and Och respectively in comparison to pre-TBI. At seven days post-TBI the average FA decreased in the CC and increased in the Och in comparison to pre-TBI. Also, the rats FA changes at four hours, twenty-four hours, three days, and seven days post-TBI were not consistent in each rat between the two (CC and Och) ROI (Figure 73 A, B). For the FA voxel base distribution of each rat refer to appendix C.

Additionally, the diffusivity behaviors across the individual rats can be summarized as follows. Within the CC ROI two of rats demonstrated a significant decrease in their AD values, three rats demonstrated a significant increase in their AD values, and one rat demonstrated insignificant changes in its FA values at four hours post-TBI in comparison to pre-TBI (Figure 73 C). At twenty-four hours post-TBI within the CC two rats demonstrated a significant decrease in their AD values, and four rats demonstrated a significant increase in their AD values in comparison to pre-TBI (Figure 73 C).At three days post-TBI within the CC one rat demonstrated a significant decrease in its AD values, and five rats demonstrated a significant increase in their AD values in comparison to pre-TBI (Figure 73 C). Finally, at seven days post-TBI within the CC two rats demonstrated a significant decrease in their AD values, and four rats demonstrated a significant increase in their AD values in comparison to pre-TBI (Figure 73 C). Within the Ochthree of rats demonstrated a significant decrease in their AD values, two rats demonstrated a significant increase in their AD values, and only one rat demonstrated insignificant changes in

its AD values at four hours post-TBI in comparison to pre-TBI (Figure 73 D). At twenty-four hours and three days post-TBI within the Och three rats demonstrated a significant decrease in their AD values, and three rats demonstrated a significant increase in their AD values in comparison to pre-TBI (Figure 73D).At seven days post-TBI within the Och two rats demonstrated a significant decrease in their AD values, three rats demonstrated a significant increase in their AD values, and one rat demonstrated no significant change in its AD values in comparison to pre-TBI (Figure 73D).Within the CC ROI one rat demonstrated a significant decrease in its RD values, and five rats demonstrated a significant increase in their RD value at four hours post-TBI in comparison to pre-TBI (Figure 73 E). At twenty-four hours post-TBI within the CC three rats demonstrated a significant decrease in their RD values, and three rats demonstrated a significant increase in their RD values in comparison to pre-TBI (Figure 73E). At three days post-TBI within the CC four rats demonstrated a significant decrease in their RD values, and two rats demonstrated a significant increase in their RD values in comparison to pre-TBI (Figure 73E). Finally, at seven days post-TBI within the CC two rats demonstrated a significant decrease in their RD values, and four rats demonstrated a significant increase in their RD values in comparison to pre-TBI (Figure 73E).Within the Och two rats demonstrated a significant decrease in their RD values, and four rats demonstrated a significant increase in their RD values at four hours post-TBI in comparison to pre-TBI (Figure 73 F). At twenty-four hours, three days and seven days post-TBI within the Och three rats demonstrated a significant decrease in their RD values, and three rats demonstrated a significant increase in their RD values in comparison to pre-TBI (Figure 73 F). At twenty-four hours, three days, and seven days post-TBI the three rats that exhibited an increase or decrease in their RD values were not the same three rats at each time point but rather various different combination of three rats within the group of six (Figure 73 F).

On average, the CC illustrated an increase in the AD values at four hours, three days, and seven days post-TBI in comparison to pre-TBI whereas the Och illustrated an increase only at seven days post-TBI compared to pre-TBI. Furthermore, on average, the CC illustrated a decrease in the AD values at twenty-four hours post-TBI, and the Och illustrated a decrease in the AD values at four hours, twenty-four hours, and three days post-TBI compared to pre-TBI. The RD on average demonstrated an increase at four hours and seven days post-TBI within the CC and at twenty-four hours and seven days post-TBI within the Och. In addition, on average a decrease in RD occurred at twenty-four hours and three days post-TBI within the CC and at four hours and three days post-TBI within the Och. Other diffusion values that were measured included diffusion trace. Within the CC, the diffusion trace decreased in one rat and increased in five rats at four hours post-TBI in comparison to pre-TBI (Figure 73 G). At twenty-four hours post-TBI within the CC, the diffusion trace decreased in one rat and increased in four rats in comparison to pre-TBI (Figure 73 G). One rat demonstrated no significant change in the diffusion trace within the CC at twenty-four hours post-TBI in comparison to pre-TBI (Figure 73 G). At three days post-TBI within the CC the diffusion trace decreased in three rats and increased in three rats compared to pre-TBI (Figure 73 G). Finally within the CC at seven days post-TBI the diffusion trace decreased in one rat, increased in four rats, and remained statistically the same in one rat in comparison to pre-TBI (Figure 73 G). Within the Och the diffusion trace decreased in three rats, and increased in three rats at four hours post-TBI in comparison to pre-TBI (Figure 73 H). At twenty-four hours post-TBI within the Och the diffusion trace decreased in one rat and increased in four rats, while one rat had no significant change in its diffusion trace values in comparison to pre-TBI (Figure 73 H). At three days post-TBI within the Och the diffusion trace decreased in five rats and increased in only one rat in comparison to pre-TBI (Figure 73 H). Finally, at seven days post-TBI within the Och the diffusion trace decreased in two rats and increased in three rats with one rat having no significant change in its diffusion trace values in comparison to pre-TBI (Figure 73 H). On average, within the CC the diffusion trace increased at

four hours, three days, and seven days post-TBI and decreased at twenty-four hours post-TBI compared to pre-TBI. Within the Och on average the diffusion trace increased at seven days post-TBI and decreased at four hours, twenty-four hours, and three days post-TBI compared to pre-TBI.

The normalized T2 values of these rats also demonstrated various changes at four hours, twenty-four hours and three days post-TBI within the CC and Och. Compared to the pre-TBI values, at four hours post-TBI the normalized T2 values within the CC decreased in four rats and increased in two rats compared to pre-TBI(Figure 73 I). At twenty-four hours post-TBI the normalized T2 values within the CC decreased in five rats and increased in one rat compared to pre-TBI (Figure 73 I). At three days post-TBI the normalized T2 values within the CC decreased in four and increased in two rats as compared to pre-TBI (Figure 73 I). Finally, at seven days post-TBI the normalized T2 values within the CC decreased in five and increased in only one rat compared to pre-TBI (Figure 73 I). Within the Och five rats demonstrated a decrease in their normalized T2 values while only one rat demonstrated an increase in its normalized T2 values at four hours post-TBI in comparison to pre-TBI (Figure 73 J). Within the Och at twenty-four hours post-TBI four rats demonstrated a decrease in their normalized T2 values and two rats demonstrated an increase in their normalized T2 values (Figure 73 J). At three days post-TBI within the Och three rats demonstrated a decrease in their normalized T2 values, two rats demonstrated an increase in their normalized T2 values, and onedemonstrated no significant change in its normalized T2 values compared to pre-TBI (Figure 73 J). Lastly, at seven days post-TBI within the Och four rats demonstrated a decrease in their normalized T2 values, one rat demonstrated an increase in its normalized T2 values, and one demonstrated no significant change in its normalized T2 values compared to pre-TBI (Figure 73 J). On average, within the CC and Och the normalized T2 values remained decreased at four hours, twenty-four hours, three days, and seven days post-TBI in comparison to pre-TBI.
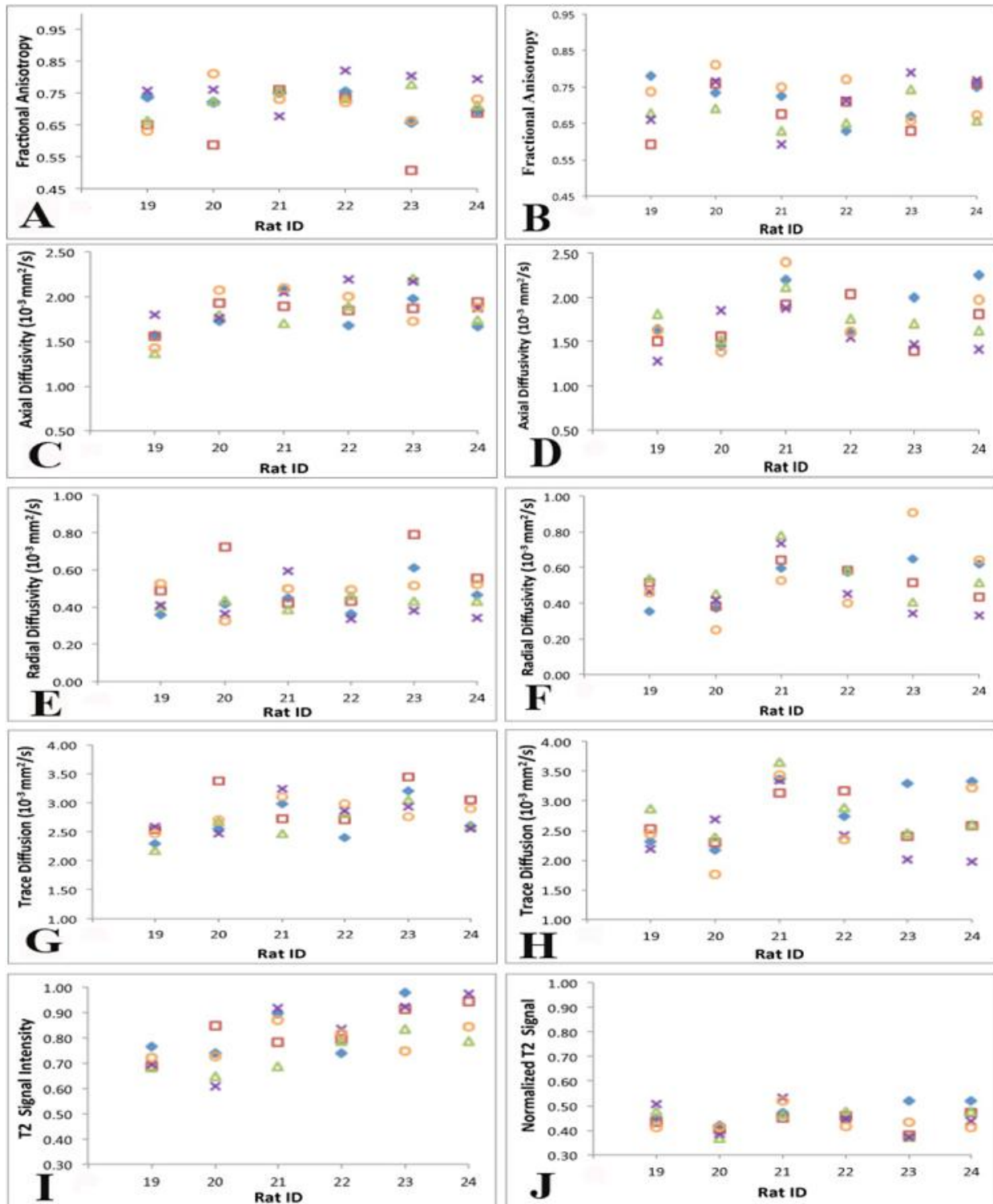
**Figure 73:** Group D's (A, B) FA, (C, D) AD, (E, F) RD, (G, H) diffusion trace, and (I, J) T2 values at pre-TBI (blue, diamond), four hours post-TBI (red, square), twenty four hours post-TBI (green, triangle), three days post-TBI (purple, x), and seven days post TBI (orange, circle) for each rat within the CC (left column) and Och (right column).

## MRI Parameters Relationship to Each Other

### *Corpus Callosum*

The normalized T2 changes post-TBI were found to be linearly correlated to various DTI parameters at four hours and three days post-TBI.  Within the CC only at four hours post-TBI and three days post TBI were the changes in the normalized T2 values linearly correlated to various DTI parameters (Figure 74).  At four hours post-TBI the FA changes illustrated a significant negative linear relationship ($R^2$ = 0.289, $p \leq$ 0.01) with the normalized T2 changes (Figure 74 A).  After four hours post-TBI within the CC the FA linear relationship with the normalized T2 was no longer statistically significant.  At four hours post-TBI the RD changes illustrated a significant positive linear relationship ($R^2$ = 0.477, $p \leq$ 0.01) with the normalized T2 changes (Figure 74 B).  In addition, the RD changes also illustrated a significant positive linear relationship ($R^2$ = 0.341, $p \leq$ 0.05) with the normalized T2 changes at three days post-TBI (Figure 74 D).  The last DTI parameter that was found to correlate with the detected changes of the normalized T2 signal post-TBI within the CC was the diffusion trace.  At four hours post-TBI the diffusion trace changes illustrated a significant positive linear relationship ($R^2$ = 0.324, $p \leq$ 0.01) with the normalized T2 changes (Figure 74 C).  Also at three days post-TBI the diffusion trace changes illustrated a significant positive linear relationship ($R^2$ = 0.500, $p \leq$ 0.01) with the normalized T2 changes (Figure 74 E).  Within the CC, the AD changes were found to have no linear relationship with the normalized T2 changes at any time point.

The FA value is derived from the radial and axial diffusivity (Chapter 4).  Within the CC the changes in the FA value seemed to be more driven by the RD changes occurring in the tissue rather by the AD changes.  The changes in the FA value seemed to be driven by RD changes because linear relationships were present between the FA and RD at four hours, twenty-four hours, and three days post-TBI while no linear relationship is present between the FA and AD at any time point.  At four hours post-TBI the RD changes illustrated a significant

negative linear relationship ($R^2$ = 0.624, p $\leq$ 0.01) with the FA changes (Figure 75 A).  At twenty-four hours post-TBI the RD changes illustrated a significant negative linear relationship ($R^2$ = 0.676, p $\leq$ 0.01) with the FA changes (Figure 75 B).  At three days post-TBI the RD changes illustrated a significant negative linear relationship ($R^2$ = 0.468, p $\leq$ 0.05) with the FA changes (Figure 75 C).
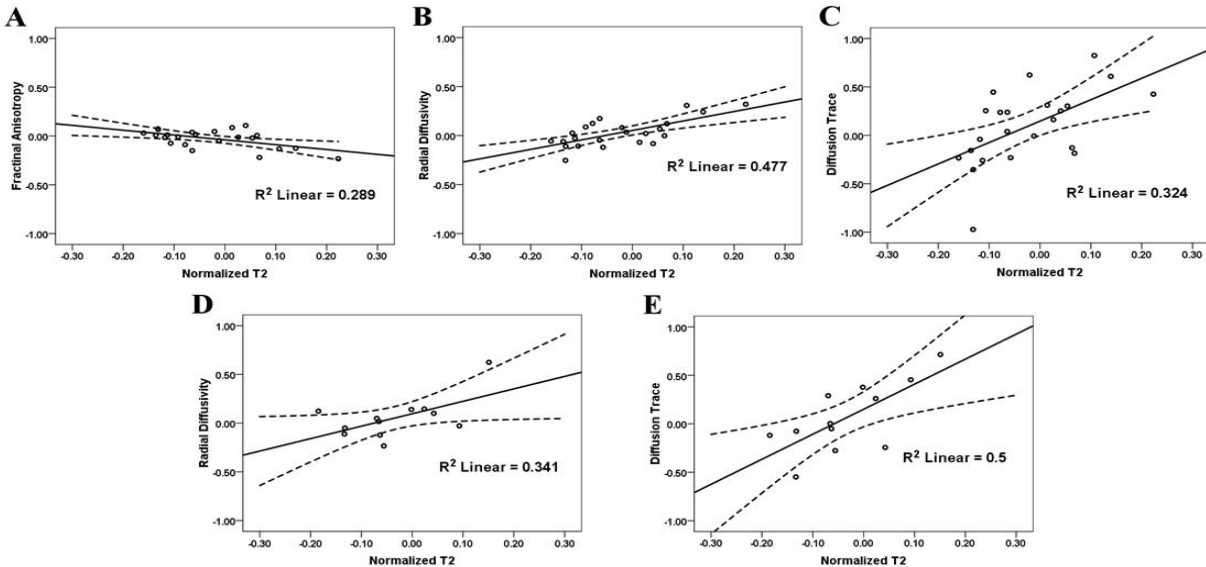


**Figure 74:** These graphs represent significant linear relationships within the CC between the changes in normalized T2 and (A) FA, (B, D) RD and (C, E) diffusion trace at four hours post-TBI (A - C) and three days post-TBI (D - E) compared to pre-TBI.  Each circle represents a data from one rat.  The x axis represents the change of the normalized T2 and the y axis represents (A) FA, (B, D) RD (diffusivity × $10^{-3}$mm$^2$/s), and (C, E) Diffusion trace (diffusivity × $10^{-3}$mm$^2$/s).  Each circle represents the data from one rat.  Dashed lines represent the 95% confidence intervals.
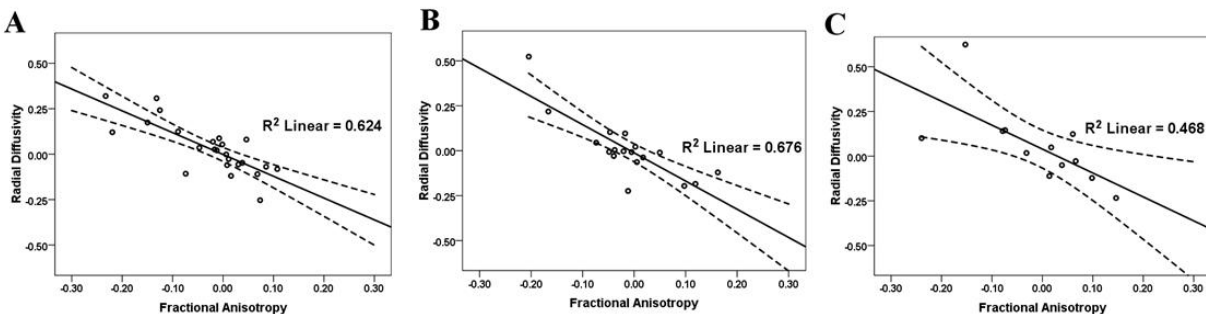


**Figure 75**: These graphs represent significant linear relationships within the CC between the changes FA and RD at (A) four hours post-TBI, (B) twenty-four hours post-TBI, and (C) three days post-TBI compared to pre-TBI.  This linear relationship is expected since FA and RD are dependent on the eigenvalues.  Each circle represents a data from one rat.  The x axis represents the change of the FA and the y axis represents RD (diffusivity × $10^{-3}$mm$^2$/s).  Each circle represents the data from one rat.  Dashed lines represent the 95% confidence intervals.

The diffusion trace value is derived from the radial and axial diffusivity (Chapter 4). Within the CC the changes in the diffusion trace value seemed to be driven by AD and RD at four hours post-TBI, since AD and RD changes illustrated a linear relationship with the diffusion trace changes. At four hours post-TBI the AD changes illustrated a significant positive linear relationship ($R^2$ = 0.534, $p \leq 0.01$) with the diffusion trace changes (Figure 76 C). In addition, at four hours post-TBI the RD changes illustrated a significant positive linear relationship ($R^2$ = 0.547, $p \leq 0.01$) with the diffusion trace changes (Figure 76 A). However, after four hours post-TBI the AD changes no longer illustrated a relationship with the diffusion trace. Only RD illustrated a positive linear relationship ($R^2$ = 0.486, $p \leq 0.05$) at three days post-TBI with the diffusion trace (Figure 76 B).
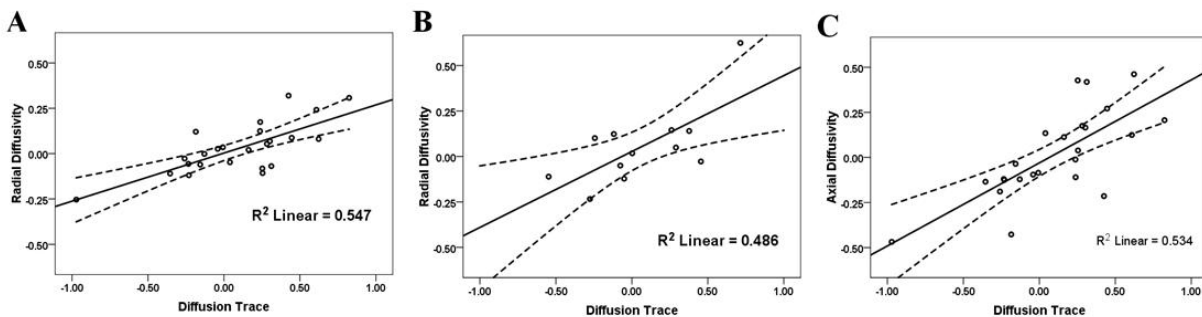


**Figure 76:** These graphs represent significant linear relationships within the CC between the changes diffusion trace and RD at (A) four hours post-TBI, and (B) 3days post-TBI, also between the trace and AD at (C) four hours post-TBI. This linear relationship is expected since diffusion trace, RD and AD are dependent on the eigenvalues. Each circle represents a data from one rat. The x axis represents the change of the diffusion trace and the y axis represents (A, B) RD (diffusivity × $10^{-3}$mm$^2$/s) and (C) AD (diffusivity × $10^{-3}$mm$^2$/s). Each circle represents the data from one rat. Dashed lines represent the 95% confidence intervals.

### *Optic Chiasm*

The normalized T2 changes post-TBI were found to be linearly correlated to various DTI parameters at four hours and there days post-TBI. Within the Och only at four hours post-TBI and three days post TBI were the changes in the normalized T2 values linearly correlated to various DTI parameter (Figure 77). At four hours post-TBI the AD changes illustrated a significant positive linear relationship ($R^2$ = 0.175, $p \leq 0.05$) with the normalized T2 changes

(Figure 77 B).  After four hours post-TBI the AD and normalized T2 linear relationship was no longer statistically significant within the Och.  At four hours post-TBI the diffusion trace changes illustrated a significant positive linear relationship ($R^2$ = 0.285, p $\leq$ 0.01) with the normalized T2 changes (Figure 77 A).  In addition, the diffusion trace changes also illustrated a significant positive linear relationship ($R^2$ = 0.443, p $\leq$ 0.05) with the normalized T2 changes at three days post-TBI (Figure 77 C).  Also, at three days post-TBI the FA changes illustrated a significant negative linear relationship ($R^2$ = 0.371, p $\leq$ 0.05) with the normalized T2 changes (Figure 77 D).  Furthermore, at three days post-TBI the RD changes illustrated a significant positive linear relationship ($R^2$ = 0.515, p $\leq$ 0.01) with the normalized T2 changes (Figure 77 E).
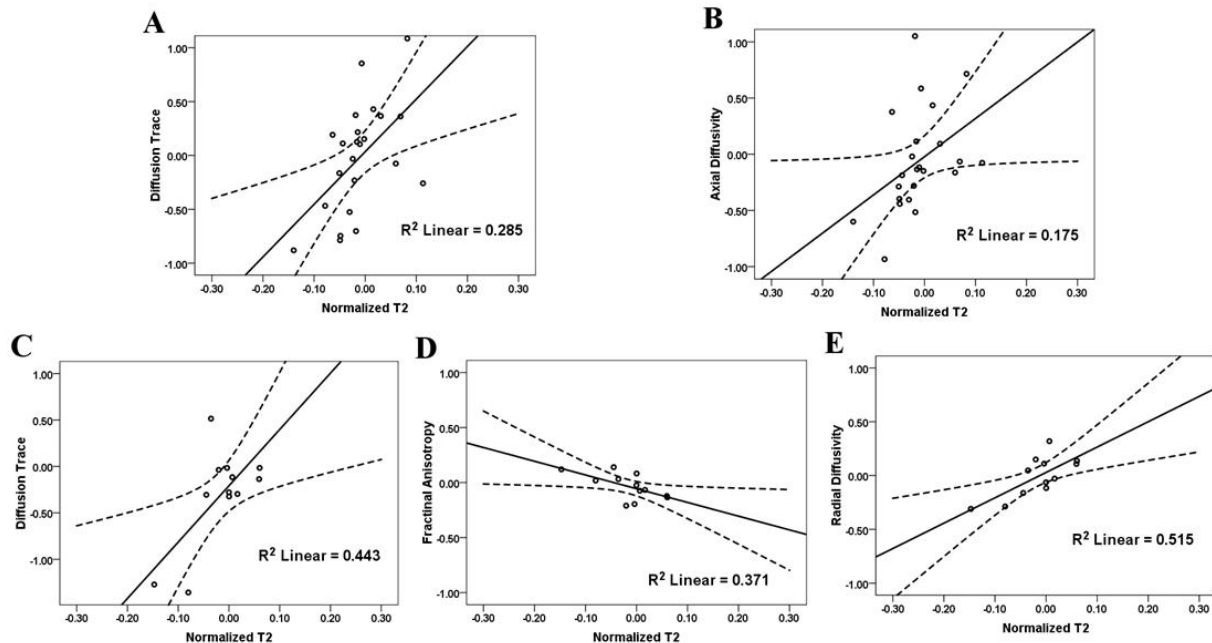


**Figure 77:** These graphs represent significant linear relationships within the Och between the changes in normalized T2 and (A, C) diffusion trace, (B) AD, (D) FA, and (C, E) RD at four hours post-TBI (A, B) and three days post-TBI (C - E) compared to pre-TBI.  Each circle represents a data from one rat.  The x axis represents the change of the normalized T2 and the y axis represents (A, C) diffusion trace (diffusivity × $10^{-3}$mm$^2$/s), (B) AD (diffusivity × $10^{-3}$mm$^2$/s), (D) FA, and (C, F) RD (diffusivity × $10^{-3}$mm$^2$/s).  Each circle represents the data from one rat. Dashed lines represent the 95% confidence intervals.

Similar to CC within the Och the changes in the FA value seemed to be driven more by the RD changes occurring in the tissue rather by the AD changes since a linear relationship was

present between the FA changes and the RD changes at four hours, twenty-four hours, and three days post-TBI while no linear relationship was present between the AD changes and the FA changes at any time point.  At four hours post-TBI the RD changes illustrated a significant negative linear relationship ($R^2$ = 0.229, $p \leq 0.05$) with the FA changes (Figure 78 A).  At twenty-four hours post-TBI the RD changes illustrated a significant negative linear relationship ($R^2$ = 0.352, $p \leq 0.05$) with the FA changes (Figure 78 B).  At three days post-TBI the RD changes illustrated a significant negative linear relationship ($R^2$ = 0.554, $p \leq 0.01$) with the FA changes (Figure 78 C).
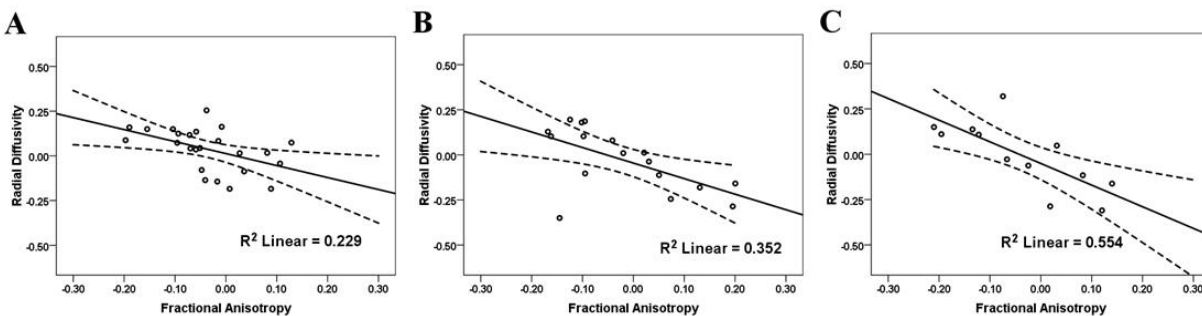


**Figure 78:** These graphs represent significant linear relationships within the Och between the changes FA and RD at (A) four hours post-TBI, (B) twenty-four hours post-TBI, and (C) three days post-TBI compared to pre-TBI.  This linear relationship is expected since FA, and RD are dependent on the eigenvalues.  Each circle represents a data from one rat.  The x axis represents the change of the FA and the y axis represents RD (diffusivity × $10^{-3}$mm$^2$/s).  Each circle represents the data from one rat.  Dashed lines represent the 95% confidence intervals.

Within the Och the changes in the diffusion trace value seemed to be driven by AD and RD at four hours, three days and seven days post-TBI, since AD and RD changes illustrated a linear relationship with the diffusion trace changes.  At twenty-four hours post-TBI, the diffusion trace seemed to be driven only by the RD changes since, the AD linear relationship with diffusion trace was absent at this time point.  At four hours post-TBI the AD changes illustrated a significant positive linear relationship ($R^2$ = 0.719, $p \leq 0.01$) with the diffusion trace changes (Figure 79 A).  In addition, at four hours post-TBI the RD changes illustrated a significant positive linear relationship ($R^2$ = 0.47, $p \leq 0.01$) with the diffusion trace changes (Figure 79 E).  However, at twenty-four hours post-TBI the AD changes no longer illustrated a relationship with

the diffusion trace but only the RD changes illustrated a positive linear relationship ($R^2 = 0.424$, $p \leq 0.01$) with the diffusion trace (Figure 79 F). In addition, at twenty-four hours post-TBI the FA changes illustrated a negative linear relationship with the diffusion trace changes (Figure 79 B). Furthermore, at three days post-TBI the AD changes illustrated a significant positive linear relationship ($R^2 = 0.548$, $p \leq 0.01$) with the diffusion trace changes (Figure 79 C) and, the RD changes illustrated a significant positive linear relationship ($R^2 = 0.585$, $p \leq 0.01$) with the diffusion trace changes (Figure 79 G). Finally, at seven days post-TBI the AD changes illustrated a significant positive linear relationship ($R^2 = 0.723$, $p \leq 0.05$) with the diffusion trace changes (Figure 79 D) and, the RD changes illustrated a significant positive linear relationship ($R^2 = 0.830$, $p \leq 0.05$) with the diffusion trace changes (Figure 79 H).
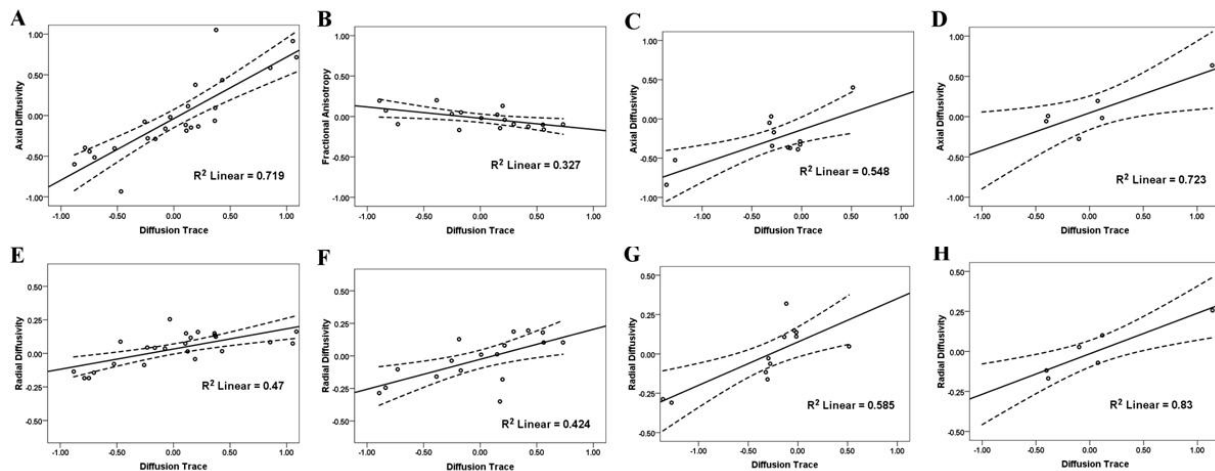


**Figure 79:** These graphs represent significant linear relationships within the Och between the changes in diffusion trace and (A, C, and D) AD, (B) FA, and (E - H) RD at (A, E) four hours post-TBI, (B, F) twenty-four hours post-TBI, (C, G) three days post-TBI and (D, H) seven days post-TBI compared to pre-TBI. This linear relationship is expected since diffusion trace, FA, RD and AD are dependent on the eigenvalues. Each circle represents a data from one rat. The x axis represents the change of the diffusion trace and the y axis represents (A, C, and D) AD (diffusivity × $10^{-3}$ mm$^2$/s), (B) FA, and (E - H) RD (diffusivity × $10^{-3}$ mm$^2$/s). Each circle represents the data from one rat. Dashed lines represent the 95% confidence intervals.

## Specific Aim 2 Discussion

Hypothesis 2: DAI is a secondary injury of TBI; therefore, as time progresses the axonal injury will become more prominent over 24 hours as delayed axotomy progresses. It was

hypothesized that the detection of DTI parameter changes are a good indicator of axonal injury progression over time. As time progresses after induction of TBI, the axonal pathology profile changes as recovery of some axons will occur and other axons will become disconnected from their distal end. It is hypothesized that this pathological profile of axonal injury over time will be reflected by the DTI parameter changes over time.

Since the DTI data in this study were acquired with b value of 800 mm/s$^2$, the DTI changes are indicative of the changes in the fast diffusion compartment in the tissue (Clark and Le Bihan 2000). Because fast diffusion compartments are believed to be a representation of the extracellular space, the DTI parameters changes are indication of the changes of the extracellular space due to injury (Clark and Le Bihan 2000; Inglis, Bossart et al. 2001; Le Bihan, Mangin et al. 2001). Therefore, the explanation of the DTI parameter changes will be focused on the possible changes that may have occurred in the extracellular space as a result of TBI.

At four hours post-TBI the FA values illustrated a decreased trend across all groups within the CC and the Och. The decrease of FA values within the Och was greater than the FA decrease within CC except for group D where the Och demonstrated a greater TAI density in comparison to CC (refer to chapter 3). Since the Och demonstrated a greater density of TAI (Chapter 3) than CC the greater decrease of FA in Och as compared to CC is consistent with the histological findings.

Immediately after induction of TBI it has been reported that the blood brain barrier (BBB) becomes more permeable (Barzo, Marmarou et al. 1996; Adelson, Whalen et al. 1998; Beaumont, Marmarou et al. 2000; O'Connor, Cernak et al. 2006). Ghabriel et al reported in rats impacted with the impact acceleration model at one hour to three hours post-TBI the tight junction between the endothelial cells of the blood vessels were open and the perivascular astrocytic end-feet were swollen (Ghabriel, Zhu et al. 2004). At twelve hours post-TBI it was

reported that the astrocytic swelling became maximal whereas the endothelial cells of the blood vessels became normal (Ghabriel, Zhu et al. 2004).  Also Beaumont et al reported that after induction of TBI to rats with the impact acceleration model, the BBB immediately and uniformly opened up for a short period of time and at four hours post-TBI the BBB returned to normal (Beaumont, Marmarou et al. 2000).  The opening of the BBB led to increased water content in the extracellular space of the brain, defined as vasogenic edema.  As early as 60 min post-TBI Barzo et al reported an increase in the brain water content in rats injured via the impact acceleration model.  Foda and Marmarou (1994) reported a widening of the extracellular space of the rat brains at six and twenty four hours after induction of TBI with the impact acceleration injury model  As well, it has been  reported that swelling of the pericapillary of the foot process of the astrocytes occurred at six and twenty-four hours post TBI (Foda and Marmarou 1994; Ghabriel, Zhu et al. 2004).  Papadopoulos et al., via diffusion measurements of fluorescence recovery after photobleaching, reported that vasogenic edema increased in the extracellular space and thereby increased diffusivity, whereas the swelling of the cells (cytotoxic edema) decreased the extracellular space and thus decreased diffusivity (Papadopoulos, Binder et al. 2005).  A decrease in diffusivity caused a reduction in the apparent diffusion coefficient (ADC) value and an increase in diffusivity  caused an increase in the ADC value since diffusion was the average of the eigenvalues (Marmarou 2007). ADC derived from diffusion-weighted imaging (DWI) was equivalent to the diffusion trace derived from diffusion tensor imaging (Hagmann, Jonasson et al. 2006); therefore, a decrease and an increase in diffusion represented a decrease and an increase in the diffusion trace respectively.  In animal studies, changes in ADC values after TBI have been shown to be related to edema (Sevick, Kanda et al. 1992; Ito, Marmarou et al. 1996; Barzo, Marmarou et al. 1997; Barzo, Marmarou et al. 1997; Kuroiwa, Nagaoka et al. 1998; Kuroiwa, Nagaoka et al. 1999; Albensi, Knoblach et al. 2000; Kuroiwa, Nagaoka et al. 2000; Kuroiwa, Miyasaka et al. 2007).

Edema can be classified as two types, vasogenic edema or cytotoxic edema. Vasogenic edema occurs as a result of BBB disruption, whereas cytotoxic edema occurs independently of BBB integrity (Unterberg, Stover et al. 2004). Vasogenic morphology is increased interstitial space (extracellular space) and not cell swelling refer to Figure 80 B (Unterberg, Stover et al. 2004). Conversely, Cytotoxic edema morphology are cell swelling caused by sustained intracellular water accumulation involving both astrocytes and neurons (Unterberg, Stover et al. 2004) resulting in decreased interstitial space (Figure 80 C).
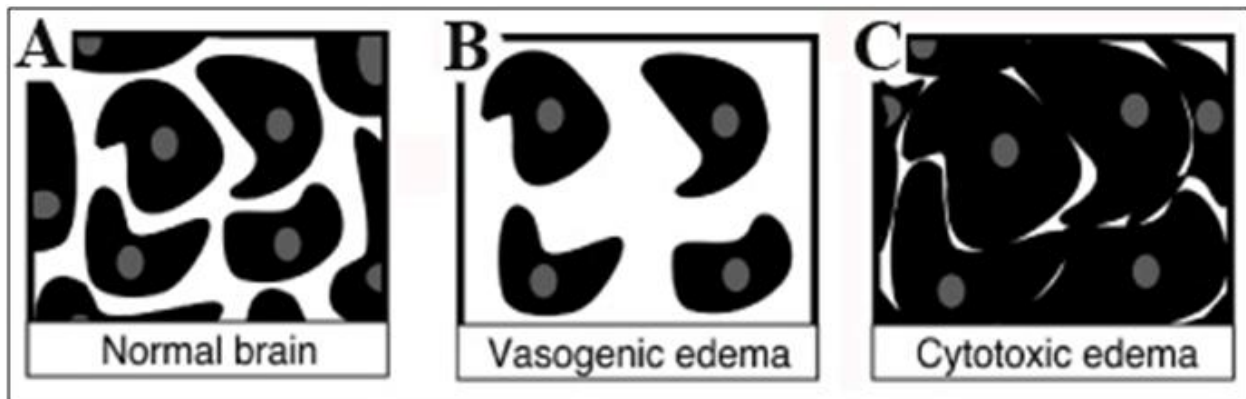


**Figure 80:** This figure represents a schematic of cells (black) and extracellular space (white) of (A) normal brain cell (B) vasogenic edema (swelling around the cells) and (C) cytotoxic edema (swelling of the cells). Note that vasogenic edema increased the extracellular space, whereas cytotoxic edema decreased the extracellular space. (Papadopoulos, Binder et al. 2005)

It has been reported that a significant increase of ADC values occurred in the presence of vasogenic edema (Ito, Marmarou et al. 1996; Barzo, Marmarou et al. 1997) whereas a significant decrease of ADC values occurred in cytotoxic edema (Sevick, Kanda et al. 1992; Ito, Marmarou et al. 1996; Kuroiwa, Miyasaka et al. 2007). Sevick et al. reported a significant inverse linear relationship between ADC and the increased brain water volume (Sevick, Kanda et al. 1992). Additionally, Kuroiwa et al reported an inverse linear correlation between decreased ADC and increased brain tissue water content (Kuroiwa, Nagaoka et al. 1998). The inverse linear relationship between the decrease in ADC and increase in brain water content indicated that ADC might be a sensitive measuring tool of cytotoxic edema. The first 60 min

post-injury ADC increased, thus signifying vasogenic edema (Ito, Marmarou et al. 1996; Barzo, Marmarou et al. 1997)  This increase was followed by a steadily decrease of ADC with the minimal value occurring at seven days post-TBI (Barzo, Marmarou et al. 1997).

In this study, the diffusion trace increased at four hours post-TBI, which might be an indication of vasogenic edema.  The impact acceleration model has been reported to increase permeability of the BBB (Beaumont, Marmarou et al. 2000; Ghabriel, Zhu et al. 2004) while widening of the extracellular space has been reported as part of the pathophysiological changes that occurred after impact (Foda and Marmarou 1994).  In addition to the increased diffusion trace, AD and RD increased as well at four hours post-TBI.  AD and RD describe three-dimensional space environment; therefore, an increase in AD and RD indicated an increase in the diffusion space volume.  Since the b value utilized during the acquisition of the DTI was less than 1500 s/mm$^2$, the increase in AD and RD indicated an increase in the extracellular space (Clark and Le Bihan 2000).  Thus, the increase in AD and RD represent vasogenic edema in the ROI (Figure 80).  Additionally, in this study FA decreased at four hours post-TBI by widening the extracellular space via vasogenic edema (Figure 80), therefore causing the  water diffusion to become less anisotropic.  Since the extracellular space between tightly aligned WM increased, the white mater fibers became less tightly aligned.  This alignment was also evident by the increase of the RD value at four hours post-TBI. In Figures 75 and 78 the relationship between FA and RD became evident as FA and RD tended to have an inverse linear relationship at four hours, twenty-four hours and three days post-TBI whereas the AD changes did not show a linear relationship with FA.  The inverse linear relationship between RD and FA supported the fact that vasogenic edema increased the extracellular space, hence increasing RD and thus decreasing the FA value.  In addition, the FA voxel distribution also supported the presence of edema.  At four hours post-TBI the FA value distribution shift to the left, which indicates that some voxels FA values have decreased.  This decrease of voxels FA values may be an

indication of injury such as vasogenic edema. As time progresses to twenty-four hours and three days post-TBI the FA distribution became wider where some voxels demonstrated a decrease in their FA values while other voxels demonstrated an increase in their FA values. The presence of increased and decreased FA values of the voxels is an indication of two types of injuries occurring at these time points such as vasogenic edema (decreased FA) and cytotoxic edema (increased FA). At seven days post-TBI the widening of the FA distribution became less than that of twenty-four hours and three days post-TBI. The distribution at seven day remained different than that of pre-TBI however, to a lesser extent compared to four hours, twenty-four hours and three days post-TBI. The change of FA distribution at seven days post-TBI in comparison to the other previous post-TBI time point may be an indication of some sort of resolution of injury. A study by Benson et al. has also demonstrated a change in the FA voxel base distribution in TBI patients in comparison to controls (Benson, Meda et al. 2007). This study did not observe a complete shift of the FA voxel base distribution post-TBI similar to that reported by Benson et al for TBI patients (Benson, Meda et al. 2007). Benson et al reported a change in the shape of TBI patients' FA histogram in comparison to controls where the TBI patients' FA distribution became leptokuric compared to control. This study has observed that post-TBI the FA voxel base distribution became platykurtic compared to the pre-TBI FA voxel base distribution. Also, Benson et al reported an increase in the peak of TBI patients' FA distribution compared to controls. This study has observed opposite results where the FA voxel base distribution peak decreased post-TBI compared to the pre-TBI distribution. The differences observed between the FA distribution in this study and Benson et al study may be due to the different imaging time utilized in these two studies. The study by Benson et al. the MRI scans was acquired approximately 35.3 months post-TBI in which loss of axons may have occurred (Benson, Meda et al. 2007). On the other hand, this study acquired the MRI scans at four hours, twenty-four hours, three days and seven days post-TBI where the injury is still at an acute stage. At 35.3 months post-TBI loss of neuronal cells may occur as a result of TBI. The

loss of neuronal cells will cause the extracellular space within the WM to become greater in width since tightly packed and coherently aligned axons become less as the amount of neurons decreases. However, from four hours to seven days post-TBI edema may play a dominant role in the change of diffusion within the extracellular space. At four hours post-TBI the dominant edema would be vasogenic edema which increases the extracellular space therefore, increasing diffusivity and decrease in the FA value (Papadopoulos, Binder et al. 2005). The presence of vasogenic edema can be seen by the increase in the voxel count of the lower FA values at four hours post-TBI. As time elapses cytotoxic edema starts to occur and becomes the more prominent type of edema. Cytotoxic edema decreases the extracellular space which causes a decrease in diffusivity thereby increases FA. The presence of cytotoxic edema can be seen by the increase in the voxel count of the higher FA values from twenty-four hours to seven days post-TBI. The increase in the voxel count of the lower and higher FA values occur together in the same post-TBI (at twenty-four hours and three days post-TBI) FA voxel base distribution supports the notion that both types (vasogenic and cytotoxic) of edema do occur at the same time.

Since the T2 relaxation parameter for water is much greater than in GM and WM, a hyperintense T2 signal represents an increase in the water volume within the ROI. Therefore, it has been established that hyperintensity of the T2 image represents an increase in water volume, thereby indicating edema (Tokutomi, Hirohata et al. 1997; Takayama, Kobayashi et al. 2000; Qiao, Malisza et al. 2001). T2 images cannot discriminate the exact cellular location (intracellular or extracellular) of the increased water and is thus is inadequate in discriminating the type of edema (vasogenic or cytotoxic) that is present (Takayama, Kobayashi et al. 2000). However, ADC has demonstrated a capability of discriminating between vasogenic and cytotoxic edema (Ito, Marmarou et al. 1996; Barzo, Marmarou et al. 1997; Takayama, Kobayashi et al. 2000). In this study, a linear relationship was observed between various DTI parameters and T2 signal intensity change after TBI. At four hours post-TBI the change in the

diffusion trace and RD values demonstrated a positive linear relationship with the change in the T2 signal. Also, at four hours post-TBI the change in the FA values demonstrated an inverse linear relationship with the T2 signal intensity. These linear relationships between the change in the DTI parameters and the T2 signal at four hours post-TBI may have been driven by edema. Edema can cause an increase in T2 signal, whereas vasogenic edema can cause an increase in diffusion trace (positive linear relationship) and a decrease in FA (inverse linear relationship). The presence of vasogenic edema at four hours post-TBI in the current study was in line with other TBI studies (Barzo, Marmarou et al. 1997; Cernak, Vink et al. 2004; Ghabriel, Zhu et al. 2004).

An electron microscope study by Ghabriel et al observed at twelve hours after induction of TBI with the weight-drop the endothelial cells of the BBB returned to normal appearance whereas the swelling of the perivascular astrocyte end-feet processes increased compared to six hours post-TBI (Ghabriel, Zhu et al. 2004). Foda et al. reported at twenty-four hours post-TBI widening of the extracellular space while the swelling of the pericapillary astrocytes feet processes were maximized (Foda and Marmarou 1994). Therefore, at twenty-four hours post-TBI both forms (vasogenic and cytotoxic) of edema coexisted. Note that vasogenic edema widened the extracellular space while cytotoxic edema decreased the extracellular space due to cellular swelling (Figure 80) (Papadopoulos, Binder et al. 2005). Papadopoulos et al. reported that vasogenic edema increased diffusion in the extracellular space while cytotoxic edema decreased diffusion in the extracellular space. Thus the vasogenic edema effect on the DTI parameters were the opposite of that of cytotoxic edema, i.e. vasogenic edema increased diffusion trace and decreased FA whereas cytotoxic edema decreased diffusion trace and increased FA (Barzo, Marmarou et al. 1997). In this study at twenty-four hours post-TBI the diffusion trace and RD values decreased from their four hours post-TBI values. The FA values at 24 hours increased in comparison to the four hours post-TBI. The decrease of the diffusion

trace and RD plus the increase in FA at 24 hours indicates the development of cytotoxic edema at this time point. However, at this time point, some values were below pre-TBI values and other values remained above pre-TBI levels. This change could be an indication of both vasogenic edema and cytotoxic edema present in the tissue at that time.

Due to the presence of vasogenic and cytotoxic edema at twenty-four hours post-TBI it has been reported that microglial and cell debris become present at this time point (Cernak, Vink et al. 2004). The microglial and cell debris in the extracellular space would hinder water diffusion in the extracellular space, thus decreasing the AD. In this study at twenty-four hours post-TBI the AD value decreased. Within the Och the AD decrease was more evident at twenty-four hours post-TBI in comparison to CC. Since the Och TAI density was greater than that observed in the CC, it could be assumed that microglial and cell debris were present to a greater degree in the Och than in the CC.

No linear correlation was found between the changes of DTI parameters and T2 values. This lack of linear correlation also supports the presence of two types (vasogenic and cytotoxic) of edema within the tissue at this time point. For example, the change in T2 values post-TBI to a more hyperintense signal indicates increased water content. Therefore, hyperintense T2 signal was the algebraic summation of the increased water content in vasogenic edema (positive T2 signal) and cytotoxic edema (positive T2 signal). On the other hand, the changes in the DTI parameters post-TBI were the algebraic sum between vasogenic edema (positive diffusion trace, positive RD, negative FA components) and cytotoxic edema (negative diffusion trace, negative RD, positive FA components) effect on diffusion (Marmarou 2003; Unterberg, Stover et al. 2004). Since vasogenic edema and cytotoxic edema had opposite effects on DTI parameters, the detected DTI change within the tissue in the presence of both edemas is driven by the predominant type of edema.

At three days post-TBI the extracellular environment changes according to the degree of the injury. Various events have been documented to occur at three days post-TBI in the Marmarou impact acceleration model, as described below. Damaged axons exhibit Wallerian degeneration at their distal end with macrophages engulfing the degenerated axonal cylinders (Povlishock and Christman 1995; Gaetz 2004). Also an increase in the amount of inflammatory cells occurs at this time point (Raghupathi 2004). Various axons exhibited multiple segmented swelling (Gaetz 2004). In addition, edema was also present at three days post-TBI where cytotoxic edema became the predominant type of edema (Barzo, Marmarou et al. 1997; Marmarou 2003). These extracellular environmental changes occurring at three days post-TBI caused varying effects on the water diffusion within the extracellular compartment. The AD changes within the CC and Och at three days post-TBI were opposite, where AD demonstrated an increase within the CC and a decrease in the Och. Within this impact injury model TAI injury density identified by the β-APP time profile was variable between these two structures (Chapter 2). The Och demonstrated the greatest increase of TAI at four hours post-TBI whereas CC demonstrated its greatest increase of TAI density at twenty-four hours post-TBI. Since the injury time profile was different between the CC and the Och, various histological events such as immune reactivity, axonal swellings and axonal degeneration might have a different time profile within the CC and the Och. One can assume since the TAI profile occurred at an earlier time point within the Och, the immunological response to injury might occur at an earlier time point within the Och as compared to the CC. Therefore immunoreactive cells would be present in the extracellular space of Och, thus hindering the diffusion parallel to the axon and causing the decrease in the AD values. However, since the cytotoxic edema occurred as a result of the initial BBB opening and not the TAI, the cytotoxic edema profile could be assumed to be similar in the Och and the CC. This similarity was evident by the RD value change at three days post-TBI. At three days post-TBI the RD decreased in both CC and Och. The decrease in RD could be an indication of predominance of the cytotoxic edema within the tissue since swelling of the

cells would cause a decrease in the extracellular space (Figure 80). In groups C and D (refer table 6) in the CC diffusion trace values were greater than their pre-TBI diffusion trace value; however, this diffusion trace value remained less than their four hours post-TBI value. Therefore, at three days post-TBI the diffusion trace values could be an indication that vasogenic and cytotoxic edema were both present and that cytotoxic edema dominated. The presence of edema in this group was supported by the fact that the T2 signal was found to be hyperintense. Within the Och group C diffusion trace at three days post-TBI increased in comparison to its pre-TBI diffusion trace value. Similar to CC, the diffusion trace within the Och group C remained less than its four hours post-TBI diffusion trace value. On the other hand, group D diffusion trace value within the Och was less than four hours post-TBI and pre-TBI diffusion trace values. At three days post-TBI the change in the trace values and the change in the T2 signal were statistically significant within the Och and the CC. Additionally, at three days post-TBI within the CC and the Och the water diffusion became more anisotropic in the extracellular space and hence increased the FA. The FA value within the CC and the Och at three days post-TBI was greater than at all the preceding time points. This increase in the FA value was linearly correlated to the RD decrease and not the AD change; thus, the increase of the FA value was related to the decrease of the extracellular space perpendicular to the axonal alignment; this increase could have come about by a swelling of the axons. This increase in fractional anisotropy might have a much more complex explanation than simply being due to edema. At three days post-TBI no linear relationship was present between the changes in FA values and T2 values within the CC. Also, within the Och a negative linear relationship was present between the change in the FA values and T2 values. If cytotoxic edema was the cause behind the FA change, there should have been a positive rather than a negative linear relationship between FA and T2.

Seven days post-TBI, DTI parameters were still significantly different from pre-TBI levels, similar to the study of Barzo et al where it was reported that ADC changes remained significantly different from control two weeks post-TBI (Barzo, Marmarou et al. 1997). Barzo et al. reported at seven days and two weeks the ADC remained less than control. This decrease of ADCwas explained by the predominance of cytotoxic edema at these time points (Barzo, Marmarou et al. 1997). In this study, at seven days post-TBI no linear relationship was observed between changes in T2 signal and DTI parameters. The lack of a linear relationship between T2 and DTI parameter changes at seven days post-TBI was an indication that edema might not be the prominent player in causing changes at this time point. At seven days post-TBI the FA increased in both the CC and the Och; however, Trace increased in the CC and decreased in the Och. In addition, at seven days post-TBI RD and AD values increased within the CC and decreased in the Och. These different findings between the CC and the Och at seven days post-TBI might be due to the varying injury time profile between the CC and the Och (Chapter 2). Within the Och and the CC the average T2 value decreased in comparison to pre-TBI; however, various animals did show an increase in T2, thus indicating edema was still present at this time point in some animals. At three days and seven days post-TBI the DTI parameters became inconsistent between the Och and the CC. This inconsistency might be due to a varying injury time profile between the two anatomical structures and the decrease in the sample size of these two groups.

# CHAPTER 8: SUMMARY, CONCLUSIONS AND RECOMMONDATIONS.

## Summary

Clinical studies have utilized diffusion tensor imaging (DTI) to study TBI and these various studies have indicated a decrease in fractional anisotropy (FA) in injured patients in comparison to control(Arfanakis, Haughton et al. 2002; Huisman, Schwamm et al. 2004; Inglese, Makani et al. 2005; Benson, Meda et al. 2007; Kraus, Susmaras et al. 2007; Xu, Rasmussen et al. 2007; Rutgers, Fillard et al. 2008; Sidaros, Engberg et al. 2008; Kumar, Saksena et al. 2010; Kinnunen, Greenwood et al. 2011). The decrease in FA in TBI patients were described as diffuse axonal injury (DAI); however, to date only one laboratory study by Mac Donald et al. has attempted to prove that decrease in relative anisotropy (RA, similar to FA RA describes ) value is indeed traumatic axonal injury (TAI, in laboratory setting DAI is referred to as TAI) (Mac Donald, Dikranian et al. 2007).

Based on the clinical and laboratory findings of previous literature the first hypothesis of this study was constructed. The first hypothesis states that the severity of TAI is characterized by the retraction ball and axonal swelling counts determined using quantitative techniques in histology. Therefore, the severity of TAI should correlate with the DTI parameters (FA, diffusion trace, AD and RD). The changes in retraction ball and swollen axons counts will correlate with the DTI parameter changes over time, since DTI parameter changes are dependent on the axonal integrity. However, the results in this study were unable to support the hypothesis that changes in DTI are an indication of DAI.

All the clinical and laboratory studies discussed above have utilized a b value less 1500 s/mm$^2$ to acquire DTI (Clark and Le Bihan 2000). The b value summarizes the influence of the gradients on the diffusion weighted images and it is proportional to the product of diffusion time

interval and the square of the length of the diffusion gradient. Since the b value utilized in these DTI studies was less than 1500 s/mm$^2$the DTI parameters represented fast water diffusion within the tissue which is considered to be the diffusion in the extracellular space rather intracellular space (Clark and Le Bihan 2000). Similarly to the previously published data, this animal study utilized a small b value (b = 0 and 800 s/mm$^2$) for DTI acquisition to further investigate if these DTI changes observed post-TBI were indeed TAI. Unlike the Mac Donald et al study, this study failed to observe a relationship between detected DTI changes (especially FA) and TAI. The discrepancy between this study and the Mac Donald study may arise from the different injury model utilized. Mac Donald utilized the controlled cortical impact (CCI) model, while this study utilized the Marmarou impact acceleration weight-drop model to induce TBI. The main difference between the Marmarou impact acceleration weight-drop model and the cortical impact model is that the weight-drop model is capable of inducing TAI with minimal focal brain lesions whereas the cortical impact model induces focal brain lesions. One possible explanation for the discrepancy between these two laboratory studies is that the detected DTI changes in the Mac Donald study that were found to be related to the TAI density may have been related to the contusion rather than TAI since increased force will increase tissue damage as well as increased TAI. Also, another discrepancy that occurred between these two studies was the fact that Mac Donald reported a constant decrease in RA across all injured rats; however, this study observed both a decrease and an increase across the injured rats. In addition to the clinical detection of a decrease in FA, an increase in FA has also been reported in some clinical mild-TBI studies (Bazarian, Zhong et al. 2007; Wilde, McCauley et al. 2008; Chu, Wilde et al. 2010; Mayer, Ling et al. 2010). The increase in FA in the clinical mild-TBI studies has been suggested to be an indication of cytotoxic edema.

Examining the clinical studies more closely, one striking feature in all the studies that reported decrease in the FA value in moderate and severe TBI patients was the time the DTI

were acquired in these patients after injury.  Most of the clinical studies acquired DTI weeks, months and years after occurrence of the injuries in patients with moderate to severe TBI (Inglese, Makani et al. 2005; Benson, Meda et al. 2007; Kraus, Susmaras et al. 2007; Xu, Rasmussen et al. 2007; Sidaros, Engberg et al. 2008; Kinnunen, Greenwood et al. 2011). Because of the long delay between TBI and the acquisition of DTI in these clinical studies, the detected DTI changes are caused by chronic change in the diffusion environment as a result of TBI.  The change in the diffusion environment around that time frame may be indication of loss of neuronal cells such as neurons.  At this time point the loss of neurons may have originated from various mechanisms including DAI, cytotoxic edema, necrosis and apoptosis of the neuronal cells.  Losing neuronal cells will cause the extracellular space within the white matter (WM) to become greater in width since tightly packed and coherently aligned axons become less as the amount of neurons decreases.  Therefore the loss of neurons will result in the decrease of FA and the increase of RD of the extracellular space as was evident in these clinical studies (Benson, Meda et al. 2007; Kraus, Susmaras et al. 2007; Sidaros, Engberg et al. 2008; Kumar, Saksena et al. 2010; Kinnunen, Greenwood et al. 2011).  Therefore, the detected changes in the DTI parameters are changes in the extracellular space rather the intracellular space since the b value utilizes was less than 1500 s/mm$^2$.  Since DAI is the breakdown of the cytoskeleton on the axons DAI is an intracellular injury rather than extracellular.  However, as a result of TBI, neurons can be lost due to DAI and other injury factors. Therefore, decreasing the number of axons in specific anatomical WM regions causes a decrease in FA in the extracellular space.

Based on the first hypothesis, a second hypothesis was also established which states that DAI is a secondary injury of TBI; therefore, as time progresses the injury will become more prominent and more damage will become evident.  Thus the early detection of DTI parameter changes should be a good indicator of axonal injury progression as time increases.  As time

progresses, after induction of TBI, the pathological profile changes, where some recovery of axons will take place while other axons will become disconnected from their distal end. This pathological profile should influence the DTI parameter changes over time. Similar to hypothesis one this hypothesis was unable to be proven since DTI acquisition was acquired with a low b value, thus imaging the extracellular space rather the intracellular space. However, over time the DTI parameters did change as a result of changes in the extracellular environment as a consequence of TBI. Even though this study was unable to prove TAI detection over time, these injured rats did demonstrate changes in the DTI parameters and various trends in which may be an indication of edema rather than DAI.

This study was the first study to detect TAI temporal profile in the corpus callosum (CC) and optic chiasm (Och) over seven days by utilizing Marmarou impact acceleration model and immunocytochemistry of beta amyloid precursor protein (β-APP) and RMO14. Histologically TAI density was highly variable in the CC between animals therefore; no statistical significance was detected across time. Unlike the CC the Och was less variable and more consistent with TAI across animal and statistical significance across time was observed. This study was the first ever to quantify TAI in the Och utilizing Marmarou impact acceleration model. The injury profiles of impaired axonal transport system (immunopositive β-APP axons) and neurofilament compaction (NFC, immunopositive RMO14 axons) were found to be temporally and anatomically variable. Within the Och the TAI density detected by β-APP was the greatest at eight hours post-TBI and decreased as time progressed. The CC greatest TAI density detected by βAPP occurred at twenty-eight hours post-TBI and decreased as time progressed. The greatest TAI density described by NFC within the Och was observed at twenty-eight hours post-TBI and decreased as time elapsed. However at seven days post-TBI the NFC density increased in comparison to three days post-TBI however this increase was not statistically significant. The CC demonstrated similar NFC density behavior as the Och. In addition to the

histological observations, DTI also detected changes across the various time points (four hours, twenty-four hours, three days and seven days post-TBI). The DTI parameter changes at four hours post-TBI (increase in diffusion trace, RD, and AD, and decrease in FA) indicate an increase in the extracellular space i.e. which may be an indication of vasogenic edema. Even though at this time point the average T2 value was decreasing, several rats did demonstrate an increase in the T2 signal after TBI. Therefore, an increased water volume appeared to occur within the tissue in various animals post-TBI. Thus, the imaging studies indicate that edema does exist within this group. At twenty-four hours post-TBI and up to seven days post-TBI the changes to the DTI parameters indicated changes from a predominantly vasogenic edema to predominantly cytotoxic edema. Unlike the conventional T2 magnetic resonance imaging where vasogenic and cytotoxic edema is represented by signal hyperintensity, DTI changes may be capable in distinguishing between vasogenic and cytotoxic edema since each type of edema has an opposite effect on the DTI paramters. Barzo et al. has also reported this (Barzo, Marmarou et al. 1997).

The Marmarou weight-drop model has been reported to induce edema after impact. The edema induced by the weight-drop model was originally predominantly vasogenic edema and then followed by cytotoxic edema, which become predominant over time and remained evident up to two weeks post-TBI (Barzo, Marmarou et al. 1997). At three days and seven days post TBI various other injury mechanisms occurred that effected the extracellular environment and thus affected the DTI parameters. Various injury mechanisms that have been reported to occur at these time points are Wallerian degeneration of axons, activated glial cells, increase in inflammatory cells, and multiple segmented welling of various axons (Povlishock and Christman 1995; Gaetz 2004; Raghupathi 2004).

One clinical study by Arfanakis et al imaged five mild-TBI patients approximately twenty-four hours or less post-TBI and from these five patients two patients were also imaged thirty

days post-TBI. Similar to our results, the Arfanakis' study demonstrated at the early time point (less than or equal to twenty-four hours post-TBI) a decrease in FA and an increase in RD (Arfanakis, Haughton et al. 2002). During the thirty day follow-up of two patients the FA and the AD increased while the RD decreased in comparison to their original values at twenty-hours post-TBI(Arfanakis, Haughton et al. 2002). These diffusion changes that have occurred in the Arfanakis et al. study were thought to be an indication of DAI since CT scans and T2 weighted imaging did not demonstrate the presence of edema or hemorrhage. However, Arfanakis utilized a b value of 0 and 1001 s/mm$^2$ and since a b value of less than 1500 s/mm$^2$ represents water diffusion in the extracellular environment the Arfanakis findings may actually have detected edema. Since DTI maps the cellular environment, it might be more sensitive in detecting changes such as edema before it becomes apparent in the CT or T2 weighted imaging.

Even though this study has failed to show a strong linear relationship between FA and axonal injury, other imaging parameters such as diffusion trace and RD, did show linear correlation with the density of immunopositive β-APP axons at 4hrs post-TBI. Therefore, diffusion Trace and RD may be the better DTI parameters for describing axonal integrity such as axonal permeability but further testing is required.

In this study, the principle eigenvalue with color-coded directional images were utilized to delineate the region of interest of the WM. The principle eigenvalue color-coded directional images made it possible to distinguish between two adjacent WM tracts such as CC, external capsule, and cingulum. Therefore, a more accurate anatomical region of interest was made possible in this study. Additionally, this study was able establish a large difference between gray matter (GM, cortex) and WM (CC) FA value in healthy rats. These FA values of GM and WM of the healthy rats were further utilized to demonstrate that across (caudal to rostral) the CC a large partial volume effect (PVE) is present and by projecting the region of interest onto

the next image a visual approximation can be made.  Since, the FA value is widely used in DTI to study disorder and injury in the central nervous system PVE needs to be addressed because a decrease in FA usually is an indication of injury or disruption to the WM.  PVE leads to decreased FA and without PVE correction false positive of injury is more prominent.

## Conclusion

1.  This study was unable to support the hypothesis that changes in DTI are an indication of DAI.

2.  DTI parameters did change post-TBI and has demonstrated various trends.

3.  This study was the first ever to quantify TAI in the Och utilizing the impact acceleration model.  The Och was found to be very consistent with TAI.

4.  Also this study was the first to study the TAI temporal profile in the CC and Och over 7 days by utilizing βAPP and RMO14.

5.  The injury profile of impaired axonal transport system and NF compaction were found to be temporally and anatomically variable.

6.  Unlike the conventional T2 MRI DTI may be capable in distinguishing between vasogenic and cytotoxic edema.

7.  In this study FA failed to show a strong relationship with axonal injury.

8.  Other imaging parameters, diffusion trace and RD, did show correlation with the density β-APP positive axons at 4hrs post-TBI.

9.  Diffusion Trace and RD may be the better DTI parameters for describing axonal integrity such as axonal permeability but further testing is required.

10. This study was able demonstrate a large difference between GM and WM FA value in healthy rats.

11. This study has also demonstrate that across the CC a large PVE is present and by projecting the region of interest onto the next image a visual approximation can be made.

12. Since FA is a widely used in DTI to study disorder and injury PVE needs to be addressed because decrease in FA usually is indication of injury or disruption to the WM. PVE leads to decreased FA and without PVE correction false positive of injury is more prominent.

13. Analysis of WM tract by using principle eigenvalue with color coded directional map made it possible to distinguish between two adjacent WM tract (i.e. such as CC, external capsule, and cingulum). Therefore, a more accurate anatomical region of interest was made possible in this study.

## Recommendations

Based on the findings of this project the Marmarou impact acceleration model has a wide variation of injury density in the CC, and if the CC is to be utilized for further studied on TAI the samples size needs to be increased. The Marmarou impact acceleration model has been documented to induce extensive TAI in the brainstem. Therefore, the WM of the brainstem such as pyramidal tract is a better anatomical region to be studied when utilizing the Marmarou impact acceleration model to induce TAI. Additional, in this study by the calculation of PVE across the CC it is recommended that images of the rat brain should be acquired with a small voxel size where the depth of the voxel is less than 1mm.

All the above explanations that have been proposed to explain the DTI changes are yet to be proven and further study is required to validate these explanations. Since the purpose of this study was to investigate if the clinical DTI changes are indeed a detection of DAI as it has

been claimed, no effort was made to further investigate other possibilities that were beyond the scope of this study. One of the most interesting conclusions in this study is the fact that detected DTI changes are not directly related to DAI. This is in line with the idea that water diffuses more quickly in the extracellular space and by utilizing a low b value the MR images events occurring in the extracellular space rather than in the intracellular space. DTI may be a more powerful imaging tool than originally thought to be if it would be possible to utilize both low and high b values. Utilizing low and high b values DTI may highlight changes in the extracellular and intracellular space as a result of injury. Nevertheless, utilizing a high b value has its own problems. As the b value increases the signal to noise ration decreases. This signal might be overcome in the future with improved hardware and increased magnetic fields strength. Also, by utilizing a large b value the brain pulsation due to cardiac output might become an imaging problem since the MRI would detect the motion artifact from the pulsation. Determining the pulsation frequency of the brain and acquiring the images in between the pulsation cycles can minimize the motion artifact from the brain pulsation. Animal studies of DTI verification are very limited but necessary. Further animal studies should be carried out to investigate the true role of edema on diffusion detected by DTI. It has been suggested by other researchers that DTI may be a sensitive method of distinguishing between vasogenic and cytotoxic edema. One must question also the sensitivity of DTI in detecting edema in comparison to the conventional T2 weighted imaging method.

Magnetic resonance DTI may be the microscope of the future, which would allow noninvasive probing into the cellular environment for diagnosis of injuries, disorders and diseases. Yet DTI is still in its infancy and improvement to this imaging method and clear understanding of the meaning of the data at the cellular and tissue level is required and can only be achieved through more correlative research such as performed in the current study.

# APPENDIX A

AD - Axial diffusivity

ADC - Apparent diffusion coefficient

AIS - Abbreviated injury severity scale

β-APP - Beta amyloid precursor protein

CC - Corpus callosum

CNS - Central nervous system

CSF - Cerebral spinal fluid

DAI - Diffuse Axonal injury

DTI - Diffusion tensor image

FA - Fractional anisotropy

GSC - Glasgow coma scale

GM - Gray matter

HDR - High dynamic range

HRP - Horseradish peroxidase

IQR - interquartile range

KSP - Lysine-serine-proline

LOC - Loss of consciousness

IAT - Impaired axonal transport

MRI - Magnetic resonance imaging

NF - Neurofilament

NFC - Neurofilament compaction

NF-L - Neurofilament light molecular weight

NF-M - Neurofilament medium molecular weight

NF-H - Neurofilament heavy molecular weight

Och - Optic chiasm

PVE - Partial volume effect

RA - Relative anisotropy

RD - Radial diffusivity

RM014 - NF-M monoclonal antibody

ROI - Region of interest

SEM - Standard error of mean

SNR - Signal to noise ratio

std - Standard deviation

TAI - Traumatic axonal injury

TBI -Traumatic Brain injury

WM - White matter

# APPENDIX B

Table B-1: The following tables represent the mean and standard deviation of the DTI parameters (FA, Trace, RD, and AD) within the V-like Region of interest of the CC at pre-TBI and four hours post-TBI of Group 1. The mean DTI parameters changes (figures 43, 47, 49, 53 and 57) are represented as the mean DTI value at four hours post-TBI minus the pre-TBI mean DTI values. The standard error of the mean difference is calculated by the following equation

$$SEM = \sqrt{\frac{Std_{PreTBI}^2}{n_{preTBI}} + \frac{Std_{PostTBI}^2}{n_{PostTBI}}}$$

| | FA | | | | | | | |
|---|---|---|---|---|---|---|---|---|
| | PreTBI | | | 4hrs PostTBI | | | 4hrs PostTBI - PreTBI | |
| Rat ID | mean | Std | n | mean | Std | n | mean | SEM |
| 1 | 0.78240 | 0.45930 | 1922 | 0.56290 | 0.01749 | 1922 | -0.21950 | 0.01048 |
| 2 | 0.70170 | 0.09038 | 2667 | 0.70800 | 0.01035 | 2667 | 0.00630 | 0.00176 |
| 3 | 0.76940 | 0.05009 | 1390 | 0.78510 | 0.07092 | 1390 | 0.01570 | 0.00233 |
| 4 | 0.74140 | 0.07661 | 2201 | 0.82670 | 0.05112 | 2049 | 0.08530 | 0.00199 |
| 5 | 0.78170 | 0.07921 | 1494 | 0.76500 | 0.05727 | 1490 | -0.01670 | 0.00253 |
| 6 | 0.71270 | 0.04031 | 400 | 0.82030 | 0.07243 | 1820 | 0.10760 | 0.00264 |

| | Trace | | | | | | | |
|---|---|---|---|---|---|---|---|---|
| | PreTBI | | | 4hrs PostTBI | | | 4hrs PostTBI - PreTBI | |
| Rat ID | mean | Std | n | mean | Std | n | mean | SEM |
| 1 | 2.09440 | 0.17328 | 1922 | 1.90910 | 0.36665 | 1922 | -0.18530 | 0.00925 |
| 2 | 2.23700 | 0.51716 | 2667 | 2.10820 | 0.10807 | 2667 | -0.12880 | 0.01023 |
| 3 | 2.24800 | 0.17823 | 1390 | 2.01800 | 0.11579 | 1390 | -0.23000 | 0.00570 |
| 4 | 2.21920 | 0.18893 | 2201 | 2.53120 | 0.19828 | 2049 | 0.31200 | 0.00595 |
| 5 | 2.66040 | 0.21112 | 1494 | 2.61920 | 0.15790 | 1490 | -0.04120 | 0.00682 |
| 6 | 2.24230 | 0.13087 | 400 | 2.49480 | 0.24745 | 1820 | 0.25250 | 0.00874 |

| | RD | | | | | | | |
|---|---|---|---|---|---|---|---|---|
| | PreTBI | | | 4hrs PostTBI | | | 4hrs PostTBI - PreTBI | |
| Rat ID | mean | Std | n | mean | Std | n | mean | SEM |
| 1 | 0.29110 | 0.05636 | 1922 | 0.41190 | 0.14643 | 1922 | 0.12080 | 0.00358 |
| 2 | 0.40900 | 0.12605 | 2667 | 0.40740 | 0.07848 | 2667 | -0.00160 | 0.00288 |
| 3 | 0.39610 | 0.06507 | 1390 | 0.27680 | 0.05986 | 1390 | -0.11930 | 0.00237 |
| 4 | 0.37070 | 0.06429 | 2201 | 0.30170 | 0.06363 | 2049 | -0.06900 | 0.00196 |
| 5 | 0.36230 | 0.10211 | 1494 | 0.38860 | 0.07517 | 1490 | 0.02630 | 0.00328 |
| 6 | 0.38840 | 0.04085 | 400 | 0.30650 | 0.10967 | 1820 | -0.08190 | 0.00328 |

| | AD | | | | | | | |
|---|---|---|---|---|---|---|---|---|
| | PreTBI | | | 4hrs PostTBI | | | 4hrs PostTBI - PreTBI | |
| Rat ID | mean | Std | n | mean | Std | n | mean | SEM |
| 1 | 1.51230 | 0.12870 | 1922 | 1.08530 | 0.15313 | 1922 | -0.42700 | 0.00456 |
| 2 | 1.44980 | 0.31595 | 2667 | 1.32860 | 0.16752 | 2667 | -0.12120 | 0.00692 |
| 3 | 1.59130 | 0.22961 | 1390 | 1.46660 | 0.14410 | 1390 | -0.12470 | 0.00727 |
| 4 | 1.50990 | 0.25348 | 2201 | 1.92830 | 0.18582 | 2049 | 0.41840 | 0.00679 |
| 5 | 1.93760 | 0.24598 | 1494 | 1.84220 | 0.15391 | 1490 | -0.09540 | 0.00751 |
| 6 | 1.46440 | 0.10783 | 400 | 1.89160 | 0.21714 | 1820 | 0.42720 | 0.00741 |

Table B-2: The following tables represent the mean and standard deviation of the DTI parameters (FA, Trace, RD, and AD) within the Och at pre-TBI and four hours post-TBI of Group 1. The post-TBI mean DTI parameters changes (figures 43, 47, 49, 53 and 57) are represented as the mean DTI values at four hours post-TBI minus the pre-TBI mean DTI values. The standard error of the mean difference is calculated by the following equation

$$SEM = \sqrt{\frac{Std_{PreTBI}^2}{n_{preTBI}} + \frac{Std_{PostTBI}^2}{n_{PostTBI}}}$$

| | FA | | | | | | | |
|---|---|---|---|---|---|---|---|---|
| | PreTBI | | | 4hrs PostTBI | | | 4hrs PostTBI - PreTBI | |
| Rat ID | mean | Std | n | mean | Std | n | mean | SEM |
| 1 | 0.73787 | 0.0755864 | 1179 | 0.690296 | 0.113867 | 2007 | -0.047574 | 0.003362458 |
| 2 | 0.636046 | 0.114024 | 1434 | 0.576961 | 0.146553 | 2619 | -0.059085 | 0.004155398 |
| 3 | 0.658753 | 0.117713 | 2180 | 0.563045 | 0.107724 | 1862 | -0.095708 | 0.003548011 |
| 4 | 0.690387 | 0.134445 | 2021 | 0.632008 | 0.153583 | 2071 | -0.058379 | 0.004509253 |
| 5 | 0.787294 | 0.114155 | 2073 | 0.590115 | 0.100572 | 2225 | -0.197179 | 0.003291228 |
| 6 | 0.723472 | 0.111302 | 601 | 0.70661 | 0.140813 | 1631 | -0.016862 | 0.005724481 |

| | Trace | | | | | | | |
|---|---|---|---|---|---|---|---|---|
| | PreTBI | | | 4hrs PostTBI | | | 4hrs PostTBI - PreTBI | |
| Rat ID | mean | Std | n | mean | Std | n | mean | SEM |
| 1 | 2.87884 | 0.670713 | 1179 | 2.35356 | 0.490611 | 2007 | -0.52528 | 0.022393906 |
| 2 | 2.56121 | 0.335643 | 1434 | 2.48599 | 0.909798 | 2619 | -0.07522 | 0.019864789 |
| 3 | 2.72421 | 0.743757 | 2180 | 2.82927 | 0.545252 | 1862 | 0.10506 | 0.02033265 |
| 4 | 2.95287 | 0.674217 | 2021 | 3.31912 | 1.07449 | 2071 | 0.36625 | 0.027971354 |
| 5 | 3.08253 | 1.04782 | 2073 | 2.61453 | 0.676071 | 2225 | -0.468 | 0.027111943 |
| 6 | 3.61815 | 1.29652 | 601 | 2.91531 | 0.979429 | 1631 | -0.70284 | 0.058181616 |

| | RD | | | | | | | |
|---|---|---|---|---|---|---|---|---|
| | PreTBI | | | 4hrs PostTBI | | | 4hrs PostTBI - PreTBI | |
| Rat ID | mean | Std | n | mean | Std | n | mean | SEM |
| 1 | 0.4999675 | 0.1828405 | 1179 | 0.42077 | 0.1726355 | 2007 | -0.0791975 | 0.006573022 |
| 2 | 0.5021175 | 0.1563525 | 1434 | 0.5375575 | 0.2749165 | 2619 | 0.03544 | 0.006775359 |
| 3 | 0.5469515 | 0.2389165 | 2180 | 0.6200505 | 0.182332 | 1862 | 0.073099 | 0.006636145 |
| 4 | 0.5088335 | 0.204955 | 2021 | 0.6439585 | 0.3384305 | 2071 | 0.135125 | 0.00872292 |
| 5 | 0.47163 | 0.275169 | 2073 | 0.559136 | 0.2028935 | 2225 | 0.087506 | 0.007418037 |
| 6 | 0.66709 | 0.4145755 | 601 | 0.5235665 | 0.2955025 | 1631 | -0.1435235 | 0.018425984 |

| | AD | | | | | | | |
|---|---|---|---|---|---|---|---|---|
| | PreTBI | | | 4hrs PostTBI | | | 4hrs PostTBI - PreTBI | |
| Rat ID | mean | Std | n | mean | Std | n | mean | SEM |
| 1 | 1.917 | 0.45635 | 1179 | 1.51217 | 0.266262 | 2007 | -0.40483 | 0.014558892 |
| 2 | 1.57354 | 0.258224 | 1434 | 1.41088 | 0.440712 | 2619 | -0.16266 | 0.010984526 |
| 3 | 1.7054 | 0.486475 | 2180 | 1.58917 | 0.342434 | 1862 | -0.11623 | 0.013097119 |
| 4 | 1.93767 | 6.68E-01 | 2021 | 2.03121 | 0.745437 | 2071 | 0.09354 | 0.022110512 |
| 5 | 2.43471 | 0.957026 | 2073 | 1.50064 | 0.364699 | 2225 | -0.93407 | 0.02239644 |
| 6 | 2.44266 | 0.763101 | 601 | 1.92706 | 0.505546 | 1631 | -0.5156 | 0.033550307 |

Table B-3: The following tables represent the mean and standard deviation of the DTI parameters (FA, Trace, RD, and AD) within the V-like Region of interest of the CC at pre-TBI and twenty-four hours post-TBI of Group 2. The mean DTI parameters changes (figures 44, 47, 50, 54 and 58) are represented as the mean DTI value at twenty-four hours post-TBI minus the pre-TBI mean DTI values. The standard error of the mean difference is calculated by the following equation

$$SEM = \sqrt{\frac{Std_{PreTBI}^2}{n_{preTBI}} + \frac{Std_{PostTBI}^2}{n_{PostTBI}}}$$

| | FA | | | | | | | |
|---|---|---|---|---|---|---|---|---|
| | PreTBI | | | 24hrs PostTBI | | | 24hrs PostTBI - PreTBI | |
| Rat ID | mean | Std | n | mean | Std | n | mean | SEM |
| 7 | 0.74650 | 0.09332 | 1775 | 0.69794 | 0.11240 | 1670 | -0.04857 | 0.00353 |
| 8 | 0.67930 | 0.08047 | 1470 | 0.84187 | 0.09164 | 1418 | 0.16257 | 0.00321 |
| 9 | 0.76730 | 0.05125 | 1726 | 0.72950 | 0.06620 | 1887 | -0.03780 | 0.00196 |
| 10 | 0.64720 | 0.09746 | 1489 | 0.74466 | 0.09535 | 1489 | 0.09746 | 0.00353 |
| 11 | 0.74910 | 0.05230 | 1794 | 0.58268 | 0.11411 | 1785 | -0.16642 | 0.00297 |
| 12 | 0.64650 | 0.06658 | 1077 | 0.60708 | 0.08557 | 1076 | -0.03942 | 0.00330 |

| | Trace | | | | | | | |
|---|---|---|---|---|---|---|---|---|
| | PreTBI | | | 24hrs PostTBI | | | 24hrs PostTBI - PreTBI | |
| Rat ID | mean | Std | n | mean | Std | n | mean | SEM |
| 7 | 2.72850 | 0.19162 | 1775 | 2.40630 | 0.32846 | 1670 | -0.32220 | 0.00924 |
| 8 | 1.78140 | 0.16996 | 1470 | 1.79210 | 0.24188 | 1418 | 0.01070 | 0.00780 |
| 9 | 2.07290 | 0.20743 | 1726 | 1.96727 | 0.16190 | 1887 | -0.10563 | 0.00623 |
| 10 | 3.29160 | 0.32948 | 1489 | 2.77772 | 0.32499 | 1489 | -0.51388 | 0.01199 |
| 11 | 2.68000 | 0.14690 | 1794 | 2.92018 | 0.67773 | 1785 | 0.24018 | 0.01641 |
| 12 | 2.72650 | 0.13119 | 1077 | 2.33617 | 0.13284 | 1076 | -0.39033 | 0.00569 |

| | RD | | | | | | | |
|---|---|---|---|---|---|---|---|---|
| | PreTBI | | | 24hrs PostTBI | | | 24hrs PostTBI - PreTBI | |
| Rat ID | mean | Std | n | mean | Std | n | mean | SEM |
| 7 | 0.41820 | 0.11315 | 1775 | 0.41175 | 0.13468 | 1670 | -0.00645 | 0.00425 |
| 8 | 0.31690 | 0.04578 | 1470 | 0.19626 | 0.10592 | 1418 | -0.12064 | 0.00306 |
| 9 | 0.31540 | 0.06326 | 1726 | 0.31938 | 0.09349 | 1887 | 0.00398 | 0.00264 |
| 10 | 0.63150 | 0.11848 | 1489 | 0.43555 | 0.16516 | 1489 | -0.19595 | 0.00527 |
| 11 | 0.40660 | 0.06586 | 1794 | 0.62497 | 0.23502 | 1785 | 0.21837 | 0.00578 |
| 12 | 0.51670 | 0.06759 | 1077 | 0.48760 | 0.11087 | 1076 | -0.02910 | 0.00396 |

| | AD | | | | | | | |
|---|---|---|---|---|---|---|---|---|
| | PreTBI | | | 24hrs PostTBI | | | 24hrs PostTBI - PreTBI | |
| Rat ID | mean | Std | n | mean | Std | n | mean | SEM |
| 7 | 1.89200 | 0.29707 | 1775 | 1.58400 | 0.20908 | 1670 | -0.30800 | 0.00871 |
| 8 | 1.14750 | 0.18027 | 1470 | 1.41925 | 0.19676 | 1418 | 0.27175 | 0.00703 |
| 9 | 1.44270 | 0.16544 | 1726 | 1.33016 | 0.15835 | 1887 | -0.11254 | 0.00540 |
| 10 | 2.03190 | 0.27590 | 1489 | 1.90773 | 0.21045 | 1489 | -0.12417 | 0.00899 |
| 11 | 1.86680 | 0.10727 | 1794 | 1.67030 | 0.30875 | 1785 | -0.19650 | 0.00773 |
| 12 | 1.69280 | 0.17314 | 1077 | 1.36053 | 0.12831 | 1076 | -0.33227 | 0.00657 |

Table B-4: The following tables represent the mean and standard deviation of the DTI parameters (FA, Trace, RD, and AD) within the Och at pre-TBI and twenty-four post-TBI of Group 2. The post-TBI mean DTI parameters changes (figures 44, 47, 50, 54 and 58ures 43, 47, 49, 53 and 57) are represented as the mean DTI values at twenty-four hours post-TBI minus the pre-TBI mean DTI values. The standard error of the mean difference is calculated by the following equation

$$SEM = \sqrt{\frac{Std_{PreTBI}^2}{n_{preTBI}} + \frac{Std_{PostTBI}^2}{n_{PostTBI}}}$$

| | FA | | | | | | | |
|---|---|---|---|---|---|---|---|---|
| | PreTBI | | | 24hrs PostTBI | | | 24hrs PostTBI - PreTBI | |
| Rat ID | mean | Std | n | mean | Std | n | mean | SEM |
| 7 | 0.628163 | 0.125591 | 1296 | 0.82354 | 0.0772745 | 1815 | 0.195377 | 0.003931997 |
| 8 | 0.61564 | 0.0808806 | 1721 | 0.533937 | 0.15709 | 1528 | -0.081703 | 0.004466669 |
| 9 | 0.711249 | 0.097516 | 1529 | 0.741877 | 0.0965417 | 1322 | 0.030628 | 0.003642731 |
| 10 | 0.75228 | 0.0982959 | 2462 | 0.584295 | 0.123929 | 1705 | -0.167985 | 0.003596157 |
| 11 | 0.784418 | 0.0977908 | 1528 | 0.622442 | 0.122542 | 1804 | -0.161976 | 0.003818712 |
| 12 | 0.747151 | 0.120624 | 1514 | 0.877815 | 0.0561107 | 1312 | 0.130664 | 0.00346556 |

| | Trace | | | | | | | |
|---|---|---|---|---|---|---|---|---|
| | PreTBI | | | 24hrs PostTBI | | | 24hrs PostTBI - PreTBI | |
| Rat ID | mean | Std | n | mean | Std | n | mean | SEM |
| 7 | 2.88554 | 0.675734 | 1296 | 1.99286 | 0.562187 | 1815 | -0.89268 | 0.022944761 |
| 8 | 2.57363 | 0.892758 | 1721 | 2.55474 | 0.703646 | 1528 | -0.01889 | 0.028056061 |
| 9 | 1.88276 | 0.285439 | 1529 | 1.63005 | 0.660214 | 1322 | -0.25271 | 0.019570417 |
| 10 | 3.45822 | 0.887081 | 2462 | 3.27121 | 1.36728 | 1705 | -0.18701 | 0.037630807 |
| 11 | 2.06248 | 0.955946 | 1528 | 2.62351 | 0.751599 | 1804 | 0.56103 | 0.030186026 |
| 12 | 2.25252 | 1.22797 | 1514 | 2.44931 | 0.543166 | 1312 | 0.19679 | 0.03494063 |

| | RD | | | | | | | |
|---|---|---|---|---|---|---|---|---|
| | PreTBI | | | 24hrs PostTBI | | | 24hrs PostTBI - PreTBI | |
| Rat ID | mean | Std | n | mean | Std | n | mean | SEM |
| 7 | 0.566924 | 0.1994985 | 1296 | 0.281312 | 0.139869 | 1815 | -0.28561205 | 0.006441142 |
| 8 | 0.5150095 | 0.190047 | 1721 | 0.5749695 | 0.2414445 | 1528 | 0.05996 | 0.007690125 |
| 9 | 0.3199575 | 0.1165065 | 1529 | 0.282953 | 0.1585145 | 1322 | -0.0370045 | 0.005280553 |
| 10 | 0.5647565 | 0.2935275 | 2462 | 0.693336 | 0.3584175 | 1705 | 0.1285795 | 0.010504295 |
| 11 | 0.313869 | 0.1851725 | 1528 | 0.416953 | 0.155717 | 1804 | 0.103084 | 0.005990115 |
| 12 | 0.44143 | 0.3546395 | 1514 | 0.260872 | 0.142468 | 1312 | -0.18055805 | 0.00992679 |

| | AD | | | | | | | |
|---|---|---|---|---|---|---|---|---|
| | PreTBI | | | 24hrs PostTBI | | | 24hrs PostTBI - PreTBI | |
| Rat ID | mean | Std | n | mean | Std | n | mean | SEM |
| 7 | 1.75294 | 0.429581 | 1296 | 1.57498 | 0.314626 | 1815 | -0.17796 | 0.014033229 |
| 8 | 1.54376 | 0.573255 | 1721 | 1.40693 | 0.350398 | 1528 | -0.13683 | 0.016471201 |
| 9 | 1.24451 | 0.191462 | 1529 | 1.12418 | 0.378485 | 1322 | -0.12033 | 0.011503659 |
| 10 | 2.37531 | 0.573914 | 2462 | 1.88395 | 7.62E-01 | 1705 | -0.49136 | 0.021782424 |
| 11 | 1.51347 | 0.720521 | 1528 | 1.26486 | 0.384948 | 1804 | -0.24861 | 0.02054022 |
| 12 | 1.48845 | 0.586958 | 1514 | 2.06325 | 0.301959 | 1312 | 0.5748 | 0.017235206 |

Table B-5: The following tables represent the mean and standard deviation of the DTI parameters (FA, Trace, RD, and AD) within the V-like Region of interest of the CC at pre-TBI and three days post-TBI of Group 3. The mean DTI parameters changes (figures 45, 48, 51, 55 and 59) are represented as the mean DTI value at three days post-TBI minus the pre-TBI mean DTI values. The standard error of the mean difference is calculated by the following equation

$$SEM = \sqrt{\frac{Std_{PreTBI}^2}{n_{preTBI}} + \frac{Std_{PostTBI}^2}{n_{PostTBI}}}$$

| | FA | | | | | | | |
|---|---|---|---|---|---|---|---|---|
| | PreTBI | | | 3days PostTBI | | | 3days PostTBI - PreTBI | |
| Rat ID | mean | Std | n | mean | Std | n | mean | SEM |
| 13 | 0.82643 | 0.07303 | 352 | 0.79483 | 0.07679 | 1474 | -0.03160 | 0.00438 |
| 14 | 0.81106 | 0.04948 | 1474 | 0.65828 | 0.11056 | 1474 | -0.15278 | 0.00315 |
| 15 | 0.82580 | 0.05113 | 1486 | 0.74706 | 0.04621 | 1486 | -0.07874 | 0.00179 |
| 16 | 0.64570 | 0.08454 | 1917 | 0.65947 | 0.07384 | 1937 | 0.01376 | 0.00256 |
| 17 | 0.81839 | 0.05314 | 1917 | 0.87874 | 0.04621 | 1917 | 0.06035 | 0.00161 |
| 18 | 0.71317 | 0.05057 | 1247 | 0.47366 | 0.08860 | 1247 | -0.23951 | 0.00289 |

| | Trace | | | | | | | |
|---|---|---|---|---|---|---|---|---|
| | PreTBI | | | 3days PostTBI | | | 3days PostTBI - PreTBI | |
| Rat ID | mean | Std | n | mean | Std | n | mean | SEM |
| 13 | 2.00139 | 0.18151 | 352 | 2.00388 | 0.17568 | 1474 | 0.00249 | 0.01070 |
| 14 | 2.00934 | 0.14227 | 1474 | 2.72338 | 0.64418 | 1474 | 0.71404 | 0.01718 |
| 15 | 1.83974 | 0.12382 | 1486 | 2.21674 | 0.19230 | 1486 | 0.37700 | 0.00593 |
| 16 | 2.39493 | 0.18683 | 1917 | 1.84710 | 0.13781 | 1937 | -0.54783 | 0.00529 |
| 17 | 2.09312 | 0.20367 | 1917 | 1.97445 | 0.17299 | 1917 | -0.11867 | 0.00610 |
| 18 | 2.22743 | 0.13389 | 1247 | 1.98347 | 0.17549 | 1247 | -0.24396 | 0.00625 |

| | RD | | | | | | | |
|---|---|---|---|---|---|---|---|---|
| | PreTBI | | | 3days PostTBI | | | 3days PostTBI - PreTBI | |
| Rat ID | mean | Std | n | mean | Std | n | mean | SEM |
| 13 | 0.25414 | 0.08881 | 352 | 0.27173 | 0.08329 | 1474 | 0.01760 | 0.00521 |
| 14 | 0.26367 | 0.06478 | 1474 | 0.88787 | 0.22918 | 1474 | 0.62420 | 0.00620 |
| 15 | 0.22430 | 0.06885 | 1486 | 0.36443 | 0.14508 | 1486 | 0.14013 | 0.00417 |
| 16 | 0.46889 | 0.10248 | 1917 | 0.35752 | 0.07758 | 1937 | -0.11137 | 0.00293 |
| 17 | 0.26119 | 0.08138 | 1917 | 0.38441 | 0.07516 | 1917 | 0.12322 | 0.00253 |
| 18 | 0.37515 | 0.07742 | 1247 | 0.47599 | 0.08527 | 1247 | 0.10084 | 0.00326 |

| | AD | | | | | | | |
|---|---|---|---|---|---|---|---|---|
| | PreTBI | | | 3days PostTBI | | | 3days PostTBI - PreTBI | |
| Rat ID | mean | Std | n | mean | Std | n | mean | SEM |
| 13 | 1.53038 | 0.05465 | 352 | 1.47584 | 0.18660 | 1474 | -0.05454 | 0.00567 |
| 14 | 1.48941 | 0.12548 | 1474 | 1.70492 | 0.35766 | 1474 | 0.21551 | 0.00987 |
| 15 | 1.39881 | 0.13497 | 1486 | 1.49322 | 0.10602 | 1486 | 0.09441 | 0.00445 |
| 16 | 1.45708 | 0.14588 | 1917 | 1.13282 | 0.15032 | 1937 | -0.32426 | 0.00477 |
| 17 | 1.57817 | 0.14059 | 1917 | 2.49221 | 0.43379 | 1917 | 0.91404 | 0.01041 |
| 18 | 1.47694 | 0.12315 | 1247 | 1.03122 | 0.07891 | 1247 | -0.44572 | 0.00414 |

Table B-6:   The following tables represent the mean and standard deviation of the DTI parameters (FA, Trace, RD, and AD) within the Och at pre-TBI and 3days post-TBI of Group 3. The post-TBI mean DTI parameters changes (figures 45, 48, 51, 55 and 59) are represented as the mean DTI values at three days post-TBI minus the pre-TBI mean DTI values.  The standard error of the mean difference is calculated by the following equation

$$SEM = \sqrt{\frac{Std^2_{PreTBI}}{n_{preTBI}} + \frac{Std^2_{PostTBI}}{n_{PostTBI}}}$$

| | FA | | | | | | | |
|---|---|---|---|---|---|---|---|---|
| | PreTBI | | | 3days PostTBI | | | 3days PostTBI - PreTBI | |
| Rat ID | mean | Std | n | mean | Std | n | mean | SEM |
| 13 | 0.747156 | 0.0838909 | 352 | 0.722563 | 0.0953865 | 1137 | -0.024593 | 0.005291095 |
| 14 | 0.846215 | 0.101448 | 1369 | 0.771779 | 0.10291 | 1542 | -0.074436 | 0.003792846 |
| 15 | 0.750464 | 0.125436 | 1561 | 0.540457 | 0.110781 | 1746 | -0.210007 | 0.004136235 |
| 16 | 0.826241 | 0.0770766 | 1275 | 0.759792 | 0.0879885 | 1275 | -0.066449 | 0.003275911 |
| 17 | 0.775606 | 0.106308 | 1749 | 0.580116 | 0.111221 | 1444 | -0.19549 | 0.003876621 |
| 18 | 0.615028 | 0.090177 | 1506 | 0.755108 | 0.133059 | 1419 | 0.14008 | 0.004228066 |

| | Trace | | | | | | | |
|---|---|---|---|---|---|---|---|---|
| | PreTBI | | | 3days PostTBI | | | 3days PostTBI - PreTBI | |
| Rat ID | mean | Std | n | mean | Std | n | mean | SEM |
| 13 | 2.03781 | 0.683455 | 352 | 1.75902 | 0.530905 | 1137 | -0.27879 | 0.039685227 |
| 14 | 1.85115 | 0.530171 | 1369 | 1.73515 | 0.712617 | 1542 | -0.116 | 0.023122417 |
| 15 | 2.22301 | 0.679124 | 1561 | 2.18562 | 0.713836 | 1746 | -0.03739 | 0.024234334 |
| 16 | 1.97316 | 0.667951 | 1275 | 1.67625 | 0.538835 | 1275 | -0.29691 | 0.024034317 |
| 17 | 2.0655 | 0.66156 | 1749 | 2.04966 | 0.349443 | 1444 | -0.01584 | 0.018297523 |
| 18 | 2.03697 | 0.556453 | 1506 | 1.73131 | 0.453695 | 1419 | -0.30566 | 0.018726012 |

| | RD | | | | | | | |
|---|---|---|---|---|---|---|---|---|
| | PreTBI | | | 3days PostTBI | | | 3days PostTBI - PreTBI | |
| Rat ID | mean | Std | n | mean | Std | n | mean | SEM |
| 13 | 0.3767865 | 0.2188215 | 352 | 0.314033 | 0.1516875 | 1137 | -0.0627535 | 0.0125007 |
| 14 | 0.1942778 | 0.1220887 | 1369 | 0.5137315 | 0.2462963 | 1542 | 0.3194538 | 0.00708715 |
| 15 | 0.3505545 | 0.1931005 | 1561 | 0.500195 | 0.2191235 | 1746 | 0.1496405 | 0.007168486 |
| 16 | 0.3014768 | 0.1881671 | 1275 | 0.273456 | 0.137287 | 1275 | -0.0280208 | 0.006523236 |
| 17 | 0.3222025 | 0.1634015 | 1749 | 0.4328695 | 0.1199465 | 1444 | 0.110667 | 0.005022878 |
| 18 | 0.427797 | 0.142977 | 1506 | 0.2658675 | 0.1491545 | 1419 | -0.1619295 | 0.005408509 |

| | AD | | | | | | | |
|---|---|---|---|---|---|---|---|---|
| | PreTBI | | | 3days PostTBI | | | 3days PostTBI - PreTBI | |
| Rat ID | mean | Std | n | mean | Std | n | mean | SEM |
| 13 | 1.32405 | 0.305791 | 352 | 1.40175 | 0.378591 | 1137 | 0.0777 | 0.019791638 |
| 14 | 1.55971 | 0.6308 | 1369 | 1.53079 | 0.510913 | 1542 | -0.02892 | 0.021446164 |
| 15 | 1.57331 | 0.42396 | 1561 | 0.0017482 | 0.0002207 | 1746 | -1.5715618 | 0.010730587 |
| 16 | 1.53742 | 0.325544 | 1275 | 1.51444 | 0.228497 | 1275 | -0.02298 | 0.01113869 |
| 17 | 1.47256 | 0.456844 | 1749 | 1.42044 | 0.344351 | 1444 | -0.05212 | 0.014193184 |
| 18 | 1.1884 | 0.331589 | 1506 | 1.24361 | 0.342208 | 1419 | 0.05521 | 0.012471414 |

Table B-7: The following tables represent the mean and standard deviation of the DTI parameters (FA, Trace, RD, and AD) within the V-like Region of interest of the CC at pre-TBI and seven days post-TBI of Group 4.  The mean DTI parameters changes (figures 45, 48, 51, 55 and 59) are represented as the mean DTI value at three days post-TBI minus the pre-TBI mean DTI values.  The standard error of the mean difference is calculated by the following equation

$$SEM = \sqrt{\frac{Std_{PreTBI}^2}{n_{preTBI}} + \frac{Std_{PostTBI}^2}{n_{PostTBI}}}$$

| | FA | | | | | | | |
|---|---|---|---|---|---|---|---|---|
| | PreTBI | | | 7days PostTBI | | | 7days PostTBI - PreTBI | |
| Rat ID | mean | Std | n | mean | Std | n | mean | SEM |
| 19 | 0.73903 | 0.06362 | 943 | 0.63072 | 0.07473 | 943 | -0.10831 | 0.00320 |
| 20 | 0.72104 | 0.09407 | 1063 | 0.81112 | 0.08840 | 1063 | 0.09008 | 0.00396 |
| 21 | 0.75156 | 0.07533 | 1063 | 0.73232 | 0.09143 | 1063 | -0.01924 | 0.00363 |
| 22 | 0.75348 | 0.07660 | 1063 | 0.71997 | 0.09803 | 1063 | -0.03351 | 0.00382 |
| 23 | 0.65771 | 0.11522 | 1063 | 0.66367 | 0.08256 | 225 | 0.00596 | 0.00654 |
| 24 | 0.69486 | 0.06610 | 1063 | 0.73099 | 0.07362 | 1063 | 0.03612 | 0.00303 |

| | Trace | | | | | | | |
|---|---|---|---|---|---|---|---|---|
| | PreTBI | | | 7days PostTBI | | | 7days PostTBI - PreTBI | |
| Rat ID | mean | Std | n | mean | Std | n | mean | SEM |
| 19 | 2.29233 | 0.20823 | 943 | 2.47146 | 0.14647 | 943 | 0.17913 | 0.00829 |
| 20 | 2.55029 | 0.19858 | 1063 | 2.70121 | 0.34980 | 1063 | 0.15092 | 0.01234 |
| 21 | 2.97495 | 0.23067 | 1063 | 3.09474 | 0.58102 | 1063 | 0.11979 | 0.01917 |
| 22 | 2.40498 | 0.21700 | 1063 | 2.98119 | 0.36804 | 1063 | 0.57621 | 0.01310 |
| 23 | 3.19805 | 0.75244 | 1063 | 2.75871 | 0.21034 | 225 | -0.43934 | 0.02700 |
| 24 | 2.60141 | 0.14096 | 1063 | 2.89938 | 0.31161 | 1063 | 0.29797 | 0.01049 |

| | RD | | | | | | | |
|---|---|---|---|---|---|---|---|---|
| | PreTBI | | | 4hrs PostTBI | | | 7days PostTBI - PreTBI | |
| Rat ID | mean | Std | n | mean | Std | n | mean | SEM |
| 19 | 0.35991 | 0.08397 | 943 | 0.52474 | 0.12090 | 943 | 0.16483 | 0.00479 |
| 20 | 0.41581 | 0.10318 | 1063 | 0.32536 | 0.13005 | 1063 | -0.09045 | 0.00509 |
| 21 | 0.44844 | 0.12612 | 1063 | 0.49990 | 0.20070 | 1063 | 0.05145 | 0.00727 |
| 22 | 0.36198 | 0.10099 | 1063 | 0.49171 | 0.17370 | 1063 | 0.12973 | 0.00616 |
| 23 | 0.61289 | 0.26969 | 1063 | 0.51374 | 0.11641 | 225 | -0.09916 | 0.01134 |
| 24 | 0.46625 | 0.10447 | 1063 | 0.52217 | 0.17971 | 1063 | 0.05592 | 0.00638 |

| | AD | | | | | | | |
|---|---|---|---|---|---|---|---|---|
| | PreTBI | | | 7days PostTBI | | | 7days PostTBI - PreTBI | |
| Rat ID | mean | Std | n | mean | Std | n | mean | SEM |
| 19 | 1.57306 | 0.21641 | 943 | 1.42447 | 0.12046 | 943 | -0.14859 | 0.00807 |
| 20 | 1.72041 | 0.24494 | 1063 | 2.06980 | 0.51955 | 1063 | 0.34939 | 0.01762 |
| 21 | 2.07783 | 0.10760 | 1063 | 2.09517 | 0.27269 | 1063 | 0.01734 | 0.00899 |
| 22 | 1.68104 | 0.19009 | 1063 | 1.99725 | 0.19388 | 1063 | 0.31621 | 0.00833 |
| 23 | 1.97253 | 0.37232 | 1063 | 1.72957 | 0.17453 | 225 | -0.24296 | 0.01630 |
| 24 | 1.66956 | 0.14657 | 1063 | 1.88008 | 0.08777 | 1063 | 0.21052 | 0.00524 |

Table B-8:   The following tables represent the mean and standard deviation of the DTI parameters (FA, Trace, RD, and AD) within the Och at pre-TBI and 3days post-TBI of Group 3. The post-TBI mean DTI parameters changes (figures 45, 48, 51, 55 and 59) are represented as the mean DTI values at three days post-TBI minus the pre-TBI mean DTI values.  The standard error of the mean difference is calculated by the following equation

$$SEM = \sqrt{\frac{Std_{PreTBI}^2}{n_{preTBI}} + \frac{Std_{PostTBI}^2}{n_{PostTBI}}}$$

| | FA | | | | | | | |
| --- | --- | --- | --- | --- | --- | --- | --- | --- |
| | PreTBI | | | 7days PostTBI | | | 7days PostTBI - PreTBI | |
| Rat ID | mean | Std | n | mean | Std | n | mean | SEM |
| 19 | 0.780887 | 0.0840832 | 1389 | 0.73786 | 0.0899295 | 1545 | -0.043027 | 0.003213174 |
| 20 | 0.732832 | 0.144926 | 1812 | 0.81113 | 0.121279 | 1820 | 0.078298 | 0.004435426 |
| 21 | 0.726104 | 0.115164 | 1609 | 0.749788 | 0.123482 | 1865 | 0.023684 | 0.004051989 |
| 22 | 0.628547 | 0.0959055 | 1874 | 0.771135 | 0.113954 | 1519 | 0.142588 | 0.003668361 |
| 23 | 0.670372 | 0.0610479 | 1867 | 0.657724 | 0.0868479 | 507 | -0.012648 | 0.004107677 |
| 24 | 0.750455 | 0.0778674 | 1482 | 0.672221 | 0.114913 | 1670 | -0.078234 | 0.003463885 |

| | Trace | | | | | | | |
| --- | --- | --- | --- | --- | --- | --- | --- | --- |
| | PreTBI | | | 7days PostTBI | | | 7days PostTBI - PreTBI | |
| Rat ID | mean | Std | n | mean | Std | n | mean | SEM |
| 19 | 2.31759 | 0.758053 | 1389 | 2.43403 | 0.874054 | 1545 | 0.11644 | 0.030136192 |
| 20 | 2.16747 | 0.608177 | 1812 | 1.76477 | 0.566102 | 1820 | -0.4027 | 0.019498996 |
| 21 | 3.3573 | 1.40403 | 1609 | 3.43313 | 1.38882 | 1865 | 0.07583 | 0.047533056 |
| 22 | 2.74219 | 0.480295 | 1874 | 2.35585 | 1.14715 | 1519 | -0.38634 | 0.031455132 |
| 23 | 3.28893 | 1.27823 | 1867 | 4.42854 | 1.18953 | 507 | 1.13961 | 0.060547692 |
| 24 | 3.32964 | 1.28172 | 1482 | 3.23007 | 1.25925 | 1670 | -0.09957 | 0.045365554 |

| | RD | | | | | | | |
| --- | --- | --- | --- | --- | --- | --- | --- | --- |
| | PreTBI | | | 4hrs PostTBI | | | 7days PostTBI - PreTBI | |
| Rat ID | mean | Std | n | mean | Std | n | mean | SEM |
| 19 | 0.3562765 | 0.1884 | 1389 | 0.456976 | 0.236733 | 1545 | 0.1006995 | 0.007863047 |
| 20 | 0.3696545 | 0.2244365 | 1812 | 0.2504715 | 0.1680885 | 1820 | -0.119183 | 0.006582022 |
| 21 | 0.5963035 | 0.402379 | 1609 | 0.525077 | 0.31219 | 1865 | -0.0712265 | 0.012364699 |
| 22 | 0.5708825 | 0.2032005 | 1874 | 0.4019845 | 0.29587 | 1519 | -0.168898 | 0.008925397 |
| 23 | 0.6509445 | 0.321065 | 1867 | 0.907368 | 0.355074 | 507 | 0.2564235 | 0.017432346 |
| 24 | 0.617123 | 0.385415 | 1482 | 0.6444935 | 0.340343 | 1670 | 0.0273705 | 0.013022822 |

| | AD | | | | | | | |
| --- | --- | --- | --- | --- | --- | --- | --- | --- |
| | PreTBI | | | 7days PostTBI | | | 7days PostTBI - PreTBI | |
| Rat ID | mean | Std | n | mean | Std | n | mean | SEM |
| 19 | 1.63693 | 0.412622 | 1389 | 1.62019 | 0.457562 | 1545 | -0.01674 | 0.01606503 |
| 20 | 1.44961 | 0.335042 | 1812 | 1.39274 | 0.434769 | 1820 | -0.05687 | 0.012876694 |
| 21 | 2.20157 | 0.778797 | 1609 | 2.3959 | 0.909662 | 1865 | 0.19433 | 0.028646976 |
| 22 | 1.60096 | 0.252227 | 1874 | 1.60864 | 0.585345 | 1519 | 0.00768 | 0.016109314 |
| 23 | 1.99427 | 0.76562 | 1867 | 2.63042 | 0.583408 | 507 | 0.63615 | 0.031389439 |
| 24 | 2.2486 | 0.708406 | 1482 | 1.97187 | 0.737777 | 1670 | -0.27673 | 0.02577906 |

# APPENDIX C

The following plots represent the CC FA histograms for each rat at pre-TBI (blue, diamond), and four hours post-TBI (red, square). The FA total range (x-axis) was divided into twenty equally spaced bins of 0.05 with marker (diamond or square) representing each bin.

The Following plots represent the CC FA histograms for each rat at pre-TBI (blue, diamond), and twenty-four hours post-TBI (green, triangle). The FA total range (x-axis) was divided into twenty equally spaced bins of 0.05 with marker (diamond or triangle) representing each bin.

The Following plots represent the CC FA histograms for each rat at pre-TBI (blue, diamond), and three days post-TBI (purple, x). The FA total range (x-axis) was divided into twenty equally spaced bins of 0.05 with marker (diamond or x) representing each bin.

Rat 17



Rat 18



Rat 19



Rat 20



Rat 21



Rat 22



Rat 23



Rat 24

The Following plots represent the CC FA histograms for each rat at pre-TBI (blue, diamond), and three days post-TBI (purple, x). The FA total range (x-axis) was divided into twenty equally spaced bins of 0.05 with marker (diamond or x) representing each bin.

The Following plots represent the Och FA histograms for each rat at pre-TBI (blue, diamond), and three days post-TBI (purple, x). The FA total range (x-axis) was divided into twenty equally spaced bins of 0.05 with marker (diamond or x) representing each bin.

The Following plots represent the Och FA histograms for each rat at pre-TBI (blue, diamond), and three days post-TBI (purple, x). The FA total range (x-axis) was divided into twenty equally spaced bins of 0.05 with marker (diamond or x) representing each bin.

The Following plots represent the Och FA histograms for each rat at pre-TBI (blue, diamond), and twenty-four hours post-TBI (green, triangle). The FA total range (x-axis) was divided into twenty equally spaced bins of 0.05 with marker (diamond or triangle) representing each bin.

The following plots represent the Och FA histograms for each rat at pre-TBI (blue, diamond), and four hours post-TBI (red, square). The FA total range (x-axis) was divided into twenty equally spaced bins of 0.05 with marker (diamond or square) representing each bin.

# REFERENCES

(1989). Federal interagency head injury task force report, United State Department of Health and Human Services.

(1998). "Rehabilitation of persons with traumatic brain injury." NIH Consens Statement **16**(1): 1-41.

Adams, J. H. (1988). "The autopsy in fatal non-missile head injuries." Curr Top Pathol **76**: 1-22.

Adams, J. H., D. Doyle, et al. (1989). "Diffuse axonal injury in head injury: definition, diagnosis and grading." Histopathology **15**(1): 49-59.

Adams, J. H., D. Doyle, et al. (1984). "Diffuse axonal injury in head injuries caused by a fall." Lancet **2**(8417-8418): 1420-1422.
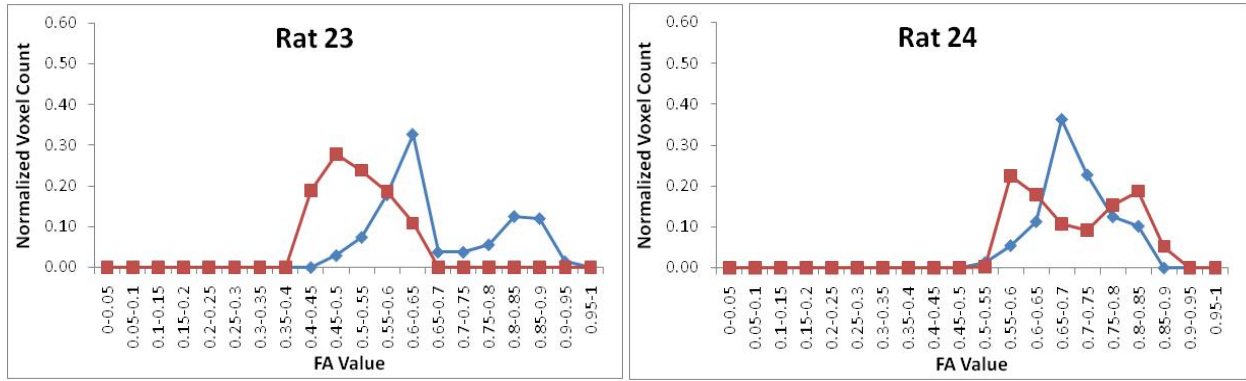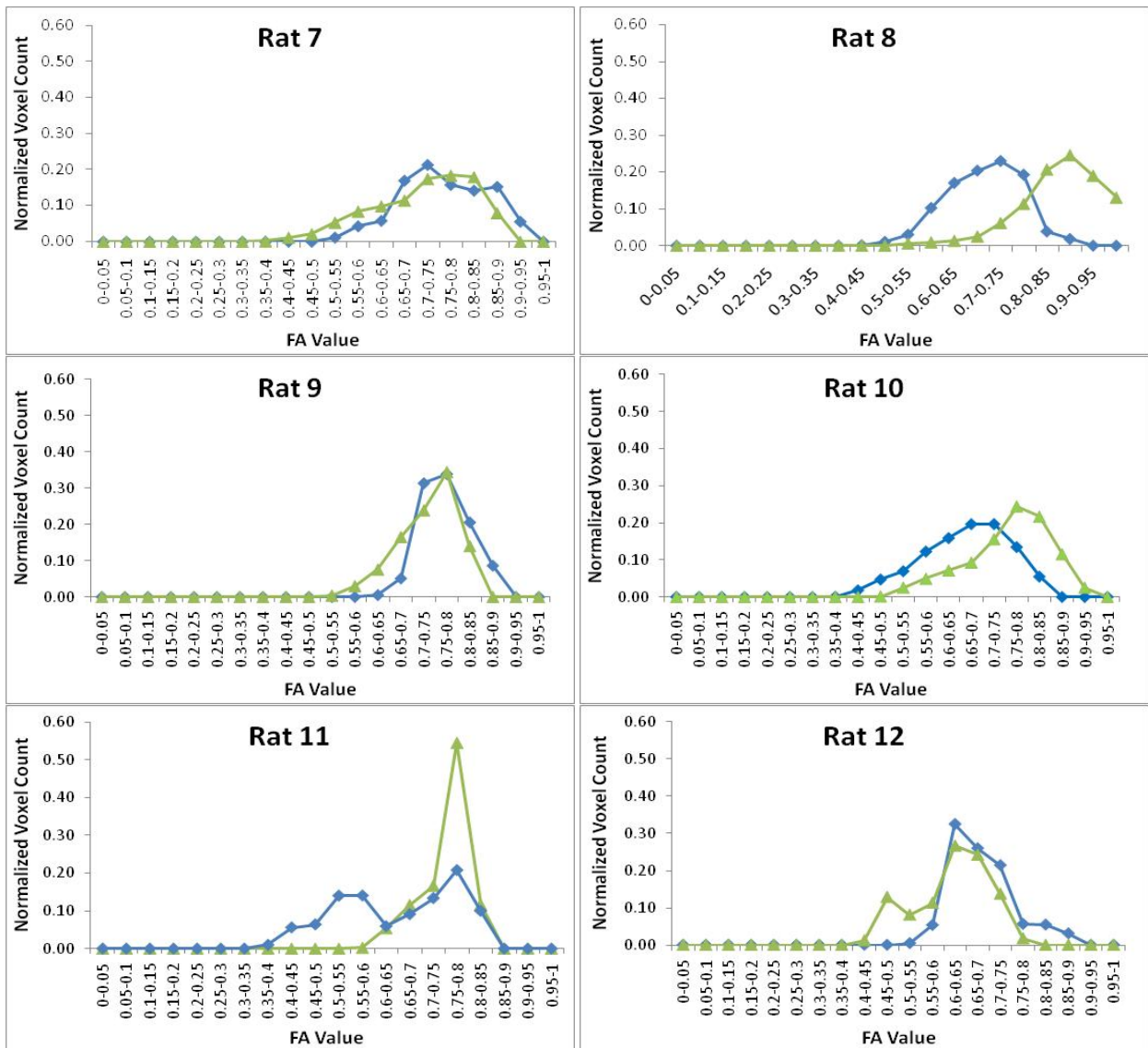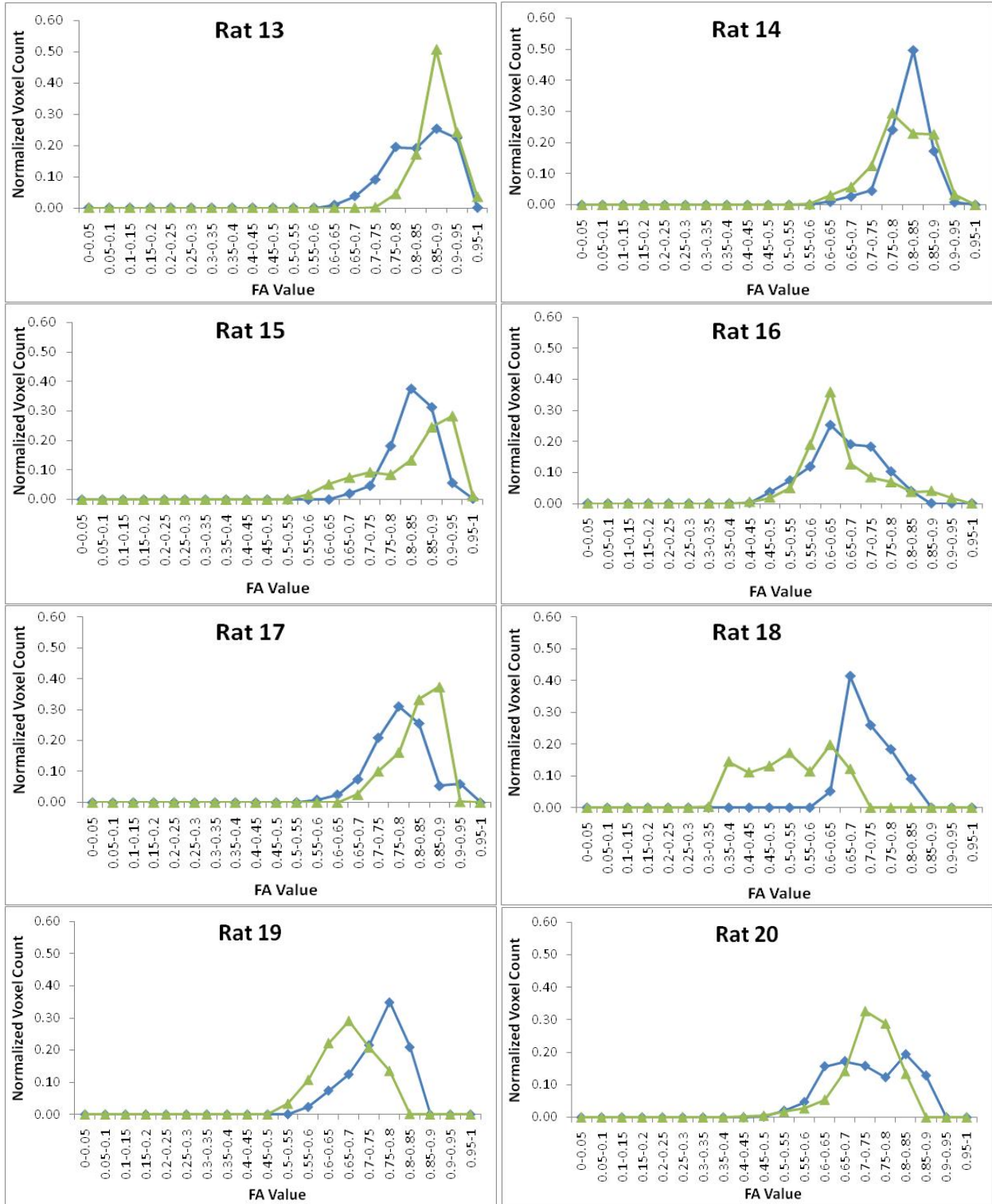
Adams, J. H., D. I. Graham, et al. (1983). "Head injury in man and experimental animals: neuropathology." Acta neurochirurgica. Supplementum **32**: 15-30.

Adams, J. H., D. I. Graham, et al. (1982). "Diffuse axonal injury due to nonmissile head injury in humans: an analysis of 45 cases." Ann Neurol **12**(6): 557-563.

Adelson, P. D., M. J. Whalen, et al. (1998). "Blood brain barrier permeability and acute inflammation in two models of traumatic brain injury in the immature rat: a preliminary report." Acta Neurochir Suppl **71**: 104-106.

Agartz, I., J. L. Andersson, et al. (2001). "Abnormal brain white matter in schizophrenia: a diffusion tensor imaging study." Neuroreport **12**(10): 2251-2254.

Albensi, B. C., S. M. Knoblach, et al. (2000). "Diffusion and high resolution MRI of traumatic brain injury in rats: time course and correlation with histology." Exp Neurol **162**(1): 61-72.

Alberts, B. (1994). Molecular biology of the cell. New York, Garland Pub.

Alexander, A. L., K. M. Hasan, et al. (2001). "Analysis of partial volume effects in diffusion-tensor MRI." Magn Reson Med **45**(5): 770-780.

Alexander, A. L., J. E. Lee, et al. (2007). "Diffusion tensor imaging of the brain." Neurotherapeutics **4**(3): 316-329.

Arfanakis, K., V. M. Haughton, et al. (2002). "Diffusion tensor MR imaging in diffuse axonal injury." AJNR Am J Neuroradiol **23**(5): 794-802.

Ashman, T. A., W. A. Gordon, et al. (2006). "Neurobehavioral consequences of traumatic brain injury." Mt Sinai J Med **73**(7): 999-1005.

Assaf, Y. and P. J. Basser (2005). "Composite hindered and restricted model of diffusion (CHARMED) MR imaging of the human brain." Neuroimage **27**(1): 48-58.

Assaf, Y., D. Ben-Bashat, et al. (2002). "High b-value q-space analyzed diffusion-weighted MRI: application to multiple sclerosis." Magn Reson Med **47**(1): 115-126.

Assaf, Y. and Y. Cohen (1996). "Detection of different water populations in brain tissue using 2H single- and double-quantum-filtered diffusion NMR spectroscopy." J Magn Reson B **112**(2): 151-159.

Assaf, Y. and Y. Cohen (2000). "Assignment of the water slow-diffusing component in the central nervous system using q-space diffusion MRS: implications for fiber tract imaging." Magn Reson Med **43**(2): 191-199.

Assaf, Y. and O. Pasternak (2008). "Diffusion tensor imaging (DTI)-based white matter mapping in brain research: a review." J Mol Neurosci **34**(1): 51-61.

Bai, J. and S. Ng (2005). "Tests for skewness, kurtosis and normality for time series data." journal of business and economic statistics **23**(1): 49-60.

Barzo, P., A. Marmarou, et al. (1996). "Magnetic resonance imaging-monitored acute blood-brain barrier changes in experimental traumatic brain injury." J Neurosurg **85**(6): 1113-1121.

Barzo, P., A. Marmarou, et al. (1997). "Biphasic pathophysiological response of vasogenic and cellular edema in traumatic brain swelling." Acta Neurochir Suppl **70**: 119-122.

Barzo, P., A. Marmarou, et al. (1997). "Contribution of vasogenic and cellular edema to traumatic brain swelling measured by diffusion-weighted imaging." J Neurosurg **87**(6): 900-907.

Basser, P. J. (1995). "Inferring microstructural features and the physiological state of tissues from diffusion-weighted images." NMR Biomed **8**(7-8): 333-344.

Basser, P. J., J. Mattiello, et al. (1994). "Estimation of the effective self-diffusion tensor from the NMR spin echo." J Magn Reson B **103**(3): 247-254.

Basser, P. J., J. Mattiello, et al. (1994). "MR diffusion tensor spectroscopy and imaging." Biophys J **66**(1): 259-267.

Basser, P. J. and C. Pierpaoli (1996). "Microstructural and physiological features of tissues elucidated by quantitative-diffusion-tensor MRI." J Magn Reson B **111**(3): 209-219.

Bazarian, J. J., J. Zhong, et al. (2007). "Diffusion tensor imaging detects clinically important axonal damage after mild traumatic brain injury: a pilot study." J Neurotrauma **24**(9): 1447-1459.

Beaulieu, C. (2002). "The basis of anisotropic water diffusion in the nervous system - a technical review." NMR Biomed **15**(7-8): 435-455.

Beaumont, A., A. Marmarou, et al. (2000). "The permissive nature of blood brain barrier (BBB) opening in edema formation following traumatic brain injury." Acta Neurochir Suppl **76**: 125-129.

Bennett, M., D. P. O'Brien, et al. (1995). "Clinicopathologic observations in 100 consecutive patients with fatal head injury admitted to a neurosurgical unit." Ir Med J **88**(2): 60-62, 59.

Benson, R. R., S. A. Meda, et al. (2007). "Global white matter analysis of diffusion tensor images is predictive of injury severity in traumatic brain injury." J Neurotrauma **24**(3): 446-459.

Blumbergs, P. C., N. R. Jones, et al. (1989). "Diffuse axonal injury in head trauma." Journal of neurology, neurosurgery, and psychiatry **52**(7): 838-841.

Blumbergs, P. C., G. Scott, et al. (1994). "Staining of amyloid precursor protein to study axonal damage in mild head injury." Lancet **344**(8929): 1055-1056.

Blumbergs, P. C., G. Scott, et al. (1995). "Topography of axonal injury as defined by amyloid precursor protein and the sector scoring method in mild and severe closed head injury." J Neurotrauma **12**(4): 565-572.

Brown, A. (2003). "Axonal transport of membranous and nonmembranous cargoes: a unified perspective." J Cell Biol **160**(6): 817-821.

Buki, A. and J. T. Povlishock (2006). "All roads lead to disconnection?--Traumatic axonal injury revisited." Acta Neurochir (Wien) **148**(2): 181-193; discussion 193-184.

Buki, A., S. A. Walker, et al. (2000). "Novel application of tyramide signal amplification (TSA): ultrastructural visualization of double-labeled immunofluorescent axonal profiles." J Histochem Cytochem **48**(1): 153-161.

Burns, J. and W. A. Hauser (2003). "The epidemiology of traumatic brain injury: a review." Epilepsia **44**(supp. 14): 2-10.

Carpenter, M. B. (1991). Core text of neuroanatomy. Baltimore, Williams & Wilkins.

Carr, H. Y. and E. M. Purcell (1954). "Effect of diffusion on free precession in nuclear magnetic resonance experiments." Physical Review **94**(3): 630-638.

Carre, E., E. Cantais, et al. (2004). "Technical aspects of an impact acceleration traumatic brain injury rat model with potential suitability for both microdialysis and PtiO2 monitoring." J Neurosci Methods **140**(1-2): 23-28.

Cernak, I. (2005). "Animal models of head trauma." NeuroRx **2**(3): 410-422.

Cernak, I., R. Vink, et al. (2004). "The pathobiology of moderate diffuse traumatic brain injury as identified using a new experimental model of injury in rats." Neurobiol Dis **17**(1): 29-43.

Christman, C. W., M. S. Grady, et al. (1994). "Ultrastructural studies of diffuse axonal injury in humans." J Neurotrauma **11**(2): 173-186.

Chu, Z., E. A. Wilde, et al. (2010). "Voxel-based analysis of diffusion tensor imaging in mild traumatic brain injury in adolescents." AJNR Am J Neuroradiol **31**(2): 340-346.

Chua, K. S., Y. S. Ng, et al. (2007). "A brief review of traumatic brain injury rehabilitation." Ann Acad Med Singapore **36**(1): 31-12.

Clark, C. A. and D. Le Bihan (2000). "Water diffusion compartmentation and anisotropy at high b values in the human brain." Magn Reson Med **44**(6): 852-859.

Cohen, Y. and Y. Assaf (2002). "High b-value q-space analyzed diffusion-weighted MRS and MRI in neuronal tissues - a technical review." NMR Biomed **15**(7-8): 516-542.

Conde, C. and A. Caceres (2009). "Microtubule assembly, organization and dynamics in axons and dendrites." Nat Rev Neurosci **10**(5): 319-332.

Conturo, T. E., R. C. McKinstry, et al. (1996). "Encoding of anisotropic diffusion with tetrahedral gradients: a general mathematical diffusion formalism and experimental results." Magn Reson Med **35**(3): 399-412.

Corrigan, J. D., A. W. Selassie, et al. (2010). "The epidemiology of traumatic brain injury." J Head Trauma Rehabil **25**(2): 72-80.

Czeiter, E., J. Pal, et al. (2008). "Traumatic axonal injury in the spinal cord evoked by traumatic brain injury." J Neurotrauma **25**(3): 205-213.

DeCarlo, L. T. (1997). "On the meaning and use of kurtosis." Psychological Methods **2**(3): 292-307.

DiLeonardi, A. M., J. W. Huh, et al. (2009). "Impaired axonal transport and neurofilament compaction occur in separate populations of injured axons following diffuse brain injury in the immature rat." Brain Res **1263**: 174-182.

Ding, Y., B. Yao, et al. (2001). "Impaired motor learning and diffuse axonal damage in motor and visual systems of the rat following traumatic brain injury." Neurol Res **23**(2-3): 193-202.

Downhill, J. E., Jr., M. S. Buchsbaum, et al. (2000). "Shape and size of the corpus callosum in schizophrenia and schizotypal personality disorder." Schizophr Res **42**(3): 193-208.

Duvdevani, R., V. Lavie, et al. (1993). "A new method for expressing axonal size: rat optic nerve analysis." J Electron Microsc (Tokyo) **42**(6): 412-414.

Finkelstein, E. A., P. S. Corso, et al. (2006). The incidence and economic burden of injuries in the United States. New York, Oxford University Press.

Foda, M. A. and A. Marmarou (1994). "A new model of diffuse brain injury in rats. Part II: Morphological characterization." J Neurosurg **80**(2): 301-313.

Gaetz, M. (2004). "The neurophysiology of brain injury." Clin Neurophysiol **115**(1): 4-18.

Geddes, D. M., R. S. Cargill, 2nd, et al. (2003). "Mechanical stretch to neurons results in a strain rate and magnitude-dependent increase in plasma membrane permeability." J Neurotrauma **20**(10): 1039-1049.

Gennarelli, T. A. (1993). "Mechanisms of brain injury." The Journal of emergency medicine **11 Suppl 1**: 5-11.

Gennarelli, T. A., J. H. Adams, et al. (1981). "Acceleration induced head injury in the monkey.I. The model, its mechanical and physiological correlates." Acta Neuropathol Suppl **7**: 23-25.

Gennarelli, T. A. and L. E. Thibault (1985). Biomechanics of head injury. Neurosurgery R. H. Wilkins and S. S. Rengachary. New York, McGraw-Hill**:** 1531-1536.

Gennarelli, T. A., L. E. Thibault, et al. (1982). "Diffuse axonal injury and traumatic coma in the primate." Ann Neurol **12**(6): 564-574.

Gennarelli, T. A., L. E. Thibault, et al. (1989). "Axonal injury in the optic nerve: a model simulating diffuse axonal injury in the brain." Journal of neurosurgery **71**(2): 244-253.

Gentleman, S. M., M. J. Nash, et al. (1993). "Beta-amyloid precursor protein (beta APP) as a marker for axonal injury after head injury." Neurosci Lett **160**(2): 139-144.

Gentleman, S. M., G. W. Roberts, et al. (1995). "Axonal injury: a universal consequence of fatal closed head injury?" Acta Neuropathol (Berl) **89**(6): 537-543.

Gentry, L. R., J. C. Godersky, et al. (1988). "Prospective comparative study of intermediate-field MR and CT in the evaluation of closed head trauma." AJR Am J Roentgenol **150**(3): 673-682.

Ghabriel, M., C. Zhu, et al. (2004). Blood-brain brarrier ultrastructural changes in impact acceleration head trauma. 7th International Neurotrauma Symposium, Aldelaide, Australia, Medimond S.r.1.

Ghajar, J. (2000). "Traumatic brain injury." Lancet **356**(9233): 923-929.

Giza, C. C. and D. A. Hovda (2001). "The Neurometabolic Cascade of Concussion." J Athl Train **36**(3): 228-235.

Gorrie, C., S. Oakes, et al. (2002). "Axonal injury in children after motor vehicle crashes: extent, distribution, and size of axonal swellings using beta-APP immunohistochemistry." J Neurotrauma **19**(10): 1171-1182.

Grady, M. S., M. R. McLaughlin, et al. (1993). "The use of antibodies targeted against the neurofilament subunits for the detection of diffuse axonal injury in humans." J Neuropathol Exp Neurol **52**(2): 143-152.

Graham, D. I., D. McLellan, et al. (1983). "The neuropathology of the vegetative state and severe disability after non-missile head injury." Acta neurochirurgica. Supplementum **32**: 65-67.

Guan, K. L. and Y. Rao (2003). "Signalling mechanisms mediating neuronal responses to guidance cues." Nat Rev Neurosci **4**(12): 941-956.

Gultekin, S. H. and T. W. Smith (1994). "Diffuse axonal injury in craniocerebral trauma. A comparative histologic and immunohistochemical study." Arch Pathol Lab Med **118**(2): 168-171.

Gutierrez, E., Y. Huang, et al. (2001). "A new model for diffuse brain injury by rotational acceleration: I model, gross appearance, and astrocytosis." J Neurotrauma **18**(3): 247-257.

Haacke, E. M., R. W. Brown, et al. (1999). Magnetic resonance imaging. New York, Wiley-Liss.

Hagmann, P., L. Jonasson, et al. (2006). "Understanding diffusion MR imaging techniques: from scalar diffusion-weighted imaging to diffusion tensor imaging and beyond." Radiographics **26 Suppl 1**: S205-223.

Hahn, E. L. (1950). "Spin echoes." Physical review **80**: 580-594.

Hoare, J., J. P. Fouche, et al. (2010). "White matter correlates of apathy in HIV-positive subjects: a diffusion tensor imaging study." J Neuropsychiatry Clin Neurosci **22**(3): 313-320.

Hofer, S. and J. Frahm (2006). "Topography of the human corpus callosum revisited--comprehensive fiber tractography using diffusion tensor magnetic resonance imaging." Neuroimage **32**(3): 989-994.

Hoffman, P. N. (1995). "The Synthesis, axonal transport, and phosphorylation of neurofilaments determine axonal caliber in myelinated nerve fibers." The neuroscientist **1**(2): 76-83.

Hornak, J. P. (1996-2011). The basics of MRI. Heneitta, NY, Interactive Learning Software.

Hortobagyi, T. and S. Al-Sarraj (2008). "The significance of diffuse axonal injury: how to diagnose it and what does it tell us?" Advances in clinical neuroscience and rehabilitation **2**(2): 16-18.

Hortobagyi, T., S. Wise, et al. (2007). "Traumatic axonal damage in the brain can be detected using beta-APP immunohistochemistry within 35 min after head injury to human adults." Neuropathol Appl Neurobiol **33**(2): 226-237.

Huh, J. W., H. L. Laurer, et al. (2002). "Rapid loss and partial recovery of neurofilament immunostaining following focal brain injury in mice." Exp Neurol **175**(1): 198-208.

Huisman, T. A., L. H. Schwamm, et al. (2004). "Diffusion tensor imaging as potential biomarker of white matter injury in diffuse axonal injury." AJNR Am J Neuroradiol **25**(3): 370-376.

Inglese, M., S. Makani, et al. (2005). "Diffuse axonal injury in mild traumatic brain injury: a diffusion tensor imaging study." J Neurosurg **103**(2): 298-303.

Inglis, B. A., E. L. Bossart, et al. (2001). "Visualization of neural tissue water compartments using biexponential diffusion tensor MRI." Magn Reson Med **45**(4): 580-587.

Ito, J., A. Marmarou, et al. (1996). "Characterization of edema by diffusion-weighted imaging in experimental traumatic brain injury." J Neurosurg **84**(1): 97-103.

Janmeya, P. A., J. F. Leterrierb, et al. (2003). "Assembly and structure of neurofilaments." Current Opinion in Colloid and Interface Science **8**: 40-47.

Jansons, K. M. and D. C. Alexander (2003). "Persistent Angular Structure: new insights from diffusion MRI data. Dummy version." Inf Process Med Imaging **18**: 672-683.

Jeffery, G. (2001). "Architecture of the optic chiasm and the mechanisms that sculpt its development." Physiol Rev **81**(4): 1393-1414.

Jellison, B. J., A. S. Field, et al. (2004). "Diffusion tensor imaging of cerebral white matter: a pictorial review of physics, fiber tract anatomy, and tumor imaging patterns." AJNR Am J Neuroradiol **25**(3): 356-369.

Jemal, A., R. Siegel, et al. (2007). "Cancer statistics, 2007." CA Cancer J Clin **57**(1): 43-66.

Jiang, H., P. C. van Zijl, et al. (2006). "DtiStudio: resource program for diffusion tensor computation and fiber bundle tracking." Comput Methods Programs Biomed **81**(2): 106-116.

Johansen-Berg, H. and T. E. J. Behrens, Eds. (2009). Diffusion MRI from quantitative measurement to in vivo neuroanatomy London, UK, Academic Press.

Kallakuri, S., J. M. Cavanaugh, et al. (2003). "The effect of varying impact energy on diffuse axonal injury in the rat brain: a preliminary study." Exp Brain Res **148**(4): 419-424.

Kallakuri, S., L. Zhang, et al. (2006). Quantification of TAI and tissue strain using experimental and computational model of TBI on rats. Biomedical Engineering Society Chicago.

Kandel, E. R., J. H. Schwartz, et al. (2000). Principles of neural science. New York, McGraw-Hill, Health Professions Division.

Kelley, B. J., O. Farkas, et al. (2006). "Traumatic axonal injury in the perisomatic domain triggers ultrarapid secondary axotomy and Wallerian degeneration." Exp Neurol **198**(2): 350-360.

Kelly, A. B., R. D. Zimmerman, et al. (1988). "Head trauma: comparison of MR and CT--experience in 100 patients." AJNR Am J Neuroradiol **9**(4): 699-708.

Keshavan, M. S., V. A. Diwadkar, et al. (2002). "Development of the corpus callosum in childhood, adolescence and early adulthood." Life Sci **70**(16): 1909-1922.

Kim, E. Y., H. J. Park, et al. (2008). "Measuring fractional anisotropy of the corpus callosum using diffusion tensor imaging: mid-sagittal versus axial imaging planes." Korean J Radiol **9**(5): 391-395.

Kinnunen, K. M., R. Greenwood, et al. (2011). "White matter damage and cognitive impairment after traumatic brain injury." Brain **134**(Pt 2): 449-463.

Kochumov, P., D. E. Williamson, et al. (2010). Neurobiology of Aging **In Press**.

Kraus, M. F., T. Susmaras, et al. (2007). "White matter integrity and cognition in chronic traumatic brain injury: a diffusion tensor imaging study." Brain **130**(Pt 10): 2508-2519.

Kumar, R., S. Saksena, et al. (2010). "Serial changes in diffusion tensor imaging metrics of corpus callosum in moderate traumatic brain injury patients and their correlation with neuropsychometric tests: a 2-year follow-up study." J Head Trauma Rehabil **25**(1): 31-42.

Kumar, S. and J. H. Hoh (2004). "Modulation of repulsive forces between neurofilaments by sidearm phosphorylation." Biochemical and biophysical research communications **324**(2): 489-496.

Kuroiwa, T., N. Miyasaka, et al. (2007). "Experimental ischemic brain edema: morphological and magnetic resonance imaging findings." Neurosurg Focus **22**(5): E11.

Kuroiwa, T., T. Nagaoka, et al. (2000). "Time course of trace of diffusion tensor [Trace(D)] and histology in brain edema." Acta Neurochir Suppl **76**: 191-194.

Kuroiwa, T., T. Nagaoka, et al. (1998). "Different apparent diffusion coefficient: water content correlations of gray and white matter during early ischemia." Stroke **29**(4): 859-865.

Kuroiwa, T., T. Nagaoka, et al. (1999). "Correlations between the apparent diffusion coefficient, water content, and ultrastructure after induction of vasogenic brain edema in cats." J Neurosurg **90**(3): 499-503.

Langlois, J. A., A. Marr, et al. (2005). "Tracking the silent epidemic and educating the public: CDC's traumatic brain injury-associated activities under the TBI Act of 1996 and the Children's Health Act of 2000." J Head Trauma Rehabil **20**(3): 196-204.

Langlois, J. A., W. Rutland-Brown, et al. (2004). Traumatic brain injury in the United States emergency department visits hospitalization and deaths. Atlanta, Center of Disease Control and Prevention.

Langlois, J. A., W. Rutland-Brown, et al. (2006). "The epidemiology and impact of traumatic brain injury: a brief overview." J Head Trauma Rehabil **21**(5): 375-378.

Le Bihan, D., J. F. Mangin, et al. (2001). "Diffusion tensor imaging: concepts and applications." J Magn Reson Imaging **13**(4): 534-546.

Le, T. H., P. Mukherjee, et al. (2005). "Diffusion tensor imaging with three-dimensional fiber tractography of traumatic axonal shearing injury: an imaging correlate for the posterior callosal "disconnection" syndrome: case report." Neurosurgery **56**(1): 189.

Li, Y., L. Zhang, et al. (2011). "Quantitative relationship between axonal injury and mechanical response in a rodent head impact acceleration model." Submitted to J Neurotrauma.

Lipton, M. L., E. Gulko, et al. (2009). "Diffusion-tensor imaging implicates prefrontal axonal injury in executive function impairment following very mild traumatic brain injury." Radiology **252**(3): 816-824.

Liu, T., H. Li, et al. (2007). "Brain tissue segmentation based on DTI data." Neuroimage **38**(1): 114-123.

Liu, T., G. Young, et al. (2006). "76-space analysis of grey matter diffusivity: methods and applications." Neuroimage **31**(1): 51-65.

Mac Donald, C. L., K. Dikranian, et al. (2007). "Diffusion tensor imaging reliably detects experimental traumatic axonal injury and indicates approximate time of injury." J Neurosci **27**(44): 11869-11876.

Mac Donald, C. L., K. Dikranian, et al. (2007). "Detection of traumatic axonal injury with diffusion tensor imaging in a mouse model of traumatic brain injury." Exp Neurol **205**(1): 116-131.

Malbouisson, A. M., M. N. Ghabriel, et al. (1985). "Axonal microtubules: a computer-linked quantitative analysis." Anat Embryol (Berl) **171**(3): 339-344.

Mamelak, A. N., L. H. Pitts, et al. (1996). "Predicting survival from head trauma 24 hours after injury: a practical method with therapeutic implications." J Trauma **41**(1): 91-99.

Margulies, S. S., L. E. Thibault, et al. (1990). "Physical model simulations of brain injury in the primate." Journal of biomechanics **23**(8): 823-836.

Marmarou, A. (2003). "Pathophysiology of traumatic brain edema: current concepts." Acta Neurochir Suppl **86**: 7-10.

Marmarou, A. (2007). "A review of progress in understanding the pathophysiology and treatment of brain edema." Neurosurg Focus **22**(5): E1.

Marmarou, A., M. A. Foda, et al. (1994). "A new model of diffuse brain injury in rats. Part I: Pathophysiology and biomechanics." J Neurosurg **80**(2): 291-300.

Marmarou, C. R. and J. T. Povlishock (2006). "Administration of the immunophilin ligand FK506 differentially attenuates neurofilament compaction and impaired axonal transport in injured axons following diffuse traumatic brain injury." Exp Neurol **197**(2): 353-362.

Marmarou, C. R., S. A. Walker, et al. (2005). "Quantitative analysis of the relationship between intra- axonal neurofilament compaction and impaired axonal transport following diffuse traumatic brain injury." J Neurotrauma **22**(10): 1066-1080.

Maxwell, W. L. and D. I. Graham (1997). "Loss of axonal microtubules and neurofilaments after stretch-injury to guinea pig optic nerve fibers." J Neurotrauma **14**(9): 603-614.

Maxwell, W. L., J. T. Povlishock, et al. (1997). "A mechanistic analysis of nondisruptive axonal injury: a review." J Neurotrauma **14**(7): 419-440.

Mayer, A. R., J. Ling, et al. (2010). "A prospective diffusion tensor imaging study in mild traumatic brain injury." Neurology **74**(8): 643-650.

McKenzie, K. J., D. R. McLellan, et al. (1996). "Is beta-APP a marker of axonal damage in short-surviving head injury?" Acta Neuropathol (Berl) **92**(6): 608-613.

Medina, D. A. and M. Gaviria (2008). "Diffusion tensor imaging investigations in Alzheimer's disease: the resurgence of white matter compromise in the cortical dysfunction of the aging brain." Neuropsychiatr Dis Treat **4**(4): 737-742.

Melhem, E. R., S. Mori, et al. (2002). "Diffusion tensor MR imaging of the brain and white matter tractography." AJR Am J Roentgenol **178**(1): 3-16.

Melvin, J. W., J. W. Lighthall, et al. (1994). "Brain injury biomechanics." SAE: 276.

Miller, C. C., S. Ackerley, et al. (2002). "Axonal transport of neurofilaments in normal and disease states." Cell Mol Life Sci **59**(2): 323-330.

Mori, S. and J. Zhang (2006). "Principles of diffusion tensor imaging and its applications to basic neuroscience research." Neuron **51**(5): 527-539.

Moseley, M. E., Y. Cohen, et al. (1990). "Diffusion-weighted MR imaging of anisotropic water diffusion in cat central nervous system." Radiology **176**(2): 439-445.

Murray, C., A. Viehman, et al. (2006). "The corpus callosum in Pick's disease, Alzheimer's disease, and amyotrophic lateral sclerosis: gliosis implies possible clinical consequence." Am J Alzheimers Dis Other Demen **21**(1): 37-43.

Nebuloni, M., A. Pellegrinelli, et al. (2001). "Beta amyloid precursor protein and patterns of HIV p24 immunohistochemistry in different brain areas of AIDS patients." Aids **15**(5): 571-575.

Newcombe, V. F., G. B. Williams, et al. (2007). "Analysis of acute traumatic axonal injury using diffusion tensor imaging." Br J Neurosurg **21**(4): 340-348.

Nicholson, C. (2004). "Diffusion and related transport mechanisms in brain tissue." Reports On Progress In Physics **64**: 815-884.

O'Connor, C. A., I. Cernak, et al. (2006). "The temporal profile of edema formation differs between male and female rats following diffuse traumatic brain injury." Acta Neurochir Suppl **96**: 121-124.

Ogata, M. and O. Tsuganezawa (1999). "Neuron-specific enolase as an effective immunohistochemical marker for injured axons after fatal brain injury." Int J Legal Med **113**(1): 19-25.

Okonkwo, D. O., E. H. Pettus, et al. (1998). "Alteration of the neurofilament sidearm and its relation to neurofilament compaction occurring with traumatic axonal injury." Brain Res **784**(1-2): 1-6.

Pal, J., Z. Toth, et al. (2006). "Selective induction of ultrastructural (neurofilament) compaction in axons by means of a new head-injury apparatus." J Neurosci Methods **153**(2): 283-289.

Papadakis, N. G., K. M. Martin, et al. (2002). "Study of the effect of CSF suppression on white matter diffusion anisotropy mapping of healthy human brain." Magn Reson Med **48**(2): 394-398.

Papadopoulos, M. C., D. K. Binder, et al. (2005). "Enhanced macromolecular diffusion in brain extracellular space in mouse models of vasogenic edema measured by cortical surface photobleaching." FASEB J **19**(3): 425-427.

Paxinos, G. and C. Watson (2005). The rat brain in stereotaxic coordinates. Amsterdam ; Boston, Elsevier Academic Press.

Pettus, E. H., C. W. Christman, et al. (1994). "Traumatically induced altered membrane permeability: its relationship to traumatically induced reactive axonal change." J Neurotrauma **11**(5): 507-522.

Pettus, E. H. and J. T. Povlishock (1996). "Characterization of a distinct set of intra-axonal ultrastructural changes associated with traumatically induced alteration in axolemmal permeability." Brain Res **722**(1-2): 1-11.

Pfefferbaum, A. and E. V. Sullivan (2003). "Increased brain white matter diffusivity in normal adult aging: relationship to anisotropy and partial voluming." Magn Reson Med **49**(5): 953-961.

Pierpaoli, C. and P. J. Basser (1996). "Toward a quantitative assessment of diffusion anisotropy." Magn Reson Med **36**(6): 893-906.

Pierpaoli, C., P. Jezzard, et al. (1996). "Diffusion tensor MR imaging of the human brain." Radiology **201**(3): 637-648.

Piper, I. R., D. Thomson, et al. (1996). "Monitoring weight drop velocity and foam stiffness as an aid to quality control of a rodent model of impact acceleration neurotrauma." J Neurosci Methods **69**(2): 171-174.

Povlishock, J. T. (1992). "Traumatically induced axonal injury: pathogenesis and pathobiological implications." Brain Pathol **2**(1): 1-12.

Povlishock, J. T. (1993). "Pathobiology of traumatically induced axonal injury in animals and man." Ann Emerg Med **22**(6): 980-986.

Povlishock, J. T., D. P. Becker, et al. (1983). "Axonal change in minor head injury." J Neuropathol Exp Neurol **42**(3): 225-242.

Povlishock, J. T., A. Buki, et al. (1999). "Initiating mechanisms involved in the pathobiology of traumatically induced axonal injury and interventions targeted at blunting their progression." Acta Neurochir Suppl **73**: 15-20.

Povlishock, J. T. and C. W. Christman (1995). "The pathobiology of traumatically induced axonal injury in animals and humans: a review of current thoughts." J Neurotrauma **12**(4): 555-564.

Povlishock, J. T., A. Marmarou, et al. (1997). "Impact acceleration injury in the rat: evidence for focal axolemmal change and related neurofilament sidearm alteration." J Neuropathol Exp Neurol **56**(4): 347-359.

Price, R. L., P. Paggi, et al. (1988). "Neurofilaments are spaced randomly in the radial dimension of axons." J Neurocytol **17**(1): 55-62.

Purves, D. (2008). Neuroscience. Sunderland, Mass., Sinauer.

Qiao, M., K. L. Malisza, et al. (2001). "Correlation of cerebral hypoxic-ischemic T2 changes with tissue alterations in water content and protein extravasation." Stroke **32**(4): 958-963.

Qiu, D., L. H. Tan, et al. (2008). "Diffusion tensor imaging of normal white matter maturation from late childhood to young adulthood: voxel-wise evaluation of mean diffusivity, fractional anisotropy, radial and axial diffusivities, and correlation with reading development." Neuroimage **41**(2): 223-232.

Raghupathi, R. (2004). "Cell death mechanisms following traumatic brain injury." Brain Pathol **14**(2): 215-222.

Reeves, T. M., L. L. Phillips, et al. (2005). "Myelinated and unmyelinated axons of the corpus callosum differ in vulnerability and functional recovery following traumatic brain injury." Exp Neurol **196**(1): 126-137.

Reilly, P. L. (2001). "Brain injury: the pathophysiology of the first hours.'Talk and Die revisited'." J Clin Neurosci **8**(5): 398-403.

Rimel, R. W., B. Giordani, et al. (1981). "Disability caused by minor head injury." Neurosurgery **9**(3): 221-228.

Rimel, R. W., B. Giordani, et al. (1982). "Moderate head injury: completing the clinical spectrum of brain trauma." Neurosurgery **11**(3): 344-351.

Roy, S., P. Coffee, et al. (2000). "Neurofilaments are transported rapidly but intermittently in axons: implications for slow axonal transport." J Neurosci **20**(18): 6849-6861.

Roy, S., B. Zhang, et al. (2005). "Axonal transport defects: a common theme in neurodegenerative diseases." Acta Neuropathol **109**(1): 5-13.

Rugg-Gunn, F. J., M. R. Symms, et al. (2001). "Diffusion imaging shows abnormalities after blunt head trauma when conventional magnetic resonance imaging is normal." J Neurol Neurosurg Psychiatry **70**(4): 530-533.

Rutgers, D. R., P. Fillard, et al. (2008). "Diffusion tensor imaging characteristics of the corpus callosum in mild, moderate, and severe traumatic brain injury." AJNR Am J Neuroradiol **29**(9): 1730-1735.

Saatman, K. E., G. Serbest, et al. (2009). Axonal Damage due to Traumatic Brain Injury. Handbook of Neurochemistry and Molecular Neurobiology. A. Lajtha, N. Banik and S. K. Ray, Springer US**:** 343-361.

Sen, P. N. (2004). "Diffusion and tissue architecture." Journal of Physics: Condensed Matter **16**: s5213-s5220.

Seoung, Y. H., H. G. Kim, et al. (2009). "Evaluation of a fractional anisotropy measurement of the corpus callosum in a normal adult brain by using diffusion tensor MRI." Journal of Korean Physical Society **55**(4): 1657-1665.

Sevick, R. J., F. Kanda, et al. (1992). "Cytotoxic brain edema: assessment with diffusion-weighted MR imaging." Radiology **185**(3): 687-690.

Sherriff, F. E., L. R. Bridges, et al. (1994). "Markers of axonal injury in post mortem human brain." Acta Neuropathol (Berl) **88**(5): 433-439.

Shimony, J. S., R. C. McKinstry, et al. (1999). "Quantitative diffusion-tensor anisotropy brain MR imaging: normative human data and anatomic analysis." Radiology **212**(3): 770-784.

Sidaros, A., A. W. Engberg, et al. (2008). "Diffusion tensor imaging during recovery from severe traumatic brain injury and relation to clinical outcome: a longitudinal study." Brain **131**(Pt 2): 559-572.

Siegel, G. J., R. W. Albers, et al., Eds. (2006). Basic neurochemistry molecluar cellular and medical aspects. Burlington, MA, Academic Press.

Siesjo, B. K., B. Hu, et al. (1999). "Is the cell death pathway triggered by the mitochondrion or the endoplasmic reticulum?" J Cereb Blood Flow Metab **19**(1): 19-26.

Slazinski, T. and M. C. Johnson (1994). "Severe diffuse axonal injury in adults and children." J Neurosci Nurs **26**(3): 151-154.

Smith, D. H., X. H. Chen, et al. (1997). "Characterization of diffuse axonal pathology and selective hippocampal damage following inertial brain trauma in the pig." J Neuropathol Exp Neurol **56**(7): 822-834.

Smith, D. H., D. F. Meaney, et al. (2003). "Diffuse axonal injury in head trauma." J Head Trauma Rehabil **18**(4): 307-316.

Smith, D. H., J. A. Wolf, et al. (1999). "High tolerance and delayed elastic response of cultured axons to dynamic stretch injury." J Neurosci **19**(11): 4263-4269.

SPSS (2007). SPSS Statisitics Base 17.0 user's guide Chicago 1-616.

Squire, L. R. (2003). Fundamental neuroscience. Amsterdam ; Boston, Academic Press.

Stejskal, E. O. and J. E. Tanner (1965). "Spin diffusion measurments: spin echoes in the presence of a time-dependent field gradient." Journal of Chemical Physics **42**(1): 288-292.

Stone, J. R., D. O. Okonkwo, et al. (2004). "Impaired axonal transport and altered axolemmal permeability occur in distinct populations of damaged axons following traumatic brain injury." <u>Exp Neurol</u> **190**(1): 59-69.

Stone, J. R., R. H. Singleton, et al. (2000). "Antibodies to the C-terminus of the beta-amyloid precursor protein (APP): a site specific marker for the detection of traumatic axonal injury." <u>Brain Res</u> **871**(2): 288-302.

Stone, J. R., R. H. Singleton, et al. (2001). "Intra-axonal neurofilament compaction does not evoke local axonal swelling in all traumatically injured axons." <u>Exp Neurol</u> **172**(2): 320-331.

Stone, J. R., S. A. Walker, et al. (1999). "The visualization of a new class of traumatically injured axons through the use of a modified method of microwave antigen retrieval." <u>Acta Neuropathol</u> **97**(4): 335-345.

Suehiro, E., R. H. Singleton, et al. (2001). "The immunophilin ligand FK506 attenuates the axonal damage associated with rapid rewarming following posttraumatic hypothermia." <u>Exp Neurol</u> **172**(1): 199-210.

Sugioka, M., H. Sawai, et al. (1995). "Changes of compound action potentials in retrograde axonal degeneration of rat optic nerve." <u>Exp Neurol</u> **132**(2): 262-270.

Takayama, H., M. Kobayashi, et al. (2000). "Diffusion-weighted imaging demonstrates transient cytotoxic edema involving the corpus callosum in a patient with diffuse brain injury." <u>Clin Neurol Neurosurg</u> **102**(3): 135-139.

Tang-Schomer, M. D., A. R. Patel, et al. (2010). "Mechanical breaking of microtubules in axons during dynamic stretch injury underlies delayed elasticity, microtubule disassembly, and axon degeneration." <u>The FASEB journal : official publication of the Federation of American Societies for Experimental Biology</u> **24**(5): 1401-1410.

Thornhill, S., G. M. Teasdale, et al. (2000). "Disability in young people and adults one year after head injury: prospective cohort study." <u>BMJ</u> **320**(7250): 1631-1635.

Thurman, D. J., C. Alverson, et al. (1999). "Traumatic brain injury in the United States: A public health perspective." J Head Trauma Rehabil **14**(6): 602-615.

Tokutomi, T., M. Hirohata, et al. (1997). "Posttraumatic edema in the corpus callosum shown by MRI." Acta Neurochir Suppl **70**: 80-83.

Tuch, D. S., T. G. Reese, et al. (2002). "High angular resolution diffusion imaging reveals intravoxel white matter fiber heterogeneity." Magn Reson Med **48**(4): 577-582.

Tuch, D. S., T. G. Reese, et al. (2003). "Diffusion MRI of complex neural architecture." Neuron **40**(5): 885-895.

Unterberg, A. W., J. Stover, et al. (2004). "Edema and brain trauma." Neuroscience **129**(4): 1021-1029.

Van den Heuvel, C., P. C. Blumbergs, et al. (1999). "Upregulation of amyloid precursor protein messenger RNA in response to traumatic brain injury: an ovine head impact model." Exp Neurol **159**(2): 441-450.

Virta, A., A. Barnett, et al. (1999). "Visualizing and characterizing white matter fiber structure and architecture in the human pyramidal tract using diffusion tensor MRI." Magn Reson Imaging **17**(8): 1121-1133.

Wang, L., C. L. Ho, et al. (2000). "Rapid movement of axonal neurofilaments interrupted by prolonged pauses." Nat Cell Biol **2**(3): 137-141.

Waxman, S. G. and J. A. Black (1988). "Unmyelinated and myelinated axon membrane from rat corpus callosum: differences in macromolecular structure." Brain Res **453**(1-2): 337-343.

Westin, C. F., S. E. Maier, et al. (2002). "Processing and visualization for diffusion tensor MRI." Med Image Anal **6**(2): 93-108.

Wiegell, M. R., H. B. Larsson, et al. (2000). "Fiber crossing in human brain depicted with diffusion tensor MR imaging." Radiology **217**(3): 897-903.

Wilde, E. A., Z. Chu, et al. (2006). "Diffusion tensor imaging in the corpus callosum in children after moderate to severe traumatic brain injury." J Neurotrauma **23**(10): 1412-1426.

Wilde, E. A., S. R. McCauley, et al. (2008). "Diffusion tensor imaging of acute mild traumatic brain injury in adolescents." Neurology **70**(12): 948-955.

Wolf, J. A., P. K. Stys, et al. (2001). "Traumatic axonal injury induces calcium influx modulated by tetrodotoxin-sensitive sodium channels." The Journal of neuroscience : the official journal of the Society for Neuroscience **21**(6): 1923-1930.

Xiao-Sheng, H., Y. Sheng-Yu, et al. (2000). "Diffuse axonal injury due to lateral head rotation in a rat model." J Neurosurg **93**(4): 626-633.

Xu, J., I. A. Rasmussen, et al. (2007). "Diffuse axonal injury in severe traumatic brain injury visualized using high-resolution diffusion tensor imaging." J Neurotrauma **24**(5): 753-765.

Yaghmai, A. and J. Povlishock (1992). "Traumatically induced reactive change as visualized through the use of monoclonal antibodies targeted to neurofilament subunits." J Neuropathol Exp Neurol **51**(2): 158-176.

Zhang, L., M. Gurao, et al. (2011). "Material characterization and computer model simulation of low density polyurethane foam used in a rodent traumatic brain injury model." Journal of neuroscience methods **198**(1): 93-98.

# ABSTRACT

# COMPARISON OF PROGRESSION OF DIFFUSE AXONAL INJURY WITH HISTOLOGICAL AND DIFFUSION TENSOR IMAGING

by

**NISRINE ZAKARIA**

**Advisor:** Dr. John M. Cavanaugh

**Major:**Biomedical Engineering

**Degree:**Doctor of Philosophy

Diffuse axonal injury, also known as traumatic axonal injury (TAI), is a major contributor to the pathology of traumatic brain injury.  However, TAI is undetectable to conventional clinical magnetic resonance (MR) imaging techniques.  Histologically, TAI is characterized by swollen axons that eventually disconnect and form axonal retraction balls (RB) in various white matter tracts.  MR-diffusion tensor imaging (MR-DTI) has been reported to be sensitive to TAI in human TBI patients by measuring water molecular diffusion motion in white matter fiber tracts. To date, only one correlative animal study has been carried out to investigate the DTI relationship to TAI, and it has reported a relationship between DTI changes and TAI.  No other animal study has validated the correlation between DTI and TAI.  Therefore, this study is the second animal study that has examined the correlation between histological observations of axonal damage in white mater tract and the DTI measurements over time.

TAI was induced in twenty-four anaesthetized male Sprague Dawley rats utilizing an impact acceleration device (Marmarou et al 1994).  T2 weighted MR images, and DTI images were acquired *in vivo* pre-impact, and four hours, twenty-four hours, three days and seven days post-impact.  The DTI images were obtained in a Bruker 4.7 Tesla scanner in six gradient

directions. Fractional anisotropy (FA), diffusion trace, axial diffusivity (AD) and radial diffusivity (RD) were calculated by using DTI Studio (Johns Hopkins University). After imaging, perfused brain tissue was processed for β-amyloid precursor protein (β-APP) and RMO14 immunocytochemistry and quantified by ImageJ software (NIH) for each time point.

β-APP and RMO14 immunoreactive axons were observed in optic chiasm (Och) and corpus callosum (CC). TAI was more prevalent and less variable in the Och in comparison to CC. In the Och and CC β-APP positive axons were more prominent at eight hours and twenty-eight hours post-TBI and decreased as time elapsed. In the Och and CC RMO14 positive axons were more prominent at twenty-eight hours post-TBI and decreased as time elapsed. However, at seven days post-TBI a modest increase of RMO14 positive axons occurred in comparison to three days post TBI.

The mean FA values of the DTI image of the Och and CC revealed a decrease of FA at four hours post-TBI ($p$<0.05). After four hours post-TBI the FA value increased and remained increased up to seven days post-TBI in the CC and Och. The other DTI parameters also changed over time.

No linear relationship was found between FA and TAI density and between AD and TAI density in the CC and Och. The diffusion trace was found to be correlated with TAI density at four hours and seven day post-TBI in the Och and CC respectively. The RD was found to be correlated with TAI density at four hours and seven days post-TBI in the Och.

This study was unable to verify that the DTI changes after TBI are an indication of TAI. However, the DTI parameters did change as time elapsed after TBI. The profile of the DTI parameter changes may be an indication of edema. In addition, other imaging parameters, diffusion trace and RD, did show correlation with the density β-APPpositive axonsand may be the better DTI parameters for describing axonal integrity such as axonal permeability.

# AUTOBIOGRAPHICAL STATEMENT

## Nisrine Zakaria

### Education

| | |
|---|---|
| 2004 – Present | **Wayne State University, USA** |
| | **Department of Biomedical Engineering** |
| | *Doctor of Philosophy* |
| 2002 – 2003 | **Wayne State University, USA** |
| | **Department of Biomedical Engineering** |
| | *Master of Philosophy* |
| 1997 – 2001 | **University of Windsor, Canada** |
| | **Department of Electrical Engineering** |
| | *Bachelor of Applied Science* |

### Awards

- Top 16 student abstract in the 25th National Neurotrauma Symposium
- Graduate-Professional Scholarship
- Engineering Dean's Honor Roll
- University of Windsor Entrance Bursary
- President's Nations Alumni Incentive

### Conferences

Srinivas Kallakuri, Yan Li, <u>Nisrine Zakaria</u>, RunZhou Zhou, Sharath Bandaru, LiYing Zhang, John Cavanaugh "Histological Assessment and Quantification of Traumatic Brain Injury in Corpus Callosum and Pyramidal Tract." Proceedings of 2011 National Neurotrauma Symposium, July 10-13, 2011, Fort Lauderdale, Florida

<u>Nisrine Zakaria</u>, Srinivas Kallakuri, John Cavanaugh, Yimin Shen, Zhifeng Kou, Yingjian Yu, E Mark Haacke. "Assessing the Potential of Diffusion Tensor Imaging as a Non-Invasive Tool for Detecting Diffuse Axonal Injuries in a Rodent Model of Traumatic Brain Injury." Proceedings of 2007 National Neurotrauma Symposium, July 30- Aug 1 2007, Kansa City, Missouri.

Zhifeng Kou, Yimin Shen, <u>Nirsine Zakaria</u>, Srinivasu Kallakuri, John Cavanaugh, Yingjian Yu, Jiani Hu, E Mark Haacke. Correlation of Fractional Anisotropy with Histology for Diffuse Axonal Injury in a Rat Model. *Joint Annual Meeting ISMRM-ESMRMB*, May 19-25, 2007, Berlin, Germany.

Zhifeng Kou, Yimin Shen, <u>Nisrine Zakaria</u>, Srini Kallakuri, John Cavanaugh, Yingjian Yu, Shunshan Li, E Mark Haacke, "Characterizing Diffuse Axonal Injury in an Animal Model Using Advanced MRI." Proceedings of 2007 Biomedical Engineering Society Annual Fall Meeting, Sept 26-29 2007, Los Angeles. To appear.

<u>Nisrine Zakaria</u>, Srinivas Kallakuri, John Cavanaugh, Yimin Shen, Zhifeng Kou, Yingjian Yu, E Mark Haacke. "Histological verification of diffusion tensor imaging as a tool for detecting diffuse axonal injury." Proceedings of 2007 Biomedical Engineering Society Annual Fall Meeting, Sept 26-29 2007, Los Angeles.

Yimin Shen, Zhifeng Kou, E Mark Haacke, <u>Nirsine Zakaria</u>, Srinivasu Kallakuri, John Cavanaugh, Yingjian Yu, Jiani Hu. Correlation of Changes in Venous Cerebral Blood Flow after Trauma in Rats Measured by Susceptibility-weighted Imaging and Fractional Anisotropy in Diffusion Tensor Imaging. *Joint Annual Meeting ISMRM-ESMRMB, May 19-25, 2007, Berlin, Germany.*

<u>Nisrine Zakaria</u>, Srinivasu Kallakuri, John M. Cavanaugh, Yimin Shen, Yingjian Yu, Zhifeng Kou, E Mark Haacke. Diffuse Axonal Injury: Comparison of Histological Observations and Diffusion Tensor Imaging (2006). *Proceedings of Biomedical Engineering Society Annual Conference*, Oct 11-14, 2006, Chicago, IL.

Srinivas Kallakuri, Lying Zhang, <u>Nisrine Zakaria</u>, John M Cavanaugh. Quantification of TAI and Tissue Strain Using Experimental and Computational Model of TBI on Rats (2006). *Proceedings of Biomedical Engineering Society Annual Conference*, Oct 11-14, 2006, Chicago, IL.